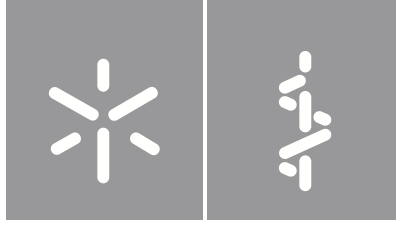Universidade do Minho
Escola de Medicina

Hugo Miguel Fernandes Silva

New insights on Retinoic Acid Signaling-Metabolism interaction during lung branching morphogenesis

New insights on Retinoic Acid Signaling-Metabolism interaction during lung branching morphogenesis

Hugo Miguel Fernandes Silva

UMinho | 2022

abril de 2022

Universidade do Minho
Escola de Medicina

Hugo Miguel Fernandes Silva

New insights on Retinoic Acid Signaling-Metabolism interaction during lung branching morphogenesis

Tese de Doutoramento
Doutoramento em Envelhecimento e Doenças Crónicas

Trabalho efetuado sob a orientação da
Doutora Rute Carina Silva Moura
e da
Doutora Catarina de Cértima Fernandes Homem

abril de 2022

DIREITOS DE AUTOR E CONDIÇÕES DE UTILIZAÇÃO DO TRABALHO POR TERCEIROS

Este é um trabalho académico que pode ser utilizado por terceiros desde que respeitadas as regras e boas práticas internacionalmente aceites, no que concerne aos direitos de autor e direitos conexos. Assim, o presente trabalho pode ser utilizado nos termos previstos na licença abaixo indicada. Caso o utilizador necessite de permissão para poder fazer um uso do trabalho em condições não previstas no licenciamento indicado, deverá contactar o autor, através do RepositóriUM da Universidade do Minho.

Licença concedida aos utilizadores deste trabalho:

ACKNOWLEDGEMENTS

Expresso os meus sinceros agradecimentos a todas as pessoas e instituições que contribuíram para a elaboração desta tese de doutoramento. Quero agradecer à Universidade do Minho, à Escola de Medicina e ao Instituto em Ciências da Vida e Saúde (ICVS). Agradeço também ao Centro de Estudos de Doenças Crónicas (CEDOC) e ao Instituto de Ciências Biomédicas Abel Salazar (ICBAS), locais onde realizei parte das tarefas práticas. Agradeço ao Programa Inter-Universitário de Doutoramento em Envelhecimento e Doenças Crónicas (PhDOC) pela oportunidade em fazer parte deste projeto, e por todas as experiências e aprendizagens que me permitiu ter. Um agradecimento especial às minhas orientadoras. À Doutora Rute Moura, que acreditou em mim desde o primeiro momento, pela paciência, compreensão, todo o apoio, disponibilidade, conselhos, discussões de ideias e por todas as noções de boas práticas laboratoriais, ensinamentos que me permitiram crescer profissional e pessoalmente. À Doutora Catarina Homem, por me ter recebido no seu laboratório, por todo o apoio, pela disponibilidade, abertura e por todas as discussões de ideias. Aos colaboradores, o Doutor Pedro Oliveira e o Doutor Marco Alves por todas as contribuições e discussões ao longo destes anos. Ao Professor Doutor Jorge Correia Pinto por todo o apoio. Aos meus colegas e companheiros de laboratório do ICVS, CEDOC, ICBAS e PhDOC. Ao Henrique, pelo companheirismo, ajuda e discussões científicas dentro e fora do laboratório ao longo destes anos. À Ana Maria, por todo o apoio, paciência e ensinamentos nas experiências do elétrodo Clark. À Márcia, por toda a ajuda nas experiências do Seahorse. Aos amigos de sempre, pelo apoio incondicional, companheirismo, força e motivação. À Maria João ... não há palavras. Obrigado por todo o apoio, motivação, compreensão, companheirismo, por estares sempre lá, por me aturares durante esta fase e por nunca teres duvidado que era possível! À minha mãe, ao meu pai, à minha irmã, à minha avó Luísa, e à restante família por todo o apoio incondicional ao longo deste percurso, pela motivação, força e pelas condições que me proporcionaram para conseguir atingir sempre as minhas metas.

STATEMENT OF INTEGRITY

I hereby declare having conducted this academic work with integrity. I confirm that I have not used plagiarism or any form of undue use of information or falsification of results along the process leading to its elaboration.

I further declare that I have fully acknowledged the Code of Ethical Conduct of the University of Minho.

RESUMO

Estudos sobre a interação da via de sinalização do Ácido Retinoico e metabolismo durante a ramificação pulmonar

A ramificação pulmonar é um processo complexo caracterizado por interações epitélio-mesênquima e coordenado por vias de sinalização que contribuem para a formação das vias respiratórias. A via de sinalização do Ácido Retinoico (AR) é crucial para o desenvolvimento pulmonar e é particularmente importante para o padrão próximo-distal e a ramificação pulmonar. Os mecanismos moleculares subjacentes aos estadios iniciais do desenvolvimento pulmonar estão bem explorados, no entanto, ainda pouco se sabe quanto ao metabolismo do pulmão embrionário. Existem evidências que sugerem que as interações entre sinalização e metabolismo são essenciais para perceber os processos de desenvolvimento embrionário. O principal objetivo desta tese foi investigar o perfil metabólico associado aos estadios iniciais da ramificação pulmonar e estudar as potenciais interações entre a via de sinalização do Ácido Retinoico e o metabolismo associados à ramificação pulmonar. Na nossa abordagem utilizamos um sistema de cultura de explantes que nos permitiu mimetizar o processo de ramificação pulmonar, usando como modelo o embrião de galinha. O metabolismo associado à ramificação pulmonar foi avaliado aos níveis de transcrito, proteína e metabolitos, através de qPCR, hibridização *in situ*, western blot e espectroscopia de ^{1}H-RMN. Os níveis de proliferação foram avaliados através de um ensaio de EdU. A função mitocondrial e capacidade respiratória dos pulmões foram analisadas através de ensaios de elétrodo Clark e Seahorse. Neste estudo descrevemos as alterações metabólicas que ocorrem ao longo do tempo e acompanham o processo de ramificação pulmonar. À medida que a ramificação pulmonar progride, o pulmão adapta-se a um metabolismo glicolítico com produção de lactato e que se assemelha ao metabolismo do tipo Warburg. Mais ainda, a modulação da via de sinalização do AR regula o metabolismo pulmonar. A estimulação da via do AR aumenta a ramificação pulmonar promovendo condições ótimas de crescimento. Por outro lado, a inibição da via do AR parece induzir um metabolismo menos eficiente e que está associado a um fenótipo pulmonar anormal. Em suma, demonstramos que o desenvolvimento pulmonar e o metabolismo estão interligados e descrevemos novas noções sobre a interação entre a sinalização e o metabolismo. Neste estudo destacamos ainda a importância da regulação metabólica durante a ramificação pulmonar e como a sinalização e o metabolismo devem ser controlados por forma a evitar o comprometimento do crescimento pulmonar.

Palavras-chave: Ácido retinoico, Embrião de galinha, Glucose, Mitocôndria, Sistema respiratório

ABSTRACT

New insights on Retinoic Acid Signaling-Metabolism interaction during lung branching morphogenesis

Lung branching morphogenesis is a complex process characterized by epithelial-mesenchymal interactions and coordinated by signaling networks that ultimately define the airway conducting system. Retinoic Acid (RA) signaling is a major player in lung development and is particularly important for proximal-distal patterning and branching morphogenesis. The molecular mechanisms involved in early lung development are well explored. However, little is known concerning embryonic lung metabolism. Moreover, growing evidence suggests that signaling-metabolism interactions are essential to understanding developmental processes. The main goal of this thesis was to investigate the metabolic profile associated with the early stages of pulmonary branching and to study potential interactions between the Retinoic Acid signaling pathway and the lung branching metabolism. In our approach, we performed an explant culture system to mimic the process of lung branching morphogenesis and used the chicken embryo as a model. Lung branching metabolism was assessed at the transcript, protein, and metabolite levels by qPCR, *in situ* hybridization, western blot, and ^{1}H-NMR spectroscopy. The proliferation status was assessed using an EdU-based assay. Mitochondrial function and the lung respiratory capacity were studied using a Clark-type electrode and a Seahorse analysis. In this study, we described the temporal metabolic changes accompanying early lung branching morphogenesis. As pulmonary branching proceeds, the lung progressively adapts to a glycolytic lactate-based metabolic profile that resembles a Warburg-like metabolism. Moreover, RA signaling modulation regulates lung branching metabolism. While RA signaling stimulation increases lung branching by promoting optimal growth conditions, RA signaling inhibition seems to induce a less efficient metabolism associated with a disease-like phenotype. In conclusion, we unveiled that lung development and metabolism are interlinked, and we brought novel insights on the signaling-metabolism interaction. This work highlights the importance of metabolic regulation during lung branching morphogenesis and how signaling and metabolism must be finely tuned to prevent lung growth impairment.

Keywords: Chicken embryo, Glucose, Mitochondria, Respiratory system, Retinoic acid

TABLE OF CONTENTS

ABBREVIATIONS

^{1}H-NMR	^{1}H-Nuclear magnetic resonance
ADH	Alcohol dehydrogenase
AEC1	Airway epithelial cell type 1
AEC2	Airway epithelial cell type 2
AKT	Protein kinase B
AMPK	Adenosine monophosphate-activated protein kinase
ATRA	All-trans retinoic acid
BC	Bronchogenic cyst
BMP	Bone morphogenetic protein
BMS	BMS493
BPD	Bronchopulmonary dysplasia
BPS	Bronchopulmonary sequestration
CC10	Clara cell marker 10
CDH	Congenital diaphragmatic hernia
CLE	Congenital lobar emphysema
COPD	Chronic obstructive pulmonary disease
COUP-TF	Chicken ovalbumin upstream promoter-transcription factor
CPAM	Congenital pulmonary airway malformation
CPT1	Carnitine palmitoyltransferase I
CRABP	Cellular retinoic acid-binding protein
CRBP	Cellular retinol-binding protein
CT	Computed Tomography
CVR	CPAM volume ratio
CYP	Cytochrome P450
ECM	Extracellular matrix
ECMO	Extracorporeal membrane oxygenation
EdU	5-ethinyl-2'-desoxyuridine
EpiSC	Epiblast stem cell
ERK	Extracellular regulated kinase
ESC	Embryonic stem cell

EUROCAT	European surveillance of congenital anomalies
FABP	Fatty acid-binding protein
FASN	Fatty acid synthase
FGF	Fibroblast growth factor
G6PD	Glucose-6-phosphate dehydrogenase
GDNF	Glial cell-derived neurotrophic factor
GLUT	Glucose transporter
HGF	Hepatocyte growth factor
HIF	Hypoxia-inducible transcription factor
Hippo	Hippo signaling pathway
HK	Hexokinase
HOX	Homeobox-containing gene
ICM	Inner cell mass
IPSC	Induced pluripotent stem cell
L-2HG	L-2-hydroxyglutarate
L-CAM	Chicken E-cadherin
LDH	Lactate dehydrogenase
LIF	Lipofibroblasts
LRAT	Lecithin retinol acyltransferase
LSD	Least significant difference
MABT	Maleic acid buffer with tween 20
MCT	Monocarboxylate transporter
miRNA/miR	MicroRNA
MRI	Magnetic resonance imaging
mTOR	Mammalian target of rapamycin
MYF	Myofibroblasts
NCOA	Nuclear receptor co-activators
NCOR	Nuclear receptor co-repressors
NOTCH	Notch signaling pathway
OCR	Oxygen consumption rate
OXPHOS	Oxidative phosphorylation
pAMPK	Phosphorylated adenosine monophosphate-activated protein kinase

PDGF	Platelet-derived growth factor
PDH	Pyruvate dehydrogenase
PFK1	Phosphofructokinase 1
PFKFB4	6-phosphofructo-2-kinase/fructose-2,6-bisphosphatase 4
PGD	6-phosphogluconate dehydrogenase
PSC	Pluripotent stem cell
PSM	Presomitic mesoderm
RA	Retinoic acid
RALDH	Retinaldehyde dehydrogenase
RAR	Retinoic acid receptor
RARE	Retinoic acid response element
RBP4	Retinol-binding protein 4
RDH	Retinol dehydrogenase
RhoA	Transforming protein rhoA
RXR	Retinoid X receptor
SEM	Standard error of the mean
SHH	Sonic hedgehog
SMO	Smoothened
SREBF1	Sterol regulatory element-binding transcription factor 1
SREBP1	Sterol regulatory element-binding protein 1
STRA6	Stimulated by retinoic acid 6
TAZ	Transcriptional coactivator with PDZ-binding motif
TCA	Tricarboxylic acid
TFAM	Transcription factor A mitochondrial
TGFβ	Transforming growth factor β
TSC	Totipotent stem cell
TTF1	Thyroid transcription factor
VAD	Vitamin A deficiency
VEGF	Vascular endothelial growth factor
WNT	Wingless-related integration site
YAP	Yes-associated protein
YY1	Yin yang 1

LIST OF FIGURES

Chapter 3.2

Retinoic Acid Signaling Regulates the Metabolic Profile of Lung Branching Morphogenesis

LIST OF TABLES

CHAPTER 1. INTRODUCTION

CHAPTER 1.1

GENERAL INTRODUCTION

Lung development is a highly orchestrated process sustained by cellular, molecular, and physical events. Lung formation requires coordinated growth, differentiation, and a continuous interplay between compartments, regulated by several developmental signaling pathways, including Retinoic Acid (RA) [1]. As the lung develops, a complex branching program shapes the airway conducting system. Later on, the airways and vasculature fuse at the distal end of the bronchial tree to generate the alveoli. This intricate structure contributes to forming a fully functional organ capable of gas exchange [2,3].

Retinoic Acid is the active metabolite from vitamin A and a key molecular player for vertebrate organogenesis and tissue homeostasis [4]. The developing respiratory system depends on RA signaling, which modulates cellular proliferation, differentiation, and patterning [5]. Moreover, during the pseudoglandular phase, RA regulates proximal-distal patterning and branching morphogenesis [6,7].

More recently, metabolism has emerged as a new player during embryonic development beyond its well-recognized bioenergetics role and has the potential to contribute to a better understanding of developmental processes. In this sense, it is essential to comprehend how metabolism impacts cellular and developmental decisions and how metabolic regulation occurs during development [8].

The introduction of this thesis is organized in the following chapters, that cover three main topics:

Chapter 1.2 addresses the current knowledge on the molecular mechanisms underlying normal and abnormal lung development. We explore the molecular networks governing all lung developmental stages, and we examine the present understanding regarding the signaling events impaired or deregulated in congenital lung disorders.

Chapter 1.3 describes in detail the RA signaling pathway. We outline the molecular events regulated by RA signaling during all lung developmental phases. Furthermore, we specify how RA signaling impairment impacts lung development.

Chapter 1.4 explores the existing knowledge on the role of metabolism during embryonic development, focusing on glycolysis. We highlight the need to study metabolic regulation, signaling-metabolism interactions, and the impact of metabolism on cellular and developmental decisions.

References:

1. Caldeira, I.; Fernandes-Silva, H.; Machado-Costa, D.; Correia-Pinto, J.; Moura, R.S. Developmental Pathways Underlying Lung Development and Congenital Lung Disorders. Cells 2021, 10(11):2987, doi:10.3390/cells10112987.
2. Warburton, D.; El-Hashash, A.; Carraro, G.; Tiozzo, C.; Sala, F.; Rogers, O.; De Langhe, S.; Kemp, P.J.; Riccardi, D.; Torday, J.; et al. Lung organogenesis. Curr. Top. Dev. Biol. 2010, 90, 73-158, doi:10.1016/S0070-2153(10)90003-3.
3. Whitsett, J.A.; Kalin, T.V.; Xu, Y.; Kalinichenko, V.V. Building and Regenerating the Lung Cell by Cell. Physiol. Rev. 2019, 99, 513-554, doi:10.1152/physrev.00001.2018.
4. Cunningham, T.J.; Duester, G. Mechanisms of retinoic acid signalling and its roles in organ and limb development. Nat. Rev. Mol. Cell Biol. 2015, 16, 110–123, doi:10.1038/nrm3932.
5. Fernandes-Silva, H.; Araújo-Silva, H.; Correia-Pinto, J.; Moura, R.S. Retinoic Acid: A Key Regulator of Lung Development. Biomolecules 2020, 10, 152, doi:10.3390/biom10010152.
6. Malpel, S.; Mendelsohn, C.; Cardoso, W.V. Regulation of retinoic acid signaling during lung morphogenesis. Development 2000, 127, 3057–3067, doi:10.1242/dev.127.14.3057.
7. Fernandes-Silva, H.; Correia-Pinto, J.; Moura, R.S. Canonical Sonic Hedgehog Signaling in Early Lung Development. J. Dev. Biol. 2017, 5, 3, doi:10.3390/jdb5010003.
8. Miyazawa, H.; Aulehla, A. Revisiting the role of metabolism during development. Development 2018, 145, doi:10.1242/dev.131110.

CHAPTER 1.2

DEVELOPMENTAL PATHWAYS UNDERLYING LUNG DEVELOPMENT AND CONGENITAL LUNG DISORDERS

Hugo Fernandes-Silva*, Inês Caldeira*, Daniela Machado-Costa, Jorge Correia-Pinto and Rute S. Moura

*These authors contributed equally to this work.

ABSTRACT

Lung organogenesis is a highly coordinated process governed by a network of conserved signaling pathways that ultimately control patterning, growth, and differentiation. This rigorously regulated developmental process culminates with the formation of a fully functional organ. Conversely, failure to correctly regulate this intricate series of events results in severe abnormalities that may compromise postnatal survival or affect/disrupt lung function through early life and adulthood. Conditions like congenital pulmonary airway malformation, bronchopulmonary sequestration, bronchogenic cysts, and congenital diaphragmatic hernia display unique forms of lung abnormalities. The etiology of these disorders is not yet completely understood; however, specific developmental pathways have already been reported as deregulated. In this sense, this review focuses on the molecular mechanisms that contribute to normal/abnormal lung growth and development and their impact on postnatal survival.

Keywords: congenital pulmonary airway malformation (CPAM); bronchopulmonary sequestration; bronchogenic cysts; congenital diaphragmatic hernia (CDH); congenital malformations

OVERVIEW

Lung development is a highly orchestrated and conserved multistage process sustained by molecular, cellular, and physical events, traversing all gestational ages. Proper lung formation relies upon the crosstalk between epithelial and mesenchymal compartments, which controls the temporal and spatial distribution of a multitude of factors and diffusible signals. Key signaling pathways play a role in this process, for instance, Fibroblast Growth Factor (FGF) [1], Retinoic Acid (RA) [2], Sonic Hedgehog (SHH) [3], Wingless-related Integration Site (WNT) [4], Transforming Growth Factor β (TGFβ), Bone Morphogenetic Protein (BMP) [5], Hippo [6], to name a few.

Congenital lung malformations arise due to abnormal embryonic development caused by an impairment of signaling and/or genetic factors. The following sections will address the key regulatory factors involved throughout the different lung developmental stages and the molecular determinants of the most common lung congenital anomalies.

LUNG DEVELOPMENT

Lung development is divided into five morphological stages that establish molecular and structural transitions: (1) embryonic; (2) pseudoglandular; (3) canalicular; (4) saccular; (5) alveolar. Due to the non-synchronous development of the lung, the timing of the stages overlaps. Primordial lung buds originate as outpunches of the primitive foregut endoderm, and the bronchial tree is generated by reinterred budding and branching of epithelial tubules [7]. The human lung epithelium derives from the endoderm, whereas the surrounding mesenchyme originates from the mesodermal germ layer [8]. Blood vessels arise from mesodermal cells surrounding the tips of branching tubules (vasculogenesis), or through migration of blood vessels from the aortic arches into the lung, by sprouting of the pulmonary artery (angiogenesis) [9]. As the lung develops, the airways and vasculature develop, fusing at the distal end of the bronchial tree to generate millions of alveolar gas exchange units. The intricate branching pattern of the airways guarantees that, during postnatal life, humidified and cleared air is uniformly distributed to alveolar units.

EMBRYONIC STAGE

The embryonic phase of human lung development is characterized by the formation of two primordial right and left buds that emerge from the foregut endoderm. Lung specification begins around the fourth post-conception week (pcw) in humans, at embryonic (E) day 9.5 in mice and E11 in rats, with a localized expression of NKX2.1 (also known as TTF1, thyroid transcription factor) in endodermal cells of the ventral anterior foregut [10,11].

The epithelial outgrowth of the primary buds requires complex interactions between local signals in the prespecified foregut endoderm and inductive paracrine signals from the surrounding mesoderm, both tightly regulated in dose, time, and space [12]. Defects in these molecular players impair foregut separation and cause abnormalities in epithelium and mesenchyme differentiation. WNT signaling, particularly WNT2 and WNT2B, plays an essential role in specifying NKX2.1 respiratory endoderm progenitors in the ventral anterior mesoderm surrounding the anterior foregut endoderm [13,14]. On the other hand, WNT2/2B expression is regulated by HOXB5 [15]. The ability of WNT/β-catenin to induce NKX2.1 endoderm progenitor fate depends on the activation of BMP signaling [16]. BMP4 is expressed in the mesenchyme surrounding the anterior foregut and appears to have an inhibitory action on the transcription factor SOX2 (which promotes esophageal fate), allowing NKX2.1 expression [16]. SHH

expression in the endoderm regulates BMP4 expression in the mesoderm through different downstream targets, such as FOXF1, GLI1, and GLI3. In its turn, SHH is regulated by mesodermal RA signaling [17].

Upon respiratory lineage specification, localized mesodermal expression of fibroblast growth factor 10 (FGF10), adjacent to the NKX2.1+ progenitors, induces FGF receptor 2b (FGFR2B) signaling resulting in primary lung bud formation due to cellular movements into the mesenchyme towards the FGF10 source. An RA-TGF-FGF10 axis triggers primary lung bud formation. Briefly, endogenous RA inhibits TGFβ signaling in the lung-specified foregut to elicit FGF10 expression and, consequently, induction of primary lung buds [18,19]. TBX4, a member of conserved T-box-containing transcription factors, influences FGF10 expression, particularly in chicken embryos. Mesodermal *tbx4* stimulates *fgf10* expression, defines its anterior-posterior (AP) mesodermal expression boundaries, and induces endoderm differentiation by triggering *nkx2.1* expression [20]. However, the genetic inactivation of TBX4 in mice does not prevent lung bud formation, suggesting a redundant role of these genes in foregut morphogenesis [21]. Figure 1 provides a schematic representation of the key genes involved in lung specification.

These early events of pulmonary development require the interplay of many other factors. For instance, the GATA family of zinc-finger transcription factors, GATA4 and GATA6, and FOXA1/2 transcription factors (Forkhead box gene superfamily) are expressed early in the endoderm and have a crucial role in survival, differentiation, and morphogenesis of the foregut [22–24]. Interestingly, these factors have pivotal roles in the formation of primary structures of the future lung (for instance, SOX2 and GATA6); they are also entangled in later phases of differentiation and specification of respiratory cell lineages.

Once primary lung buds are formed, epithelial tubules undergo extensive branching morphogenesis that culminates in the formation of the bronchial tree and the future alveolar region.
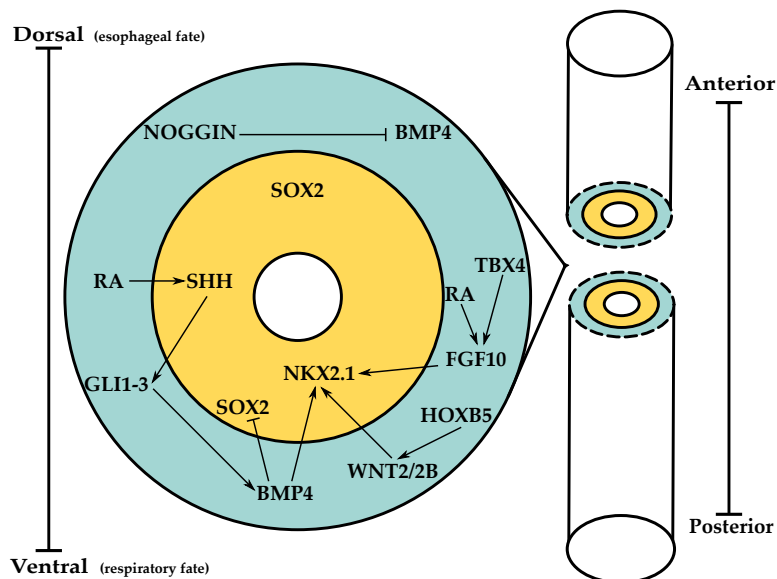
Figure 1 - Summary of the molecular players involved in lung specification. A BMP gradient elicits dorsal SOX2 expression (esophageal progenitors) vs. ventral NKX2.1 expression (respiratory progenitors). Yellow, endoderm; blue, mesoderm.

PSEUDOGLANDULAR STAGE

During the pseudoglandular phase (5–17 pcw human, E12–16.5 mouse, and E13–E18.5 rat), each main lung bud initiates a repetitive process of outgrowth, elongation, and bifurcation of the airway epithelium into the surrounding mesenchyme, a process called branching morphogenesis. This process is repeated over several generations; a reiterated combination of three processes, domain branching, planar bifurcation, and orthogonal bifurcation, will give rise to the respiratory bronchial tree [25,26]. Blood vessel development occurs concomitantly with epithelial branching, and vessels start to run along the airway, except that vessels branch more slowly [27]. Simultaneously, the proximal-distal axis of the developing lung is established. Additionally, as the airway tree is laid down, it begins to differentiate with cartilage; mucous glands and smooth muscle are already present [28].

Branching mechanisms are governed by intensive crosstalk between the epithelial and mesenchymal compartments, which in turn is regulated by a network of signaling cascades that control cellular processes, including extracellular matrix remodeling, proliferation, and differentiation in a temporal-spatial manner. Lung bud outgrowth, branching, and subsequent bud arrest result from the dynamic activity of SHH, FGF10, Sprouty 2 (SPRY2), TGFβ, and BMP4 [12,29].

FGF signaling, in particular FGF10, is essential for branching morphogenesis; in fact, *fgf10−/−* mice die at birth due to complete abrogation of pulmonary branching morphogenesis [30]. FGF10 is

expressed in the distal lung mesenchyme, specifically at sites of branch point formation and outgrowth; it acts in a paracrine fashion on the adjacent epithelium, where its cognate receptor FGFR2 is expressed [31,32], prompting a signaling cascade that culminates in the expression of SPRY2, SHH, and BMP4, which subsequently regulate the response and outgrowth of the lung bud [33,34]. This interaction is repeated each time a new series of bud initiation and outgrowth is initiated - the buds that branch from the preexisting ones grow towards the regions of high FGF10 expression [35]. Recently, there has been emerging evidence for a critical role of mammalian target of rapamycin (mTOR) complexes in coordinating branching morphogenesis and defining organ structural complexity [36]. FGF10/ FGFR2b downstream signaling through ERK1/2 (extracellular regulated kinase 1/2) and mTORC1, which is active in the epithelial progenitor cells at the tip of the airway tube, induce outward growth towards FGF10 induction signaling, controlling the duration of this event (a determinant of branch length and patterning of the airway tree) [37]. Furthermore, though the mechanisms that link vascular growth to airway branching remain unknown, it is recognized that mTORC1 directly links the primary cues for airway (FGF10) and vascular (VEGF-A; vascular endothelial growth factor A) growth in the pulmonary branching morphogenesis program [38]. The secretion of VEGF from the branching epithelium initiates the differentiation of mesenchyme progenitor cells into vascular tissue and is regulated by hypoxia-inducible transcription factors (HIFs). From the three HIF-α isoforms expressed in the developing lung, HIF-1α, present in the branching epithelium, plays a major role in early pulmonary vasculogenesis [39]. Land *et al.* demonstrated that FGF10 induces mTORC1 activity via SPRY2 in fetal airway epithelium, and that amplifies HIF-1α vasculogenic activity to drive VEGF-A expression and secretion from the airway endoderm [37]. The RA pathway has also been recognized as a crucial regulator for correct lung formation in mammalian [40,41] and chicken models [42]. Impairment of the RA signaling (by interfering with RDH10 or RALDH2) undermines branching morphogenesis and, thus, lung formation [43,44]. Likewise, WNT signaling is also a key regulator of lung branching morphogenesis [45,46]; targeted deletion of β-catenin [47] or the expression of the Dickkopf-1 (DKK1) WNT antagonist hamstrings normal lung branching [48]. Ligands such as WNT5A, WNT2A, and WNT7B play crucial roles in lung epithelial and mesenchymal growth/differentiation through a WNT-FGF crosstalk [49–52].

Branching morphogenesis also depends on the timely expression of numerous transcription factors. Among the subgroup of homeobox-containing genes (HOX family), HOXB5 is essential for establishing AP airway patterning. *hoxb5* is highly expressed during the pseudoglandular period, in the mesenchymal compartment, surrounding active branching sites [42,53]. As branching morphogenesis is completed and lung development progresses, *hoxb5* expression diminishes. Additionally, *sox2* and *sox9*,

belonging to the SRY-related HMG-box family of transcription factors, regulate cell specification and differentiation. In the mouse, the proximal-distal patterning of the respiratory tree is defined by a distinct expression of SOX9 (and ID2) in the distal epithelium and SOX2 in the proximal airway epithelium. SOX2 is restricted to the pulmonary epithelium and is undetectable at the tips of the emerging secondary bronchi, whereas SOX9 expression delimits branching epithelium and originates distal pulmonary cell lineages [54]. In fact, it has been shown that loss of *sox2* expression at branching sites is required for branching morphogenesis to occur [55]. SOX2-SOX9 spatial distribution along the lung epithelium is regulated by FGF10 signaling; FGF10 induces *sox9* expression in the distal epithelium thus maintaining SOX9+ multipotent progenitor cells in an undifferentiated and stimulating their self-renewal; conversely, FGF10 inhibits *sox2* expression, and proximal cellular fate, in the distal lung [56]. Furthermore, loss of SOX2 signaling impairs the differentiation of secretory and multiciliated cells that line the proximal airway epithelium in the subsequent lung stage [57].

More recently, the Hippo effectors YAP (Yes-associated protein) and TAZ (transcriptional coactivator with PDZ-binding motif) have been described as having important growth-modulator functions in branching morphogenesis and epithelial cell differentiation. YAP functions at the transition zone between the airway and the distal lung compartments and controls *sox2* expression, thus promoting proximal airway differentiation [58,59]. In the absence of YAP, epithelial progenitors are unable to respond to local cues and, consequently, control SOX2 levels and spatial distribution and properly form airways [59]. Furthermore, Volckaert and colleagues proposed that cytoplasmatic YAP activity in the proximal epithelium promotes epithelial lineage commitment by inhibiting the β-catenin signaling pathway and FGF10 [60].

MicroRNAs (miRNAs/miR) also contribute to the lung developmental program. For instance, in this stage, miR-326 negatively regulates SHH signaling by targeting GLI2 and SMO (Smoothened) [61]. miR-142-3p regulates the proliferation and differentiation of mesenchymal progenitors by controlling the level of WNT signaling [62]. Mouse miR-17 (and its paralogs miR-20a and miR-106b) is expressed in the epithelium and controls branching morphogenesis through an FGF10-mediated molecular mechanism targeting MAPK14 and STAT3 [63]. Overexpression or deletion of the miR17–92 cluster (belonging to the miR-17 family) leads to increased proliferation/decreased differentiation or hypoplastic lungs, respectively, pointing to a crucial role in lung branching morphogenesis [64,65]. Moreover, *miR-200b−/−* mice display disturbed airway distal lung branching and impairment in lung parenchyma [66]. miR-449a is crucial in the pseudoglandular to canalicular transition, and its inhibition results in increased *mycn* and *sox9* mRNA and Ki-67 and SOX9 protein levels [67]. Furthermore, overexpression of rat miR-127 results

in decreased terminal number of buds and increased terminal and internal bud sizes, suggesting an important role during lung morphogenesis [68]. In chicken, the expression pattern of miRNA processing machinery *drosha*, *dgcr8*, *exportin-5*, and *dicer1* was described, thus supporting the importance of these regulatory elements during the early stages of branching morphogenesis [69]. Branching morphogenesis is also highly influenced by biomechanical forces, such as the transmural pressure in the chest cavity and smooth muscle contractions that influence the synchronization of the branching events [70]. HIPPO/YAP signaling regulates myosin light chain kinase activity, creating mechanical forces that influence cell shape required for branching [71]. In addition, recent data highlighted the importance of metabolic regulation during the early stages of lung branching morphogenesis [72]. The key signaling pathways underlying branching morphogenesis are shown in Figure 2.
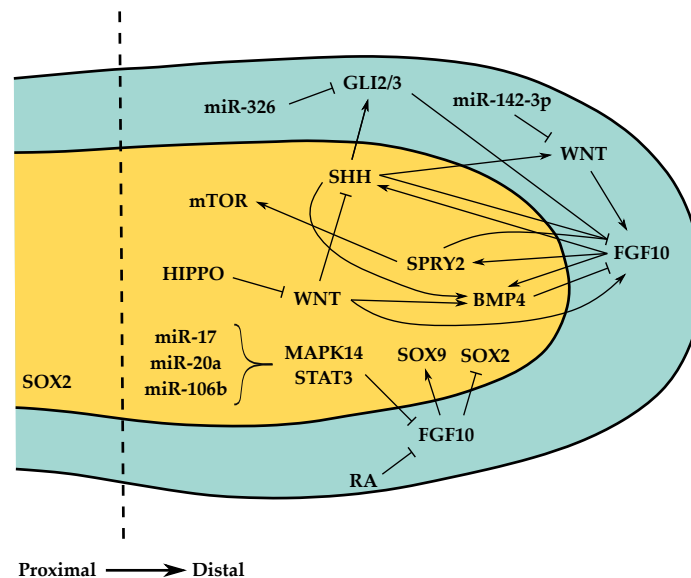
Figure 2 - Signaling pathways that mediate epithelial-mesenchymal interactions during pseudoglandular stage, specifically in the distal epithelial tip. SOX2+ cells define proximal epithelial cell lineages whereas SOX9+ cells define distal epithelial cell lineages. Yellow, epithelium; blue, mesenchyme.

Furthermore, the extracellular matrix (ECM) undergoes a series of remodeling events for the branching process to occur. ECM composition/structure plays a decisive role in lung development and organ architecture; it directly affects the availability and activity of soluble factors (as, for instance, FGF) by influencing their diffusion rates and the accessibility of their receptors [73]. ECM components, particularly fibronectin, laminin, and collagen, actively participate in the epithelium and mesenchyme interactions by accumulating within the clefts that mark the branch points. Fibronectin deposition possibly regulates cellular migration by fixing some cells at the cleft, while the un-fixed ones can migrate and

proliferate distally [74]. By the end of the pseudoglandular phase, the complete human airway structure has been established, and airway epithelial differentiation is proceeding.

CANALICULAR STAGE

The canalicular stage spans pcw 16–26 in human (E16.5–E17.5 in mouse and around E18.5–E20 in rat) [25]. During this period, the existing epithelial airways continue to increase in size, and the epithelial terminal buds project into the distal airspaces as their surrounding mesenchyme thins, giving rise to the primitive pulmonary acini (terminal sacs), the primitive alveoli. This phase is also characterized by alveolar cellular differentiation. Distal epithelial cells differentiate into alveolar epithelial cells type 1 (AEC1) and type 2 (AEC2), also known as type 1 and type 2 pneumocytes. AEC2 are responsible for surfactant production and serve as AEC1 progenitor cells, whereas AEC1 are responsible for gas exchange. One of the key signaling pathways for the determination of cellular fate is NOTCH signaling. NOTCH transmembrane receptors mediate communication between neighboring cells and have a central role in balancing differentiation of multiciliated vs. secretory lineages in the proximal airway epithelium; loss of NOTCH signaling leads to the absence of secretory cells and airways populated by multiciliated cells [75]. HIPPO signaling ceases branching morphogenesis and promotes alveolar differentiation through degradation of β-catenin in the epithelium, disrupting the WNT-FGF feedback loop and directing bud tip epithelial progenitors to differentiate [76]. Finally, both human and mouse miR-449a are upregulated in the distal lung, throughout the canalicular stage, to promote distal epithelium differentiation by regulating N-MYC and SOX9 but has no effect in SOX2 expression [67]. Figure 3 illustrates the signaling events governing the canalicular stage.

Lastly, vascularization begins during this phase. The course of capillaries leaning against the distal epithelium airspaces and the continued angiogenic process contribute to the formation of the first thinned air-blood barrier in the future alveolar ducts and saccules [77].

13
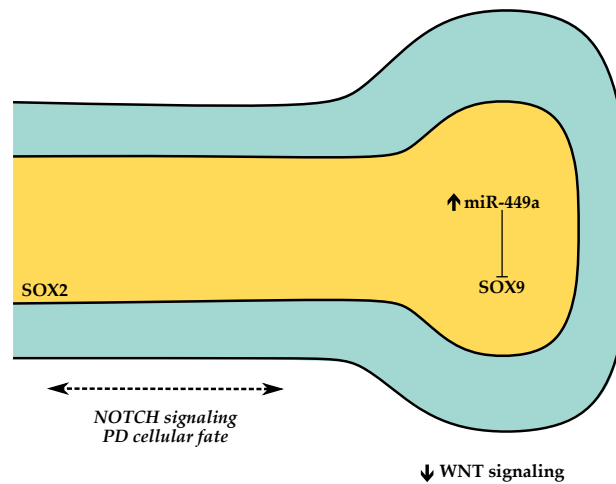
Figure 3 - Simplified representation of the signaling pathways implicated in the canalicular stage. Proximal SOX2+ cells generate conducting airway cells (neuroendocrine, secretory, multiciliated and basal). Distal SOX9+ cells generate alveolar epithelial cells.

SACCULAR STAGE

The saccular phase, occurring between pcw 24 and 38 in humans (between E17.5–Postnatal day (P) 4 in mouse and E21–P4 in rat), is an intermediate phase in which branching morphogenesis ceases, and alveolarization is yet to commence. This intermediate stage is necessary since branching morphogenesis and alveolarization do not occur simultaneously [12]. Furthermore, this period is characterized by the widening and further division of the distal airspaces into numerous thin-walled terminal saccules, the alveoli precursors. The expansion of the future gas exchange region causes the condensation of the mesenchyme in-between airspaces, originating a thick immature primary septum at locations where two airspaces meet. [25]. Capillary networks remain very close to septal surfaces and are separated by a dense central layer of mesenchyme that forms a core of connective tissue [25]. During this period, the exceptional expansion of the prospective respiratory airspaces leads to a decrease in the interstitial tissue, which greatly impacts capillary arrangement. As each saccule further increases in size, blood vessels become closely associated and form a capillary bilayer wrapping each saccule. This process is crucial for alveoli formation and subsequent gas exchange [8]. Compared to the mature lung, the capillaries are embedded in a broad interstitial layer that is very poor in extracellular fibers but is very cellular [8]. Nonetheless, soon after, elastin starts to be deposited under the epithelium, which prepares the lungs for further alveolar formation.

The primary septa's surface is mainly covered by AEC1 and AEC2, which continue to differentiate and populate the distal tubules. The surfactant system of AEC2 maturates and lamellar bodies appear, and surfactant secretion is detected [25]. With the development and maturation of the surfactant system during the saccular phase, the chances of survival to early premature infants' increase [78].

RA signaling pathway seems to play an important role in preparing the lungs for sacculation and, later, in preparing for alveolar formation. Throughout the saccular stage, expression levels of the RA receptor-alpha (RARα) transcript decrease, which seems to be essential for sacculation and differentiation of mature AEC1. RA receptor-beta (RARβ) expression increases significantly in the saccular phase, matching AEC1 and AEC2 induction, pointing to a plausible role in preparing the lungs for alveolarization [79]. Similarly, loss of WNT signaling has been proven to be required to facilitate the transition from canalicular to saccular phase and allow air sac formation in the canalicular-saccular stages [80]. Interestingly, activation of WNT signaling results in the expansion of AEC2, whereas its inhibition constrains AEC2 development and shunts alveolar epithelial development toward the AEC1 cell lineage. These findings revealed that a wave of WNT-dependent AEC2 expansion is required for lung alveologenesis and maturation [81]. Moreover, studies from YAP/TAZ loss-of-function mouse mutants have shown that HIPPO signaling pathway plays a key role in promoting AEC1 fate [82]. miR-26a-1/miR-26a-2 knockout mice exhibit alterations in the morphology of distal epithelial cells, and display an increase in AEC2 cell number in the saccular stage with a concomitant increase in surfactant production; this study points to a role of miR-26a in lung maturation [83]. miR-127 expression levels are highest during the saccular/alveolar stage, and its spatial distribution shifts from mesenchymal to epithelial cells, suggesting a role in the cellular reorganization and differentiation of alveolar epithelial cells [68]. During sacculation, miR-17-92 should be repressed by HDAC3 to allow proper TGF-β signaling crucial for AEC1 remodeling [84]. Figure 4 displays the main signaling events in this phase.
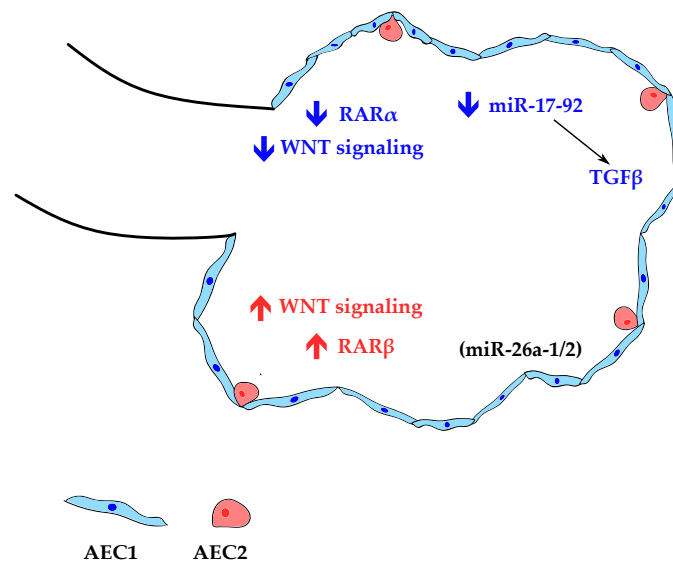
Figure 4 - Simplified scheme of the signaling pathways involved in alveolar epithelial cell type 1 (AEC1) and type 2 (AEC2) differentiation during the saccular stage. Blue label: AEC1 differentiation; red label: AEC2 differentiation. (miR), present in the lung compartment.

ALVEOLAR STAGE

The final alveolar stage refers to the process of alveoli formation (alveologenesis, also known as alveolization) that gives rise to the functional units for gas exchange. The timing of alveolar development varies among species. In humans, some alveoli are already formed before birth, and this process continues postnatally until young adulthood, whereas in mice, it is mainly a postnatal process. Alveologenesis can be divided into classical (or bulk) alveolarization (week 36 of gestation~3 years), continued alveolarization (birth-young adulthood), and microvascular maturation (week 36 of gestation—young adulthood) [25].

During classical alveolization, new secondary septa, risen from the pre-existing septa, grow from the saccular walls to subdivide the distal saccules into smaller units, the alveoli, broadening the surface area for gas exchange [28]. Like the primary septa, the secondary septa initially display a double capillary network [85]. Endothelial cells, myofibroblasts progenitors, fibroblasts, and lipofibroblasts cover the secondary septa, and matrix elastic fibers are deposited at the tip of the crests [85,86].

Classic alveolarization starts rather rapidly, but as it switches to continued alveolarization, the rate of increase in the number of alveoli declines [87,88]. Moreover, throughout postnatal lung development, the size and surface area of alveoli remain singularly stable in mice and humans. Simultaneously, microvascular maturation occurs, and the double-layered capillary network observed in

the immature primary and secondary septa fuse into a more efficient single-layered one in a thin septum [25]. This process involves multi-focal fusing of capillary segments and preferential growth of the mature single-layer capillary network [85]. Since it is now widely recognized that alveolarization continues until young adulthood, the timing of microvascular maturation was re-examined. Based on stereological estimations performed during rat lung development, microvascular maturation occurs in parallel to alveolarization and continues as long as new septa or alveoli are formed [25]. Once the alveolus has matured, every AEC1 has become in close contact with the endothelium. Reciprocal crosstalk between the airway epithelium and the vascular endothelium has been investigated in mice and found to be crucial for the prosperous development of one another. In pericytes, which are mesenchymal cells that strongly interact with endothelial and epithelial cells, mechanosensitive YAP1/TAZ signaling is stimulated to release hepatocyte growth factor (HGF), which is important for effective secondary septation [89]. In addition, the respiratory epithelium is a source of alveolar epithelium-derived VEGF-A that promotes vascularization [90].

Alveologenesis involves extensive cellular and tissue remodeling that culminates in the establishment of a large gas exchange surface area. Remodeling processes include the final specification and maturation of AEC2, surfactant synthesis, AEC1 flattening, and mesenchymal differentiation. Several signaling events are associated with the processes of secondary septation and alveolarization. For instance, platelet-derived growth factor A chain (PDGF-A) and its receptor (PDGFRα/β) have been shown to play key roles in myofibroblast differentiation and production of elastin [91]. In PDGF-A deficient mice, alveolarization failed to occur and exhibited reduced elastic fibers deposition, showing that the appearance of elastin and alveolar crests are closely linked [92]. Bundles of elastin laid down by myofibroblasts restrain the differentiating alveolar cells that are expanding into sacculi as development proceeds. This remodeling process is driven by mesenchymal cells, such as the alveolar myofibroblasts (MYF), which are stimulated by PDGF-A and SHH. Furthermore, the contractibility of the MYFs physically shapes the alveolus. Additionally, WNT-responsive AEC2 receives WNT ligands from the mesenchymal cells and proliferate during this time, increasing surfactant production, which is crucial for the shift to air breathing [81].

Ephrin-B2 has been shown to play an important role in endothelial cells. Loss of ephrin-B2 signaling impairs the normal development of secondary septa and disrupts the deposition of several matrix proteins [93]. Additionally, the TGF superfamily of transforming growth factors has received great attention as a mediator of normal and aberrant lung alveolarization [94,95]. BMP, the alternative branch of the TGF-β superfamily, is also implicated in postnatal lung maturation, particularly surfactant

production in neonates during respiratory adaptation to the extrauterine environment [96]. Furthermore, evidence from *fgfr3*/*fgfr4* double null mice points to a critical role for FGF signaling in controlling the alveolarization process since these animals fail to undergo secondary septation [97]. Moreover, these animals did not present the typical downregulation of elastin production that occurs at the end of this process. Finally, the retinoids have been recognized as alveolar morphogens, especially RA, which is crucial for alveolar formation [85,86]. Both increased and decreased RA signaling impair alveolar development. Several studies have demonstrated an association between vitamin A deficiency and major histological alterations, including thinner alveolar walls, airspace enlargement, and an increase in alveolar breaks [98]. On the other hand, increased epithelial RA signaling by transgenic expression of a dominant active RARα resulted in lung immaturity and a blockage in distal epithelial maturation, preventing the appearance of AEC1 cells [79]. Despite all evidence, the precise mechanism by which RA functions to regulate alveolarization is not entirely understood. Notwithstanding, the paracrine regulation of lung myofibroblast proliferation and elastin synthesis by RA is dependent on the interaction with FGF signaling, specifically FGF18 [99]. RA also acts in an autocrine manner to regulate proliferation and tube formation in endothelial cells [100]. The main interactions eliciting alveologenesis are displayed in Figure 5.
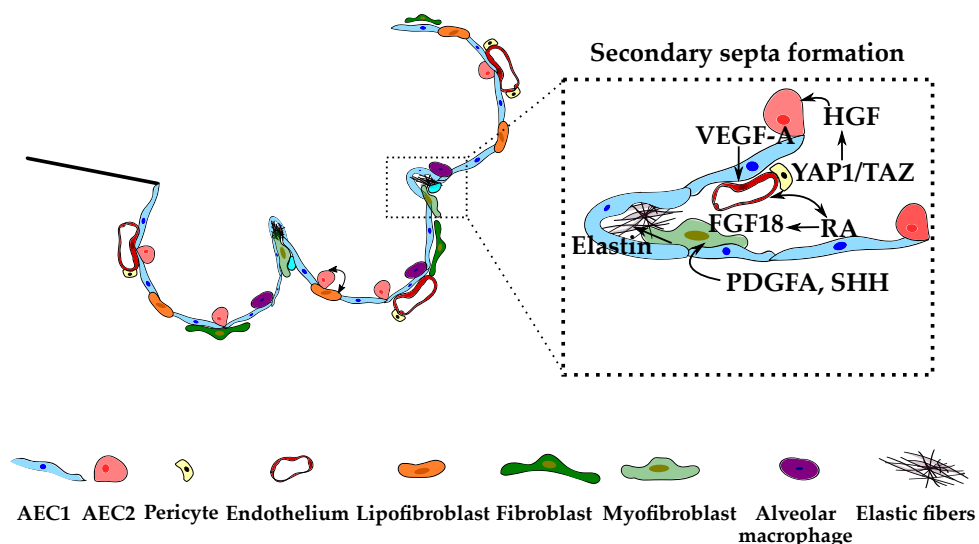
Figure 5 - Schematic representation of the signaling events occurring during alveologenesis, particularly secondary septa formation. Left image: alveolar niche. Right image: magnification of the secondary septa.

Finally, it has been demonstrated that targeting miR-34a partially improves alveologenesis in the hyperoxia-induced alveolar impairment mice model [101]. miR-29b supplementation improves

alveolarization in mice that were exposed to neonatal hyperoxia and maternal inflammation [102]. miR-876-3p gain of function improved alveolar structures in the bronchopulmonary dysplasia mice model [103]. Mice miR-421 inhibition improves bronchopulmonary dysplasia condition by targeting *fgf10* [104].

CONGENITAL LUNG MALFORMATIONS

Congenital lung malformations arise during development and include numerous anatomical anomalies of the lung and respiratory tree. They are usually detected prenatally by ultrasonography and comprise congenital pulmonary airway malformation (CPAM), bronchopulmonary sequestration (BPS), bronchogenic cysts (BC), and more rarely bronchial atresia, congenital lobar emphysema (CLE), and congenital tracheal obstruction. This section focuses on the molecular and genetic determinants of the most frequent anomalies: CPAM, BPS, and BC. Congenital diaphragmatic hernia (CDH) is not usually included in this group; however, since the lung is also highly affected in this condition, we have also incorporated evidence related to lung hypoplasia.

CONGENITAL PULMONARY AIRWAY MALFORMATION

Congenital Pulmonary Airway Malformation (CPAM), previously known as Congenital Cystic Adenomatoid Malformation (CCAM), is a rare but clinically significant developmental disorder. CPAMs are the most common congenital lung abnormalities, with an estimated incidence between 1 in 25,000–35,000 live births [105]. However, recent data and reports from the European Surveillance of Congenital Anomalies (EUROCAT) suggest a much higher prevalence of this disorder [106,107]. CPAMs are associated with significant infant morbidity and mortality due to associated complications such as lung hypoplasia, respiratory distress, and fetal hydrops [108,109].

CPAM is characterized by dilation of the airways and consequent cystic lesions within the lung parenchyma; it displays a disorganized spatial arrangement of tissues where multicystic masses replace the normal lung and are connected to the tracheal-bronchial system. Most of the cases involve a single pulmonary lobe, and bilateral lesions are uncommon. Stocker's classification subdivides CPAM into five types based on clinical, macroscopic, and microscopic criteria [110,111]. CPAM type 1 is the more frequent cystic lesion (~60% frequency) and comprises multiple large cysts (2–10 cm) or a single dominant cyst. In this case, cysts are lined by ciliated pseudostratified columnar epithelium, and the walls are composed of fibromuscular connective tissue with cartilage presence, in some cases. CPAM type 2 lesion (~20% frequency) consists of smaller cysts (0.5–2 cm) with a sponge-like appearance. Cystic

structures are lined by ciliated cuboidal or columnar epithelium, and walls are formed by a small portion of fibromuscular connective tissue. CPAM type 3 (~10% frequency) is characterized by multiple microscopic cysts (0.5 cm) with an adenomatoid appearance, resembling a bronchiolar structure. The more recently added subtypes are CPAM type 0 and type 4. CPAM type 0 (~2% frequency), also known as acinar dysplasia, consists of solid lesions with tracheal or bronchial-like structures composed of cartilage and smooth muscle. Lastly, CPAM type 4 (~10% frequency) or distal acinar-alveolar malformation consists of varying-sized cysts lined by type 1 and type 2 alveolar cells. All five CPAM subtypes originate from different locations of the pulmonary airway structure, from proximal tracheobronchial (type 0) to bronchial/bronchiolar/alveolar (type 1, 2, 3), to distal acinar (type 4) [109,110,112].

To perform an antenatal practical evaluation of CPAMs, Adzick's classification system based on gross anatomy and sonographic appearance is widely accepted. This classification has a relevant degree of prognosis and distinguishes between microcystic and macrocystic lesions [113]. Macrocystic lesions are composed of a single or several large cysts (≥ 0.5 cm) and appear as fluid-filled structures in the ultrasound. On the other hand, microcystic lesions are smaller (≤ 0.5 cm), solid, and bulky. While microcystic lesions are associated with a poor prognosis due to associations with hydrops, macrocystic lesions usually have a more favorable prognosis [113]. Nonetheless, several other classification systems have been proposed throughout the years [114].

The pathogenesis of CPAM remains uncertain, although it is believed that defective airway proximo-distal patterning and abnormal lung branching are associated with pulmonary cysts formation [108,114]. Some authors consider CPAM a hamartomatous abnormality, while others hypothesize that CPAM is caused by a focal arrest of lung development during different stages of branching morphogenesis. Numerous molecular mechanisms have been explored as potential contributors to CPAM etiology [112,114,115]. For instance, altered cellular processes such as increased cell proliferation and decreased apoptosis are typically associated with CPAM lesions [116]. The protein levels of cell adhesion molecules such as Integrin and E-cadherin are altered in CPAMs, suggesting uncharacteristic cytoplasmic signaling [117]. Platelet-derived growth factor (PDGF-BB) has maximal activity in the canalicular phase, stimulating lung growth by increasing proliferation but later, in the saccular stage, PDGF-BB action decreases. *In utero* resected CPAM lesions with rapid growth and associated hydrops show high PDGF-BB mRNA and protein expression levels. Moreover, PDGF-BB has a high and specific expression in the mesenchymal compartment of epithelial-lined cysts [118]. Glial Cell-Derived Neurotrophic Factor (GDNF) is expressed in the epithelial and endothelial compartments during lung organogenesis but is absent

postnatally. Conversely, in postnatal resected CPAMs, GDNF is highly expressed in the epithelium suggesting a dysregulation of the GDNF signaling pathway [119]. Decreased mRNA and protein levels of Fatty Acid-binding Protein-7 (FABP-7) are observed in CPAM specimens compared to normal fetal lungs, suggesting a potential decrease in glucocorticoid response in CPAM lesions [120]. In addition, Clara Cell marker 10 (CC10) overexpression is observed in CPAM cysts [115]. Also, KRAS signaling and PI3K-AKT-mTOR pathway may play a role in the pathogenesis of CPAM lesions [121]. Increased protein expression of Vascular Endothelial Growth Factor Receptor 2 (VEGFR2) is observed in postnatal CPAM, compared to normal lung, pointing to a role for the VEGF system in these congenital lesions [122].

An imbalance of early developmental markers is also observed in CPAMs. HOXB5 transcription factor is highly expressed during the pseudoglandular period. Nonetheless, the protein expression levels decrease in the canalicular phase and, in the alveolar phase, expression is negligible [42,53]. In CPAM lesions, HOXB5 protein expression levels are increased and present in the mesenchyme adjacent to abnormal branched airways, resembling a phenotype of earlier developmental stages [123]. Likewise, TTF1 is also crucial in regulating early lung development. In CPAM lesions, TTF1 presents differential expression patterns. In CPAM types 1 and 2 TTF1 expression pattern resembles typical pseudoglandular stage lungs. On the other hand, CPAM type 4 lesion presents TTF1 spatial distribution comparable to the canalicular stage [124]. Another study detected increased *hoxb5*, *ttf1*, and *fgf9* and decreased *fgf7* expression levels in fetal CPAM lesions, but no differences were noticed for *fgf10* and *fgfr2* in both fetal and postnatal CPAM lesions [125].

FGF10 is a mesenchymal growth factor critical for the epithelial-mesenchymal interactions that occur during lung branching. Rat fetal lung localized overexpression of *fgf10* at distinct developmental stages induces CPAM-like lesions. Depending on the localization/stage, *fgf10* overexpression induces macrocystic and microcystic malformations highly similar to those observed in humans [126]. Heterotopic overexpression of *fgf7* and *fgf10* and orthotopic expression of *fgf9* in transgenic mice disrupted pulmonary morphogenesis, pointing towards a role in cysts formation [127–129]. Moreover, mesenchyme-free epithelial explant cultures with FGF7 supplementation promoted epithelial proliferation, leading to the formation of cyst-like structures [130]. In addition, mouse microRNA-processing enzyme DICER mutant lungs result in upregulation of mesenchymal *fgf10* expression and, consequently, lung branching arrest and large epithelial pouches (cystic-like) [131]. This mechanism may involve intermediary *shh* downregulation [132,133]. Yin Yang 1 (YY1) transcription factor lung epithelial mutations cause abrogated mouse lung branching and airway dilation comparable to human CPAMs. This phenotype can be justified by reduced *shh* expression and subsequent upregulation of mesenchymal

fgf10 in an YY1-SHH-FGF10 molecular axis [132,133]. Epithelial cell-specific deletion of small GTPase *cdc42* in fetal mice disrupts epithelial cell polarity, proliferation, and mitotic spindle orientation, resulting in dilated respiratory tubules. This phenotype was accompanied by broader *fgf10* mesenchymal expression and decreased *shh* and *ptc1* (Cell Surface Transmembrane PATCHED 1) [134]. Combined deletion of *foxa1* and *foxa2* transcription factors disrupts pulmonary branching after E12.5 and result in the formation of large cysts at E15.5 and afterward. This morphological phenotype was associated with decreased *shh* expression [24]. Loss of WNT signaling receptor Frizzled 2 (*fzd2*) in the mouse lung epithelium causes large cysts formation in the distal region of the lung. Moreover, cysts formation was associated with decreased epithelial RhoA (Transforming Protein RhoA) signaling and no impact on WNT/β-Catenin signaling. Though, increased *fgf10* expression and decreased *fgfr2* and *shh* were observed [135]. Combined mutations of Histone Deacetylases *hdac1* and *hdac2* in the developing lung epithelium resulted in defects in branching morphogenesis and cysts formation in mouse E12.5 lungs [136]. E18.5 mouse lungs with epithelial *bmpr1a* (Bone Morphogenetic Protein Receptor Type 1A) deletion develop dramatic defects, with lungs containing large-fluid spaces [137]. Similar phenotypes occur under mouse conditional deletion of the proto-oncogene *mycn* [138]. Conditional mutation of the HIPPO pathway effector *yap* also results in dilated cyst-like structures [59]. *sox2* gene has a critical role during lung branching morphogenesis. *sox2* is expressed in non-branching regions and absent from branching sites. Overexpression of SOX2 in mouse lung epithelium disrupts branching morphogenesis and results in cystic-like structures. This data suggests that forced proximal epithelial differentiation leads to the CPAM phenotype [55]. Modulating the timing of ectopic *sox2* expression of branching regions results in cystic lesions that resemble the spectrum of human CPAMs [139]. Embryonic airway epithelial markers SOX2 and TTF1 are also present in adult human CPAMs, resembling the epithelial expression of the developing lung. Additionally, the Retinoic Acid signaling component Retinal Dehydrogenase 1 (RALDH1) shows weak expression in adult CPAM lesions [140]. In mouse epithelial-specific studies, both gain and loss of function of *sox9* gene resulted in cystic-like structures at distal epithelial branch tips [54]. Transgenic Notch signaling misexpression in lung mice prevents the differentiation of alveolar cell types and results in distal abnormal cysts, which express typical proximal markers. Such data suggests defective proximal-distal patterning [141]. While many studies focus on the epithelial compartment, recent data revealed that CPAM lesions also impact the adjacent mesenchymal tissues with alterations in airway smooth muscle cells and extracellular protein products such as elastin [142]. Although significant advances have been made in understanding the molecular basis of CPAM, the pathogenesis of this

congenital defect remains quite unknown. Still, CPAM is considered a unique model to study the molecular pathogenesis of isolated structural birth defects [121].

Considerable progress has been made in the diagnosis and treatment of CPAM lesions. However, the management of CPAM is still a matter of debate. Prenatal diagnosis of CPAM is crucial for the supervision of patients in the prenatal and postnatal periods. Most abnormal lung lesions are detected as early as the 20th week of gestation. Fetal ultrasonography is usually used to detect lesions' growth and potential complications and allows the calculation of the CPAM volume ratio (CVR), a value used to predict the prenatal course. When ultrasound is unreliable or inconclusive, evaluation is performed by Magnetic Resonance Imaging (MRI). Frequently, CPAMs tend to increase in size until the 28th gestational week, reach a plateau, and then start to regress. Fetal intervention is necessary when there is a persistent mediastinal shift and/or hydrops develops. CPAM prenatal interventions include systemic corticosteroid therapy, thoracoamniotic shunts or single-needle thoracentesis, and fetal lobectomy by minimally invasive procedures or open surgery [108,114,143,144]. Most babies require respiratory support at birth, and postnatal examinations combine several imaging methods such as Computed Tomography (CT) and X-ray. The exact optimal time for surgery is still inconclusive, but early interventions are recommended in symptomatic offspring. Neonatal resection is recommended for symptomatic patients, while asymptomatic resection remains controversial. There are three general indications to operate in asymptomatic cases: risk of malignancy, risk of complications (such as the risk of infection and pneumothorax), and potential for compensatory lung growth with earlier resection. The optimal operative management methods use minimally invasive approaches, with thoracoscopic techniques adopted over traditional thoracotomy [108,143–145]. According to the existing data, no apparent decrease in lung function is observed after surgery in the short term. As for the long term, children who undergo surgery display normal exercise tolerance and similar quality of life compared to otherwise healthy children [108].

BRONCHOPULMONARY SEQUESTRATION

Bronchopulmonary sequestration (BPS) is a rare congenital malformation of the lower respiratory tract characterized by a non-functioning mass of lung tissue with an anomalous arterial supply from systemic circulation (usually the aorta) not involved in lung oxygenation [146]. In this disorder, embryonic pulmonary tissue detaches from the tracheobronchial tree and then degenerates into a cyst alongside the normal developing lung. Concurrently, an abnormal connection between this cystic structure and systemic circulation occurs [147]. BPS is classified as intralobar (ILS) or extralobar (ELS), depending on their location in the lung [148]. ILS is located inside a normal pulmonary lobe and shares a common pleura.

In opposition, ELS is separated by the visceral pleura and forms a separate lobe [149]. Moreover, ELS is often linked with other congenital malformations, including congenital diaphragmatic hernia (CDH), congenital bronchopulmonary foregut malformations, CPAM, congenital heart disease, pulmonary hypoplasia, vertebral anomalies, and colonic duplication [148].

Bronchopulmonary sequestration accounts for 1.1% to 1.8% of all congenital bronchopulmonary anomalies. Intralobar cysts are more common, predominantly on the left lower lobe, and are frequently diagnosed in adolescent or adult patients; failure of earlier diagnosis can lead to repeated pneumonia and hemoptysis [150–153]. Conversely, ELS is a disease confined to neonates because of the high frequency of concomitant congenital abnormalities [154,155]. Pulmonary sequestration is not believed to be familial; however, some rare cases point to the possibility of a genetic predisposition for this condition [156,157].

Human studies have established that both types of BPS are commonly associated with CPAM [158–161]. The aberrant features of BPS and CPAM lesions are thought to be due to alterations in cell adhesion mechanisms that lead to atypical cell migration and proliferation during early lung branching morphogenesis. In fact, altered $\alpha 2\beta 1$-integrin signaling triggers alterations in cell-cell adhesion and, consequently, changes in epithelial cell migration and cell proliferation [117]. In addition, $\beta 1$-integrin signaling is essential for the migration of epithelial cells during lung development [162]. It has been demonstrated that abnormal Hoxb5 regulation triggers alterations in branching, such as the formation and persistence of immature and dysfunctional tissue, and is associated with BPS [123,163]. Additionally, in BPS, there is a decrease in $\alpha 2$-integrin protein levels, which is consistent with HOXB5 downregulation and its well-known role as a regulator of integrins and E-cadherins [164].

In the past, BPS malformations were thought to be rare and were mainly seen in autopsy cases, associated with other developmental abnormalities such as CDH, hydrops, and polyhydramnios. Nowadays, BPS is identified on prenatal ultrasound, and fetus outcome depends on the location of the lesion. Lesions located below the diaphragm usually have a more favorable prognosis, while intrathoracic lesions are commonly correlated with poor prognostic due to associations to hydrothorax, which can lead to fetal hydrops, polyhydramnios, and fetal death. In this case, a thoracoamniotic shunting may be required [165]. Postnatal complications, such as respiratory distress, infection, intrathoracic bleeding, hemoptysis, cardiac failure, and the potential risk of malignancy require early surgical excision.

BRONCHOGENIC CYST

Bronchogenic cyst (BC) is a developmental anomaly that results from abnormal budding of the primitive foregut. BCs are isolated choristomas characterized by closed respiratory epithelium-lined sacs with walls composed of cartilage. Other bronchial structures can also be found in BCs, such as smooth muscle and mucous glands. BC lesions are typically unilocular and fluid or mucus-filled. Though they can locate anywhere along the foregut, they are frequently localized in the mediastinum, adjacent to the carina region. BCs can also arise in the lung parenchyma, but no communication occurs with the airways [109,143,166].

The molecular mechanisms underlying BCs are still unknown. However, it is believed that abnormal growth of the upper gastrointestinal and respiratory tracts contributes to this condition. Moreover, BCs are not typically associated with genetic or chromosomal differences [167].

Bronchogenic cysts rarely require prenatal intervention. However, occasionally, they become large and cause complications, such as external compression and resulting hydrops. Prenatal interventions to remove BC lesions include thoracentesis or thoracoamniotic shunts to relieve fluid accumulation; resection is only necessary for rare complications. Nonetheless, removing BCs in the postnatal period is preferred considering the high risk of infection associated with prenatal procedures. Still, BCs always need to be removed due to the risk of becoming malignant [109,143,166].

When asymptomatic and not detected by prenatal ultrasound, BC lesions are only detected postnatally due to an infection or mass-related symptoms (congenital lobar overinflation, dysphagia, hemothorax, respiratory distress, dyspnea, recurrent pneumonia, or hemorrhage). Correct diagnosis using X-ray, CT, and MRI and subsequent management are crucial since BCs can become malignant. Postnatal treatment consists of surgical enucleation or resection by lobectomy using Video-Assisted Thoracoscopic Surgery (VATS) whenever possible. Definite diagnosis is determined by histopathology, and recurrence is improbable after complete resection [109,143,166,168]. Children with bronchogenic cysts have normal lung function after lesions removal [167].

CONGENITAL DIAPHRAGMATIC HERNIA

Congenital Diaphragmatic Hernia (CDH) is a congenital condition, with a prevalence rate between 1 in 2500–3000 live births [169]. CDH is characterized by a defect in the diaphragm that leads to the protrusion of the abdominal content into the thoracic cavity, impacting lung growth and development [170]. Human diaphragm development starts approximately at the fourth week of gestation, and by week 12, it is already fully formed. Closure of the diaphragm occurs typically around the eighth week of

gestation, and sealing of the left side occurs one week later than the right side [171,172]. Based on the anatomical position of the defect, CDH can be classified into the posterolateral (Bochdalek hernia), anterior (Morgagni hernia), and central hernia [172,173]. In CDH, abnormal pulmonary development is characterized by decreased terminal branching leading to hypoplasia, reduced gas exchange area, thickened alveolar walls, and increased interstitial tissue. Concurrently, the pulmonary circulation is also profoundly affected, triggering persistent pulmonary hypertension, contributing to higher mortality and morbidity [174]. Consequently, babies with CDH often suffer from cardiorespiratory failure at birth [175].

The pathogenesis of CDH is still not fully understood. Chromosomal anomalies such as aneuploidies, structural rearrangements, copy number variants, single-gene mutations, and monogenic syndromes contribute to the heterogenic etiology of CDH [176,177]. Nonetheless, only 30% of the CDH cases have been associated with genetic factors and, for this reason, several animal models have been used to study this condition. Teratogenic and genetic rodent models have contributed to disentangling CDH pathophysiology and unravelling the molecular mechanisms underlying lung underdevelopment and diaphragmatic defect. On the other hand, large experimental animal models (sheep and rabbit) have been valuable to improve surgical approaches and prenatal therapies [174,178,179].

One of the most used teratogenic models is the mouse/rat nitrofen model. Nitrofen is an herbicide (considered a 2B class carcinogen) that disrupts critical pathways for diaphragm development, lung branching morphogenesis, and alveolar differentiation, mimicking human CDH defects [178,179]. Data obtained from the nitrofen model revealed that pulmonary hypoplasia could be settled without the diaphragmatic defect. These findings lead to the proposal of the dual-hit hypothesis, which explains lung hypoplasia in CDH as the result of two independent developmental insults: an early insult that occurs before diaphragmatic closure and a late insult that follows the appearance of the diaphragmatic defect and, consequently, herniation of abdominal organs into the thoracic cavity [180,181].

The molecular characterization of the nitrofen model revealed that nitrofen targets several steps/components of RA signaling. For instance, it inhibits retinal dehydrogenase 2 activity (RALDH2), a key enzyme in the RA synthetic pathway, and downregulates the retinol storage enzyme, lecithin:retinol acyltransferase (LRAT), and the RA-degrading enzyme CYP26. At the genomic level, it causes mutations in the STRA6 membrane receptor for serum retinol and deletions on the 15q chromosome, which contains the encoding gene for a cellular retinoic acid-binding protein (CRABP1). Conversely, antenatal administration of RA to the nitrofen model clearly reduced CDH incidence [182,183]. Furthermore, human studies detected low retinol levels in infants diagnosed with CDH compared to non-CDH babies

[184,185]. In summary, it seems that a disruption in the RA pathway could be responsible for the morphological changes seen in CDH [174,179,186–188].

As stated previously in this review, lung development requires a synchronized pool of several growth factors/signaling pathways to give rise to a fully functional organ. Alongside RA, other signaling pathways underlying early and late pulmonary epithelial differentiation and mesenchymal development, such as FGF, BMP, WNT, are downregulated in the nitrofen-induced CDH model, thus contributing to lung hypoplasia [186]. In some cases, these findings have been corroborated with human data from amniotic fluid [189] or lung tissue [190,191]. Additionally, transcription factors and ECM components also contribute to the etiology of diaphragmatic defects and associated lung abnormalities. For instance, GATA4, a retinoic acid-inducible transcription factor, is essential for diaphragm and lung organogenesis. Hence, the lack of GATA4 during mouse development causes CDH [192,193]. Concurrently, knockout mice for NR2F2 (formerly called COUP-TFII) and ZFPM2 (also known as FOG2), both modulators of RA transcriptional activity, exhibit diaphragmatic hernia and lung hypoplasia [194,195]. Ablation of several other RA-dependent transcription factors such as WT1, SOX7, GATA6, and MYRF leads to CDH development, causing different types of herniation and pulmonary underdevelopment [196–199]. GLI, KIF7, and PBX1 knockout mice have revealed a role for SHH signaling in CDH [200–202]. Knockout mice for SLIT3, ROBO1, GPC3, NDST1, FREM1, FRAS1, and FREM2 uncovered their function in different aspects of normal diaphragm development [174,179,203].

More recently, epigenetic alterations, particularly microRNAs, have been associated with CDH pathophysiology. Several miRNAs have been associated with different lung developmental stages [204]. In the CDH context, miR-200b is upregulated in both human and animal samples. Moreover, tracheal fluid from CDH survivor babies that underwent FETO (fetoscopic endoluminal tracheal occlusion) exhibited elevated levels of miR-200b when compared to non-survivors [205,206]. Furthermore, the same group demonstrated that miR-200b prenatal treatment reduces the incidence of CDH defects in the nitrofen model [207]. The authors suggest that this upsurge in miR-200b levels may result from compensatory mechanisms to promote lung maturation [208].

Despite the relatively low prevalence rate of this congenital condition, the mortality rate is considerably high. Long-term outcomes depend on the characteristics of the diaphragmatic defect [170,209], and CDH survivors have a high risk of long-term morbidities and a lower quality of life. CDH lesions can be identified by ultrasonography around the 22–24th week of gestation; prenatal MRI can also be performed to predict prenatal course [171]. Fetal interventions, such as FETO, have been associated with increased survival among some CDH-infants; however, studies are still ongoing to further determine

patient risk/benefit [209,210]. Postnatal surgical intervention to repair the diaphragmatic effect is required, and the surgical approach depends on the size/type of defect. However, babies born with CDH exhibit life-threatening pulmonary hypertension that needs to be resolved before surgery. Lung-protective ventilator strategies or "gentle ventilation", extracorporeal membrane oxygenation (ECMO), and cardiopulmonary pre-operative stabilization are strategies currently used to tackle hypertension and improve patient outcomes [211–213].

CONCLUDING REMARKS

During embryonic development, coordinated growth and differentiation are essential to the formation of fully functional organs. In the particular case of the lung, a continuous interplay between lung compartments is precisely regulated by distinct developmental pathways. Table 1 summarizes the key molecular signals involved in each stage of development.

A deeper understanding of the mechanisms controlling lung morphogenesis is crucial for managing congenital/neonatal respiratory diseases. Furthermore, it is highly relevant for developing new strategies to improve the regenerative response of the lung to injury. With this review, we aimed to describe the key signaling pathways underlying normal lung development. Additionally, we reviewed the current knowledge regarding the signaling events impaired in congenital lung lesions. Congenital lung lesions present several alterations in both the epithelial and mesenchymal compartments that, altogether, contribute to the abnormal lung phenotype. Table 2 summarizes the molecular players known to be altered in CPAM and CDH. Nonetheless, more studies are in demand to determine the etiology of these congenital conditions.

Table 1 - Summary of the molecular players and corresponding major events underlying normal lung development.

Stage	Major Events	Molecular Players	Expression Site	Function
Embryonic	Lung bud develops from the foregut; Tracheoesophageal septation	NKX2.1 (or TTF1)	Endoderm	Specification of respiratory progenitors Epithelial marker
		TBX4	Mesoderm	Induction of endodermal differentiation (*nkx2.1*-dependnent) & budding (*fgf10*-dependent)
		WNT2/2B	Mesoderm	Specification of NKX2.1 respiratory progenitors
		GATA4/6	Endoderm	Formation of primary lung structures Differentiation of visceral endoderm
		SHH/ GLI1-3	Endoderm/ Mesoderm	Embryonic foregut development
		FOXF1	Mesoderm	Lung & gastrointestinal morphogenesis Regulation of mesenchymal-epithelial interactions
		FOXA1/A2	Endoderm	Specification of foregut endoderm Branching morphogenesis
Pseudoglandular	Formation of bronchial buds; Branching morphogenesis; Formation of bronchial tree and blood vessels; Cellular differentiation (cartilage, smooth muscle)	FGF10/ FGFR2	Mesenchyme/ Epithelium	Lung bud outgrowth
		SPRY2	Distal epithelium	Negatively regulates FGF10 signaling Inhibits lung budding
		TGFβ	Mesenchyme/ Epithelium	Lung branching
		BMP4	Epithelium of distal tips	Negatively regulates FGF10 signaling Inhibits lung budding
		SHH	Epithelium	Branching morphogenesis
		RDH10	Lung buds	Lung bud outgrowth
		RALDH2	Mesothelial region	Lung growth and branching
		WNT7B	Distal epithelium	Branching morphogenesis
		WNT2A	Distal lung mesothelium	Mesenchymal cell proliferation
		WNT5A	Mesenchyme/ Epithelium	Tracheal development/ Distal lung morphogenesis
		β-Catenin	Airway epithelium	Branching morphogenesis Epithelial differentiation and proliferation
		HOXB5	Mesenchyme	Anterior-posterior patterning Directing epithelial morphogenesis
		SOX2	Proximal epithelium	Proximal-distal patterning
		SOX9	Distal epithelium	Proximal-distal patterning
		miR-17 miR-20a miR-106b	Epithelium	FGF10-mediated epithelial branching morphogenesis

		miR-200b	Epithelium & Mesenchyme	Distal airway branching
		miR-449a	Distal epithelium	Regulation of differentiation & proliferation
		miR-326	Mesenchyme	SHH signaling modulator
		miR-142-3p	Mesenchyme	Proliferation & differentiation of mesenchymal progenitors Control of WNT signaling
Canalicular	Formation of distal most airways; Alveolar cellular differentiation; Appearance of the first air-blood barrier; Surfactant production initiation	NOTCH		Determination of cellular fate Development of microvasculature network
		miR-449a	Distal epithelium	Regulation of differentiation & proliferation
Saccular	Formation of thin-walled terminal saccules (alveoli precursors); Maturation of vasculature and surfactant system	RARα	Epithelium	Sacculation & differentiation of mature AEC1
		RARβ	Epithelium	AEC1 & AEC2 induction
		miR-26a-1/ miR-26a-2	Alveolar epithelial cells	Pulmonary surfactant synthesis
		miR-17-92	Epithelium	AEC1 remodeling
Alveolar	Alveologenesis: establishment of secondary septa and alveoli formation; Microvascular maturation: single-layered capillary network formation	VEGF-A	Epithelium	Vascular development
		PDGF-A/ PDGFRα/β	Epithelium/ Mesenchyme	Myofibroblast differentiation Elastin production Secondary septation & alveolarization
		Ephrin-B2	Microvasculature	Secondary septation & alveolarization
		miR-34a		Impairs alveolarization
		miR-29b		Promotes alveolarization
		miR-876-3p		Promotes alveolarization
		miR-421	Alveolar epithelial cells	Disrupts alveolarization

Table 2 - Summary of the molecular players impaired in congenital lung diseases.

Congenital Lung Disease	Altered Epithelial Signaling/Expression	Altered Mesenchymal Signaling/Expression	References
	Integrin	Integrin	[117]
	E-cadherin	-	[117]
	-	PDGF-BB	[118]
	GDNF	-	[119]
	-	FABP-7	[120]
	CC10	-	[115]
	KRAS; PI3K-AKT-mTOR	-	[121]
	VEGFR2	-	[122]
	-	HOXB5	[123,125]
	TTF1/Nkx2.1	-	[124,125,140]
	fgf9	-	[125,129]
	-	fgf7	[125,127,130]
	-	fgf10	[126,128,131,132,134,135]
	fgfr2	-	[135]
CPAM	DICER	-	[131]
	yy1	-	[132,133]
	shh	-	[24,132,134]
	cdc42	-	[134]
	-	ptc1	[134]
	foxa1; foxa2	-	[24]
	fzd2	-	[135]
	RhoA	-	[135]
	hdac1; hdac2	-	[136]
	bmpr1a	-	[137]
	mycn	-	[138]
	Yap	-	[59]
	SOX2	-	[55,139,140]
	SOX9	-	[54]
	Notch	-	[141]
	-	Elastin	[142]
	-	RALDH2	[187]
	RAR	RAR	[186]
	-	STRA6	[174,187]
	Midkine	Midkine	[186]
	FGF signaling	-	-
	-	FGF10	[189]
	FGF2	FGF2	[186]
	-	FGF7	[189,190]
	FGF9	-	[186]
	-	FGF18	[191]
	FGFR2	FGFR2	[186]
	FGFR3	FGFR3	[186]
	BMP signaling	-	-
	BMP4	-	[186]
CDH	BMP7	-	[186]
	BMPR2	-	[186]
	WNT signaling	-	-
	-	WNT2	[186]
	WNT5A	WNT5A	[186]
	WNT7B	-	[186]
	-	GATA6	[198]
	-	GATA4	[192,193]
	-	NR2F2	[194]
	ZFPM2	-	[195]
	-	WT1	[196]
	-	MYRF	[199]
	-	GLI	[200]
	-	KIF7	[201]

-	PBX1	[202]
-	SLIT3	[174,179,203]
ROBO1	ROBO1	[174,179]
NDST1	-	[174,179]
FREM1	-	[174,179]
-	FRAS1	[174,179]
-	FREM2	[174]
miR-200b	miR-200b	[207]

REFERENCES

1. Danopoulos, S.; Shiosaki, J.; Al Alam, D. FGF Signaling in Lung Development and Disease: Human Versus Mouse. Front. genet. 2019, 10, 170, doi:10.3389/fgene.2019.00170.
2. Fernandes-Silva, H.; Araújo-Silva, H.; Correia-Pinto, J.; Moura, R.S. Retinoic Acid: A Key Regulator of Lung Development. Biomolecules 2020, 10, 152, doi:10.3390/biom10010152.
3. Fernandes-Silva, H.; Correia-Pinto, J.; Moura, R.S. Canonical Sonic Hedgehog Signaling in Early Lung Development. J. Dev. Biol. 2017, 5, 3, doi:10.3390/jdb5010003.
4. Pongracz, J.E.; Stockley, R.A. Wnt signalling in lung development and diseases. Respir. Res. 2006, 7, 15–15, doi:10.1186/1465-9921-7-15.
5. Bellusci, S.; Henderson, R.; Winnier, G.; Oikawa, T.; Hogan, B.L. Evidence from normal expression and targeted misexpression that bone morphogenetic protein (Bmp-4) plays a role in mouse embryonic lung morphogenesis. Development 1996, 122, 1693–1702, doi:10.1242/dev.122.6.1693.
6. Yeung, B.; Yu, J.; Yang, X. Roles of the Hippo pathway in lung development and tumorigenesis. Int. J. Cancer 2016, 138, 533–539, doi:10.1002/ijc.29457.
7. Cardoso, W.V. Molecular regulation of lung development. Annu. Rev. Physiol. 2001, 63, 471–494, doi:10.1146/annurev.physiol.63.1.471.
8. Burri, P.H. Fetal and postnatal development of the lung. Annu. Rev. Physiol. 1984, 46, 617–628, doi:10.1146/annurev.ph.46.030184.003153.
9. deMello, D.E.; Sawyer, D.; Galvin, N.; Reid, L.M. Early fetal development of lung vasculature. Am. J. Respir. Cell Mol. Biol. 1997, 16, 568–581, doi:10.1165/ajrcmb.16.5.9160839.
10. Minoo, P.; Su, G.; Drum, H.; Bringas, P.; Kimura, S. Defects in tracheoesophageal and lung morphogenesis in Nkx2.1(-/-) mouse embryos. Dev. Biol. 1999, 209, 60–71, doi:10.1006/dbio.1999.9234.
11. Kimura, S.; Hara, Y.; Pineau, T.; Fernandez-Salguero, P.; Fox, C.H.; Ward, J.M.; Gonzalez, F.J. The T/ebp null mouse: thyroid-specific enhancer-binding protein is essential for the organogenesis of the thyroid, lung, ventral forebrain, and pituitary. Genes Dev. 1996, 10, 60–69, doi:10.1101/gad.10.1.60.
12. Herriges, M.; Morrisey, E.E. Lung development: orchestrating the generation and regeneration of a complex organ. Development 2014, 141, 502–513, doi:10.1242/dev.098186.
13. Goss, A.M.; Tian, Y.; Tsukiyama, T.; Cohen, E.D.; Zhou, D.; Lu, M.M.; Yamaguchi, T.P.; Morrisey, E.E. Wnt2/2b and beta-catenin signaling are necessary and sufficient to specify lung progenitors in the foregut. Dev. Cell 2009, 17, 290–298, doi:10.1016/j.devcel.2009.06.005.
14. Harris-Johnson, K.S.; Domyan, E.T.; Vezina, C.M.; Sun, X. beta-Catenin promotes respiratory progenitor identity in mouse foregut. Proc. Natl. Acad. Sci. 2009, 106, 16287–16292, doi: 10.1073/pnas.0902274106.
15. Hrycaj, S.M.; Dye, B.R.; Baker, N.C.; Larsen, B.M.; Burke, A.C.; Spence, J.R.; Wellik, D.M. Hox5 Genes Regulate the Wnt2/2b-Bmp4-Signaling Axis during Lung Development. Cell Rep. 2015, 12, 903–912, doi:10.1016/j.celrep.2015.07.020.

16.   Domyan, E.T.; Ferretti, E.; Throckmorton, K.; Mishina, Y.; Nicolis, S.K.; Sun, X. Signaling through BMP receptors promotes respiratory identity in the foregut via repression of Sox2. Development 2011, 138, 971–981, doi:10.1242/dev.053694.

17.   Rankin, S.A.; Han, L.; McCracken, K.W.; Kenny, A.P.; Anglin, C.T.; Grigg, E.A.; Crawford, C.M.; Wells, J.M.; Shannon, J.M.; Zorn, A.M. A Retinoic Acid-Hedgehog Cascade Coordinates Mesoderm-Inducing Signals and Endoderm Competence during Lung Specification. Cell Rep. 2016, 16, 66–78, doi:10.1016/j.celrep.2016.05.060.

18.   Chen, F.; Desai, T.J.; Qian, J.; Niederreither, K.; Lü, J.; Cardoso, W.V. Inhibition of Tgfβ signaling by endogenous retinoic acid is essential for primary lung bud induction. Development 2007, 134, 2969–2979, doi:10.1242/dev.006221.

19.   Chen, F.; Cao, Y.; Qian, J.; Shao, F.; Niederreither, K.; Cardoso, W.V. A retinoic acid–dependent network in the foregut controls formation of the mouse lung primordium. J. Clin. Invest. 2010, 120, 2040–2048, doi:10.1172/JCI40253.

20.   Sakiyama, J.; Yamagishi, A.; Kuroiwa, A. Tbx4-Fgf10 system controls lung bud formation during chicken embryonic development. Development 2003, 130, 1225–1234, doi:10.1242/dev.00345.

21.   Naiche, L.A.; Papaioannou, V.E. Loss of Tbx4 blocks hindlimb development and affects vascularization and fusion of the allantois. Development 2003, 130, 2681–2693, doi:10.1242/dev.00504.

22.   Kuo, C.T.; Morrisey, E.E.; Anandappa, R.; Sigrist, K.; Lu, M.M.; Parmacek, M.S.; Soudais, C.; Leiden, J.M. GATA4 transcription factor is required for ventral morphogenesis and heart tube formation. Genes Dev. 1997, 11, 1048–1060, doi:10.1101/gad.11.8.1048.

23.   Yang, H.; Lu, M.M.; Zhang, L.; Whitsett, J.A.; Morrisey, E.E. GATA6 regulates differentiation of distal lung epithelium. Development 2002, 129, 2233–2246, doi:10.1242/dev.129.9.2233.

24.   Wan, H.; Dingle, S.; Xu, Y.; Besnard, V.; Kaestner, K.H.; Ang, S.L.; Wert, S.; Stahlman, M.T.; Whitsett, J.A. Compensatory roles of Foxa1 and Foxa2 during lung morphogenesis. J. Biol. Chem. 2005, 280, 13809–13816, doi:10.1074/jbc.M414122200.

25.   Schittny, J.C. Development of the lung. Cell Tissue Res. 2017, 367, 427–444, doi:10.1007/s00441-016-2545-0.

26.   Metzger, R.J.; Klein, O.D.; Martin, G.R.; Krasnow, M.A. The branching programme of mouse lung development. Nature 2008, 453, 745–750, doi:10.1038/nature07005.

27.   deMello, D.E.; Reid, L.M. Embryonic and Early Fetal Development of Human Lung Vasculature and Its Functional Implications. Pediatr. Dev. Pathol. 2000, 3, 439–449, doi:10.1007/s100240010090.

28.   Nikolić, M.Z.; Sun, D.; Rawlins, E.L. Human lung development: recent progress and new challenges. Development 2018, 145, doi:10.1242/dev.163485.

29.   Saito, A.; Horie, M.; Nagase, T. TGF-beta Signaling in Lung Health and Disease. Int. J. Mol. Sci. 2018, 19, doi:10.3390/ijms19082460.

30.   Sekine, K.; Ohuchi, H.; Fujiwara, M.; Yamasaki, M.; Yoshizawa, T.; Sato, T.; Yagishita, N.; Matsui, D.; Koga, Y.; Itoh, N. Fgf10 is essential for limb and lung formation. Nat. Genet. 1999, 21, 138–141, doi:10.1038/5096.

31.   Moura, R.S.; Coutinho-Borges, J.P.; Pacheco, A.P.; daMota, P.O.; Correia-Pinto, J. FGF Signaling Pathway in the Developing Chick Lung: Expression and Inhibition Studies. PLoS ONE 2011, 6, e17660, doi:10.1371/journal.pone.0017660.

32.   Bellusci, S.; Grindley, J.; Emoto, H.; Itoh, N.; Hogan, B.L. Fibroblast growth factor 10 (FGF10) and branching morphogenesis in the embryonic mouse lung. Development 1997, 124, 4867–4878, doi:10.1242/dev.124.23.4867.

33. Moura, R.S.; Silva-Gonçalves, C.; Vaz-Cunha, P.; Correia-Pinto, J. Expression analysis of Shh signaling members in early stages of chick lung development. Histochem. Cell Biol. 2016, 146, 457–466, doi:10.1007/s00418-016-1448-1.

34. Mailleux, A.A.; Tefft, D.; Ndiaye, D.; Itoh, N.; Thiery, J.P.; Warburton, D.; Bellusci, S. Evidence that SPROUTY2 functions as an inhibitor of mouse embryonic lung growth and morphogenesis. Mech. Dev. 2001, 102, 81–94, doi:10.1016/s0925-4773(01)00286-6.

35. Park W.Y.; Miranda, B.; Lebeche, D.; Hashimoto, G.; Cardoso, W.V. FGF-10 is a chemotactic factor for distal epithelial buds during lung development. Dev. Biol. 1998, 201, 125–134, doi:10.1006/dbio.1998.8994.

36. Land, S.C.; Scott, C.L.; Walker, D. mTOR signalling, embryogenesis and the control of lung development. Semin. Cell Dev. Biol. 2014, 36, 68–78, doi:10.1016/j.semcdb.2014.09.023.

37. Scott, C.L.; Walker, D.J.; Cwiklinski, E.; Tait, C.; Tee, A.R.; Land, S.C. Control of HIF-1{alpha} and vascular signaling in fetal lung involves cross talk between mTORC1 and the FGF-10/FGFR2b/Spry2 airway branching periodicity clock. Am. J. Physiol. Lung Cell Mol. Physiol. 2010, 299, L455–471, doi:10.1152/ajplung.00348.2009.

38. Walker, D.J.; Land, S.C. Regulation of vascular signalling by nuclear Sprouty2 in fetal lung epithelial cells: Implications for co-ordinated airway and vascular branching in lung development. Comp. Biochem. Physiol. B Biochem. Mol. Biol. 2018, 224, 105‑114, doi:10.1016/j.cbpb.2018.01.007.

39. Groenman, F.; Rutter, M.; Caniggia, I.; Tibboel, D.; Post, M. Hypoxia-inducible factors in the first trimester human lung. J. Histochem. Cytochem. 2007, 55, 355–363, doi:10.1369/jhc.6A7129.2006.

40. Malpel, S.; Mendelsohn, C.; Cardoso, W.V. Regulation of retinoic acid signaling during lung morphogenesis. Development 2000, 127, 3057–3067, doi:10.1242/dev.127.14.3057.

41. Chazaud, C.; Dolle, P.; Rossant, J.; Mollard, R. Retinoic acid signaling regulates murine bronchial tubule formation. Mech. Dev. 2003, 120, 691–700, doi:10.1016/s0925-4773(03)00048-0.

42. Fernandes-Silva, H.; Vaz-Cunha, P.; Barbosa, V.B.; Silva-Goncalves, C.; Correia-Pinto, J.; Moura, R.S. Retinoic acid regulates avian lung branching through a molecular network. Cell. Mol. Life Sci. 2017, 74, 4599–4619, doi:10.1007/s00018-017-2600-3.

43. Rhinn, M.; Schuhbaur, B.; Niederreither, K.; Dollé, P. Involvement of retinol dehydrogenase 10 in embryonic patterning and rescue of its loss of function by maternal retinaldehyde treatment. Proc. Natl. Acad. Sci. 2011, 108, 16687–16692, doi:10.1073/pnas.1103877108.

44. Wang, Z.; Dollé, P.; Cardoso, W.V.; Niederreither, K. Retinoic acid regulates morphogenesis and patterning of posterior foregut derivatives. Dev. Biol. 2006, 297, 433–445, doi:10.1016/j.ydbio.2006.05.019.

45. Aros, C.J.; Pantoja, C.J.; Gomperts, B.N. Wnt signaling in lung development, regeneration, and disease progression. Commun. Biol. 2021, 4, 601, doi:10.1038/s42003-021-02118-w.

46. Moura, R.S.; Carvalho-Correia, E.; daMota, P.; Correia-Pinto, J. Canonical Wnt Signaling Activity in Early Stages of Chick Lung Development. PLoS ONE 2014, 9, e112388, doi:10.1371/journal.pone.0112388.

47. Mucenski, M.L.; Wert, S.E.; Nation, J.M.; Loudy, D.E.; Huelsken, J.; Birchmeier, W.; Morrisey, E.E.; Whitsett, J.A. beta-Catenin is required for specification of proximal/distal cell fate during lung morphogenesis. J. Biol. Chem. 2003, 278, 40231–40238, doi:10.1074/jbc.M305892200.

48. De Langhe, S.P.; Sala, F.G.; Del Moral, P.M.; Fairbanks, T.J.; Yamada, K.M.; Warburton, D.; Burns, R.C.; Bellusci, S. Dickkopf-1 (DKK1) reveals that fibronectin is a major target of Wnt signaling in branching morphogenesis of the mouse embryonic lung. Dev. Biol. 2005, 277, 316–331, doi:10.1016/j.ydbio.2004.09.023.

49. Li, C.; Xiao, J.; Hormi, K.; Borok, Z.; Minoo, P. Wnt5a participates in distal lung morphogenesis. Dev. Biol. 2002, 248, 68–81, doi:10.1006/dbio.2002.0729.

50. Li, C.; Hu, L.; Xiao, J.; Chen, H.; Li, J.T.; Bellusci, S.; Delanghe, S.; Minoo, P. Wnt5a regulates Shh and Fgf10 signaling during lung development. Dev. Biol. 2005, 287, 86–97, doi:10.1016/j.ydbio.2005.08.035.

51. Shu, W.; Jiang, Y.Q.; Lu, M.M.; Morrisey, E.E. Wnt7b regulates mesenchymal proliferation and vascular development in the lung. Development 2002, 129, 4831–4842, doi:10.1242/dev.129.20.4831.

52. Rajagopal, J.; Carroll, T.J.; Guseh, J.S.; Bores, S.A.; Blank, L.J.; Anderson, W.J.; Yu, J.; Zhou, Q.; McMahon, A.P.; Melton, D.A. Wnt7b stimulates embryonic lung growth by coordinately increasing the replication of epithelium and mesenchyme. Development 2008, 135, 1625–1634, doi:10.1242/dev.015495.

53. Volpe, M.V.; Ramadurai, S.M.; Mujahid, S.; Vong, T.; Brandao, M.; Wang, K.T.; Pham, L.D.; Nielsen, H.C. Regulatory Interactions between Androgens, Hoxb5, and TGFβ Signaling in Murine Lung Development. Biomed Res. Int. 2013, 2013, 320249, doi:10.1155/2013/320249.

54. Rockich, B.E.; Hrycaj, S.M.; Shih, H.P.; Nagy, M.S.; Ferguson, M.A.; Kopp, J.L.; Sander, M.; Wellik, D.M.; Spence, J.R. Sox9 plays multiple roles in the lung epithelium during branching morphogenesis. Proc. Natl. Acad. Sci. 2013, 110, E4456–4464, doi:10.1073/pnas.1311847110.

55. Gontan, C.; de Munck, A.; Vermeij, M.; Grosveld, F.; Tibboel, D.; Rottier, R. Sox2 is important for two crucial processes in lung development: branching morphogenesis and epithelial cell differentiation. Dev. Biol. 2008, 317, 296–309, doi:10.1016/j.ydbio.2008.02.035.

56. Chang, D.R.; Martinez Alanis, D.; Miller, R.K.; Ji, H.; Akiyama, H.; McCrea, P.D.; Chen, J. Lung epithelial branching program antagonizes alveolar differentiation. Proc. Natl. Acad. Sci. 2013, 110, 18042–18051, doi:10.1073/pnas.1311760110.

57. Que, J.; Luo, X.; Schwartz, R.J.; Hogan, B.L.M. Multiple roles for Sox2 in the developing and adult mouse trachea. Development 2009, 136, 1899–1907, doi:10.1242/dev.034629.

58. Szymaniak, A.D.; Mahoney, J.E.; Cardoso, W.V.; Varelas, X. Crumbs3-Mediated Polarity Directs Airway Epithelial Cell Fate through the Hippo Pathway Effector Yap. Dev. Cell 2015, 34, 283–296, doi:10.1016/j.devcel.2015.06.020.

59. Mahoney, J.E.; Mori, M.; Szymaniak, A.D.; Varelas, X.; Cardoso, W.V. The hippo pathway effector Yap controls patterning and differentiation of airway epithelial progenitors. Dev. Cell 2014, 30, 137–150, doi:10.1016/j.devcel.2014.06.003.

60. Volckaert, T.; Yuan, T.; Yuan, J.; Boateng, E.; Hopkins, S.; Zhang, J.S.; Thannickal, V.J.; Fassler, R.; De Langhe, S.P. Hippo signaling promotes lung epithelial lineage commitment by curbing Fgf10 and beta-catenin signaling. Development 2019, 146, doi:10.1242/dev.166454.

61. Jiang, Z.; Cushing, L.; Ai, X.; Lu, J. miR-326 is downstream of Sonic hedgehog signaling and regulates the expression of Gli2 and smoothened. Am. J. Respir. Cell Mol. Biol. 2014, 51, 273–283, doi:10.1165/rcmb.2013-0127OC.

62. Carraro, G.; Shrestha, A.; Rostkovius, J.; Contreras, A.; Chao, C.M.; El Agha, E.; Mackenzie, B.; Dilai, S.; Guidolin, D.; Taketo, M.M.; et al. miR-142-3p balances proliferation and differentiation of mesenchymal cells during lung development. Development 2014, 141, 1272–1281, doi:10.1242/dev.105908.

63. Carraro, G.; El-Hashash, A.; Guidolin, D.; Tiozzo, C.; Turcatel, G.; Young, B.M.; De Langhe, S.P.; Bellusci, S.; Shi, W.; Parnigotto, P.P.; et al. miR-17 family of microRNAs controls FGF10-mediated embryonic lung epithelial branching morphogenesis through MAPK14 and STAT3 regulation of E-Cadherin distribution. Dev. Biol. 2009, 333, 238–250, doi:10.1016/j.ydbio.2009.06.020.

64. Lu, Y.; Thomson, J.M.; Wong, H.Y.; Hammond, S.M.; Hogan, B.L. Transgenic over-expression of the microRNA miR-17-92 cluster promotes proliferation and inhibits differentiation of lung epithelial progenitor cells. Dev. Biol. 2007, 310, 442–453, doi:10.1016/j.ydbio.2007.08.007.

65. Ventura, A.; Young, A.G.; Winslow, M.M.; Lintault, L.; Meissner, A.; Erkeland, S.J.; Newman, J.; Bronson, R.T.; Crowley, D.; Stone, J.R.; et al. Targeted deletion reveals essential and overlapping functions of the miR-17 through 92 family of miRNA clusters. Cell 2008, 132, 875–886, doi:10.1016/j.cell.2008.02.019.

66. Khoshgoo, N.; Visser, R.; Falk, L.; Day, C.A.; Ameis, D.; Iwasiow, B.M.; Zhu, F.; Ozturk, A.; Basu, S.; Pind, M.; et al. MicroRNA-200b regulates distal airway development by maintaining epithelial integrity. Sci. Rep. 2017, 7, 6382, doi:10.1038/s41598-017-05412-y.

67. Sanford, E.L.; Choy, K.W.; Donahoe, P.K.; Tracy, A.A.; Hila, R.; Loscertales, M.; Longoni, M. MiR-449a Affects Epithelial Proliferation during the Pseudoglandular and Canalicular Phases of Avian and Mammal Lung Development. PLoS ONE 2016, 11, e0149425, doi:10.1371/journal.pone.0149425.

68. Bhaskaran, M.; Wang, Y.; Zhang, H.; Weng, T.; Baviskar, P.; Guo, Y.; Gou, D.; Liu, L. MicroRNA-127 modulates fetal lung development. Physiol. Genomics 2009, 37, 268–278, doi:10.1152/physiolgenomics.90268.2008.

69. Moura, R.S.; Vaz-Cunha, P.; Silva-Goncalves, C.; Correia-Pinto, J. Characterization of miRNA processing machinery in the embryonic chick lung. Cell Tissue Res. 2015, 362, 569–575, doi:10.1007/s00441-015-2240-6.

70. Nelson, C.M.; Gleghorn, J.P.; Pang, M.-F.; Jaslove, J.M.; Goodwin, K.; Varner, V.D.; Miller, E.; Radisky, D.C.; Stone, H.A. Microfluidic chest cavities reveal that transmural pressure controls the rate of lung development. Development 2017, 144, 4328–4335, doi:10.1242/dev.154823.

71. Lin, C.; Yao, E.; Zhang, K.; Jiang, X.; Croll, S.; Thompson-Peer, K.; Chuang, P.-T. YAP is essential for mechanical force production and epithelial cell proliferation during lung branching morphogenesis. eLife 2017, 6, e21130, doi:10.7554/eLife.21130.

72. Fernandes-Silva, H.; Alves, M.G.; Araújo-Silva, H.; Silva, A.M.; Correia-Pinto, J.; Oliveira, P.F.; Moura, R.S. Lung branching morphogenesis is accompanied by temporal metabolic changes towards a glycolytic preference. Cell Biosci. 2021, 11, 134, doi:10.1186/s13578-021-00654-w.

73. Zhou, Y.; Horowitz, J.C.; Naba, A.; Ambalavanan, N.; Atabai, K.; Balestrini, J.; Bitterman, P.B.; Corley, R.A.; Ding, B.-S.; Engler, A.J.; et al. Extracellular matrix in lung development, homeostasis and disease. Matrix Biol. 2018, 73, 77–104, doi:10.1016/j.matbio.2018.03.005.

74. McGowan, S.E. Extracellular matrix and the regulation of lung development and repair1. FASEB J. 1992, 6, 2895–2904, doi:10.1096/fasebj.6.11.1644255.

75. Tsao, P.-N.; Vasconcelos, M.; Izvolsky, K.I.; Qian, J.; Lu, J.; Cardoso, W.V. Notch signaling controls the balance of ciliated and secretory cell fates in developing airways. Development 2009, 136, 2297–2307, doi:10.1242/dev.034884.

76. Volckaert, T.; De Langhe, S.P. Wnt and FGF mediated epithelial-mesenchymal crosstalk during lung development. Dev. Dyn. 2015, 244, 342–366, doi:10.1002/dvdy.24234.

77. Vu, T.H.; Alemayehu, Y.; Werb, Z. New insights into saccular development and vascular formation in lung allografts under the renal capsule. Mech. Dev. 2003, 120, 305–313, doi:10.1016/S0925-4773(02)00451-3.

78. Madurga, A.; Mižíková, I.; Ruiz-Camp, J.; Morty, R.E. Recent advances in late lung development and the pathogenesis of bronchopulmonary dysplasia. Am. J. Physiol. Lung Cell Mol. Physiol. 2013, 305, L893–L905, doi:10.1152/ajplung.00267.2013.

79. Wongtrakool, C.; Malpel, S.; Gorenstein, J.; Sedita, J.; Ramirez, M.I.; Underhill, T.M.; Cardoso, W.V. Down-regulation of Retinoic Acid Receptor α Signaling Is Required for Sacculation and Type

I Cell Formation in the Developing Lung. J. Biol. Chem. 2003, 278, 46911–46918, doi:10.1074/jbc.M307977200.

80. Fumoto, K.; Takigawa-Imamura, H.; Sumiyama, K.; Kaneiwa, T.; Kikuchi, A. Modulation of apical constriction by Wnt signaling is required for lung epithelial shape transition. Development 2017, 144, 151–162, doi:10.1242/dev.141325.

81. Frank, D.B.; Peng, T.; Zepp, J.A.; Snitow, M.; Vincent, T.L.; Penkala, I.J.; Cui, Z.; Herriges, M.J.; Morley, M.P.; Zhou, S.; et al. Emergence of a Wave of Wnt Signaling that Regulates Lung Alveologenesis by Controlling Epithelial Self-Renewal and Differentiation. Cell Rep. 2016, 17, 2312–2325, doi:10.1016/j.celrep.2016.11.001.

82. Nantie, L.B.; Young, R.E.; Paltzer, W.G.; Zhang, Y.; Johnson, R.L.; Verheyden, J.M.; Sun, X. Lats1/2 inactivation reveals Hippo function in alveolar type I cell differentiation during lung transition to air breathing. Development 2018, 145, doi:10.1242/dev.163105.

83. Sun, Y.F.; Kan, Q.; Yang, Y.; Zhang, Y.H.; Shen, J.X.; Zhang, C.; Zhou, X.Y. Knockout of microRNA26a promotes lung development and pulmonary surfactant synthesis. Mol. Med. Rep. 2018, 17, 5988–5995, doi:10.3892/mmr.2018.8602.

84. Wang, Y.; Frank, D.B.; Morley, M.P.; Zhou, S.; Wang, X.; Lu, M.M.; Lazar, M.A.; Morrisey, E.E. HDAC3-Dependent Epigenetic Pathway Controls Lung Alveolar Epithelial Cell Remodeling and Spreading via miR-17-92 and TGF-beta Signaling Regulation. Dev. Cell 2016, 36, 303–315, doi:10.1016/j.devcel.2015.12.031.

85. Burri, P.H. Structural Aspects of Postnatal Lung Development – Alveolar Formation and Growth. Neonatology 2006, 89, 313–322, doi:10.1159/000092868.

86. Morrisey; Hogan, B.L.M. Preparing for the first breath: genetic and cellular mechanisms in lung development. Dev. Cell 2010, 18, 8–23, doi:10.1016/j.devcel.2009.12.010.

87. Hyde, D.M.; Blozis, S.A.; Avdalovic, M.V.; Putney, L.F.; Dettorre, R.; Quesenberry, N.J.; Singh, P.; Tyler, N.K. Alveoli increase in number but not size from birth to adulthood in rhesus monkeys. Am. J. Physiol. Lung Cell Mol. Physiol. 2007, 293, L570–L579, doi:10.1152/ajplung.00467.2006.

88. Tschanz, S.A.; Salm, L.A.; Roth-Kleiner, M.; Barré, S.F.; Burri, P.H.; Schittny, J.C. Rat lungs show a biphasic formation of new alveoli during postnatal development. J. Appl. Physiol. 2014, 117, 89–95, doi:10.1152/japplphysiol.01355.2013.

89. Mammoto, A.; Mammoto, T. Vascular Niche in Lung Alveolar Development, Homeostasis, and Regeneration. Front Bioeng Biotechnol 2019, 7, 318, doi:10.3389/fbioe.2019.00318.

90. Yamamoto, H.; Jun Yun, E.; Gerber, H.-P.; Ferrara, N.; Whitsett, J.A.; Vu, T.H. Epithelial–vascular cross talk mediated by VEGF-A and HGF signaling directs primary septae formation during distal lung morphogenesis. Dev. Biol. 2007, 308, 44–53, doi:10.1016/j.ydbio.2007.04.042.

91. Boström, H.; Gritli-Linde, A.; Betsholtz, C. PDGF-a/PDGF alpha-receptor signaling is required for lung growth and the formation of alveoli but not for early lung branching morphogenesis. Dev. Dyn. 2002, 223, 155–162, doi:10.1002/dvdy.1225.

92. Lindahl, P.; Karlsson, L.; Hellstrom, M.; Gebre-Medhin, S.; Willetts, K.; Heath, J.K.; Betsholtz, C. Alveogenesis failure in PDGF-A-deficient mice is coupled to lack of distal spreading of alveolar smooth muscle cell progenitors during lung development. Development 1997, 124, 3943–3953, doi:10.1242/dev.124.20.3943.

93. Wilkinson, G.A.; Schittny, J.C.; Reinhardt, D.P.; Klein, R. Role for ephrinB2 in postnatal lung alveolar development and elastic matrix integrity. Dev. Dyn. 2008, 237, 2220–2234, doi:10.1002/dvdy.21643.

94. Alejandre-Alcázar, M.A.; Michiels-Corsten, M.; Vicencio, A.G.; Reiss, I.; Ryu, J.; de Krijger, R.R.; Haddad, G.G.; Tibboel, D.; Seeger, W.; Eickelberg, O.; et al. TGF-β signaling is dynamically

regulated during the alveolarization of rodent and human lungs. Dev. Dyn. 2008, 237, 259–269, doi:10.1002/dvdy.21403.

95. Alejandre-Alcázar, M.A.; Shalamanov, P.D.; Amarie, O.V.; Sevilla-Pérez, J.; Seeger, W.; Eickelberg, O.; Morty, R.E. Temporal and spatial regulation of bone morphogenetic protein signaling in late lung development. Dev. Dyn. 2007, 236, 2825–2835, doi:10.1002/dvdy.21293.

96. Luo, Y.; Chen, H.; Ren, S.; Li, N.; Mishina, Y.; Shi, W. BMP signaling is essential in neonatal surfactant production during respiratory adaptation. Am. J. Physiol. Lung Cell Mol. Physiol. 2016, 311, L29–L38, doi:10.1152/ajplung.00391.2015.

97. Weinstein, M.; Xu, X.; Ohyama, K.; Deng, C.X. FGFR-3 and FGFR-4 function cooperatively to direct alveogenesis in the murine lung. Development 1998, 125, 3615–3623, doi:10.1242/dev.125.18.3615.

98. Baybutt, R.C.; Hu, L.; Molteni, A. Vitamin A Deficiency Injures Lung and Liver Parenchyma and Impairs Function of Rat Type II Pneumocytes. J. Nutr. 2000, 130, 1159–1165, doi:10.1093/jn/130.5.1159.

99. Perl, A.-K.T.; Gale, E. FGF signaling is required for myofibroblast differentiation during alveolar regeneration. Am. J. Physiol. Lung Cell Mol. Physiol. 2009, 297, L299–L308, doi:10.1152/ajplung.00008.2009.

100. Yun, E.J.; Lorizio, W.; Seedorf, G.; Abman, S.H.; Vu, T.H. VEGF and endothelium-derived retinoic acid regulate lung vascular and alveolar development. Am. J. Physiol. Lung Cell Mol. Physiol. 2016, 310, L287–298, doi:10.1152/ajplung.00229.2015.

101. Ruiz-Camp, J.; Quantius, J.; Lignelli, E.; Arndt, P.F.; Palumbo, F.; Nardiello, C.; Surate Solaligue, D.E.; Sakkas, E.; Mizikova, I.; Rodriguez-Castillo, J.A.; et al. Targeting miR-34a/Pdgfra interactions partially corrects alveologenesis in experimental bronchopulmonary dysplasia. EMBO Mol. Med. 2019, 11, e9448, doi:10.15252/emmm.201809448.

102. Durrani-Kolarik, S.; Pool, C.A.; Gray, A.; Heyob, K.M.; Cismowski, M.J.; Pryhuber, G.; Lee, L.J.; Yang, Z.; Tipple, T.E.; Rogers, L.K. miR-29b supplementation decreases expression of matrix proteins and improves alveolarization in mice exposed to maternal inflammation and neonatal hyperoxia. Am. J. Physiol. Lung Cell Mol. Physiol. 2017, 313, L339–L349, doi:10.1152/ajplung.00273.2016.

103. Lal, C.V.; Olave, N.; Travers, C.; Rezonzew, G.; Dolma, K.; Simpson, A.; Halloran, B.; Aghai, Z.; Das, P.; Sharma, N.; et al. Exosomal microRNA predicts and protects against severe bronchopulmonary dysplasia in extremely premature infants. JCI Insight 2018, 3, e93994, doi:10.1172/jci.insight.93994.

104. Yuan, H.S.; Xiong, D.Q.; Huang, F.; Cui, J.; Luo, H. MicroRNA-421 inhibition alleviates bronchopulmonary dysplasia in a mouse model via targeting Fgf10. J. Cell. Biochem. 2019, 120, 16876–16887, doi:10.1002/jcb.28945.

105. Laberge, J.M.; Flageole, H.; Pugash, D.; Khalife, S.; Blair, G.; Filiatrault, D.; Russo, P.; Lees, G.; Wilson, R.D. Outcome of the prenatally diagnosed congenital cystic adenomatoid lung malformation: a Canadian experience. Fetal Diagn. Ther. 2001, 16, 178–186, doi:10.1159/000053905.

106. Lau, C.T.; Kan, A.; Shek, N.; Tam, P.; Wong, K.K. Is congenital pulmonary airway malformation really a rare disease? Result of a prospective registry with universal antenatal screening program. Pediatr. Surg. Int. 2017, 33, 105–108, doi:10.1007/s00383-016-3991-1.

107. EUROCAT. Prevalence tables. Cystic adenomatous malf of lung. Available online: https://eu-rd-platform.jrc.ec.europa.eu/eurocat/eurocat-data/prevalence_en (accessed on 06/07/2021).

108. Wong, K.K.Y.; Flake, A.W.; Tibboel, D.; Rottier, R.J.; Tam, P.K.H. Congenital pulmonary airway malformation: advances and controversies. Lancet Child Adolesc. Health 2018, 2, 290–297, doi:10.1016/S2352-4642(18)30035-X.

109. Correia-Pinto, J.; Gonzaga, S.; Huang, Y.; Rottier, R. Congenital lung lesions–underlying molecular mechanisms. Semin. Pediatr. Surg. 2010, 19, 171–179, doi:10.1053/j.sempedsurg.2010.03.003.

110. Stocker, J.T. Cystic lung disease in infants and children. Fetal Pediatr. Pathol. 2009, 28, 155–184, doi:10.1080/15513810902984095.

111. Stocker, J.T.; Madewell, J.E.; Drake, R.M. Congenital cystic adenomatoid malformation of the lung. Classification and morphologic spectrum. Hum. Pathol. 1977, 8, 155–171, doi:10.1016/s0046-8177(77)80078-6.

112. Ursini, W.P.; Ponce, C.C. Congenital pulmonary airway malformation. Autops. Case Rep. 2018, 8, e2018022, doi:10.4322/acr.2018.022.

113. Adzick, N.S.; Harrison, M.R.; Glick, P.L.; Golbus, M.S.; Anderson, R.L.; Mahony, B.S.; Callen, P.W.; Hirsch, J.H.; Luthy, D.A.; Filly, R.A.; et al. Fetal cystic adenomatoid malformation: prenatal diagnosis and natural history. J. Pediatr. Surg. 1985, 20, 483–488, doi:10.1016/s0022-3468(85)80470-x.

114. David, M.; Lamas-Pinheiro, R.; Henriques-Coelho, T. Prenatal and Postnatal Management of Congenital Pulmonary Airway Malformation. Neonatology 2016, 110, 101–115, doi:10.1159/000440894.

115. Morotti, R.A.; Cangiarella, J.; Gutierrez, M.C.; Jagirdar, J.; Askin, F.; Singh, G.; Profitt, S.A.; Wert, S.E.; Whitsett, J.A.; Greco, M.A. Congenital cystic adenomatoid malformation of the lung (CCAM): evaluation of the cellular components. Hum. Pathol. 1999, 30, 618–625, doi:10.1016/s0046-8177(99)90084-9.

116. Cass, D.L.; Quinn, T.M.; Yang, E.Y.; Liechty, K.W.; Crombleholme, T.M.; Flake, A.W.; Adzick, N.S. Increased cell proliferation and decreased apoptosis characterize congenital cystic adenomatoid malformation of the lung. J. Pediatr. Surg. 1998, 33, 1043–1046, doi:10.1016/s0022-3468(98)90528-0.

117. Volpe, M.V.; Chung, E.; Ulm, J.P.; Gilchrist, B.F.; Ralston, S.; Wang, K.T.; Nielsen, H.C. Aberrant cell adhesion molecule expression in human bronchopulmonary sequestration and congenital cystic adenomatoid malformation. Am. J. Physiol. Lung Cell Mol. Physiol. 2009, 297, L143–152, doi:10.1152/ajplung.90618.2008.

118. Liechty, K.W.; Crombleholme, T.M.; Quinn, T.M.; Cass, D.L.; Flake, A.W.; Adzick, N.S. Elevated platelet-derived growth factor-B in congenital cystic adenomatoid malformations requiring fetal resection. J. Pediatr. Surg. 1999, 34, 805–809; discussion 809-810, doi:10.1016/s0022-3468(99)90377-9.

119. Fromont-Hankard, G.; Philippe-Chomette, P.; Delezoide, A.L.; Nessmann, C.; Aigrain, Y.; Peuchmaur, M. Glial cell-derived neurotrophic factor expression in normal human lung and congenital cystic adenomatoid malformation. Arch. Pathol. Lab. Med. 2002, 126, 432–436, doi:10.5858/2002-126-0432-GCDNFE.

120. Wagner, A.J.; Stumbaugh, A.; Tigue, Z.; Edmondson, J.; Paquet, A.C.; Farmer, D.L.; Hawgood, S. Genetic analysis of congenital cystic adenomatoid malformation reveals a novel pulmonary gene: fatty acid binding protein-7 (brain type). Pediatr. Res. 2008, 64, 11–16, doi:10.1203/PDR.0b013e318174eff8.

121. Swarr, D.T.; Peranteau, W.H.; Pogoriler, J.; Frank, D.B.; Adzick, N.S.; Hedrick, H.L.; Morley, M.; Zhou, S.; Morrisey, E.E. Novel Molecular and Phenotypic Insights into Congenital Lung Malformations. Am. J. Respir. Crit. Care Med. 2018, 197, 1328–1339, doi:10.1164/rccm.201706-1243OC.

122. Weber, S.C.; Sallmon, H.; Sarioglu, N.; Degenhardt, P.; Buhrer, C.; Rudiger, M.; Koehne, P. The expression of vascular endothelial growth factor and its receptors in congenital

bronchopulmonary cystic malformations. Eur. J. Pediatr. Surg. 2012, 22, 127–132, doi:10.1055/s-0032-1308692.

123. Volpe, M.V.; Pham, L.; Lessin, M.; Ralston, S.J.; Bhan, I.; Cutz, E.; Nielsen, H.C. Expression of Hoxb-5 during human lung development and in congenital lung malformations. Birt. Defects Res. A. Clin. Mol. Teratol. 2003, 67, 550–556, doi:10.1002/bdra.10086.

124. Morotti, R.A.; Gutierrez, M.C.; Askin, F.; Profitt, S.A.; Wert, S.E.; Whitsett, J.A.; Greco, M.A. Expression of thyroid transcription factor-1 in congenital cystic adenomatoid malformation of the lung. Pediatr. Dev. Pathol. 2000, 3, 455–461, doi:10.1007/s100240010092.

125. Jancelewicz, T.; Nobuhara, K.; Hawgood, S. Laser microdissection allows detection of abnormal gene expression in cystic adenomatoid malformation of the lung. J. Pediatr. Surg. 2008, 43, 1044–1051, doi:10.1016/j.jpedsurg.2008.02.027.

126. Gonzaga, S.; Henriques-Coelho, T.; Davey, M.; Zoltick, P.W.; Leite-Moreira, A.F.; Correia-Pinto, J.; Flake, A.W. Cystic adenomatoid malformations are induced by localized FGF10 overexpression in fetal rat lung. Am. J. Respir. Cell Mol. Biol. 2008, 39, 346–355, doi:10.1165/rcmb.2007-0290OC.

127. Simonet, W.S.; DeRose, M.L.; Bucay, N.; Nguyen, H.Q.; Wert, S.E.; Zhou, L.; Ulich, T.R.; Thomason, A.; Danilenko, D.M.; Whitsett, J.A. Pulmonary malformation in transgenic mice expressing human keratinocyte growth factor in the lung. Proc. Natl. Acad. Sci. 1995, 92, 12461–12465, doi:10.1073/pnas.92.26.12461.

128. Clark, J.C.; Tichelaar, J.W.; Wert, S.E.; Itoh, N.; Perl, A.K.; Stahlman, M.T.; Whitsett, J.A. FGF-10 disrupts lung morphogenesis and causes pulmonary adenomas in vivo. Am. J. Physiol. Lung Cell Mol. Physiol. 2001, 280, L705–715, doi:10.1152/ajplung.2001.280.4.L705.

129. White, A.C.; Xu, J.; Yin, Y.; Smith, C.; Schmid, G.; Ornitz, D.M. FGF9 and SHH signaling coordinate lung growth and development through regulation of distinct mesenchymal domains. Development 2006, 133, 1507–1517, doi:10.1242/dev.02313.

130. Cardoso, W.V.; Itoh, A.; Nogawa, H.; Mason, I.; Brody, J.S. FGF-1 and FGF-7 induce distinct patterns of growth and differentiation in embryonic lung epithelium. Dev. Dyn. 1997, 208, 398–405, doi:10.1002/(SICI)1097-0177(199703)208:3<398::AID-AJA10>3.0.CO;2-X.

131. Harris, K.S.; Zhang, Z.; McManus, M.T.; Harfe, B.D.; Sun, X. Dicer function is essential for lung epithelium morphogenesis. Proc. Natl. Acad. Sci. 2006, 103, 2208–2213, doi:10.1073/pnas.0510839103.

132. Boucherat, O.; Landry-Truchon, K.; Berube-Simard, F.A.; Houde, N.; Beuret, L.; Lezmi, G.; Foulkes, W.D.; Delacourt, C.; Charron, J.; Jeannotte, L. Epithelial inactivation of Yy1 abrogates lung branching morphogenesis. Development 2015, 142, 2981–2995, doi:10.1242/dev.120469.

133. Boucherat, O.; Jeannotte, L.; Hadchouel, A.; Delacourt, C.; Benachi, A. Pathomechanisms of Congenital Cystic Lung Diseases: Focus on Congenital Cystic Adenomatoid Malformation and Pleuropulmonary Blastoma. Paediatr. Respir. Rev. 2016, 19, 62–68, doi:10.1016/j.prrv.2015.11.011.

134. Wan, H.; Liu, C.; Wert, S.E.; Xu, W.; Liao, Y.; Zheng, Y.; Whitsett, J.A. CDC42 is required for structural patterning of the lung during development. Dev. Biol. 2013, 374, 46–57, doi:10.1016/j.ydbio.2012.11.030.

135. Kadzik, R.S.; Cohen, E.D.; Morley, M.P.; Stewart, K.M.; Lu, M.M.; Morrisey, E.E. Wnt ligand/Frizzled 2 receptor signaling regulates tube shape and branch-point formation in the lung through control of epithelial cell shape. Proc. Natl. Acad. Sci. 2014, 111, 12444–12449, doi:10.1073/pnas.1406639111.

136. Wang, Y.; Tian, Y.; Morley, M.P.; Lu, M.M.; Demayo, F.J.; Olson, E.N.; Morrisey, E.E. Development and regeneration of Sox2+ endoderm progenitors are regulated by a Hdac1/2-Bmp4/Rb1 regulatory pathway. Dev. Cell 2013, 24, 345–358, doi:10.1016/j.devcel.2013.01.012.

137. Eblaghie, M.C.; Reedy, M.; Oliver, T.; Mishina, Y.; Hogan, B.L. Evidence that autocrine signaling through Bmpr1a regulates the proliferation, survival and morphogenetic behavior of distal lung epithelial cells. Dev. Biol. 2006, 291, 67–82, doi:10.1016/j.ydbio.2005.12.006.

138. Okubo, T.; Knoepfler, P.S.; Eisenman, R.N.; Hogan, B.L. Nmyc plays an essential role during lung development as a dosage-sensitive regulator of progenitor cell proliferation and differentiation. Development 2005, 132, 1363–1374, doi:10.1242/dev.01678.

139. Ochieng, J.K.; Schilders, K.; Kool, H.; Boerema-De Munck, A.; Buscop-Van Kempen, M.; Gontan, C.; Smits, R.; Grosveld, F.G.; Wijnen, R.M.; Tibboel, D.; et al. Sox2 regulates the emergence of lung basal cells by directly activating the transcription of Trp63. Am. J. Respir. Cell Mol. Biol. 2014, 51, 311–322, doi:10.1165/rcmb.2013-0419OC.

140. Taylor, B.; Rice, A.; Nicholson, A.G.; Hind, M.; Dean, C.H. Mechanism of lung development in the aetiology of adult congenital pulmonary airway malformations. Thorax 2020, 75, 1001–1003, doi:10.1136/thoraxjnl-2020-214752.

141. Guseh, J.S.; Bores, S.A.; Stanger, B.Z.; Zhou, Q.; Anderson, W.J.; Melton, D.A.; Rajagopal, J. Notch signaling promotes airway mucous metaplasia and inhibits alveolar development. Development 2009, 136, 1751–1759, doi:10.1242/dev.029249.

142. Jiang, Y.; Luo, Y.; Tang, Y.; Moats, R.; Warburton, D.; Zhou, S.; Lou, J.; Pryhuber, G.S.; Shi, W.; Wang, L.L. Alteration of cystic airway mesenchyme in congenital pulmonary airway malformation. Sci. Rep. 2019, 9, 5296, doi:10.1038/s41598-019-41777-y.

143. Zobel, M.; Gologorsky, R.; Lee, H.; Vu, L. Congenital lung lesions. Semin. Pediatr. Surg. 2019, 28, 150821, doi:10.1053/j.sempedsurg.2019.07.004.

144. Beksac, M.S.; Fadiloglu, E.; Tanacan, A.; Unal, C.; Tepe, N.B.; Aydin, E.; Orgul, G.; Yurdakok, M. Outcomes of Cases of Prenatally-Diagnosed Congenital Pulmonary Airway Malformation. Rev. Bras. Ginecol. Obstet. 2019, 41, 654–659, doi:10.1055/s-0039-1697983.

145. Barroso, C.; Felizes, A.; Silva, A.R.; Braga, I.; Gonçalves, M.; Salgado, H.; Gonçalves, A.; Cadilhe, A.; Pereira, A.; Santos, M.J.; et al. Thoracoscopic Lobectomy for Congenital Pulmonary Airway Malformation with Prenatal Diagnosis. Port J Pediatr 2021, 52, 30–37, doi:10.25754/pjp.2021.20046.

146. Vieira, J.; Rego, A.; Oliveira, A.; Sa Ferreira, D.; Furtado, A.; Couceiro, A.; Miranda, J.A.; Leal, F.; Vouga, L. Bronchopulmonary sequestration–a 12-year experience. Rev. Port. Pneumol. 2006, 12, 489–501, doi:10.1016/S0873-2159(15)30455-4.

147. Kabnick, E.M.; Adler, L.; Susin, M.; Helfgott, A.; Alexander, L.L.; Tafreshi, M. Pulmonary sequestration. J. Natl. Med. Assoc. 1984, 76, 907–908, 911-902.

148. Estes, M.E.Z. Bronchopulmonary sequestration: Improving practice by evaluating for a missed diagnosis. Nurse Pract. 2017, 42, 51–55, doi:10.1097/01.NPR.0000511775.59497.cb.

149. Agee, C.; Walls, J.T.; Curtis, J.J.; Lababidi, Z. Bronchopulmonary sequestration. Mo. Med. 1989, 86, 271–274.

150. Franko, J.; Bell, K.; Pezzi, C.M. Intraabdominal pulmonary sequestration. Curr. Surg. 2006, 63, 35–38, doi:10.1016/j.cursur.2005.04.004.

151. Carter, R. Pulmonary sequestration. Ann. Thorac. Surg. 1969, 7, 68–88, doi:10.1016/s0003-4975(10)66147-4.

152. Arjun, P.; Palangadan, S.; Haque, A.; Ramachandran, R. Intralobar sequestration. Lung India 2017, 34, 559–561, doi:10.4103/lungindia.lungindia_51_17.

153. Aryal, G.; Pathak, V. Bronchopulmonary sequestration presenting as recurrent pneumonia. Wis. Med. J. 2011, 110, 240–242.

154. Shah, M.A.; Shah, I. Not all hemoptysis is tuberculosis - It could be intralobar bronchopulmonary sequestration. Lung India 2019, 36, 72–73, doi:10.4103/lungindia.lungindia_425_17.

155. Cooke, C.R. Bronchopulmonary sequestration. Respir. Care 2006, 51, 661–664.

156. Abuhamad, A.Z.; Bass, T.; Katz, M.E.; Heyl, P.S. Familial recurrence of pulmonary sequestration. Obstet. Gynecol. 1996, 87, 843–845.

157. Becker, J.; Hernandez, A.; Dipietro, M.; Coran, A.G. Identical twins concordant for pulmonary sequestration communicating with the esophagus and discordant for the VACTERL association. Pediatr. Surg. Int. 2005, 21, 541–546, doi:10.1007/s00383-005-1452-3.

158. Aulicino, M.R.; Reis, E.D.; Dolgin, S.E.; Unger, P.D.; Shah, K.D. Intra-abdominal pulmonary sequestration exhibiting congenital cystic adenomatoid malformation. Report of a case and review of the literature. Arch. Pathol. Lab. Med. 1994, 118, 1034–1037.

159. Cass, D.L.; Crombleholme, T.M.; Howell, L.J.; Stafford, P.W.; Ruchelli, E.D.; Adzick, N.S. Cystic lung lesions with systemic arterial blood supply: a hybrid of congenital cystic adenomatoid malformation and bronchopulmonary sequestration. J. Pediatr. Surg. 1997, 32, 986–990, doi:10.1016/s0022-3468(97)90383-3.

160. Conran, R.M.; Stocker, J.T. Extralobar sequestration with frequently associated congenital cystic adenomatoid malformation, type 2: report of 50 cases. Pediatr. Dev. Pathol. 1999, 2, 454–463, doi:10.1007/s100249900149.

161. McLean, S.E.; Pfeifer, J.D.; Siegel, M.J.; Jensen, E.R.; Schuler, P.M.; Hirsch, R.; Mychaliska, G.B. Congenital cystic adenomatoid malformation connected to an extralobar pulmonary sequestration in the contralateral chest: common origin? J. Pediatr. Surg. 2004, 39, e13–17, doi:10.1016/j.jpedsurg.2004.04.044.

162. Coraux, C.; Zahm, J.M.; Puchelle, E.; Gaillard, D. Beta(1)-integrins are involved in migration of human fetal tracheal epithelial cells and tubular morphogenesis. Am. J. Physiol. Lung Cell Mol. Physiol. 2000, 279, L224–234, doi:10.1152/ajplung.2000.279.2.L224.

163. Volpe, M.V.; Ramadurai, S.M.; Pham, L.D.; Nielsen, H.C. Hoxb-5 down regulation alters Tenascin-C, FGF10 and Hoxb gene expression patterns in pseudoglandular period fetal mouse lung. Front. Biosci. 2007, 12, 860–873, doi:10.2741/2108.

164. Cillo, C.; Cantile, M.; Mortarini, R.; Barba, P.; Parmiani, G.; Anichini, A. Differential patterns of HOX gene expression are associated with specific integrin and ICAM profiles in clonal populations isolated from a single human melanoma metastasis. Int. J. Cancer 1996, 66, 692–697, doi:10.1002/(SICI)1097-0215(19960529)66:5<692::AID-IJC18>3.0.CO;2-6.

165. Langston, C. New concepts in the pathology of congenital lung malformations. Semin. Pediatr. Surg. 2003, 12, 17–37, doi:10.1053/spsu.2003.00001.

166. Annunziata, F.; Bush, A.; Borgia, F.; Raimondi, F.; Montella, S.; Poeta, M.; Borrelli, M.; Santamaria, F. Congenital Lung Malformations: Unresolved Issues and Unanswered Questions. Front. Pediatr. 2019, 7, 239, doi:10.3389/fped.2019.00239.

167. CHOP. The Children's Hospital of Philadelphia. Bronchogenic Cyst. Available online: https://www.chop.edu/conditions-diseases/bronchogenic-cyst (accessed on 23/07/2021).

168. Durell, J.; Lakhoo, K. Congenital cystic lesions of the lung. Early Hum. Dev. 2014, 90, 935–939, doi:10.1016/j.earlhumdev.2014.09.014.

169. McGivern, M.R.; Best, K.E.; Rankin, J.; Wellesley, D.; Greenlees, R.; Addor, M.C.; Arriola, L.; de Walle, H.; Barisic, I.; Beres, J.; et al. Epidemiology of congenital diaphragmatic hernia in Europe: a register-based study. Arch. Dis. Child. Fetal Neonatal Ed. 2015, 100, F137–144, doi:10.1136/archdischild-2014-306174.

170. Chandrasekharan, P.K.; Rawat, M.; Madappa, R.; Rothstein, D.H.; Lakshminrusimha, S. Congenital Diaphragmatic hernia - a review. Matern. Health. Neonatol. Perinatol. 2017, 3, 6, doi:10.1186/s40748-017-0045-1.

171. Kosinski, P.; Wielgos, M. Congenital diaphragmatic hernia: pathogenesis, prenatal diagnosis and management - literature review. Ginekol. Pol. 2017, 88, 24–30, doi:10.5603/GP.a2017.0005.
172. Keijzer, R.; Puri, P. Congenital diaphragmatic hernia. Semin. Pediatr. Surg. 2010, 19, 180–185, doi:10.1053/j.sempedsurg.2010.03.001.
173. Leeuwen, L.; Fitzgerald, D.A. Congenital diaphragmatic hernia. J. Paediatr. Child Health 2014, 50, 667–673, doi:10.1111/jpc.12508.
174. van Loenhout, R.B.; Tibboel, D.; Post, M.; Keijzer, R. Congenital diaphragmatic hernia: comparison of animal models and relevance to the human situation. Neonatology 2009, 96, 137–149, doi:10.1159/000209850.
175. Chatterjee, D.; Ing, R.J.; Gien, J. Update on Congenital Diaphragmatic Hernia. Anesth. Analg. 2020, 131, 808–821, doi:10.1213/ANE.0000000000004324.
176. Cannata, G.; Caporilli, C.; Grassi, F.; Perrone, S.; Esposito, S. Management of Congenital Diaphragmatic Hernia (CDH): Role of Molecular Genetics. Int. J. Mol. Sci. 2021, 22, 6353, doi:10.3390/ijms22126353.
177. Kardon, G.; Ackerman, K.G.; McCulley, D.J.; Shen, Y.; Wynn, J.; Shang, L.; Bogenschutz, E.; Sun, X.; Chung, W.K. Congenital diaphragmatic hernias: from genes to mechanisms to therapies. Dis. Model. Mech. 2017, 10, 955–970, doi:10.1242/dmm.028365.
178. Chiu, P.P. New Insights into Congenital Diaphragmatic Hernia - A Surgeon's Introduction to CDH Animal Models. Front. Pediatr. 2014, 2, 36, doi:10.3389/fped.2014.00036.
179. Nakamura, H.; Doi, T.; Puri, P.; Friedmacher, F. Transgenic animal models of congenital diaphragmatic hernia: a comprehensive overview of candidate genes and signaling pathways. Pediatr. Surg. Int. 2020, 36, 991–997, doi:10.1007/s00383-020-04705-0.
180. Jesudason, E.C.; Connell, M.G.; Fernig, D.G.; Lloyd, D.A.; Losty, P.D. Early lung malformations in congenital diaphragmatic hernia. J. Pediatr. Surg. 2000, 35, 124–127, doi:10.1016/s0022-3468(00)80028-7.
181. Keijzer, R.; Liu, J.; Deimling, J.; Tibboel, D.; Post, M. Dual-hit hypothesis explains pulmonary hypoplasia in the nitrofen model of congenital diaphragmatic hernia. Am. J. Pathol. 2000, 156, 1299–1306, doi:10.1016/S0002-9440(10)65000-6.
182. Baptista, M.J.; Melo-Rocha, G.; Pedrosa, C.; Gonzaga, S.; Teles, A.; Estevao-Costa, J.; Areias, J.C.; Flake, A.W.; Leite-Moreira, A.F.; Correia-Pinto, J. Antenatal vitamin A administration attenuates lung hypoplasia by interfering with early instead of late determinants of lung underdevelopment in congenital diaphragmatic hernia. J. Pediatr. Surg. 2005, 40, 658–665, doi:10.1016/j.jpedsurg.2005.01.034.
183. Thebaud, B.; Tibboel, D.; Rambaud, C.; Mercier, J.C.; Bourbon, J.R.; Dinh-Xuan, A.T.; Archer, S.L. Vitamin A decreases the incidence and severity of nitrofen-induced congenital diaphragmatic hernia in rats. Am. J. Physiol. 1999, 277, L423–429, doi:10.1152/ajplung.1999.277.2.L423.
184. Major, D.; Cadenas, M.; Fournier, L.; Leclerc, S.; Lefebvre, M.; Cloutier, R. Retinol status of newborn infants with congenital diaphragmatic hernia. Pediatr. Surg. Int. 1998, 13, 547–549, doi:10.1007/s003830050399.
185. Beurskens, L.W.; Tibboel, D.; Lindemans, J.; Duvekot, J.J.; Cohen-Overbeek, T.E.; Veenma, D.C.; de Klein, A.; Greer, J.J.; Steegers-Theunissen, R.P. Retinol status of newborn infants is associated with congenital diaphragmatic hernia. Pediatrics 2010, 126, 712–720, doi:10.1542/peds.2010-0521.
186. Montalva, L.; Zani, A. Assessment of the nitrofen model of congenital diaphragmatic hernia and of the dysregulated factors involved in pulmonary hypoplasia. Pediatr. Surg. Int. 2019, 35, 41–61, doi:10.1007/s00383-018-4375-5.

187. Montedonico, S.; Nakazawa, N.; Puri, P. Congenital diaphragmatic hernia and retinoids: searching for an etiology. Pediatr. Surg. Int. 2008, 24, 755–761, doi:10.1007/s00383-008-2140-x.

188. Pereira-Terra, P.; Moura, R.S.; Nogueira-Silva, C.; Correia-Pinto, J. Neuroendocrine factors regulate retinoic acid receptors in normal and hypoplastic lung development. J. Physiol. 2015, 593, 3301–3311, doi:10.1113/JP270477.

189. Candilera, V.; Bouche, C.; Schleef, J.; Pederiva, F. Lung growth factors in the amniotic fluid of normal pregnancies and with congenital diaphragmatic hernia. J. Matern. Fetal Neonatal Med. 2016, 29, 2104–2108, doi:10.3109/14767058.2015.1076387.

190. Boucherat, O.; Benachi, A.; Chailley-Heu, B.; Franco-Montoya, M.L.; Elie, C.; Martinovic, J.; Bourbon, J.R. Surfactant maturation is not delayed in human fetuses with diaphragmatic hernia. PLoS Med. 2007, 4, e237, doi:10.1371/journal.pmed.0040237.

191. Boucherat, O.; Benachi, A.; Barlier-Mur, A.M.; Franco-Montoya, M.L.; Martinovic, J.; Thebaud, B.; Chailley-Heu, B.; Bourbon, J.R. Decreased lung fibroblast growth factor 18 and elastin in human congenital diaphragmatic hernia and animal models. Am. J. Respir. Crit. Care Med. 2007, 175, 1066–1077, doi:10.1164/rccm.200601-050OC.

192. Merrell, A.J.; Ellis, B.J.; Fox, Z.D.; Lawson, J.A.; Weiss, J.A.; Kardon, G. Muscle connective tissue controls development of the diaphragm and is a source of congenital diaphragmatic hernias. Nat. Genet. 2015, 47, 496–504, doi:10.1038/ng.3250.

193. Jay, P.Y.; Bielinska, M.; Erlich, J.M.; Mannisto, S.; Pu, W.T.; Heikinheimo, M.; Wilson, D.B. Impaired mesenchymal cell function in Gata4 mutant mice leads to diaphragmatic hernias and primary lung defects. Dev. Biol. 2007, 301, 602–614, doi:10.1016/j.ydbio.2006.09.050.

194. You, L.R.; Takamoto, N.; Yu, C.T.; Tanaka, T.; Kodama, T.; Demayo, F.J.; Tsai, S.Y.; Tsai, M.J. Mouse lacking COUP-TFII as an animal model of Bochdalek-type congenital diaphragmatic hernia. Proc. Natl. Acad. Sci. 2005, 102, 16351–16356, doi:10.1073/pnas.0507832102.

195. Ackerman, K.G.; Herron, B.J.; Vargas, S.O.; Huang, H.; Tevosian, S.G.; Kochilas, L.; Rao, C.; Pober, B.R.; Babiuk, R.P.; Epstein, J.A.; et al. Fog2 is required for normal diaphragm and lung development in mice and humans. PLoS Genet. 2005, 1, 58–65, doi:10.1371/journal.pgen.0010010.

196. Clugston, R.D.; Klattig, J.; Englert, C.; Clagett-Dame, M.; Martinovic, J.; Benachi, A.; Greer, J.J. Teratogen-induced, dietary and genetic models of congenital diaphragmatic hernia share a common mechanism of pathogenesis. Am. J. Pathol. 2006, 169, 1541–1549, doi:10.2353/ajpath.2006.060445.

197. Wat, M.J.; Beck, T.F.; Hernandez-Garcia, A.; Yu, Z.; Veenma, D.; Garcia, M.; Holder, A.M.; Wat, J.J.; Chen, Y.; Mohila, C.A.; et al. Mouse model reveals the role of SOX7 in the development of congenital diaphragmatic hernia associated with recurrent deletions of 8p23.1. Hum. Mol. Genet. 2012, 21, 4115–4125, doi:10.1093/hmg/dds241.

198. Morrisey, E.E.; Tang, Z.; Sigrist, K.; Lu, M.M.; Jiang, F.; Ip, H.S.; Parmacek, M.S. GATA6 regulates HNF4 and is required for differentiation of visceral endoderm in the mouse embryo. Genes Dev. 1998, 12, 3579–3590, doi:10.1101/gad.12.22.3579.

199. Qi, H.; Yu, L.; Zhou, X.; Wynn, J.; Zhao, H.; Guo, Y.; Zhu, N.; Kitaygorodsky, A.; Hernan, R.; Aspelund, G.; et al. De novo variants in congenital diaphragmatic hernia identify MYRF as a new syndrome and reveal genetic overlaps with other developmental disorders. PLoS Genet. 2018, 14, e1007822, doi:10.1371/journal.pgen.1007822.

200. Kim, P.C.; Mo, R.; Hui Cc, C. Murine models of VACTERL syndrome: Role of sonic hedgehog signaling pathway. J. Pediatr. Surg. 2001, 36, 381–384, doi:10.1053/jpsu.2001.20722.

201. Coles, G.L.; Ackerman, K.G. Kif7 is required for the patterning and differentiation of the diaphragm in a model of syndromic congenital diaphragmatic hernia. Proc. Natl. Acad. Sci. 2013, 110, E1898–1905, doi:10.1073/pnas.1222797110.

202. Russell, M.K.; Longoni, M.; Wells, J.; Maalouf, F.I.; Tracy, A.A.; Loscertales, M.; Ackerman, K.G.; Pober, B.R.; Lage, K.; Bult, C.J.; et al. Congenital diaphragmatic hernia candidate genes derived from embryonic transcriptomes. Proc. Natl. Acad. Sci. 2012, 109, 2978–2983, doi:10.1073/pnas.1121621109.

203. Yu, L.; Hernan, R.R.; Wynn, J.; Chung, W.K. The influence of genetics in congenital diaphragmatic hernia. Semin. Perinatol. 2020, 44, 151169, doi:10.1053/j.semperi.2019.07.008.

204. Boateng, E.; Krauss-Etschmann, S. miRNAs in Lung Development and Diseases. Int. J. Mol. Sci. 2020, 21, 2765, doi:10.3390/ijms21082765.

205. Pereira-Terra, P.; Deprest, J.A.; Kholdebarin, R.; Khoshgoo, N.; DeKoninck, P.; Munck, A.A.; Wang, J.; Zhu, F.; Rottier, R.J.; Iwasiow, B.M.; et al. Unique Tracheal Fluid MicroRNA Signature Predicts Response to FETO in Patients With Congenital Diaphragmatic Hernia. Ann. Surg. 2015, 262, 1130–1140, doi:10.1097/SLA.0000000000001054.

206. Mulhall, D.; Khoshgoo, N.; Visser, R.; Iwasiow, B.; Day, C.; Zhu, F.; Eastwood, P.; Keijzer, R. miR-200 family expression during normal and abnormal lung development due to congenital diaphragmatic hernia at the later embryonic stage in the nitrofen rat model. Pediatr. Surg. Int. 2020, 36, 1429–1436, doi:10.1007/s00383-020-04757-2.

207. Khoshgoo, N.; Kholdebarin, R.; Pereira-Terra, P.; Mahood, T.H.; Falk, L.; Day, C.A.; Iwasiow, B.M.; Zhu, F.; Mulhall, D.; Fraser, C.; et al. Prenatal microRNA miR-200b Therapy Improves Nitrofen-induced Pulmonary Hypoplasia Associated With Congenital Diaphragmatic Hernia. Ann. Surg. 2019, 269, 979–987, doi:10.1097/SLA.0000000000002595.

208. Wagner, R.; Montalva, L.; Zani, A.; Keijzer, R. Basic and translational science advances in congenital diaphragmatic hernia. Semin. Perinatol. 2020, 44, 151170, doi:10.1053/j.semperi.2019.07.009.

209. Tsao, K.; Johnson, A. Fetal tracheal occlusion for congenital diaphragmatic hernia. Semin. Perinatol. 2020, 44, 151164, doi:10.1053/j.semperi.2019.07.003.

210. Kirby, E.; Keijzer, R. Congenital diaphragmatic hernia: current management strategies from antenatal diagnosis to long-term follow-up. Pediatr. Surg. Int. 2020, 36, 415–429, doi:10.1007/s00383-020-04625-z.

211. Reiss, I.; Schaible, T.; van den Hout, L.; Capolupo, I.; Allegaert, K.; van Heijst, A.; Gorett Silva, M.; Greenough, A.; Tibboel, D.; Consortium, C.E. Standardized postnatal management of infants with congenital diaphragmatic hernia in Europe: the CDH EURO Consortium consensus. Neonatology 2010, 98, 354–364, doi:10.1159/000320622.

212. Bhatnagar, S.N.; Sarin, Y.K. Management of Congenital Diaphragmatic Hernia in Newborn - Paradigm Shift and Ethical Issues. Indian J. Pediatr. 2017, 84, 629–635, doi:10.1007/s12098-017-2374-5.

213. Hofmann, S.R.; Stadler, K.; Heilmann, A.; Hausler, H.J.; Fitze, G.; Kamin, G.; Nitzsche, K.I.; Hahn, G.; Dinger, J. Stabilisation of cardiopulmonary function in newborns with congenital diaphragmatic hernia using lung function parameters and hemodynamic management. Klin. Padiatr. 2012, 224, e1–e10, doi:10.1055/s-0031-1299731.

CHAPTER 1.3

RETINOIC ACID: A KEY REGULATOR OF LUNG DEVELOPMENT

Hugo Fernandes-Silva*, Henrique Araújo-Silva*, Jorge Correia-Pinto and Rute S. Moura

*These authors contributed equally to this work.

ABSTRACT

Retinoic Acid (RA) is a key molecular player in embryogenesis and adult tissue homeostasis. In embryo development, RA plays a crucial role in the formation of different organ systems, namely, the respiratory system. During lung development, there is a spatiotemporal regulation of RA levels that assures the formation of a fully functional organ. RA signaling influences lung specification, branching morphogenesis, and alveolarization by regulating the expression of particular target genes. Moreover, cooperation with other developmental pathways is essential to shape lung organogenesis. This review focuses on the events regulated by Retinoic Acid during lung developmental phases and pulmonary vascular development; also, it aims to provide a snapshot of RA interplay with other well-known regulators of lung development.

Keywords: vitamin A; retinol; respiratory system; lung specification; branching morphogenesis; alveologenesis

GENERAL INTRODUCTION

Retinoic Acid (RA), the active metabolite of retinol (Vitamin A), plays countless roles in different organs and tissues. In the adult, RA is crucial for immune, nervous and reproductive systems, as well as for vision and skin renewal. Throughout embryogenesis, RA acts as a potent morphogen that mediates cellular signaling and transcriptional regulation, thus modulating numerous aspects of embryo development [1–3]. RA levels must be tightly regulated, if not, RA can act as a teratogen, rather than a morphogen. In fact, deficiency or excess of RA causes severe congenital malformations that may affect somite, skeletal, spinal cord, limb, heart, pancreas, eye, diaphragm, and lung development [2].

Regarding lung development, RA regulates cellular events such as proliferation, differentiation, patterning, and maturation [4]. Evidently, this signaling pathway "does not walk alone", and the interplay with other well-known regulators is critical for proper lung formation. This review highlights the role of Retinoic Acid signaling all through lung development, its interaction with other signaling pathways, and its impact on fetal and adult diseases.

RETINOIC ACID SIGNALING PATHWAY OVERVIEW

In the blood, serum retinol travels in association with Retinol-binding protein 4 (RBP4) [5]. At the target tissues, retinol may enter the cells through two distinct mechanisms: (1) membrane transport through the Stimulated by retinoic acid 6 (STRA6) membrane transporter [6] or (2) membrane diffusion, dependent on gradient concentration, as a result of its hydrophobic structure [7]. Once in the cytosol, retinol molecules are sequestered by membrane systems and bind to Cellular retinol-binding protein 1 (CRBP1), which plays a role in vitamin A cytoplasmic trafficking [8].

Inside the cell, retinol can either be interconverted into retinyl esters, to serve as cellular storage, in a reaction catalyzed by Lecithin retinol acyltransferase (LRAT) [9]; or undergo the 2-steps oxidative pathway to generate RA for signaling. In this case, the conversion of retinol into retinal is performed by the Retinol dehydrogenase (RDH) family, primarily by RDH10 [10,11]. Alcohol dehydrogenase (ADH) enzymes convert retinol into retinal, only when retinol is not associated with CRBP1 [12]. This reversible reaction is mediated, in the opposite direction, by Dehydrogenase/Reductase SDR family, particularly DHSR3 [11,13]. The second oxidative step is the irreversible conversion of retinal into RA, catalyzed by Retinaldehyde dehydrogenase (RALDH). There are three main subtypes RALDH1, RALDH2, and RALDH3 [14,15] that display diverse expression patterns throughout organogenesis [16]. RA intracellular levels must be tightly controlled to maintain the appropriate RA concentration and consequent tissue distribution. Cytochrome P450 (CYP) subfamily 26 of enzymes degrade the excess of RA to avoid detrimental effects [17]. Among the three subtypes (CYP26A1, CYP26B1, and CYP26C1), CYP26A1 is particularly important during embryonic development [17].

Either acting on the producing cell (autocrine signaling) or the receiving cell (paracrine signaling), RA is transferred into the nucleus by Cellular retinoic acid-binding protein 2 (CRABP2) [18]. Once inside the nucleus, RA binds to specific nuclear transcription factors named Retinoic acid receptors (RARs), of which there are three main subtypes RARα, RARβ, and RARγ [19]. On its turn, RARs bind to Retinoid X receptors (RXRα, RXRβ, and RXRγ) to form heterodimers [19] that recognize specific DNA sequences (Retinoic acid response element - RARE) in the promotor region of RA target genes [20]. In the canonical model, RA-RAR-RXR complex binds to RAREs and induces conformational changes that promote the replacement of co-repressors by co-activators. Nuclear receptor co-activators (NCOA) recruit Histone acetylases and trithorax proteins, which trigger chromatin relaxation and induce gene transcription [1]. In contrast, when RA is absent, RAR-RXR heterodimers bind to RARE and recruit Nuclear receptor co-repressors (NCOR). NCOR recruits repressive factors such as Histone deacetylases and Polycomb

repressive complex 2. This interaction results in chromatin condensation and gene silencing [1]. In Figure 1, the main events of the RA signaling pathways are illustrated.
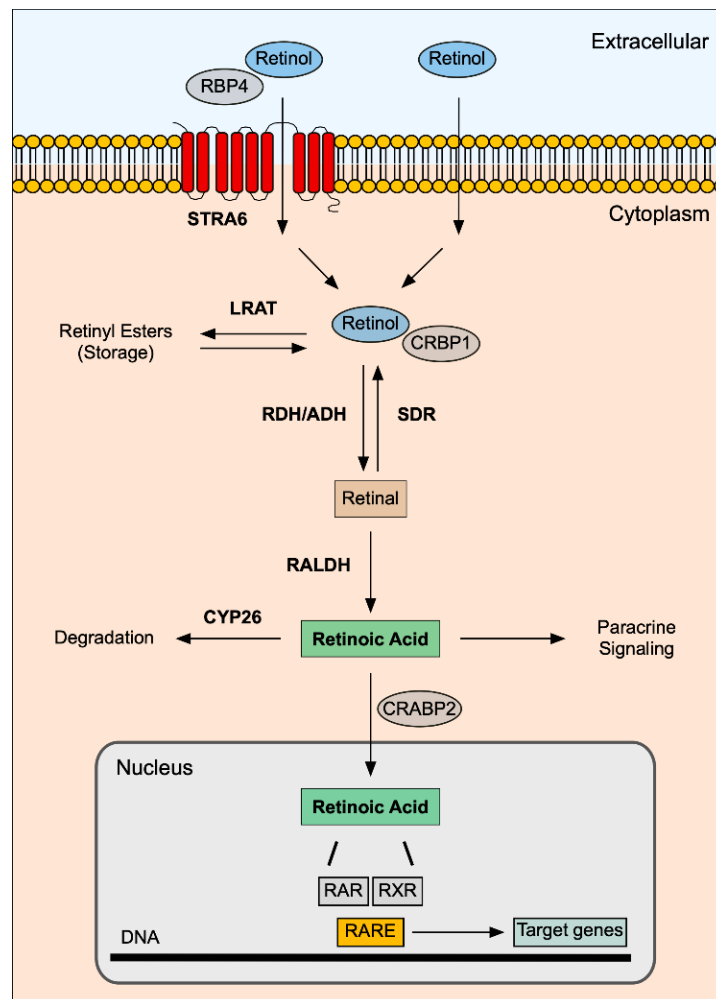
Figure 1 - Retinoic Acid signaling pathway. Retinol travels in the bloodstream in association with RBP4. Retinol can enter the target cell handled by STRA6 (binds RBP4 with high affinity), or by membrane diffusion. Inside the cell, retinol travels in association with CRBP1. Retinol can be interconverted into Retinyl esters (cellular storage) by LRAT, or be transformed into retinal by RDH/ADH enzymes. Afterward, retinal is oxidized to Retinoic Acid by RALDH enzymes. CYP26 degradative enzymes tightly regulate the intracellular levels of Retinoic Acid. Retinoic Acid can travel to the neighboring cells to act in a paracrine fashion or be transported to the nucleus bound to CRABP2. In the nucleus, Retinoic Acid interacts with RAR and RXR nuclear receptors, which form a heterodimer that recognizes RARE sequences in the promoter region of target genes, thus modulating transcription.

LUNG DEVELOPMENT AND RETINOIC ACID

Lung development is a highly coordinated and multistage process governed by mechanical, anatomical, and biochemical events. In humans, it begins around the fourth week after conception and continues into the post-natal period approximately until 22 years of age [21–23]. The mature lung displays a tree-like tubular system connected to the trachea and a highly branched vascular system. The

conducting (proximal) airways differ from the respiratory (distal) airways. In fact, towards the distal portion of the lung, the airways become progressively smaller/narrower, ending in the alveolar region where gas exchange occurs [24,25].

In humans, lung organogenesis initiates with the appearance of an endodermal bud on the ventral side of the anterior foregut around the fourth week of gestation. The endodermal evagination leads to the formation of the two lung buds and trachea, surrounded by mesoderm and a vascular network [25]. Lung epithelium is endoderm-derived and lines the airways and the alveoli. The conducting airways are generated by a highly regulated dichotomous branching morphogenesis commencing on the 5th week of gestation, giving rise to a complex network with numerous terminal branches. The continuous bifurcation of the epithelial bud tips relies on the close interaction between epithelium and mesenchyme. The mesenchyme at the tips is particularly important since it contains precursor cells that will differentiate into smooth muscle that stabilize the cleft between the newly formed buds. At the same time, diffusible signals act in both compartments, orchestrating lung organogenesis processes [26–28]. The alveolar cellular differentiation begins between the 16th and the 24th week of gestation. During this phase, bronchial epithelial cells differentiate into alveolar epithelial cells type 1 (AEC1) and type 2 (AEC2), also known as type 1 and type 2 pneumocytes, respectively. AEC2 act as AEC1 progenitor cells and are responsible for surfactant production, whereas AEC1 are responsible for gas exchange. From the 24th week onwards, tissue projection into the distal airspaces gives rise to structures resembling sacs, the primitive alveoli, lined with AEC1 and AEC2. Although the alveoli are formed at birth, their maturation begins approximately five weeks after birth, with the formation of a fine air-blood barrier composed by a thin epithelial sheet, an endothelial layer, and a basement membrane. Even though in the first years of life, the alveolar size remains constant, in adolescence, with the enlargement of the thoracic cage, it increases [29–31].

The crosstalk between the epithelial and mesenchymal compartment is conveyed by several diffusible signals from multiple signaling pathways including Sonic Hedgehog (SHH) [32], Wingless-related Integration Site (WNT) [33], Transforming Growth Factor β (TGFβ), Bone Morphogenetic Protein (BMP) [34], Fibroblast Growth Factor (FGF) [35], Hippo [36], and Retinoic Acid [4], just to name a few. In the next sections, we will dissect the role of RA throughout the five lung developmental phases, namely, embryonic, pseudoglandular, canalicular, saccular, and alveolar (Figure 2), and also in lung vascular development.
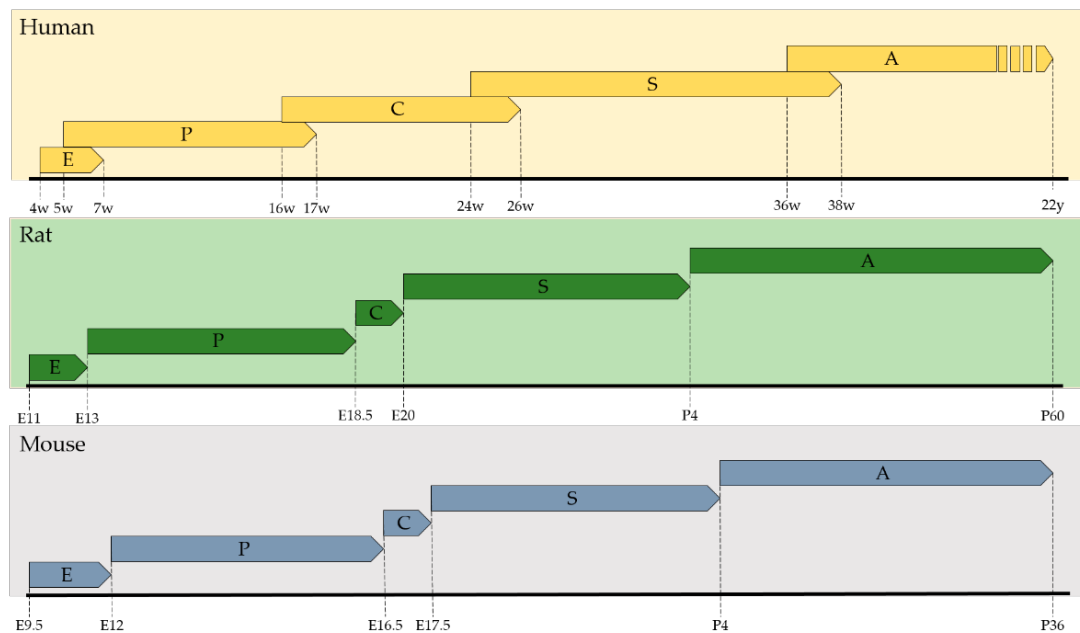
Figure 2 - Lung developmental phases. Time scale of human, rat and mouse lung developmental phases (E = Embryonic; P = Pseudoglandular; C = Canalicular; S = Saccular; A = Alveolar). The phases are defined largely by morphological standards and may overlap in time. Adapted from [30].

EMBRYONIC PHASE

The respiratory system is specified from the anterior foregut endoderm approximately at embryonic day 9.5 (E9.5) in mouse and around the 4th week of gestation in humans [30]. Initially, the anterior foregut begins as a sole epithelial tube surrounded by mesoderm. Lung and trachea specification begins with the establishment of a localized expression domain of the transcription factor NKX2.1 (also known as TTF1) in the ventral wall of the anterior foregut [37]. The expression of *nkx2.1* on the ventral side, distally to the rudimentary trachea, leads to the evagination of the two primary lung buds [25]. The epithelial outgrowth of the primary buds is supported by diffusible signals from the mesoderm tightly regulated both in time, dosage, and space. Briefly, WNT2 and WNT2b expression specify NKX2.1+ respiratory endoderm progenitors in the ventral anterior mesoderm that surrounds the anterior foregut endoderm [38]. The expression of NKX2.1 also depends on BMP signaling activation. Endodermal SHH regulates BMP4 expression in the ventral mesenchyme surrounding the ventral foregut, mainly through the transcription factors FOXF1, GLI1, and GLI3. BMP signaling represses the expression of the transcription factor SOX2 (that promotes esophageal fate), thus enabling NKX2.1 endodermal expression [39]. After respiratory lineage specification, FGF10 mesodermal expression requires TGFβ inhibition, mediated by RA signaling, to conduct outgrowth and extension of the primary lung buds [40].

RA signaling machinery is present in the foregut at the beginning of lung organogenesis. At E9.5, *raldh2* is highly and ubiquitously expressed in the anterior foregut, specifically in the mesenchyme neighboring the prospective trachea and lung primordia, suggesting that RA is being synthesized. Moreover, at this gestational age, a high local RAR activation is also detected in all layers of the foregut where trachea and primordial lung are emerging. This expression pattern is consistent with the hypothesis that RA acts on its receptors present in the epithelium in early lung development. At E10, *raldh2* levels are preserved in the tracheal mesenchyme and proximal lung but decrease towards the distal lung. Conversely, *cyp26* is not detected between E9.5–10; consequently, at these stages, RA synthesis is not compensated by its degradation, pointing to a crucial role for RA in the formation of the lung bud primordium. It is worth noting that, as lung morphogenesis proceeds, *cyp26* is progressively expressed, therefore controlling RA levels [41].

Disruption of RA signaling in *in vitro* mouse foregut cultures impairs lung bud initiation [42]. Likewise, *raldh2−/−* knockout mice and dams exposed to severe vitamin A deficiency during gestation display lung agenesis [43,44]. *In vitro* studies revealed that RA induces *fgf10* expression in the foregut mesoderm, where lung initiates, which then activates FGFR2 signaling in the endoderm and induces primary bud morphogenesis [42]. By further dissecting *raldh2−/−* knockout mice, it was uncovered that RARβ mediates *fgf10* induction by RA. Differential activation of RARα and RARβ has opposite effects in *fgf10* mesodermal expression; nonetheless, both receptors are needed for proper lung development [44]. Furthermore, it has been shown that endogenous RA acts via WNT and TGFβ signaling to control *fgf10* expression. RA downregulates TGFβ activity in the foregut mesoderm, thus allowing local expression of *fgf10*, which is crucial for primary lung bud induction [40]. Conversely, RA facilitates the activation of WNT signaling, crucial for the appearance/maintenance of the respiratory field, by inhibiting the expression of a WNT/β-catenin antagonist (Dickkopf1) [45]. Hence, an RA-dependent fine-tuned equilibrium of the WNT/TGFβ/FGF10 axis is mandatory to permit both respiratory progenitors' expansion and lung primordium formation.

RA acts in both endoderm and mesoderm to provide a niche for lung induction by regulating the expression of signals that will induce the lung and the competence to respond. In early somite stages, RA pre-patterns the lateral plate mesoderm and establishes the anterior foregut region that will form the respiratory niche. Subsequently, RA signaling promotes endodermal Hedgehog (HH) expression, which, mediated by mesenchymal GLI transcription factors, is indispensable for *wnt2/2b* and *bmp4* expression; subsequently, *wnt2/2b* and *bmp4* act on the endoderm to promote *nkx2.1* expression. The RA-HH-WNT signaling cascade that coordinates respiratory lineage specification is conserved between frog, mouse,

and human [46]. Moreover, RA/RAR activity regulates the competence of the endoderm to activate the NKX2.1+ respiratory program in response to mesodermal WNT and BMP, independently of HH, during early somite stages of development.

Recently, it has been shown that RA signaling has different roles during endoderm organogenesis, acting in a distinct temporal and spatial pattern. In early gastrula stages (mouse E6–7.5), during endoderm formation, RA induces hindgut and pancreatic stages but inhibits foregut fate. Conversely, in early somitogenesis (mouse E7.5–8.5), during endoderm patterning, RA suppresses pharyngeal and promotes respiratory fate in the anterior endoderm. Finally, lung induction (mouse E9.5) relies on the RA/WNT/BMP axis previously described [46]. However, RA actions are only possible because, during the gastrula stage, WNT/BMP signaling specifies endodermal competence domains and, consequently, how cells respond to signals during the subsequent phases [47].

PSEUDOGLANDULAR PHASE

Lung branching morphogenesis occurs during the pseudoglandular phase (E12–16.5 mouse; E13–E18.5 rat; 5–17 weeks, human), and it is characterized by reiterative splitting of the airway epithelium into the surrounding mesenchyme [48]. The development of new generations of terminal buds contributes to defining the airway conducting system. This process is tightly regulated by a network of signaling cascades that operate via epithelial-mesenchymal interactions [30]. The RA pathway has been recognized as a critical regulator of pulmonary branching [4,41,49,50]. In fact, in *rdh10–/–* mutants, primary lung bud growth is arrested and branching morphogenesis impaired, thus preventing the formation of the lung [51]. Likewise, *raldh2–/–* mouse embryos display defective growth and branching, resulting in hypoplastic lungs [43].

RA signaling machinery is dynamically expressed during branching morphogenesis. For instance, *stra6* mouse transcript is present in the mesenchyme surrounding the bronchi [52]. Conversely, as lung branching initiates, *crbp* transcripts are present in both epithelial and mesenchymal compartments, and later its expression is restricted to the mesenchyme [53]. In the embryonic mouse lung, *raldh2* is expressed along the mesothelium surface at sites of low branching activity. By comparing *fgf10* and *raldh2* expression patterns, it is possible to observe that regions, where *fgf10* is expressed, are low in *raldh2* [41,54]. Conversely, *raldh1* mRNA is present in the proximal region of the bronchi [41,49], while *raldh3* is weakly expressed in the epithelium of the main bronchus [16]. Importantly, RA bioavailability must be balanced to avoid detrimental concentrations. As secondary buds start to emerge, *cyp26* expression displays a proximal-distal epithelial gradient with high expression at distal sites. In the

mesenchymal compartment, *cyp26* is present between the secondary buds contributing to the regulation of RA levels in this region [41].

Retinoic Acid signaling response is, ultimately, transduced through RAR and RXR nuclear receptors that recognize RARE sequences in the promoter region of RA-target genes. The importance of RAR is particularly evident in *rarαβ2* mouse mutants, which exhibit lung agenesis and hypoplasia due to the absence of left lung budding and altered branching morphogenesis [55]. In the developing lung, *rarα1* and *rarα2* are ubiquitously expressed [49,56], whereas *rarβ* expression is restricted to the proximal bronchi epithelium and the proximal subepithelial and subpleural mesenchyme [41,49,53]. In opposition, *rarγ* transcripts are faintly and ubiquitously expressed in the embryonic lung; indeed, RARγ knockouts do not affect lung branching [41,49,53,56–58]. Throughout branching, RARE-lacZ reporter activity is detected in the proximal bronchial region with a pattern that strongly overlaps *rarβ* expression. Moreover, RARE-lacZ lacks from both the distal bud epithelium and the mesenchymal compartment [41]. Furthermore, RXR can be sequestered by Chicken Ovalbumin upstream promoter-transcription factors (COUP-TFs), resulting in RA signaling inhibition. *coup-tfII* expression is found in the lung mesenchyme, particularly higher in the mesenchyme between the secondary buds, but absent from the pulmonary epithelium [41]. Recently, RA signaling was characterized in the embryonic chicken lung [50]. For instance, *stra6* is expressed in the periepithelial mesenchyme surrounding the epithelium as it occurs in the mouse lung [50,52]. *raldh2*, *raldh3*, *cyp26a1*, and *rarα* expression patterns are comparable to their mammalian counterparts. Curiously, *rarβ* has a stage-dependent expression that is present in the proximal region of the mesenchymal compartment [50]. It is worth mentioning that while in the mammalian lung RA signaling members are distributed between the mesenchymal and epithelial compartments, in the chick lung, all members seem to be restricted to the mesenchyme [50]. Nonetheless, transcripts like *stra6* and *raldh2* display highly conserved expression patterns. Moreover, the complementary expression pattern between *raldh2* and *fgf10* is conserved, with *raldh2* being expressed in the ventral region, and *fgf10* in the dorsal pulmonary region [50,59].

RA signaling must be finely tuned so that mammalian lung branching morphogenesis may occur. In the mesenchymal compartment, RA is produced in the mesothelial region, at low branching sites, by RALDH2. Conversely, RA synthesis is regulated by CYP26 and COUP-TFs in the mesenchyme between the secondary buds [41]. A gradient of RA is produced from the pleura to the periepithelial mesenchyme that surrounds the distal region of the growing bud. RA availability regulates *fgf10* that is typically expressed in the mesenchyme surrounding the distal bud tips [41,54]; for this reason, *raldh2−/−* mouse embryos phenotype is rescued by RA and FGF10 supplementation [43]. Concurrently, in the epithelial

compartment, RA is produced in the proximal bronchi by RALDH1 [41,49] and may act through RARβ, which is detected in the same region [41,49,53]. RA epithelial levels are regulated by CYP26, which displays a gradient from the distal to the proximal region of the epithelial bronchi [41]. Intriguingly, *stra6* expression in the periepithelial mesenchyme, surrounding the epithelial bronchi, may play a role in retinol trafficking between epithelium and mesenchyme [52].

The role of RA signaling during pulmonary branching was uncovered by performing RA stimulation/inhibition studies. Mouse lung explants exposed to RA display an increase in lung branching in a dose-dependent manner [60]. Furthermore, RA supplementation can increase pulmonary branching in nitrofen-induced hypoplastic lungs, which display decreased RALDH2 activity [61]. Similarly, rat lung explants treated with exogenous RA exhibit an increase in the number of peripheral airway buds, epithelial perimeter, and the total area of the lung [62]. Likewise, RA supplementation, in the chicken model, revealed a dose-dependent increase in lung branching [50]. Furthermore, RA-exposed lung explants can display morphological alterations that resemble a more immature branching configuration; specifically, the formation of typical distal bud-like structures is impaired, promoting a more proximal-like phenotype [41,63,64]. Nevertheless, in some studies, a reduced number of terminal buds is observed in RA-treated lungs [41,56,63,64].

RA pathway modulation studies revealed a series of feedback control mechanisms underlying pulmonary branching morphogenesis. For instance, *crbpl* and *raldh1* expression are susceptible to be modulated by activation/inhibition of the RA cascade [49,56]. This feedback loop mechanism may regulate RA synthesis in the proximal epithelial buds [49]. On the other hand, RA supplementation increases both *rarβ* and RARβ but decreases RARα and RARγ [56,62].

RA downstream targets are not only signaling machinery components, but also members of other pathways. For instance, RA can directly downregulate *fgf10* expression or indirectly by stimulating the SHH pathway (through increasing *shh* expression) and, consequently, decrease *fgf10* transcript levels in the distal region of the lung [41,49,54,64,65]. Moreover, *bmp4* is also negatively modulated by RA signaling stimulation [41]. The interaction between RA, FGF, SHH, and BMP4 is crucial for branching and proximal-distal patterning [41,49,54,64–67]. In the proximal epithelium, RA modulates the expression of *foxa2*, a known regulator of epithelial differentiation and pulmonary branching [49,68]. RA pathway stimulation promotes *tgfβ3* expression in the lobar bronchial mesenchyme, pleura region, and bronchial epithelium [49], and downregulates *cftr* epithelial expression in the lobar bronchial and bronchial epithelium [49]. In fact, mammalian lung branching morphogenesis can be divided into two RA responsive centers: the distal epithelial region where *shh*, and *bmp4* are expressed and interact with *fgf10*

mesenchymal expression; and the proximal epithelial region where RA regulates *tgfβ3*, *foxa2* and *cftr* [41,49,54,65].

There are other RA downstream targets described in the embryonic mammalian lung, namely *hoxa2*, *hoxa5*, *hoxb5*, and *hoxb6*, which are related to patterning. Moreover, RA regulates HOXB5 protein levels, and *hoxa2* and *hoxb6* proximal-distal patterns [64,69,70]. In addition, disruption of the RA pathway results in altered murine smooth muscle phenotype and a consequent increase in the expression of *acta2* and *myh11* [71]. During chick lung branching, RA supplementation does not affect *sox2* but decreases *sox9* expression (patterning-related genes); however, it affects *sox9* spatial distribution, which is progressively excluded from the distal regions of the lung. Still, the new distal branches do not exhibit proximal appearance [50,72,73]. Furthermore, RA signaling stimulation, of the embryonic chick lung, increases the expression of *rarβ*, *hoxb5*, and *meis2*; alters the spatial distribution of *cyp26a1*, *id2*, *tgfβ2*, and *sox9*; and has a very modest effect on *fgf10*, *fgfr2*, and *sox2*. Even though RA machinery is confined to the mesenchymal compartment, it can influence the expression of epithelial genes such as *shh*, *sox9*, and *fgfr2* [50]. In the chicken model, RA signaling stimulates early pulmonary branching and contributes to pulmonary branching proximal-distal patterning [50].

CANALICULAR PHASE

The canalicular phase occurs between post-conception weeks 16 and 26 in human, E18.5–E20 in rat, and around E16.5–E17.5 in mouse [30]. During this phase, the epithelial airways continue to increase in size, and the terminal buds extend into the airspaces, forming the primitive pulmonary acini (terminal sacs) [74]. Simultaneously, distal mesenchyme, although still abundant at this phase, becomes progressively thinner. Additionally, early differentiation of AEC1 and AEC2 occurs, establishing an elementary gas exchange surface [25,75]; this respiratory region is morphologically different from the more proximal conducting airways [76–78]. Moreover, the bronchioalveolar duct junctions appear when epithelial differentiation happens and correspond to a stem cell niche; the location of this junction stays constant throughout life [79–81]. Finally, in this phase, vascularization begins. The continuous angiogenic process and juxtaposition of capillaries in close contact with the distal respiratory epithelium create the first air-blood barrier in the future alveolar ducts and saccules [82,83].

The role of RA in the canalicular phase has not been particularly dissected so far. However, in this phase, with the occurrence of cytodifferentiation of the columnar epithelium, the level of *rarα* transcripts decreases [84]. RA is a key regulator of cellular growth, proliferation, differentiation, and embryogenesis *per se*, and one cannot discard that it may contribute to this phase of lung morphogenesis.

For instance, Retinoic Acid is a major regulator of angiogenesis and vasculogenesis [85], and the organization of the pulmonary vascular bed initiates during the canalicular period. Therefore, RA may be involved in the development of the lung vascular system (please refer to Vascular Development section).

SACCULAR PHASE

The pulmonary saccular phase is characterized by the widening and growing of the terminal airways, which contribute to forming clusters of larger airspaces called saccules. During this phase (weeks 24–38 in human; E20–P4 in rat; E17.5–P4 in mouse), the enlargement of the future gas-exchange region causes condensation of the mesenchyme in-between airspaces, establishing the primary septa. Primary septa are composed of a double layer of capillaries separated by a central layer of mesenchyme. The majority of the primary septa surface is covered by AEC1, and the remaining surface is occupied by AEC2. Throughout this phase, lamellar bodies appear, and surfactant secretion initiates. Smooth muscle cell precursors start to form a network of elastic fiber and collagen fibrils that prepare the lung for alveolarization [30,86,87].

rar transcripts are present in the embryonic rat and mouse lung during the canalicular phase [84,88]. The expression levels of *rarα* transcript decrease in this phase [84], which seems to be required to allow sacculation and the differentiation program that contributes to forming mature AEC1 [88]. On the other hand, *rarβ* expression increases significantly in the late saccular period. This increase in *rarβ* matches AEC1 and AEC2 induction, suggesting a role for *rarβ* in preparing the lung for the alveolar phase. Low expression levels of *rarγ* were detected in this period [84]. Such findings point to a crucial role of the RA signaling pathway in preparing the lung for sacculation, and later, during the saccular phase, to prepare the lung for alveolarization.

ALVEOLAR PHASE

Alveologenesis or alveolarization is the process by which the gas exchange functional units, the alveoli, are generated. Alveoli formation is mainly a postnatal event, and it is time and species-dependent. For instance, mammals like deer, guinea pigs, or sheep are born with functional alveoli; mother-dependent mammals like mice, rats, and humans are born with primitive alveoli and, so, alveologenesis continues postnatally [89]. In mouse and rat, alveologenesis occurs entirely in the postnatal period, approximately from P4 to P36 and P4 to P60, respectively [23,25,30]. In humans, part of the alveoli is formed before birth, but their genesis continues postnatally. Alveologenesis is divided into three phases:

classical alveolarization (week 36 until ~3 years), microvascular maturation (week 36 until young adulthood), and continued alveolarization (~2 years until young adulthood) [30].

Throughout the canalicular and saccular phases, the terminal tubes are transformed into small saccules separated by the primary septum. During classical alveologenesis, the sacs are subdivided by the ingrowth of secondary septum, the outline of the future alveoli. Myofibroblast progenitors, endothelial cells, fibroblasts, and lipofibroblasts (LIFs) cover the secondary septa, and matrix proteins such elastin are deposited at the tip [23,25,90,91]. At first, alveolarization is quite fast (known as "bulk alveolarization"), but then, this process is slowed down, giving rise to the continued alveolarization. As the alveoli mature, the surrounding capillaries are remodeled, forming the capillary unit, and the endothelial cells are located in the proximity of the AEC1 cells permitting an efficient gas exchange. This process is known as microvascular maturation and occurs simultaneously with alveolarization [23,25,30,90–93].

Secondary septation is intimately associated with several signaling events. For example, platelet-derived growth factor α (PDGFα) regulates myofibroblast differentiation and elastin production; TGFβ regulates elastin expression [90,91,94], whereas ephrin B2 plays an essential role in endothelial cells. Furthermore, *fgfr3/fgfr4* double null mice fail to generate the secondary septa pointing to a role for FGF signaling in controlling this event [95]. Finally, RA is crucial for proper alveolar formation [23,25].

Alveologenesis in the developing lung is partially regulated by vitamin A [96], and endogenous RA is present in the postnatal lung [97,98]. Retinoids have been recognized over the years as alveolar morphogens and possible therapeutic mediators [99]. Different studies have demonstrated that vitamin A deficiency induces major histological changes in the lung, namely: airspace enlargement, thinner alveolar walls, more alveolar breaks, and an increase in the mean free distance in the air spaces [100]. Furthermore, vitamin A deficiency impairs lung epithelial function in rodents and promotes bronchopulmonary dysplasia (BPD) in humans [101,102]. The precise mechanism by which RA regulates alveolar formation remains poorly understood, although RA regulation of myofibroblast proliferation was shown to rely on intact FGF signaling [25]. Conversely, RA supplementation in explant culture induces septation, and retinol treatment of premature lambs promotes alveologenesis [103].

RA signaling machinery is differentially expressed during alveologenesis. For instance, in mice, CRBPI is present in the alveolar walls and exhibits higher expression levels around P9, whereas CRBPII is detected during alveolar formation at P4 [97]. Furthermore, in the rat model, CRABP levels rise shortly after birth, reach its maximum values at P10, and at P21 it is barely detected. These genes were upregulated during alveologenesis in whole rat lung, and isolated LIFs [104], and the alterations in the

expression levels coincide with the morphological transformation of primitive saccules into differentiated alveoli [105,106]. Likewise, RALDH1 and RALDH2 are expressed in a temporal and spatial regulated manner in the lung and are associated with different patterns of alveolar cell wall proliferation. For example, in mice, RALDH1 levels are higher at P4, and it is found in LIFs populating alveolar walls, like CRBPI, and in the bronchial epithelium. Conversely, RALDH2 peaks just before birth, it slowly declines during alveologenesis, and it is expressed in the bronchial epithelium and pleural mesothelial cells but not in the alveolar walls [107]. Secondary septation is RALDH/RA-dependent. Epithelium-derived vascular endothelial growth factor A (VEGFA) regulates RALDH levels and, consequently, RA production by endothelial cells. RA acts as a paracrine factor to induce the expression of FGF18 by lung fibroblasts that, on its turn, regulates elastin deposition [108].

RA and RAR receptors are crucial for septation and secondary crest formation [94]. RARα, RARβ, and RARγ were identified in rat lung isolated LIFs and in postnatal mice lung, namely RARα1, RARβ2, RARβ4, and RARγ2 [107]. RARs are present in the alveolar walls, bronchial epithelium, pleura, and bronchial vascular smooth muscle. Their expression changes with time and, in mouse, increases significantly at P4 [97]. Lungs from *rarα−/−* mice are similar to wild type at P14 (end of septation), but, at P50, the alveoli number and surface area are decreased. These results hint that RARα is not vital for alveolar septation, but it may have a role in later phases of alveologenesis [109]. Conversely, increased RA signaling of a dominant active RARα receptor in the epithelium leads to lung immaturity [88]. In *rarβ−/−* mice (exon 10 deletion), septation occurs earlier and faster; also, the administration of RARβ specific agonists in the rat model impairs septation. Overall, it seems that RARβ negatively controls the septation process [110]. However, RARβ seems to be important for neonatal alveolar growth, as disclosed by studying a different *rarβ−/−* mutant (exon 6 deletion) that displayed a decreased surface area of gas exchange [111]. RARγ is required for alveoli formation during the first 28 postnatal days. *rarγ−/−* display a decrease in the elastic tissue of the whole lung, and the alveoli number. In contrast, the distance between the alveolar walls and the mean chord length increased. Additionally, in lipofibroblasts, the trophoelastin mRNA decreased at P12 [94]. Moreover, RARγ agonist's administration promotes alveolar repair in an animal model of emphysema [112]. Altogether, it seems that RARγ positively regulates pulmonary septation. Furthermore, in cultured LIFs, it was demonstrated that RARβ and RARγ increase at birth, which corresponds to the peak of RA storage. The increase in RARγ is temporary since it decreases after P2 (RA in the LIFs also decreases after postnatal day 2). In summary, RA may act at RARγ level in the early postnatal period [107]. RAR heterodimerizes with RXR before binding to DNA. Homozygous null RXR-α mice die *in utero*. Additionally, null for RARγ and heterozygote for RXR-α present

decreased elastin expression in the LIFs at P10; and a decrease in pulmonary elastic tissue in the alveolar septa and not at the airway or vascular walls at P28 [94].

After the administration of retinyl palmitate to pregnant rats, the levels of retinyl esters increase in the fetal and postnatal lung [113], which implies that fetal lungs store retinol or retinyl esters from the progenitor. The lung is the second biggest storing place of retinoids following the liver [114]. LIFs are the main retinoid reservoir of the lung and contain all the components of the pathway [104,114,115]; consequently, they can uptake circulating retinol or hydrolyze stored retinyl esters and convert them into retinol or RA [116,117]. LIFs are localized in the septating tissue adjacent to AEC2 [118]. LIFs generate all-trans retinoic acid (ATRA) that acts autocrinally to upregulate elastin gene expression and synthesis, thus playing a crucial role in the induction of septal eruption [116,119,120]. Moreover, ATRA acts paracrinally to induce proliferation of the adjacent AEC2 [121,122], gene expression [115], and angiogenesis in microvascular endothelial cells [123]. After birth, esters start to disappear from the lung and are converted into active forms, like retinol and RA [98,104,124]. Retinyl esters are abundant in the last three prenatal days (similar amount comparing to the liver) [117], and its depletion correlates with lung maturation [98]. Retinoid clearance is associated with changes in the epithelium of the conducting airways. Specifically, cell phenotype alters from stratified columnar epithelium with goblet cells to keratinizing squamous epithelium [125].

RA regulates positively or negatively the expression of many genes. Among them, RA is important for the synthesis of the surfactant proteins SPA, SPB, and SPC. Administration of retinyl palmitate at high doses to pregnant rats elevates both total phospholipid and the desaturated portion of phosphatidylcholine of the pulmonary surfactant. However, SPA concentration remains unchanged. Additionally, repetitive RA administration increases surfactant phospholipid content [126]. On the other hand, RA also has inhibitory actions. In some studies, it was shown that RA decreases the expression of both mRNA and protein levels of SPA [127].

Regenerative processes are intimately connected with the reawakening of developmental programs [128], and RA has been described as important in alveolar regeneration. Exogenous ATRA, RARα and RARγ agonists and 4-oxo RA can induce alveolar regeneration in adult rats displaying emphysema and partially rescue their phenotype [110,112,129]. On the contrary, pan RXR agonist, 13-cis RA, and retinol were not regeneration inducers, and RARβ was not required for regeneration [130]. In some studies, ATRA was shown to induce apoptosis, a normal process in wound healing, in rats previously treated with elastase, rescuing the alveolar surface area whereas, in others, RA did not affect lung function [131,132]. Recently, using lung organoid models, it was shown that RA pathway stimulation led to a

decrease in the organoid size and inhibited epithelial proliferation. In contrast, RA pathway inhibition promoted epithelial proliferation in mice lung organoids and human organoids from chronic obstructive pulmonary disease (COPD) patients. In the mouse model, increased proliferation happened with concomitant suppression of epithelial differentiation from the airway and alveolar epithelium. Furthermore, cell proliferation was intermediated by YAP (yes-associated protein) activation and FGF signaling. Lastly, the inhibition of Histone deacetylase in combination with ATRA was proposed as a potential method to restore adult lung epithelial cell differentiation [133]. An *in silico* study provided the first clues regarding the possible role of ATRA in minimizing inflammation in elastase-induced emphysema in rat lungs and, therefore, in alveolar epithelium regeneration. It was proposed that ATRA can bind to receptors and ligands of both ERK and JAK-STAT signaling pathways, namely, TNF-α, IL6ST, TNFR1, and IL6. Furthermore, ATRA showed more binding efficiency for TNF-α and IL6ST and can potentially regulate both ERK and JAK-STAT pathways by acting at its first steps. ATRA administration restored lung histology, the proteases/antiproteases balance (imbalance is characteristic of emphysema condition), the levels of inflammatory markers and antioxidants, and the expression of candidate genes of ERK and JAK-STAT. In conclusion, ATRA reduces inflammation and improves alveolar epithelium regeneration in rat lung with emphysema [134].

VASCULAR DEVELOPMENT

The pulmonary vasculature forms synchronously with the airways by a process called distal angiogenesis [135]. Actually, disruption of lung vascular development impairs airway and alveolar formation, a feature that characterizes some congenital lung diseases [136]. VEGFA plays a crucial role in the interaction between the epithelial and endothelial compartment [137]. On its turn, new endothelial cells are bordered by pericytes that require PDGFβ signaling [138]. As it occurs with airway formation, fine-tuning of multiple signaling pathways is essential for vascular development [136].

RA signaling regulates the proliferation of endothelial cells during vasculogenesis in mice embryos and yolk sacs [139]. In the particular case of the lung, Schmidt *et al.* [140] suggested that prenatal administration of RA improves lung vascularization and VEGF expression in a rat model of congenital diaphragmatic hernia (CDH). Later in development, during alveologenesis, endothelial cells produce RA that promotes FGF18 expression in adjacent mesenchymal cells, thus regulating elastin production. Simultaneously, RA acts autocrinally controlling endothelial cell proliferation and tube formation [108]. More recently, it has been demonstrated that RA signaling is involved in pericyte migration, angiogenesis, and collagen IV expression [141].

RA and Lung Disease

Retinoic Acid is a key regulator of pulmonary organogenesis and homeostasis by orchestrating the different phases of lung development. Impairment of RA signaling has catastrophic effects on the development of the respiratory system. Such defects include lung hypoplasia, pulmonary agenesis, lack of esophageal-tracheal septum, and congenital diaphragmatic hernia (CDH) both in animal models and in humans [4,55,142,143]. Dietary vitamin A deficiency (VAD) during pregnancy represents a major concern in developing countries who do not have access to well-balanced food intake and, consequently, are more prone to develop RA-associated fetal lung diseases [3]. The genetic burden, particularly the presence of mutations in the RA machinery, also contributes to developing more or less dramatic lung phenotypes.

In the particular case of CDH, which is characterized by a spectrum of lung hypoplasia and consequent pulmonary hypertension, several studies reported a defective RA signaling [61,143]. CDH has been observed in infants with decreased levels of serum retinol and RBP; and in individuals with deletions in chromosome 15q, where the RA signaling machinery components are located. Moreover, *rarαβ2* knockout animals display unilateral lung agenesis, contralateral lung hypoplasia, and diaphragmatic defects, which are features of CDH [55,142–144]. Furthermore, vitamin A/RA supplementation has a very positive effect on nitrofen-induced rat model of CDH (inhibition of RALDH2). In this case, RA pathway stimulation reduces CDH incidence, improves lung hypoplasia, vascular abnormalities, and, consequently, lung development [143].

Chronic respiratory disorders such as pulmonary fibrosis, lung cancer, emphysema, and COPD, are also VAD-related. Likewise, under VAD conditions, childhood asthma and respiratory infections are promoted [3,145]. On the other hand, retinoids can be applied to promote alveolarization of premature infants at risk of bronchopulmonary dysplasia; or to stimulate the alveolar development and de novo surfactant production of CDH-associated pulmonary hypoplasia [146–148].

Final Remarks

The importance of RA signaling during embryonic development and, specifically, during pulmonary organogenesis is indisputable. From lung specification to alveologenesis, RA signaling fine-tunes the epithelial-mesenchymal interactions that trigger the formation of a fully functional organ. With this review, we aimed to describe the current knowledge regarding the role of RA in the distinct phases of lung development. Alterations in this signaling pathway cause major developmental defects, but that,

by itself, would be a topic for an extensive review. Table 1 summarizes: (1) the specific RA components/crosstalk involved in each of the phases; (2) the phenotype when RA components are silenced, demonstrating its involvement in the etiology of some developmental lung diseases. Moreover, and considering Retinoic Acid role in the later phases, RA might be a suitable candidate to improve some chronic diseases in the adult by promoting regenerating/repair events.

Table 1 - Summary of Retinoic Acid components, crosstalk, and knockouts during lung development.

Lung Developmental Phase	RA Pathway Machinery	RA Pathway Targets	Knockouts with Lung Phenotype	References
Embryonic	cyp26 raldh2 RARα, β, γ	fgf10, FGFR2 WNT, wnt2/2b TGFβ HH bmp4 nkx2.1	raldh2−/− (lung agenesis)	[40–47]
Pseudoglandular	stra6 crbp raldh1, 2, 3 cyp26 rarα1, α2, β, γ coup-tfII	fgf10, fgfr2 shh bmp4 foxa2 tgfβ2, β3 cftr hoxa2, a5, b5, b6 HOXB5 acta myh11 sox2, sox9, id2 meis2 crbpl raldh1 rarβ, RARα, β, γ	rdh10−/− (absence of lung, primary lung bud growth arrested and branching impaired) raldh2−/− (hypoplastic lungs, defective growth and branching) rarαβ2−/− (lung agenesis and hypoplasia, absence of lung budding, altered branching)	[16,41,43,49–58,62,64,69–71]
Canalicular	RARα	-	-	[84]
Saccular	rarα, β, γ	-	-	[84,88]
Alveolar	CRBPI, II CRABP RALDH1, 2 RARα, β, γ RXR	VEGFA FGF signaling SPA, B, C, spa YAP TNF-α, TNFR1 IL6, IL6ST	rarα−/− (↓ alveolar number and surface area) rarβ−/− (early & faster septation; ↓ surface area) rarγ−/− (↓ elastic tissue, ↓ alveoli number, ↑ distance between the alveolar walls) rxrα−/− (embryonic lethality) rarγ−/−, rxrα+/− (↓ elastic tissue at the alveolar septa)	[88,94,97,104,107–112,123,126,127,130,134]

↓, decrease; ↑, increase

REFERENCES

1. Cunningham, T.J.; Duester, G. Mechanisms of retinoic acid signalling and its roles in organ and limb development. Nat. Rev. Mol. Cell Biol. 2015, 16, 110–123, doi:10.1038/nrm3932.

2. Ghyselinck, N.B.; Duester, G. Retinoic acid signaling pathways. Development 2019, 146, doi:10.1242/dev.167502.

3. Timoneda, J.; Rodríguez-Fernández, L.; Zaragozá, R.; Marín, M.P.; Cabezuelo, M.T.; Torres, L.; Viña, J.R.; Barber, T. Vitamin A Deficiency and the Lung. Nutrients 2018, 10, doi:10.3390/nu10091132.

4. Cardoso, W.V.; Chen, F. Retinoic Acid in the Developing Lung and Other Foregut Derivatives. In The Retinoids: Biology, Biochemistry, and Disease, Dollé, P., Neiderreither, K., eds.; John Wiley & Sons: IncHoboken, NJ, USA, 2015; pp. 371–382; doi:10.1002/9781118628003.ch16.

5. Quadro, L.; Blaner, W.S.; Salchow, D.J.; Vogel, S.; Piantedosi, R.; Gouras, P.; Freeman, S.; Cosma, M.P.; Colantuoni, V.; Gottesman, M.E. Impaired retinal function and vitamin A availability in mice lacking retinol-binding protein. EMBO J. 1999, 18, 4633–4644, doi:10.1093/emboj/18.17.4633.

6. Kawaguchi, R.; Yu, J.; Honda, J.; Hu, J.; Whitelegge, J.; Ping, P.; Wiita, P.; Bok, D.; Sun, H. A membrane receptor for retinol binding protein mediates cellular uptake of vitamin A. Science 2007, 315, 820–825, doi:10.1126/science.1136244.

7. Fex, G.; Johannesson, G. Retinol transfer across and between phospholipid bilayer membranes. Biochim. Biophys Acta 1988, 944, 249–255, doi:10.1016/0005-2736(88)90438-5.

8. Napoli, J.L. Cellular retinoid binding-proteins, CRBP, CRABP, FABP5: Effects on retinoid metabolism, function and related diseases. Pharm. Thera. 2017, 173, 19–33, doi:10.1016/j.pharmthera.2017.01.004.

9. Kim, Y.K.; Wassef, L.; Hamberger, L.; Piantedosi, R.; Palczewski, K.; Blaner, W.S.; Quadro, L. Retinyl ester formation by lecithin: Retinol acyltransferase is a key regulator of retinoid homeostasis in mouse embryogenesis. J. Biol. Chem. 2008, 283, 5611–5621, doi:10.1074/jbc.M708885200.

10. Sandell, L.L.; Sanderson, B.W.; Moiseyev, G.; Johnson, T.; Mushegian, A.; Young, K.; Rey, J.P.; Ma, J.X.; Staehling-Hampton, K.; Trainor, P.A. RDH10 is essential for synthesis of embryonic retinoic acid and is required for limb, craniofacial, and organ development. Genes Dev. 2007, 21, 1113–1124, doi:10.1101/gad.1533407.

11. Shannon, S.R.; Moise, A.R.; Trainor, P.A. New insights and changing paradigms in the regulation of vitamin A metabolism in development. Wiley Interdiscip. Rev. Dev. Biol. 2017, 6, doi:10.1002/wdev.264.

12. Napoli, J.L. Physiological insights into all-trans-retinoic acid biosynthesis. Biochim. Biophys Acta 2012, 1821, 152–167, doi:10.1016/j.bbalip.2011.05.004.

13. Feng, L.; Hernandez, R.E.; Waxman, J.S.; Yelon, D.; Moens, C.B. Dhrs3a regulates retinoic acid biosynthesis through a feedback inhibition mechanism. Dev. Biol. 2010, 338, 1–14, doi:10.1016/j.ydbio.2009.10.029.

14. Duester, G. Retinoic acid synthesis and signaling during early organogenesis. Cell 2008, 134, 921–931, doi:10.1016/j.cell.2008.09.002.

15. Rhinn, M.; Dollé, P. Retinoic acid signalling during development. Development 2012 139, 843–858, doi:10.1242/dev.065938.

16. Niederreither, K.; Fraulob, V.; Garnier, J.M.; Chambon, P.; Dollé, P. Differential expression of retinoic acid-synthesizing (RALDH) enzymes during fetal development and organ differentiation in the mouse. Mech. Dev. 2002, 110, 165–171, doi: 10.1016/s0925-4773(01)00561-5.

17. Ross, A.C.; Zolfaghari, R. Cytochrome P450s in the regulation of cellular retinoic acid metabolism. Annu. Rev. Nutr. 2011, 31, 65–87, doi:10.1146/annurev-nutr-072610-145127.

18. Ong, D.E. Cellular transport and metabolism of vitamin A: Roles of the cellular retinoid-binding proteins. Nutr. Rev. 1994, 5, S24–S31, doi:10.1111/j.1753-4887.1994.tb01383.x.

19. Chambon, P. A decade of molecular biology of retinoic acid receptors. FASEB J. 1996, 10, 940–954, doi:10.1096/fasebj.10.9.8801176.

20. Metzler, M.A.; Sandell, L.L. Enzymatic Metabolism of Vitamin A in Developing Vertebrate Embryos. Nutrients 2016, 8, doi:10.3390/nu8120812.

21. Quanjer, P.H.; Stanojevic, S.; Cole, T.J.; Baur, X.; Hall, G.L.; Culver, B.H.; Enright, P.L.; Hankinson, J.L.; Ip, M.S.M.; Zheng, J.; et al. Multi-ethnic reference values for spirometry for the 3-95-yr age range: The global lung function 2012 equations. Eur. Respir. J. 2012, 40, 1324–1343, doi:10.1183/09031936.00080312.

22. Stocks, J.; Hislop, A.; Sonnappa, S.; Early lung development: Lifelong effect on respiratory health and disease. Lancet Respir. Med. 2013, 1,728–742, doi:10.1016/S2213-2600(13)70118-8.

23. Burri, P.H. Structural Aspects of Postnatal Lung Development–Alveolar Formation and Growth. Biol. Neonate 2006, 89, 313–322, doi:10.1159/000092868.

24. Hogan, B.L.M.; Barkauskas, C.E.; Chapman, H.A.; Epstein, J.A.; Jain, R.; Hsia, C.C.W.; Niklason, L.; Calle, E.; Le, A.; Randell, S.H.; et al. Repair and regeneration of the respiratory system: Complexity, plasticity, and mechanisms of lung stem cell function. Cell Stem Cell 2014, 15, 123–138, doi:10.1016/j.stem.2014.07.012.

25. Morrisey, E.E.; Hogan, B.L.M. Preparing for the First Breath: Genetic and Cellular Mechanisms in Lung Development. Dev. Cell 2010, 1, 8–23, doi:10.1016/j.devcel.2009.12.010.

26. McCulley, D.; Wienhold, M.; Sun, X. The pulmonary mesenchyme directs lung development. Curr. Opin. Genet. Dev. 2015, 32, 98–105, doi:10.1016/j.gde.2015.01.011.

27. Warburton, D.; Perin, L.; Defilippo, R.; Bellusci, S.; Shi, W.; Driscoll, B. Stem/progenitor cells in lung development, injury repair, and regeneration. Proc. Am. Thorac. Soc. 2008, 5, 703–706, doi:10.1513/pats.200801-012AW.

28. Kim, H.Y.; Pang, M.F.; Varner, V.D.; Kojima, L.; Miller, E.; Radisky, D.C.; Nelson, C.M. Localized Smooth Muscle Differentiation Is Essential for Epithelial Bifurcation during Branching Morphogenesis of the Mammalian Lung. Dev. Cell 2015, 34, 719–726, doi:10.1016/j.devcel.2015.08.012.

29. Warburton, D.; El-Hashash, A., Carraro, G.; Tiozzo, C.; Sala, F.; Rogers, O.; De Langhe, S.; Kemp, P.J.; Riccardi, D.; Torday, J.; et al. Chapter Three-Lung Organogenesis. In Current Topics in Developmental Biology; Koopman, P.; Academic Press: Cambridge, MA, USA, 2010; Volume 90, pp. 73–158, doi:10.1016/S0070-2153(10)90003-3.

30. Schittny, J.C. Development of the lung. Cell Tissue Res. 2017, 367, 427–444, doi: 10.1007/s00441-016-2545-0.

31. Herriges, M.; Morrisey, E.E. (2014) Lung development: Orchestrating the generation and regeneration of a complex organ. Development 2014, 141, 502–513, doi:10.1242/dev.098186.

32. Fernandes-Silva, H.; Correia-Pinto, J.; Moura, R.S.; Canonical Sonic Hedgehog Signaling in Early Lung Development. J. Dev. Biol. 2017, 5, 3, doi:10.3390/jdb5010003.

33. Hussain, M.; Xu, C.; Lu, M.; Wu, X.; Tang, L.; Wu, X. Wnt/β-catenin signaling links embryonic lung development and asthmatic airway remodeling. Biochim. Biophys Acta Mol. Basis Dis. 2017, 1863, 3226–3242, doi:10.1016/j.bbadis.2017.08.031.

34. Ning, J.; Zhao, Y.; Ye, Y.; Yu, J. Opposing roles and potential antagonistic mechanism between TGF-β and BMP pathways: Implications for cancer progression. EBioMedicine 2019, 41, 702–710, doi:10.1016/j.ebiom.2019.02.033.

35. Danopoulos, S.; Shiosaki, J.; Al Alam, D. FGF Signaling in Lung Development and Disease: Human Versus Mouse. Front. Genet. 2019, 10, 170, doi:10.3389/fgene.2019.00170.

36. Yeung, B.; Yu, J.; Yang, X. Roles of the Hippo pathway in lung development and tumorigenesis. Int. J. Cancer 2016, 138, 533–539, doi:10.1002/ijc.29457.

37. Lazzaro, D.; Price, M.; Felice, M.D.E.; Lauro, R.D.I. The transcription factor TTF-1 is expressed at the onset of thyroid and lung morphogenesis and in restricted regions of the foetal brain. Development 1991, 113, 1093–1104, doi:10.1242/dev.113.4.1093

38. Goss, A.M.; Tian, Y., Tsukiyama, T.; Cohen, E.D.; Zhou, D.; Lu, M.M.; Yamaguchi, T.P.; Morrisey, E.E. Wnt2/2b and -Catenin Signaling Are Necessary and Sufficient to Specify Lung Progenitors in the Foregut. Dev. Cell 2009 17, 290–298, doi:10.1016/j.devcel.2009.06.005.

39. Domyan, E.T.; Ferretti, E.; Throckmorton, K.; Mishina, Y.; Nicolis, S.K.; Sun, X. Signaling through BMP receptors promotes respiratory identity in the foregut via repression of Sox2. Development 2011, 138, 971–981, doi:10.1242/dev.053694.

40. Chen, F.; Desai, T.J.; Qian, J.; Niederreither, K.; Lü, J.; Cardoso, W.V. Inhibition of Tgf signaling by endogenous retinoic acid is essential for primary lung bud induction. Development 2007, 134, 2969–2979, doi:10.1242/dev.006221.

41. Malpel, S.; Mendelsohn, C.; Cardoso, W.V. Regulation of retinoic acid signaling during lung morphogenesis. Development 2000, 127, 3057–3067, doi:10.1242/dev.127.14.3057.

42. Desai, T.J.; Malpel, S.; Flentke, G.R.; Smith, S.M.; Cardoso, W.V. Retinoic acid selectively regulates Fgf10 expression and maintains cell identity in the prospective lung field of the developing foregut. Dev. Biol. 2004, 273, 402–415, doi:10.1016/j.ydbio.2004.04.039.

43. Wang, Z.; Dollé, P.; Cardoso, W.V.; Niederreither, K. Retinoic acid regulates morphogenesis and patterning of posterior foregut derivatives. Dev. Biol. 2006, 297, 433-445, doi:10.1016/j.ydbio.2006.05.019.

44. Desai, T.J.; Chen, F.; Lü, J.; Qian, J.; Niederreither, K.; Dollé, P.; Chambon, P.; Cardoso, W.V. Distinct roles for retinoic acid receptors alpha and beta in early lung morphogenesis. Dev. Biol. 2006, 291, 12–24, doi:10.1016/j.ydbio.2005.10.045.

45. Chen, F.; Cao, Y.; Qian, J.; Shao, F.; Niederreither, K.; Cardoso, W.V. A retinoic acid–dependent network in the foregut controls formation of the mouse lung primordium. J. Clin. Invest. 2010, 120, 2040–2048, doi:10.1172/JCI40253.

46. Rankin, S.A.; Han, L.; Kyle, W.; Wells, J.M.; John, M.; Zorn, A.M.; Rankin, S.A.; Han, L.; Mccracken, K.W.; Kenny, A.P.; et al. Article A Retinoic Acid-Hedgehog Cascade Coordinates Mesoderm-Inducing Signals and Endoderm Competence during Lung Specification. Cell Reports 2016, 16, 66–78, doi:10.1016/j.celrep.2016.05.060.

47. Rankin, S.A.; McCracken, K.W.; Luedeke, D.M.; Han, L.; Wells, J.M.; Shannon, J.M.; Zorn, A.M. Timing is everything: Reiterative Wnt, BMP and RA signaling regulate developmental competence during endoderm organogenesis. Dev. Biol. 2018, 434, 121–132, doi:10.1016/j.ydbio.2017.11.018.

48. Metzger, R.J.; Klein, O.D.; Martin, G.R.; Krasnow, M.A. The branching programme of mouse lung development. Nature 2008, 453, 745–750, doi:10.1038/nature07005.

49. Chazaud, C.; Dollé, P.; Rossant, J.; Mollard, R. Retinoic acid signaling regulates murine bronchial tubule formation. Mech. Dev. 2003, 120, 691–700, doi:10.1016/s0925-4773(03)00048-0.

50. Fernandes-Silva, H.; Vaz-Cunha, P.; Barbosa, V.B.; Silva-Gonçalves, C.; Correia-Pinto, J.; Moura, R.S. Retinoic acid regulates avian lung branching through a molecular network. Cell Mol. Life Sci. 2017 74, 4599–4619, doi:10.1007/s00018-017-2600-3.

51. Rhinn, M.; Schuhbaur, B.; Niederreither, K.; Dollé, P. Involvement of retinol dehydrogenase 10 in embryonic patterning and rescue of its loss of function by maternal retinaldehyde treatment. Proc. Natl. Acad. Sci. USA 2011, 108, 16687–16692, doi:10.1073/pnas.1103877108.

52. Bouillet, P.; Sapin, V.; Chazaud, C.; Messaddeq, N.; Décimo, D.; Dollé, P.; Chambon, P. Developmental expression pattern of Stra6, a retinoic acid-responsive gene encoding a new type of membrane protein. Mech. Dev. 1997, 63, 173–186, doi:10.1016/s0925-4773(97)00039-7.

53. Dollé, P.; Ruberte, E.; Leroy, P.; Morriss-Kay, G.; Chambon, P. Retinoic acid receptors and cellular retinoid binding proteins. I. A systematic study of their differential pattern of transcription during mouse organogenesis. Development 1990, 110, 1133–1151, doi:10.1242/dev.110.4.1133.

54. Bellusci, S.; Grindley, J.; Emoto, H.; Itoh, N.; Hogan, B.L. Fibroblast growth factor 10 (FGF10) and branching morphogenesis in the embryonic mouse lung. Development 1997, 124, 4867–4878, doi:10.1242/dev.124.23.4867.

55. Mendelsohn, C.; Lohnes, D.; Décimo, D.; Lufkin, T.; LeMeur, M.; Chambon, P.; Mark, M. Function of the retinoic acid receptors (RARs) during development (II). Multiple abnormalities at various stages of organogenesis in RAR double mutants. Development 1994 120, 2749–2771, doi:10.1242/dev.120.10.2749.

56. Mollard, R.; Ghyselinck, N.B.; Wendling, O.; Chambon, P.; Mark, M. Stage-dependent responses of the developing lung to retinoic acid signaling. Int. J. Dev. Biol. 2000, 44, 457–462.

57. Lohnes, D.; Mark, M.; Mendelsohn, C.; Dollé, P.; Dierich, A.; Gorry, P.; Gansmuller, A.; Chambon, P. Function of the retinoic acid receptors (RARs) during development (I). Craniofacial and skeletal abnormalities in RAR double mutants. Development 1994, 120, 2723–2748, doi:10.1242/dev.120.10.2723.

58. Lü, J.; Qian, J.; Izvolsky, K.I.; Cardoso, W.V. Global analysis of genes differentially expressed in branching and non-branching regions of the mouse embryonic lung. Dev. Biol. 2004, 273, 418–435, doi:10.1016/j.ydbio.2004.05.035.

59. Moura, R.S.; Coutinho-Borges, J.P.; Pacheco, A.P.; Damota, P.O.; Correia-Pinto, J. FGF signaling pathway in the developing chick lung: Expression and inhibition studies. PLoS ONE 2011, 6, doi:10.1371/journal.pone.0017660.

60. Schuger, L.; Varani, J.; Mitra, R.Jr.; Gilbride, K. Retinoic acid stimulates mouse lung development by a mechanism involving epithelial-mesenchymal interaction and regulation of epidermal growth factor receptors. Dev. Biol. 1993, 159, 462–473, doi:10.1006/dbio.1993.1256.

61. Montedonico, S.; Nakazawa, N.; Puri, P. Retinoic acid rescues lung hypoplasia in nitrofen-induced hypoplastic foetal rat lung explants. Pediatr. Surg. Int. 2006, 22, 2–8, doi:10.1007/s00383-005-1571-x.

62. Pereira-Terra, P.; Moura, R.S.; Nogueira-Silva, C.; Correia-Pinto, J. Neuroendocrine factors regulate retinoic acid receptors in normal and hypoplastic lung development. J. Physiol. 2015, 593, 3301–3311, doi:10.1113/JP270477.

63. Cardoso, W.V.; Williams, M.C.; Mitsialis, S.A.; Joyce-Brady, M.; Rishi, A.K.; Brody, J.S. Retinoic acid induces changes in the pattern of airway branching and alters epithelial cell differentiation in the developing lung in vitro. Am. J. Respir. Cell Mol. Biol. 1995, 12, 464–476, doi:10.1165/ajrcmb.12.5.7742011.

64. Cardoso, W.V.; Mitsialis, S.A.; Brody, J.S.; Williams, M.C. Retinoic acid alters the expression of pattern-related genes in the developing rat lung. Dev. Dyn. 1996, 207, 47–59, doi:10.1002/(SICI)1097-0177(199609)207:1<47::AID-AJA6>3.0.CO;2-W.

65. Urase, K.; Mukasa, T.; Igarashi, H.; Ishii, Y.; Yasugi, S.; Momoi, M.Y.; Momoi, T. Spatial expression of Sonic hedgehog in the lung epithelium during branching morphogenesis. Biochem. Biophys. Res. Commun. 1996, 225, 161–166, doi:10.1006/bbrc.1996.1147.

66. Lebeche, D.; Malpel, S.; Cardoso, W.V. Fibroblast growth factor interactions in the developing lung. Mech. Dev. 1999, 86, 125–136, doi:10.1016/s0925-4773(99)00124-0.

67. Weaver, M.; Yingling, J.M.; Dunn, N.R.; Bellusci, S.; Hogan, B.L. Bmp signaling regulates proximal-distal differentiation of endoderm in mouse lung development. Development 1999, 126, 4005–4015, doi:10.1242/dev.126.18.4005.

68. Zhou, L.; Dey, C.R.; Wert, S.E.; Yan, C.; Costa, R.H.; Whitsett, J.A. Hepatocyte nuclear factor-3beta limits cellular diversity in the developing respiratory epithelium and alters lung

morphogenesis in vivo. Dev. Dyn. 1997, 210, 305–314, doi:10.1002/(SICI)1097-0177(199711)210:3<305::AID-AJA10>3.0.CO;2-9.

69. Bogue, C.W.; Gross, I.; Vasavada, H.; Dynia, D.W.; Wilson, C.M.; Jacobs, H.C. Identification of Hox genes in newborn lung and effects of gestational age and retinoic acid on their expression. Am. J. Physiol. 1994, 266, L448–L454, doi:10.1152/ajplung.1994.266.4.L448.

70. Volpe, M.V.; Vosatka, R.J.; Nielsen, H.C. Hoxb-5 control of early airway formation during branching morphogenesis in the developing mouse lung. Biochim. Biophys. Acta 2000, 1475, 337–345, doi:10.1016/s0304-4165(00)00087-8.

71. Chen, F.; Marquez, H.; Kim, Y.K.; Qian, J.; Shao, F.; Fine, A.; Cruikshank, W.W.; Quadro, L.; Cardoso, W.V. Prenatal retinoid deficiency leads to airway hyperresponsiveness in adult mice. J. Clin. Invest. 2014, 124, 801–811, doi:10.1172/JCI70291.

72. Gontan, C.; de Munck, A.; Vermeij, M.; Grosveld, F.; Tibboel, D.; Rottier, R. Sox2 is important for two crucial processes in lung development: Branching morphogenesis and epithelial cell differentiation. Dev. Biol. 2008, 317, 296–309, doi:10.1016/j.ydbio.2008.02.035.

73. Rockich, B.; Hrycaj, S.M.; Shih, H.P.; Nagy, M.S.; Ferguson, M.A.; Kopp, J.L.; Sander, M.; Wellik, D.M.; Spence, J.R. Sox9 plays multiple roles in the lung epithelium during branching morphogenesis. Proc. Natl. Acad. Sci. USA 2013, 110, E4456–E4464, doi:10.1073/pnas.1311847110.

74. deMello, D.E.; Reid, L.M. Embryonic and early fetal development of human lung vasculature and its functional implications. Pediatr. Dev. Pathol. 2000, 3, 439–449, doi:10.1007/s100240010090.

75. Ornitz, D.M.; Yin, Y. Signaling networks regulating development of the lower respiratory tract. Cold Spring Harb. Perspect. Biol. 2012, 4, doi:10.1101/cshperspect.a008318.

76. Boyden, E.A. The structure of the pulmonary acinus in a child of six years and eight months. Am. J. Anat. 1971, 132, 275–299, doi:10.1002/aja.1001320302.

77. Kitaoka, H.; Burri, P.H.; Weibel, E.R. Development of the human fetal airway tree: Analysis of the numerical density of airway endtips. Anat. Rec. 1996, 244, 207–213, doi:10.1002/(SICI)1097-0185(199602)244:2<207::AID-AR8>3.0.CO;2-Y.

78. DiMaio, M.; Gil, J.; Ciurea, D.; Kattan, M. Structural maturation of the human fetal lung: A morphometric study of the development of air-blood barriers. Pediatr. Res. 1989, 26, 88–93, doi:10.1203/00006450-198908000-00002.

79. McQualter, J.L.; Yuen, K.; Williams, B.; Bertoncello, I. Evidence of an epithelial stem/progenitor cell hierarchy in the adult mouse lung. Proc. Natl. Acad. Sci. USA 2010, 107, 1414–1419, doi:10.1073/pnas.0909207107.

80. Nolen-Walston, R.D.; Kim, C.F.; Mazan, M.R.; Ingenito, E.P.; Gruntman, A.M.; Tsai, L.; Boston, R.; Woolfenden, A.E.; Jacks, T.; Hoffman, A.M. Cellular kinetics and modeling of bronchioalveolar stem cell response during lung regeneration. Am. J. Physiol. Lung Cell Mol. Physiol. 2008, 294, 1158–1166, doi:10.1152/ajplung.00298.2007.

81. Barré, S.F.; Haberthür, D.; Cremona, T.P.; Stampanoni, M.; Schittny, J.C. The total number of acini remains constant throughout postnatal rat lung development. Am. J. Physiol. Lung Cell. Mol. Physiol. 2016, 311, L1082–L1089, doi:10.1152/ajplung.00325.2016.

82. DeMello, D.E.; Sawyer, D.; Galvin, N.; Reid, L.M. Early Fetal Development of Lung Vasculature. Am. J. Respir. Cell Mol. Biol. 1997, 16, 568–581, doi:10.1165/ajrcmb.16.5.9160839.

83. Vu, T.H.; Alemayehu, Y.; Werb, Z. New insights into saccular development and vascular formation in lung allografts under the renal capsule. Mech. Dev. 2003, 120, 305–313, doi:10.1016/s0925-4773(02)00451-3.

84. Grummer, M.A.; Thet, L.A.; Zachman, R.D. Expression of retinoic acid receptor genes in fetal and newborn rat lung. Pediatr. Pulmonol. 1994, 17, 234–238, doi:10.1002/ppul.1950170406.

85. Pawlikowski, B.; Wragge, J.; Siegenthaler, J.A. Retinoic acid signaling in vascular development. Genesis 2019, 57, e23287, doi:10.1002/dvg.23287.

86. Kumar, V.H.; Lakshminrusimha, S.; El, Abiad. M.T.; Chess, P.R.; Ryan, R.M. Growth factors in lung development. Adv. Clin. Chem. 2005, 40, 261–316, doi:10.1016/s0065-2423(05)40007-4.

87. Nikolić, M.Z.; Sun, D.; Rawlins, E.L. Human lung development: Recent progress and new challenges. Development 2018, 145, doi:10.1242/dev.163485.

88. Wongtrakool, C.; Malpel, S.; Gorenstein, J.; Sedita, J.; Ramirez, M.I.; Underhill, T.M.; Cardoso, W.V. Down-regulation of retinoic acid receptor alpha signaling is required for sacculation and type I cell formation in the developing lung. J. Biol. Chem. 2003, 278, 46911–46928, doi:10.1074/jbc.M307977200.

89. Massaro, G.D. Formation of Pulmonary Alveoli and Gas-Exchange Surface Area: Quantitation and Regulation. Annu. Rev. Physiol. 1996, 58, 73–92, doi:10.1146/annurev.ph.58.030196.000445.

90. Boström, H.; Willetts, K.; Pekny, M.; Levéen, P.; Lindahl, P.; Hedstrand, H.; Pekna, M.; Hellström, M.; Gebre-Medhin, S.; Schalling, M. et al. PDGF-A signaling is a critical event in lung alveolar myofibroblast development and alveogenesis. Cell 1996, 85, 863–873, doi:10.1016/s0092-8674(00)81270-2.

91. Lindahl, P.; Karlsson, L.; Hellström, M.; Gebre-Medhin, S.; Willetts, K.; Heath, J.K.; Betsholtz, C. Alveogenesis failure in PDGF-A-deficient mice is coupled to lack of distal spreading of alveolar smooth muscle cell progenitors during lung development. Development 1997, 124, 3943–3953, doi:10.1242/dev.124.20.3943.

92. Burri, P.H. Postnatal growth and maturation of the lung. Chest 1975, 67, 2S–3S, doi:10.1378/chest.67.2_supplement.2s.

93. Caduff, J.H.; Fischer, L.C.; Burri, P.H. Scanning electron microscope study of the developing microvasculature in the postnatal rat lung. Anat. Rec. 1986, 216, 154–164, doi:10.1002/ar.1092160207.

94. McGowan, S.; Jackson, S.K.; Jenkins-Moore, M.; Dai, H.H.; Chambon, P.; Snyder, J.M. Mice bearing deletions of retinoic acid receptors demonstrate reduced lung elastin and alveolar numbers. Am. J. Respir. Cell Mol. Biol 2000, 23, 162–167, doi:10.1165/ajrcmb.23.2.3904.

95. Weinstein, M.; Xu, X.; Ohyama, K.; Deng, C.X. FGFR-3 and FGFR-4 function cooperatively to direct alveogenesis in the murine lung. Development 1998, 125, 3615–3623, doi:10.1242/dev.125.18.3615.

96. Massaro, G.D.; Massaro, D. Treatment with retinoic acid increases the number of pulmonary alveoli. FASEB J. 1996, 270, L305–L310, doi:10.1152/ajplung.1996.270.2.L305.

97. Hind. M.; Corcoran. J.; Maden. M. Temporal/spatial expression of retinoid binding proteins and RAR isoforms in the postnatal lung. Am. J. Physiol. Lung Cell Mol. Physiol. 2002, 282, L468–L476, doi:10.1152/ajplung.00196.2001.

98. Geevarghese, S.K.; Chytil, F. Depletion of retinyl esters in the lungs coincides with lung prenatal morphological maturation. Biochem. Biophys. Res. Commun. 1994, 200, 529–535, doi:10.1006/bbrc.1994.1480.

99. McGowan, S.E. Contributions of retinoids to the generation and repair of the pulmonary alveolus. Chest 2002, 121, 206S–208S, doi:10.1378/chest.121.5_suppl.206s.

100. Baybutt, R.C.; Hu, L.; Molteni, A. Vitamin A Deficiency Injures Lung and Liver Parenchyma and Impairs Function of Rat Type II Pneumocytes. J. Nutr. 2000, 130, 1159–1165, doi:10.1093/jn/130.5.1159.

101. Biesalski, H.K.; Nohr, D. Importance of vitamin-A for lung function and development. Mol. Asp. Med. 2003, 24, 431–440, doi:10.1016/s0098-2997(03)00039-6.

102. Verma, R.P.; Mcculloch, K.M.; Worrell, L.; Vidyasagar, D. Vitamin A deficiency and severe bronchopulmonary dysplasia in very low birthweight infants. Am. J. Perinatol. 1996, 13, 389–393, doi:10.1055/s-2007-994376.

103. Albertine, K.H.; Jones, G.P.; Starcher, B.C.; Bohnsack, J.F.; Davis, P.L.; Cho, S.C.; Carlton, D.P.; Bland, R.D. Chronic lung injury in preterm lambs: Disordered respiratory tract development. Am. J. Respir. Crit. Care Med. 1999, 159, 945–958, doi:10.1164/ajrccm.159.3.9804027.

104. McGowan, S.E.; Harvey, C.S.; Jackson, S.K. Retinoids, retinoic acid receptors, and cytoplasmic retinoid binding proteins in perinatal rat lung fibroblasts. Am. J. Physiol. Lung Cell Mol. Physiol. 1995, 269, L463–L472, doi:10.1152/ajplung.1995.269.4.L463.

105. Powell, J.T.; Whitney, P.L. Postnatal development of rat lung. Changes in lung lectin, elastin, acetylcholinesterase and other enzymes. Biochem. J. 1980, 188, 1–8, doi:10.1042/bj1880001.

106. Ong, D.E.; Chytil, F. Changes in levels of cellular retinol and retinoic acid binding proteins of liver and lung during perinatal development of rat. Proc. Natl. Acad. Sci. USA 1976, 73, 3976–3978, doi:10.1073/pnas.73.11.3976.

107. Hind, M.; Corcoran, J.; Maden, M. Alveolar proliferation, retinoid synthesizing enzymes, and endogenous retinoids in the postnatal mouse lung different roles for Aldh-1 and Raldh-2. Am. J. Respir Cell Mol. Biol. 2002, 26, 67–73, doi:10.1165/ajrcmb.26.1.4575.

108. Yun, E.J.; Lorizio, W.; Seedorf, G.; Abman, S.H.; Vu, T.H. VEGF and endothelium-derived retinoic acid regulate lung vascular and alveolar development. Am. J. Physiol. Lung Cell Mol. Physiol. 2016, 310, L287–L298, doi:10.1152/ajplung.00229.2015.

109. Massaro, G.D.; Massaro, D.; Chambon, P. Retinoic acid receptor-α regulates pulmonary alveolus formation in mice after, but not during, perinatal period. Am. J. Physiol. Lung Cell Mol. Physiol. 2003, 284, 2002–2004, doi:10.1152/ajplung.00245.2002.

110. Massaro, G.D.; Massaro, D.; Chan, W.Y.; Clerch, L.B.; Ghyselinck, N.; Chambon, P.; Chandraratna, R.A.S. Retinoic acid receptor- : An endogenous inhibitor of the perinatal formation of pulmonary alveoli. Physiol. Genom. 2001, 4, 51–57, doi:10.1152/physiolgenomics.2000.4.1.51.

111. Snyder, J.M.; Jenkins-Moore, M.; Jackson, S.K.; Goss, K.L.; Dai, H.H.; Bangsund, P.J.; Giguere, V.; Mcgowan, S.E. Alveolarization in retinoic acid receptor- -deficient mice. Pediatr. Res. 2005, 57, 384–391, doi:10.1203/01.PDR.0000151315.81106.D3.

112. Massaro, G.D.; Massaro, D. Retinoic acid treatment abrogates elastase-induced pulmonary emphysema in rats. Nat. Med. 1997, 3, 675–677, doi:10.1038/nm0697-675.

113. Shenai, J.P.; Chytil, F. Effect of maternal vitamin-A administration on fetal lung vitamin-A stores in the perinatal rat. Biol. Neonate 1990, 58, 318–325, doi:10.1159/000243286.

114. Okabe, T.; Yorifuji, H.; Yamada, E.; Takaku, F. Isolation and characterization of vitamin-A-storing lung cells. Exp. Cell Res. 1984, 154, 125–135, doi:10.1016/0014-4827(84)90673-6.

115. Dirami, G.; Massaro, G.D.; Clerch, L.B.; Ryan, U.S.; Reczek, P.R.; Massaro, D. Lung retinol storing cells synthesize and secrete retinoic acid, an inducer of alveolus formation. Am. J. Physiol. Lung Cell Mol. Physiol. 2018, 286, 249–256, doi:10.1152/ajplung.00140.2003.

116. McGowan, S.E.; Torday, J.S. The pulmonary lipofibroblast (lipid interstitial cell) and its contributions to alveolar development. Annu. Rev. Physiol. 1997, 59, 43–62, doi:10.1146/annurev.physiol.59.1.43.

117. Shenai, J.P.; Chytil, F. Vitamin A storage in lungs during perinatal development in the rat. Biol. Neonate 1990, 57, 126–132, doi:10.1159/000243172.

118. Burri, P.H. The postnatal growth of the rat lung III. Morphology. Anat. Rec. 1974, 180, 77–98, doi:10.1002/ar.1091800109.

119. Mcgowan, S.E.; Doro, M.M.; Jackson, S.K. Endogenous retinoids increase perinatal elastin gene expression in rat lung fibroblasts and fetal explants. Am. J. Physiol. Lung Cell Mol. Physiol. 1997, 273, L410–L416, doi:10.1152/ajplung.1997.273.2.L410.

120. Liu, R.; Harvey, C.S.; McGowan, S.E. Retinoic acid increases elastin in neonatal rat lung fibroblast cultures. Am. J. Physiol. Lung Cell Mol. Physiol. 1993, 265, L430–L437, doi:10.1152/ajplung.1993.265.5.L430.

121. Nabeyrat, E.; Besnard, V.; Corroyer, S.; Cazals, V.; Clement, A. Retinoic acid-induced proliferation of lung alveolar epithelial cells: Relation with the IGF system. Am. J. Physiol. Lung Cell Mol. Physiol. 1998, 275, 71–79, doi:10.1152/ajplung.1998.275.1.L71.

122. Nabeyrat, E.; Corroyer, S.; Epaud, R.; Besnard, R.I.E.; Corroyer, S.; Epaud, R. Retinoic acid-induced proliferation of lung alveolar epithelial cells is linked to p21(CIP1) downregulation. Am. J. Physiol. Lung Cell Mol. Physiol. 2000, 278, L42–L50, doi:10.1152/ajplung.2000.278.1.L42.

123. Ng-Blichfeldt, J.P.; Alçada, J.; Montero, M.A.; Dean, C.H.; Griesenbach, U.; Griffiths, M.J.; Hind, M. Deficient retinoid-driven angiogenesis may contribute to failure of adult human lung regeneration in emphysema. Thorax 2017, 72, 510–521, doi:10.1136/thoraxjnl-2016-208846.

124. Zachman, R.D.; Kakkad, B.; Chytil, F. Perinatal rat lung retinol (vitamin A) and retinyl palmitate. Pediatr. Res. 1984, 18, 1297–1299, doi:10.1203/00006450-198412000-00015.

125. Wolbach, S.B.; Howe, P.R. Tissue Changes Following Deprivation of Fat-Soluble A Vitamin. J. Exp. Med. 1925, 42, 753–791, doi:10.1084/jem.42.6.753.

126. Fraslon, C.; Bourbon, J.R. Retinoids control surfactant phospholipid biosynthesis in fetal rat lung. Am. J. Physiol. Lung Cell Mol. Physiol. 1994, 266, L705–L712, doi:10.1152/ajplung.1994.266.6.L705.

127. Metzler, M.D.; Snyder, J.M. Retinoic acid differentially regulates expression of surfactant-associated proteins in human fetal lung. Endocrinology 1993, 133, 1990–1998, doi:10.1210/endo.133.5.8404646.

128. Maden, M.; Hind, M. Retinoic acid in alveolar development, maintenance and regeneration. In Proceedings of the Philosophical Transactions of the Royal Society B: Biological Sciences, 2004; Vol. 359, pp. 799–808, doi:10.1098/rstb.2004.1470.

129. Hind, M.; Maden, M. Retinoic acid induces alveolar regeneration in the adult mouse lung. Eur. Respir J. 2004, 23, 20–27, doi:10.1183/09031936.03.00119103.

130. Maden, M. Retinoids have differing efficacies on alveolar regeneration in a dexamethasone-treated mouse. Am. J. Respir Cell Mol. Biol. 2006, 35, 260–267, doi:10.1165/rcmb.2006-0029OC.

131. Belloni, P.N.; Garvin, L.; Mao, C.P.; Bailey-Healy, I.; Leaffer, D. Effects of all-trans-retinoic acid in promoting alveolar repair. Chest 2000, 117, 235S–241S, doi:10.1378/chest.117.5_suppl_1.235s.

132. Srinivasan, G.; Bruce, E.N.; Houtz, P.K.; Bruce, M.C. Dexamethasone-induced changes in lung function are not prevented by concomitant treatment with retinoic acid. Am. J. Physiol. Lung Cell Mol. Physiol. 2002, 283, 275–287, doi:10.1152/ajplung.00423.2001.

133. Ng-Blichfeldt, J.P.; Gosens, R.; Dean, C.; Griffiths, M.; Hind, M. Regenerative pharmacology for COPD: Breathing new life into old lungs. Thorax 2019, 74, 890–897, doi:10.1136/thoraxjnl-2018-212630.

134. Uniyal, S.; Dhasmana, A.; Tyagi, A.; Muyal, J.P. ATRA reduces inflammation and improves alveolar epithelium regeneration in emphysematous rat lung. Biomed. Pharmacother. 2018, 108, 1435–1450, doi:10.1016/j.biopha.2018.09.166.

135. Parera, M.C.; Van Dooren, M.; Van Kempen, M.; De Krijger, R.; Grosveld, F.; Tibboel, D.; Rottier, R. Distal angiogenesis: A new concept for lung vascular morphogenesis. Am. J. Physiol. Lung Cell Mol. Physiol. 2005, 288, 141–149, doi:10.1152/ajplung.00148.2004.

136. Kool, H.; Mous, D.; Tibboel, D.; de Klein, A.; Rottier, R.J. Pulmonary vascular development goes awry in congenital lung abnormalities. Birth Defects Res. Part. C Embryo Today Rev. 2014, 102, 343–358, doi:10.1002/bdrc.21085.

137. Yamamoto, H.; Jun Yun, E.; Gerber, H.P.; Ferrara, N.; Whitsett, J.A.; Vu, T.H. Epithelial-vascular cross talk mediated by VEGF-A and HGF signaling directs primary septae formation during distal lung morphogenesis. Dev. Biol. 2007, 308, 44–53, doi:10.1016/j.ydbio.2007.04.042.

138. Armulik, A.; Abramsson, A.; Betsholtz, C. Endothelial/pericyte interactions. Circ. Res. 2005, 97, 512–523, doi:10.1161/01.RES.0000182903.16652.d7.

139. Lai, L.; Bohnsack, B.L.; Niederreither, K.; Hirschi, K.K. Retinoic acid regulates endothelial cell proliferation during vasculogenesis. Development 2003, 130, 6465–6474, doi:10.1242/dev.00887.

140. Schmidt, A.F.; Gonçalves, F.L.L.; Regis, A.C.; Gallindo, R.M.; Sbragia, L. Prenatal retinoic acid improves lung vascularization and VEGF expression in CDH rat. Am. J. Obs. Gynecol. 2012, 207, 76, doi:10.1016/j.ajog.2012.04.025.

141. Kool, H.M.; Bürgisser, P.E.; Edel, G.G.; de Kleer, I.; Boerema-de Munck, A.; de Laat, I.; Chrifi, I.; Cheng, C.; van Cappellen, W.A.; Kremers, G.J.; et al. Inhibition of retinoic acid signaling induces aberrant pericyte coverage and differentiation resulting in vascular defects in congenital diaphragmatic hernia. Am. J. Physiol. Lung Cell Mol. Physiol. 2019, 317, 317–331, doi:10.1152/ajplung.00104.2018.

142. Beurskens, N.; Klaassens, M.; Rottier, R.; de Klein, A.; Tibboel, D. Linking animal models to human congenital diaphragmatic hernia. Birth Defects Res. A Clin. Mol. Teratol. 2007, 79, 565–572, doi:10.1002/bdra.20370.

143. Kardon, G.; Ackerman, K.G.; McCulley, D.J.; Shen, Y.; Wynn, J.; Shang, L.; Bogenschutz, E.; Sun, X.; Chung, W.K. Congenital diaphragmatic hernias: From genes to mechanisms to therapies. Dis Model. Mech. 2017, 10, 955–970, doi:10.1242/dmm.028365.

144. Major, D.; Cadenas, M.; Fournier, L.; Leclerc, S.; Lefebvre, M.; Cloutier, R. Retinol status of newborn infants with congenital diaphragmatic hernia. Pediatr. Surg. Int. 1998, 13, 547–549, doi:10.1007/s003830050399.

145. Marquez, H.A.; Cardoso, W.V. Vitamin A-retinoid signaling in pulmonary development and disease. Mol. Cell Pediatr. 2016, 3, 28, doi:10.1186/s40348-016-0054-6.

146. Pierce, R.A.; Joyce, B.; Officer, S.; Heintz, C.; Moore, C.; McCurnin, D.; Johnston, C.; Maniscalco, W. Retinoids increase lung elastin expression but fail to alter morphology or angiogenesis genes in premature ventilated baboons. Pediatr. Res. 2007, 61, 703–709, doi:10.1203/pdr.0b013e318053661d.

147. Hind, M.; Gilthorpe, A.; Stinchcombe, S.; Maden, M. Retinoid induction of alveolar regeneration: From mice to man? Thorax 2009, 64, 451–457, doi:10.1136/thx.2008.105437.

148. Friedmacher, F.; Hofmann, A.D.; Takahashi, T.; Takahashi, H.; Kutasy, B.; Puri, P. Prenatal administration of all-trans retinoic acid upregulates leptin signaling in hypoplastic rat lungs with experimental congenital diaphragmatic hernia. Pediatr. Surg. Int. 2014, 30, 1183–1190, doi:10.1007/s00383-014-3605-8.

CHAPTER 1.4

DEVELOPMENT AND GLYCOLYSIS DEPENDENCE

Hugo Fernandes-Silva, Jorge Correia-Pinto and Rute S. Moura

ABSTRACT

Proper embryonic development depends not only on highly regulated genetic programs but also on the metabolic state that may influence gene function. In the particular case of glycolysis, once viewed merely as an energy supply pathway, it is considered far more than that nowadays. In this chapter, we aim to describe the current knowledge regarding the role of the glycolytic pathway during embryonic development. Briefly, we will address how metabolism coordinates embryonic development through metabolic rewiring to cope with developmental programs, metabolism-signaling interactions, and metabolic transcriptional and epigenetic control during development. This topic is a promising area that, for sure, will bring new and exciting findings that will enrich our knowledge about embryonic development.

Keywords: Embryonic development; Metabolism; Glucose; Lactate; Warburg effect; Temporal regulation; Metabolic shift; Glycolytic gradient; Cell signaling

METABOLISM AND EMBRYONIC DEVELOPMENT: GENERAL CONSIDERATIONS

Metabolic studies played a prominent role in the early history of developmental biology, then modern molecular biology took the stage, and the development-metabolism field fell into oblivion [1]. More recently, the interest in the potential implications of metabolism during embryonic development emerged again. How metabolism influences cellular and developmental decisions, how the metabolic flux adapts to the energy needs during organism development, and how metabolism coordinates with developmental progression are some of the in-vogue topics [1–3].

Metabolism can contribute to embryonic development through two distinct biochemical perspectives. The bioenergetic role consists of canonical metabolic activities such as providing energy or macromolecules for cellular building blocks; the metabolic signaling function provides modulatory or instructive roles to regulate cellular programs [2]. Still, little is known concerning the intrinsic and extrinsic cues that might regulate metabolism during development. Alterations in substrate availability or growth environment and intrinsic developmental programs might trigger metabolic changes or play a role in the coordination between metabolism and development [2].

TEMPORAL CONTROL AND METABOLIC SWITCHES DURING EMBRYONIC DEVELOPMENT

The timing of metabolic rewiring seems to be related to developmental progression. Moreover, specific developmental programs are accompanied by precise metabolic changes. For instance, pyruvate is the preferential energy source upon embryo fertilization in early mouse development, and embryos cannot use glucose until the 8-cell stage. Then, a metabolic shift occurs, with glucose becoming the predominant substrate [4–7]. While the lactate and pyruvate substrates act synergistically and are sufficient to support embryo development until the morula stage, glucose is necessary to support the morula to blastocyst transition [8]. Both hexokinase (HK) and phosphofructokinase 1 (PFK1) enzymes are responsible for glycolysis regulation in these pre-implantation stages [4,6]. Moreover, lactate dehydrogenase (LDH) plays a crucial role in lactate regulation, and the resultant amount of lactate can influence pyruvate uptake and metabolism in the embryo [9]. In this sense, during early embryonic development, totipotent stem cells (TSCs) rely on pyruvate utilization, with HK and PFK1 playing a crucial role in metabolism control, while pluripotent stem cells (PSCs) use glucose with increased lactate synthesis [10].

Post-implantation mouse embryos show considerable aerobic glycolysis with the production of significant amounts of lactate [11]. Murine embryos redirect the glucose carbon flow into the pentose phosphate pathway by suppressing the glycolytic enzymes PFK1 and aldolase. Alongside, there is an increase in the glycolytic fraction that serves lactate biosynthesis. Such metabolic changes can result from intrinsic developmental programs occurring during the chorioallantoic branching stage, following placental development [12]. Embryonic stem cells (ESCs) are isolated from the inner cell mass (ICM) of pre-implantation embryos, while epiblast stem cells (EpiSCs) represent cells from the post-implantation epiblast, a later developmental stage. The evaluation of the bioenergetic profile of mouse ESCs and EpiSCs (distinct pluripotent stages) revealed that mouse ESCs are metabolic bivalent, while EpiSCs are almost exclusively glycolytic. Such metabolic switch demonstrates a relationship between the specific metabolic profile and the pluripotent developmental stage in early embryonic development [13]. Subsequently, the glycolytic activity of the embryo decreases as development progresses [14].

During *Drosophila* larval development, aerobic glycolysis is activated to promote biomass production and, consequently, support growth and body mass increase. This metabolic feature resembles the Warburg effect and supports massive cell proliferation in this phase [15]. Moreover, *Drosophila* larval neuroblast cells are highly dependent on aerobic glycolysis while proliferating. During cell cycle exit and

terminal differentiation, a metabolic switch to an oxidative phosphorylation (OXPHOS) metabolism is observed [16]. Likewise, dividing progenitor cells of the *Xenopus* retina display a high glycolytic metabolic profile. However, upon final differentiation, retinal neurons switch metabolism towards OXPHOS [17]. In *Drosophila* wing discs, supercompetitor cells boost the glycolytic activity to promote proliferation under competitive conditions [18]. Glycolytic metabolism seems to play a role in cell competition mechanisms of growing tissues since intercellular heterogeneity of metabolism contributes to the selection of winner against loser cells during this cell-cell interaction process [18].

Lung branching morphogenesis is another example where temporal control of metabolism and a gradual metabolic shift contributes to shaping a developmental process. A recent study showed that the developing lung gradually adapts to a glycolytic lactate-based metabolism to sustain the pulmonary branching energetic demands, resembling a Warburg-like effect. Besides, *ldha* and *ldhb* isoforms displayed a compartment-specific expression pattern, also suggesting a spatial regulation of metabolism. This work uncovered temporal metabolic changes synchronous with branching morphogenesis, thus illustrating the importance of metabolic regulation during organogenesis [19].

SIGNALING-METABOLISM INTERACTIONS DURING EMBRYONIC DEVELOPMENT

Throughout embryonic development, signaling-metabolism interactions contribute to shaping specific developmental processes. For instance, a glycolytic activity gradient is linked to mouse embryo presomitic mesoderm (PSM) differentiation and development [20]. Elevated glycolysis was reported in the posterior more undifferentiated region of the PSM; conversely, oxygen consumption in the anterior region of PSM is higher. This suggests an aerobic glycolysis signature in the posterior PSM region, without differences at the proliferation level. Such data points towards an intrinsic link between this glycolytic gradient and PSM formation [20]. In a different study, the same glycolytic gradient contributing to PSM development was reported in the mouse and chicken embryos [21]. Moreover, PSM glycolytic activity is coordinated with a fibroblast growth factor/wingless integration site (FGF/WNT) signaling network. In this molecular mechanism, FGF signaling controls the expression of glycolytic enzymes, influencing the glycolytic activity, which impacts WNT signaling. Then, a WNT signaling gradient is required to maintain FGF activation [21]. More recently, a study using chicken embryos and human tail bud-like cells differentiated from induced pluripotent stem cells (IPSCs) revealed that the tailbud exhibits an inverted pH gradient. The PSM posterior region has a more acidic extracellular pH and a more basic intracellular

pH, and this feature depends on the glycolytic activity [22]. In this sense, glycolysis affects the intracellular pH through the production of lactate, which is exported together with protons to the extracellular space via monocarboxylate transporters (MCTs). The resulting higher intracellular pH favors non-enzymatic acetylation of β-catenin and promotes mesoderm induction. In this model, FGF promotes glycolytic activity, regulating the intracellular pH. The more basic intracellular pH induces WNT signaling, contributing to PSM differentiation and development [22].

6-phosphofructo-2-kinase/fructose-2,6-bisphosphatase 4 (PFKFB4) is a crucial glycolysis regulator and was recently described to control dorsal ectoderm patterning of frog embryos during the gastrulation stage. Signaling-metabolism interactions involving a PFKFB4-dependent protein kinase B (AKT) signaling mechanism are essential for dorsal ectoderm progenitors' specification into neural and non-neural ectoderm, neural crest, or placodes. Moreover, this particular PFKFB4 function is glycolysis-independent and contributes to overall ectoderm development and survival [23].

In *Drosophila*, a short pulse of NOTCH signaling stimulates glycolysis and increases lactate production to the detriment of the Krebs cycle [24]. Loss of NOTCH signaling in *Drosophila* wing discs and human microvascular cells is associated with the downregulation of glycolytic genes. In this sense, NOTCH signaling regulates glucose catabolism and promotes a glycolytic shift towards the Warburg effect, contributing to *Drosophila* wing disc growth and development [24]. Similarly, NOTCH signaling regulates the expression of glycolysis-related genes in *Zebrafish* neural tissue development. Still, NOTCH metabolic regulation depends on the developmental stage and the specific neural tissue context [25].

METABOLISM, GENE EXPRESSION REGULATION AND EPIGENETIC CONTROL IN EMBRYONIC DEVELOPMENT

Metabolism may play a role in regulating gene expression and epigenetic control during embryonic development. In the compacted morula stage, trophectoderm (TE) (will become placenta) and ICM (will become the embryo) precursors are first evident. In this developmental period, glucose is metabolized by multiple pathways and initiates signaling and transcriptional events that eventually control TE but not ICM cell fate [26]. Besides, stem cells primarily depend on glycolysis and switch to an OXPHOS metabolism during differentiation. In naïve ESCs, active glycolysis contributes to the intracellular accumulation of acetyl-CoA, which facilitates histone acetylation and promotes the expression of pluripotent genes [27]. On the other hand, suppression of glycolysis and acetyl-CoA production results in deacetylation and early ESCs differentiation. In this sense, a glycolytic switch triggers loss of pluripotency

and histone acetylation, suggesting a link between cellular metabolism and ESCs differentiation via epigenetic control [27].

Once thought of as a metabolic waste product, L-2-hydroxyglutarate (L-2HG) was recently observed in *Drosophila* larvae at specific developmental stages, namely under aerobic glycolysis stimulated conditions. L-2HG is derived from glucose oxidation through production by LDH. Moreover, L-2HG can function as a signaling molecule, modulating heterochromatin formation and regulating gene expression. This report suggests another mechanistic link between metabolism, embryonic development, and gene expression programs [28].

METABOLISM, GLYCOLYSIS, AND EMBRYONIC DEVELOPMENT: CONCLUSIONS AND FUTURE PERSPECTIVES

Once thought of as a housekeeping process, metabolism is tightly regulated and linked to cell decisions and developmental progression [1,3,29]. Throughout embryonic development, glycolytic metabolism is controlled both in time and space to sustain the stage-required energetic demands. Moreover, the metabolic flux can rewire to cope with developmental programs. Besides, metabolism can respond to signaling pathways and modulate them. Still, a role for glycolysis in both transcriptional regulation and epigenetic control starts to be perceived.

In this chapter, several examples demonstrate that development depends on metabolic switches. Aerobic glycolysis seems to be a feature of several developmental programs, which might be explained by the need for fast growth and proliferation, similar to what occurs in the Warburg effect of cancer systems [30]. Glycolytic metabolism promotes fast ATP synthesis, uncouples from mitochondria, and provides anabolism with metabolic intermediates for biosynthetic pathways [30].

Development and metabolism are undeniably interlinked, and this emerging field is gaining interest among developmental biologists. This field is still up and coming, and future mechanistic studies exploring metabolic regulation and the interaction between classical signaling pathways and metabolism will certainly contribute to a better understanding of developmental processes.

REFERENCES

1.   Krejci, A.; Tennessen, J.M. Metabolism in time and space - exploring the frontier of developmental biology. Development 2017, 144, 3193-3198, doi:10.1242/dev.150573.

2. Miyazawa, H.; Aulehla, A. Revisiting the role of metabolism during development. Development 2018, 145, doi:10.1242/dev.131110.

3. Cable, J.; Pourquie, O.; Wellen, K.E.; Finley, L.W.S.; Aulehla, A.; Gould, A.P.; Teleman, A.; Tu, W.B.; Garrett, W.S.; Miguel-Aliaga, I.; et al. Metabolic decisions in development and disease-a Keystone Symposia report. Ann. N. Y. Acad. Sci. 2021, 1506, 55-73, doi:10.1111/nyas.14678.

4. Barbehenn, E.K.; Wales, R.G.; Lowry, O.H. Measurement of metabolites in single preimplantation embryos; a new means to study metabolic control in early embryos. J. Embryol. Exp. Morphol. 1978, 43, 29-46, doi:10.1242/dev.43.1.29.

5. Leese, H.J.; Barton, A.M. Pyruvate and glucose uptake by mouse ova and preimplantation embryos. J. Reprod. Fertil. 1984, 72, 9-13, doi:10.1530/jrf.0.0720009.

6. Johnson, M.T.; Mahmood, S.; Patel, M.S. Intermediary metabolism and energetics during murine early embryogenesis. J. Biol. Chem. 2003, 278, 31457-31460, doi:10.1074/jbc.R300002200.

7. Brinster, R.L. Studies on the Development of Mouse Embryos in Vitro. II. The Effect of Energy Source. J. Exp. Zool. 1965, 158, 59-68, doi:10.1002/jez.1401580106.

8. Brown, J.J.; Whittingham, D.G. The roles of pyruvate, lactate and glucose during preimplantation development of embryos from F1 hybrid mice in vitro. Development 1991, 112, 99-105, doi:10.1242/dev.112.1.99.

9. Lane, M.; Gardner, D.K. Lactate regulates pyruvate uptake and metabolism in the preimplantation mouse embryo. Biol. Reprod. 2000, 62, 16-22, doi:10.1095/biolreprod62.1.16.

10. Shyh-Chang, N.; Daley, G.Q.; Cantley, L.C. Stem cell metabolism in tissue development and aging. Development 2013, 140, 2535-2547, doi:10.1242/dev.091777.

11. Clough, J.R.; Whittingham, D.G. Metabolism of [14C]glucose by postimplantation mouse embryos in vitro. J. Embryol. Exp. Morphol. 1983, 74, 133-142, doi:10.1242/dev.74.1.133.

12. Miyazawa, H.; Yamaguchi, Y.; Sugiura, Y.; Honda, K.; Kondo, K.; Matsuda, F.; Yamamoto, T.; Suematsu, M.; Miura, M. Rewiring of embryonic glucose metabolism via suppression of PFK-1 and aldolase during mouse chorioallantoic branching. Development 2017, 144, 63-73, doi:10.1242/dev.138545.

13. Zhou, W.; Choi, M.; Margineantu, D.; Margaretha, L.; Hesson, J.; Cavanaugh, C.; Blau, C.A.; Horwitz, M.S.; Hockenbery, D.; Ware, C.; et al. HIF1alpha induced switch from bivalent to exclusively glycolytic metabolism during ESC-to-EpiSC/hESC transition. EMBO J. 2012, 31, 2103-2116, doi:10.1038/emboj.2012.71.

14. Wales, R.G.; Martin, K.L.; Leese, H.J. Glucose utilization by components of the mouse conceptus during early embryogenesis. J. Reprod. Fertil. 1995, 104, 125-132, doi:10.1530/jrf.0.1040125.

15. Tennessen, J.M.; Baker, K.D.; Lam, G.; Evans, J.; Thummel, C.S. The Drosophila estrogen-related receptor directs a metabolic switch that supports developmental growth. Cell Metab. 2011, 13, 139-148, doi:10.1016/j.cmet.2011.01.005.

16. Homem, C.C.F.; Steinmann, V.; Burkard, T.R.; Jais, A.; Esterbauer, H.; Knoblich, J.A. Ecdysone and mediator change energy metabolism to terminate proliferation in Drosophila neural stem cells. Cell 2014, 158, 874-888, doi:10.1016/j.cell.2014.06.024.

17. Agathocleous, M.; Love, N.K.; Randlett, O.; Harris, J.J.; Liu, J.; Murray, A.J.; Harris, W.A. Metabolic differentiation in the embryonic retina. Nat. Cell Biol. 2012, 14, 859-864, doi:10.1038/ncb2531.

18. de la Cova, C.; Senoo-Matsuda, N.; Ziosi, M.; Wu, D.C.; Bellosta, P.; Quinzii, C.M.; Johnston, L.A. Supercompetitor status of Drosophila Myc cells requires p53 as a fitness sensor to reprogram metabolism and promote viability. Cell Metab. 2014, 19, 470-483, doi:10.1016/j.cmet.2014.01.012.

19. Fernandes-Silva, H.; Alves, M.G.; Araujo-Silva, H.; Silva, A.M.; Correia-Pinto, J.; Oliveira, P.F.; Moura, R.S. Lung branching morphogenesis is accompanied by temporal metabolic changes towards a glycolytic preference. Cell Biosci. 2021, 11, 134, doi:10.1186/s13578-021-00654-w.

20. Bulusu, V.; Prior, N.; Snaebjornsson, M.T.; Kuehne, A.; Sonnen, K.F.; Kress, J.; Stein, F.; Schultz, C.; Sauer, U.; Aulehla, A. Spatiotemporal Analysis of a Glycolytic Activity Gradient Linked to Mouse Embryo Mesoderm Development. Dev. Cell 2017, 40, 331-341 e334, doi:10.1016/j.devcel.2017.01.015.

21. Oginuma, M.; Moncuquet, P.; Xiong, F.; Karoly, E.; Chal, J.; Guevorkian, K.; Pourquie, O. A Gradient of Glycolytic Activity Coordinates FGF and Wnt Signaling during Elongation of the Body Axis in Amniote Embryos. Dev. Cell 2017, 40, 342-353 e310, doi:10.1016/j.devcel.2017.02.001.

22. Oginuma, M.; Harima, Y.; Tarazona, O.A.; Diaz-Cuadros, M.; Michaut, A.; Ishitani, T.; Xiong, F.; Pourquie, O. Intracellular pH controls WNT downstream of glycolysis in amniote embryos. Nature 2020, 584, 98-101, doi:10.1038/s41586-020-2428-0.

23. Pegoraro, C.; Figueiredo, A.L.; Maczkowiak, F.; Pouponnot, C.; Eychene, A.; Monsoro-Burq, A.H. PFKFB4 controls embryonic patterning via Akt signalling independently of glycolysis. Nat. Commun. 2015, 6, 5953, doi:10.1038/ncomms6953.

24. Slaninova, V.; Krafcikova, M.; Perez-Gomez, R.; Steffal, P.; Trantirek, L.; Bray, S.J.; Krejci, A. Notch stimulates growth by direct regulation of genes involved in the control of glycolysis and the tricarboxylic acid cycle. Open Biol. 2016, 6, 150155, doi:10.1098/rsob.150155.

25. Kuwabara, S.; Yamaki, M.; Yu, H.; Itoh, M. Notch signaling regulates the expression of glycolysis-related genes in a context-dependent manner during embryonic development. Biochem. Biophys. Res. Commun. 2018, 503, 803-808, doi:10.1016/j.bbrc.2018.06.079.

26. Chi, F.; Sharpley, M.S.; Nagaraj, R.; Roy, S.S.; Banerjee, U. Glycolysis-Independent Glucose Metabolism Distinguishes TE from ICM Fate during Mammalian Embryogenesis. Dev. Cell 2020, 53, 9-26 e24, doi:10.1016/j.devcel.2020.02.015.

27. Moussaieff, A.; Rouleau, M.; Kitsberg, D.; Cohen, M.; Levy, G.; Barasch, D.; Nemirovski, A.; Shen-Orr, S.; Laevsky, I.; Amit, M.; et al. Glycolysis-mediated changes in acetyl-CoA and histone acetylation control the early differentiation of embryonic stem cells. Cell Metab. 2015, 21, 392-402, doi:10.1016/j.cmet.2015.02.002.

28. Li, H.; Chawla, G.; Hurlburt, A.J.; Sterrett, M.C.; Zaslaver, O.; Cox, J.; Karty, J.A.; Rosebrock, A.P.; Caudy, A.A.; Tennessen, J.M. Drosophila larvae synthesize the putative oncometabolite L-2-hydroxyglutarate during normal developmental growth. Proc. Natl. Acad. Sci. 2017, 114, 1353-1358, doi:10.1073/pnas.1614102114.

29. Gandara, L.; Wappner, P. Metabo-Devo: A metabolic perspective of development. Mech. Dev. 2018, 154, 12-23, doi:10.1016/j.mod.2018.02.004.

30. Vander Heiden, M.G.; Cantley, L.C.; Thompson, C.B. Understanding the Warburg effect: the metabolic requirements of cell proliferation. Science 2009, 324, 1029-1033, doi:10.1126/science.1160809.

CHAPTER 2. AIMS

Lung branching morphogenesis is characterized by epithelial-mesenchymal interactions and coordinated by a complex network of conserved signaling pathways that ultimately define the airway conducting system. Retinoic Acid signaling is fundamental for vertebrate embryonic development, and it is a major player in lung organogenesis. Retinoic Acid modulates multiple aspects of embryonic lung development, specifically proximal-distal patterning and lung branching morphogenesis. The signaling mechanisms involved in early lung development are quite well studied; conversely, little is known about embryonic lung metabolism. The main goal of this work was to explore the metabolic profile associated with the early stages of pulmonary branching and examine a hypothetical interaction between Retinoic Acid signaling and lung metabolism throughout branching morphogenesis.

This thesis aims to accomplish the following specific objectives:

- Investigate the metabolic profile underpinning pulmonary branching morphogenesis

- Determine how the Retinoic Acid signaling influences lung metabolism in the branching stages

- Explore new insights on the signaling-metabolism interaction in the context of lung development

CHAPTER 3. RESULTS

CHAPTER 3.1

LUNG BRANCHING MORPHOGENESIS IS ACCOMPANIED BY TEMPORAL METABOLIC CHANGES TOWARDS A GLYCOLYTIC PREFERENCE

Hugo Fernandes-Silva, Marco G. Alves, Henrique Araújo-Silva,

Ana M. Silva, Jorge Correia-Pinto, Pedro F. Oliveira and Rute S. Moura

ABSTRACT

Lung branching morphogenesis is characterized by epithelial-mesenchymal interactions that ultimately define the airway conducting system. Throughout this process, energy and structural macromolecules are necessary to sustain the high proliferative rates. The extensive knowledge of the molecular mechanisms underlying pulmonary development contrasts with the lack of data regarding the embryonic lung metabolic requirements. Here, we studied the metabolic profile associated with the early stages of chicken pulmonary branching. In this study, we used an *ex vivo* lung explant culture system and analyzed the consumption/production of extracellular metabolic intermediates associated with glucose catabolism (alanine, lactate, and acetate) by ^{1}H-NMR spectroscopy in the culture medium. Then, we characterized the transcript levels of metabolite membrane transporters (*glut1*, *glut3*, *glut8*, *mct1*, *mct3*, *mct4*, and *mct8*) and glycolytic enzymes (*hk1*, *hk2*, *pfk1*, *ldha*, *ldhb*, *pdha*, and *pdhb*) by qPCR. *ldha* and *ldhb* mRNA spatial localization was determined by *in situ* hybridization. Proliferation was analyzed by directly assessing DNA synthesis using an EdU-based assay. Additionally, we performed western blot to analyze LDHA and LDHT protein levels. Finally, we used a Clark-Type Electrode to assess the lung explant's respiratory capacity. Glucose consumption decreases, whereas alanine, lactate, and acetate production progressively increase as branching morphogenesis proceeds. mRNA analysis revealed variations in the expression levels of key enzymes and transporters from the glycolytic pathway. *ldha* and *ldhb* displayed a compartment-specific expression pattern that resembles proximal-distal markers. In addition, high proliferation levels were detected at active branching sites. LDH protein expression levels suggest that LDHB may account for the progressive rise in lactate. Concurrently, there is a stable oxygen consumption rate throughout branching morphogenesis. This report describes the temporal metabolic changes that accompany the early stages of chicken lung branching morphogenesis. Overall, the embryonic chicken lung seems to shift to a glycolytic lactate-based metabolism as pulmonary branching occurs. Moreover, this metabolic rewiring might play a crucial role during lung development.

Keywords: Metabolism, Respiratory system, Warburg effect, Lactate dehydrogenase, Chicken embryo

BACKGROUND

Pulmonary branching morphogenesis is an intricate process governed by epithelial-mesenchymal interactions and is dependent on complex signaling events. This process occurs throughout the early stages of embryonic lung development and defines the respiratory airway structure [1]. In the chicken,

Gallus gallus, the primordial lung appears around day 3 of embryogenesis as a protuberance from the primitive foregut [2]. During this process, the mesobronchus grows distally, and the new secondary bronchi sprout laterally into the surrounding mesenchymal compartment [1,3]. This lateral or monopodial branching is exceptionally similar to the domain branching subroutine characteristic of the mammalian lung system [4,5]. Moreover, the molecular events underlying the development of the avian respiratory system are highly conserved with the mammalian and point to similar functions [6]. For instance, FGF (Fibroblast Growth Factor), WNT (Wingless-related Integration Site), SHH (Sonic Hedgehog), and Retinoic Acid signaling pathways were described as playing critical roles in chicken pulmonary branching morphogenesis [7–11].

The signaling mechanisms involved in early lung development are quite well studied in several animal models [10,12,13]; however, little is known concerning the embryonic lung metabolic needs [14,15]. As for the mammalian adult lung metabolic requirements, it has been shown that they are achieved through the uptake and catabolism of glucose, which represents the primary fuel to the adult lung tissue [16–18]. The coordination between signaling and metabolism is now emerging as a key concept for understanding developmental processes. Therefore, it is of major importance to investigate how metabolism contributes and is dynamically regulated during animal development [19,20].

Recent studies have demonstrated that glycolysis can serve additional roles beyond the classical bioenergetics purpose and contribute to shaping embryonic development both in time and space. For instance, during the murine chorioallantoic branching stage, the developing embryo redirects glucose carbon flow into the pentose phosphate pathway by suppressing phosphofructokinase 1 (PFK1) and aldolase; concomitantly, there is an increase in the glycolytic fraction to serve lactate biosynthesis. This study suggests a rewiring of glycolytic metabolism in the whole embryo, and over time, to promote accurate chorioallantoic branching [21]. Moreover, Slaninova *et al.* showed that loss of NOTCH signaling in *Drosophila* and human microvascular cells resulted in the downregulation of pivotal glycolytic genes; in opposition, a short pulse of NOTCH signaling stimulates glycolysis and increases lactate production, in detriment of Tricarboxylic Acid (TCA) cycle activity [22]. Overall, these results revealed that NOTCH signaling promotes a glycolytic shift that resembles the Warburg effect [22]. Furthermore, *Drosophila* larval neuroblast cells, while proliferating, depend on aerobic glycolysis. However, during cell cycle exit and terminal differentiation, cell metabolism switches from aerobic glycolysis to an OXPHOS-based metabolism [23]. More recently, Bulusu *et al.* described a glycolytic activity gradient that contributes to Presomitic Mesoderm (PSM) differentiation and development in the mouse embryo [24]. Additionally, it

has been shown that there is an FGF/Wnt coordinated glycolytic gradient that regulates cell motility and controls specification, thus contributing to PSM development in the chicken embryo [25].

This study aimed to investigate the metabolic profile underpinning the early stages of pulmonary branching morphogenesis. Chicken embryonic lungs were used to perform *ex vivo* lung explant culture. Extracellular metabolites associated with glucose catabolism (alanine, lactate, and acetate) were evaluated by ^{1}H Nuclear Magnetic Resonance (^{1}H-NMR) spectroscopy in the culture medium. The expression patterns/levels of key enzymes and transporters from the glycolytic pathway were assessed by *in situ* hybridization and qPCR, namely: glucose transporters (*glut1*, *glut3*, and *glut8*), monocarboxylate transporters (*mct1*, *mct3*, *mct4*, and *mct8*), and metabolic-related enzymes such as hexokinase (*hk1* and *hk2*), phosphofructokinase (*pfk1*), lactate dehydrogenase (*ldha* and *ldhb*) and pyruvate dehydrogenase (*pdha* and *pdhb*). Proliferation status was determined by directly assessing DNA synthesis using an EdU-based assay. Additionally, the protein expression levels of LDH were determined by western blot. Lastly, the respiratory capacity of explants was evaluated by measuring the basal oxygen consumption rate (OCR).

This report describes, for the first time, the temporal metabolic changes that accompany the early stages of chicken lung branching morphogenesis. In our experimental setting, the embryonic chicken lung shows a glycolytic preference with a shift to lactate production as pulmonary branching proceeds.

RESULTS

Lung branching morphogenesis is accompanied by temporal metabolite changes

To describe the metabolic alterations that occur during the early stages of chicken pulmonary branching, *in vitro* lung explant culture was performed using stages b1, b2, and b3 (1, 2, or 3 secondary buds formed per bronchus, respectively) that correspond to the first three branching stages (Fig. 1a); new branches are clearly seen with the epithelial marker *l-cam* (Fig. 1a). Explant culture allows assessing extracellular metabolite fluctuations while in a controlled environment. Briefly, the culture system was performed for 48 h and refreshed at D1 (24 h); medium was collected at D0 (0 h; to be used as reference/control), D1, and D2 (48 h), and then analyzed by ^{1}H-NMR spectroscopy. Metabolite production/consumption was calculated following the mathematical formula | (D1-D0) + (D2-D0) |, expressed in pmol, and normalized to the total amount of protein. From the ^{1}H-NMR spectra analysis, it was possible to detect the following metabolites: glucose, alanine, lactate, and acetate (Fig. 1b). Additionally, morphometric analysis was performed to assess branching, revealing a gradual increment

of the epithelial compartment when comparing between stages (B1 *vs* B2 *vs* B3), which implies an increase in lung branching morphogenesis (Figure S1).

The ^{1}H-NMR results revealed that glucose consumption, by the embryonic lung, decreases from B1 ($3.8 \times 10^{7} \pm 1.7 \times 10^{6}$ pmol/mg protein) to B2 ($3.2 \times 10^{7} \pm 2.0 \times 10^{6}$ pmol/mg protein) ($p < 0.05$) and from B1 to B3 ($3.3 \times 10^{7} \pm 4.7 \times 10^{5}$ pmol/mg protein) ($p < 0.05$) (Fig. 1c). Alanine is produced (Fig. 1d), revealing a statistically significant increase from B1 ($1.3 \times 10^{6} \pm 4.6 \times 10^{5}$ pmol/mg protein) to B3 ($2.9 \times 10^{6} \pm 2.2 \times 10^{5}$ pmol/mg protein) ($p < 0.05$). Likewise, a progressive upsurge in lactate production is detected (Fig. 1e). Indeed, the production of lactate during branching increases from stage B1 ($1.6 \times 10^{7} \pm 2.3 \times 10^{6}$ pmol/mg protein) and from stage B2 ($1.9 \times 10^{7} \pm 1.8 \times 10^{6}$ pmol/mg protein) to B3 ($2.5 \times 10^{7} \pm 9.7 \times 10^{5}$ pmol/mg protein) ($p < 0.01$ and $p < 0.05$, respectively). Similarly, acetate production (Fig. 1f) increases through lung branching stages, namely from B1 ($2.1 \times 10^{6} \pm 3.0 \times 10^{5}$ pmol/mg protein) to B3 ($3.2 \times 10^{6} \pm 1.6 \times 10^{5}$ pmol/mg protein) ($p < 0.05$).
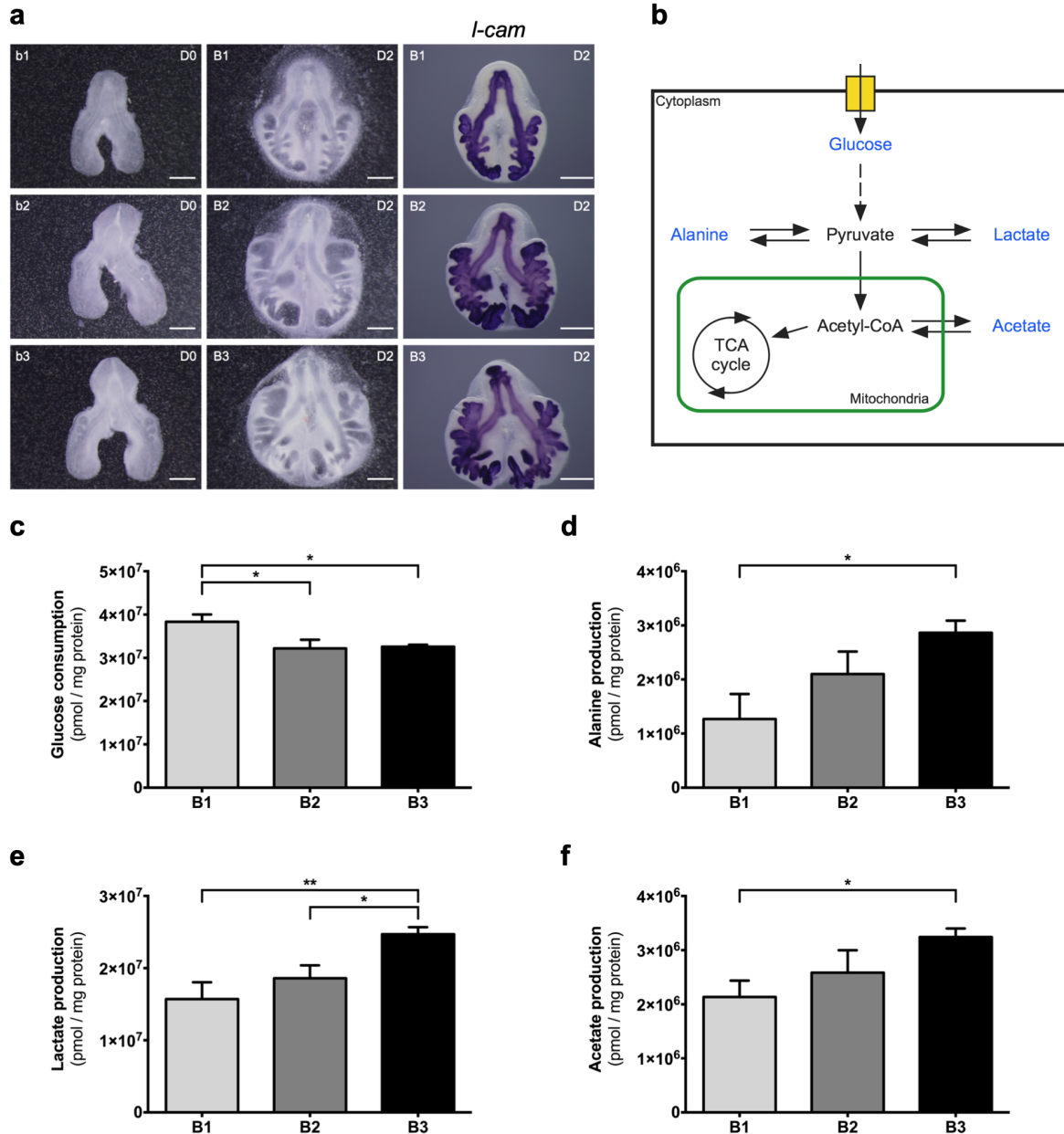
Figure 1 - Extracellular metabolite fluctuations throughout early stages of lung branching. a Representative examples of embryonic chicken lungs at D0 (0 h) (b1, b2, b3) and D2 (48 h) (B1, B2, B3) of explant culture, and corresponding *in situ* hybridization for *l-cam*, (n = 5/stage). *l-cam* is an epithelial marker, showing active branching formation. Scale bar: 500 μm. **b** Schematic representation of the glucose catabolism pathway and the potential pyruvate destinations. Blue labeling indicates the metabolites that were detected and quantified in the ^{1}H-NMR spectroscopy analysis. **c** Glucose consumption, **d** Alanine production, **e** Lactate production, and **f** Acetate production, during 48 h of explant culture. The medium was refreshed at D1 (24 h). Medium samples were collected at D1 (24 h) and D2 (48 h). D0 media samples were used as control. Metabolite consumption or production was calculated following the mathematical formula | (D1-D0) + (D2-D0) |. Metabolite data was normalized to the total amount of protein. Results are expressed as | mean | ± SEM (n ≥ 5/stage). One-Way ANOVA and Fisher's LSD test were performed. Significantly different results are indicated as: *p < 0.05; **p < 0.01.

Key glycolytic enzymes and transporters are present in the embryonic chicken lung

To characterize the molecular machinery underlying the metabolic variations associated with early branching stages, key enzymes and transporters involved in glucose catabolism were evaluated by qPCR (Fig. 2a). For this purpose, b1 to b3 lung explants were collected at 0 h and after 48 h of culture (Fig. 1a) and assessed for the expression of *glut1*, *glut3*, *glut8*, *mct1*, *mct3*, *mct4*, *mct8*, *hk1*, *hk2*, *pfk1*, *ldha*, *ldhb*, *pdha*, and *pdhb*.

glut1, *glut3*, and *glut8* transcripts (Fig. 2b–d) are present in all three pulmonary stages. *glut1* displays an increase in the expression levels from b1 (0 h) to B1 (48 h) with $p < 0.01$ (Fig. 2b). Similarly, *glut3* expression levels (Fig. 2c) increase between b1 and B1 ($p < 0.05$), and also between b2 and B2 ($p < 0.05$). After 48 h, both *glut1* and *glut3* expression levels decrease from B1 to B3 ($p < 0.01$; $p < 0.05$). Likewise, *glut8* transcript (Fig. 2d) decreases from B2 to B3 ($p < 0.05$).

mct1 and *mct8* transcripts (Fig. 2e, f) display a similar tendency in the embryonic chicken lung. Both *mct1* and *mct8* exhibit an increase from b1 to B1 ($p < 0.05$; $p < 0.01$) and then a decrease from B1 to B3 ($p < 0.05$; $p < 0.01$). After 48 h, MCT transcripts behave comparably to GLUTs. *mct3* and *mct4* expression levels were virtually undetectable in the embryonic chicken lung (data not shown).

hk1 transcript (Fig. 3a) is present in the three pulmonary stages studied and displays statistically significant differences between b2 and B2 ($p < 0.05$). Also, *hk1* expression decreases from B2 to B3 ($p < 0.05$). *hk2* mRNA levels are practically null in the embryonic chick lung (data not shown).

pfk1 expression levels are maintained between groups (Fig. 3b), except for a statistically significant increase between B2 and B3 ($p < 0.05$).

Concerning *ldha* transcript (Fig. 3c), an increase in the expression levels from b1 to B1 ($p < 0.001$) and from b3 to B3 is detected ($p < 0.05$). After 48 h, both B2 and B3 lungs display a decrease in *ldha* levels compared to B1 lungs ($p < 0.05$). *ldhb* (Fig. 3d) is present in all the stages and time points analyzed, and statistically significant differences were observed only between b1 and B1 lungs ($p < 0.05$).

pdha expression levels (Fig. 3e) are moderately maintained among the groups studied. On the opposite, *pdhb* transcript levels (Fig. 3f) increase from b1 to B1 ($p < 0.05$) but decrease between B1 and B3 lungs ($p < 0.01$).

For all transcripts, fold variation was expressed as the change that occurs from 0 to 48 h of explant culture (Figs. 2g and 3g). Major variations were observed in stages b1 and b2 for glucose transporters (*glut1* and *glut3*) and monocarboxylate transporters (*mct1* and *mct8*) (Fig. 2g). Still, the b3/B3 stages exhibited only minor variations in the same groups of transcripts (Fig. 2g). *hk1* and *ldha* showed a potential synergism with symmetric behavior regarding the fold variation (Fig. 3g). *ldhb* revealed

a fold variation decrease for all stages, from 0 to 48 h. Still, no major expression variations were observed in *pfk1*, *pdha*, and *pdhb* (Fig. 3g).
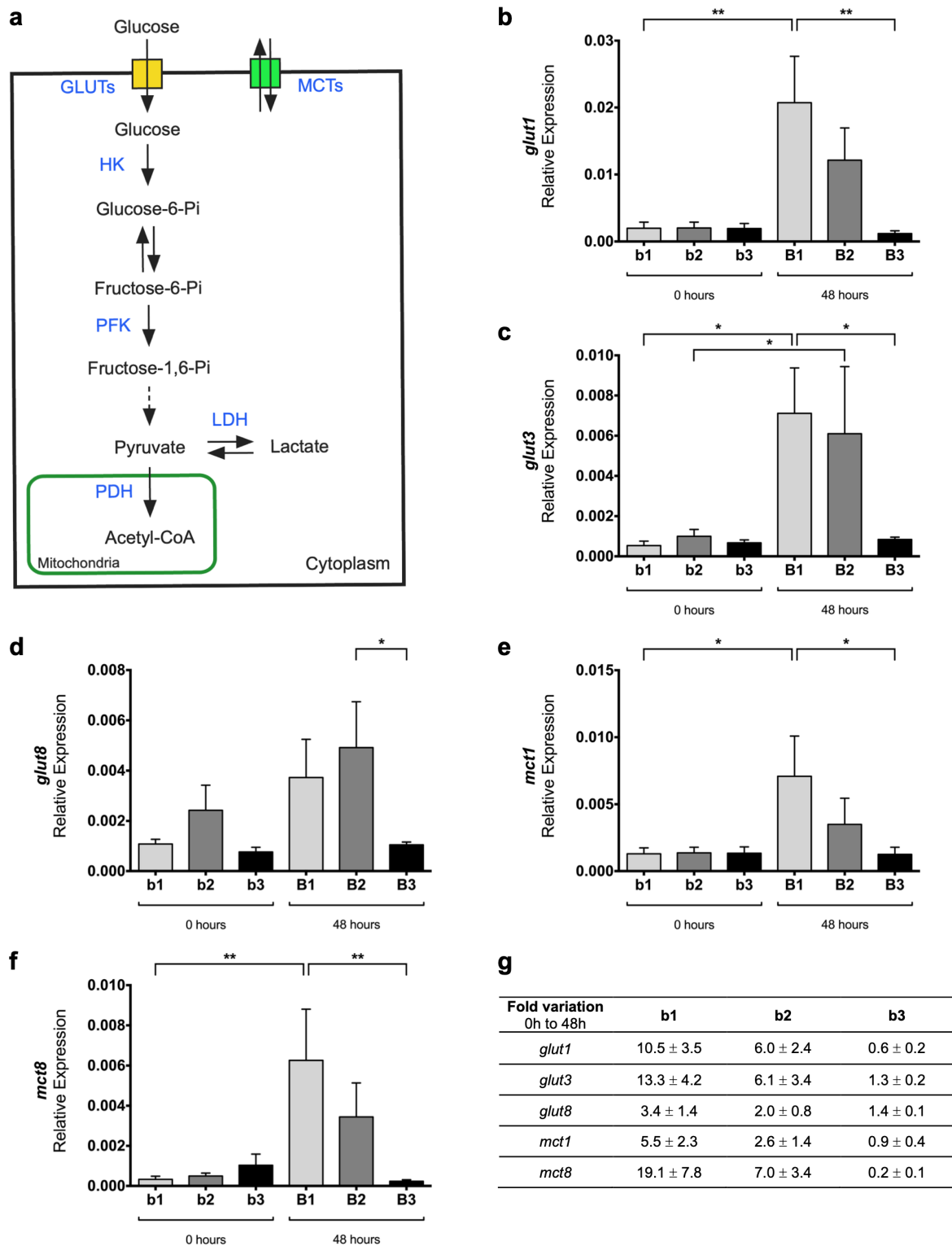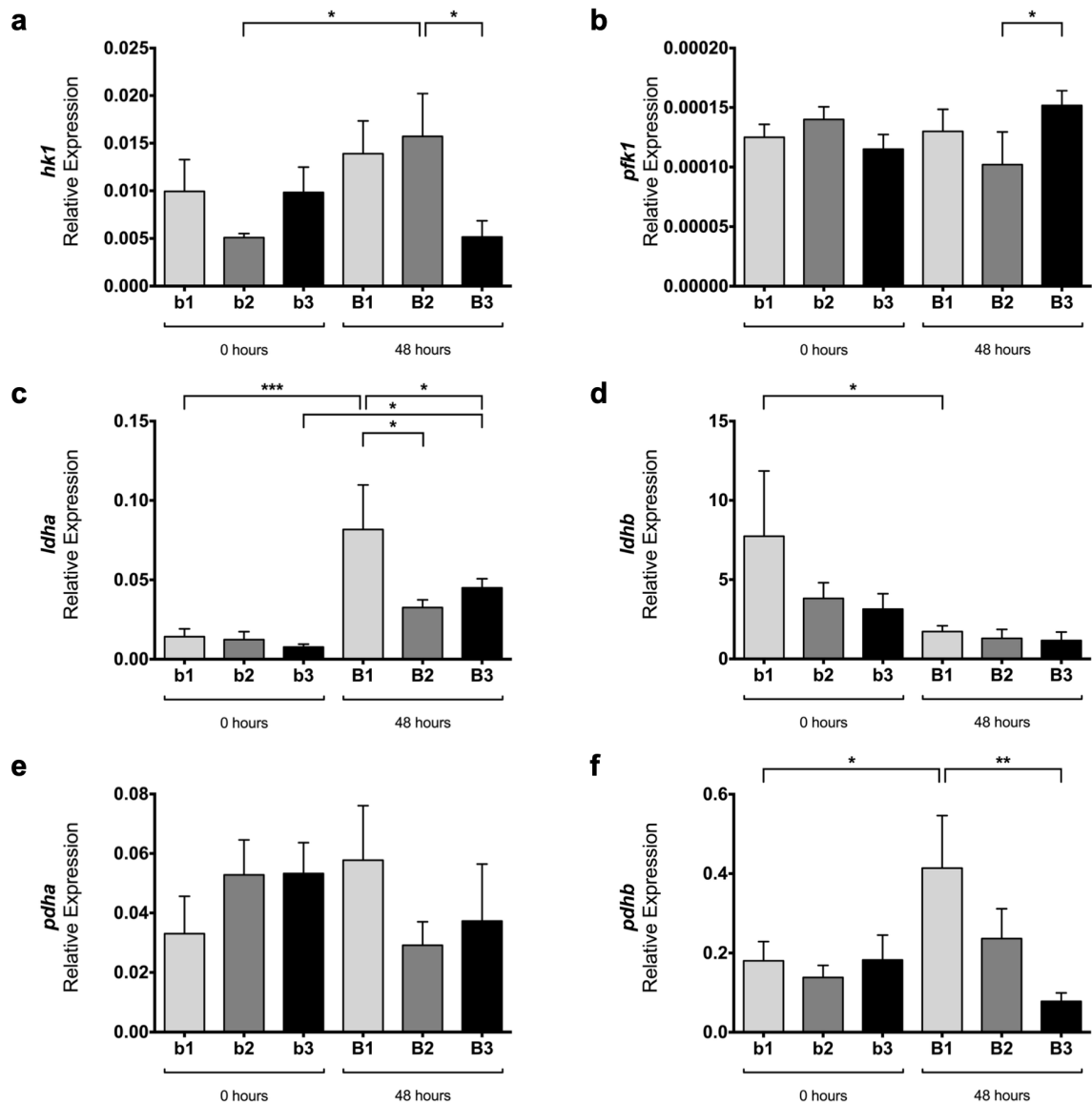
Figure 2 - mRNA expression levels of glucose catabolism transporters in early stages of lung branching. a Schematic representation of the glucose catabolism pathway. Blue labeling indicates the enzymes and transporters that were evaluated by qPCR. Relative expression levels of **b** *glut1*, **c** *glut3*, **d** *glut8*, **e** *mct1*, and **f** *mct8* in embryonic lungs at D0 (0 h) (b1, b2, b3) and D2 (48 h) (B1, B2, B3) of explant culture. **g** Expression fold variation, from 0 to 48 h of explant culture, for *glut1*, *glut3*, *glut8*, *mct1*, and *mct8*. mRNA expression levels were normalized for both *18s* and *actin-β* housekeeping genes. Results are expressed in arbitrary units, as mean ± SEM (n ≥ 5/stage/condition). One-Way ANOVA and Fisher's LSD test were performed. Significantly different results are indicated as: *$p < 0.05$; **$p < 0.01$.

Figure 3 - mRNA expression levels of glucose catabolism enzymes in early stages of lung branching. Relative expression levels of **a** *hk1*, **b** *pfk1*, **c** *ldha*, **d** *ldhb*, **e** *pdha*, and **f** *pdhb*, in embryonic lungs at D0 (0 h) (b1, b2, b3) and D2 (48 h) (B1, B2, B3) of explant culture. **g** Expression fold variation, from 0 to 48 h of explant culture, for *hk1*, *pfk1*, *ldha*, *ldhb*, *pdha*, and *pdhb*. mRNA expression levels were normalized for both *18s* and *actin-β* housekeeping genes. Results are expressed in arbitrary units, as mean ± SEM (n ≥ 5/stage/condition). One-Way ANOVA and Fisher's LSD test were performed. Significantly different results are indicated as: *$p < 0.05$; **$p < 0.01$; ***$p < 0.001$.

ldha and _lhdb_ exhibit region-specific expression patterns in the embryonic lung

To study the spatial distribution of lactate dehydrogenase, the expression pattern of _ldha_ and _ldhb_ was characterized by _in situ_ hybridization. Afterward, representative lungs from the three branching stages were processed for histological sectioning.

ldha mRNA is present in the proximal epithelium of the lung, namely in the trachea region (Fig. 4a, dark arrowhead; 4b, black rectangle). _ldha_ transcript is also expressed in the more distal region of the main bronchus (Fig. 4a, dagger). However, it is not expressed in the main bronchus epithelium and secondary bronchi (Fig. 4c, black arrow and asterisk, respectively). This expression pattern is conserved among the three branching stages but decreases throughout branching morphogenesis, namely for stage b3. Slide sectioning of the hybridized lungs confirmed the presence of _ldha_ in both mesenchymal and epithelial compartments of the embryonic trachea (Fig. 4d).

ldhb transcript is completely absent from the proximal region of the lung (Fig. 4e, dark arrowhead) and the epithelium of the primary bronchus (Fig. 4f, black arrow). _ldhb_ is strongly expressed in the distal-most region of the lung (Fig. 4e, dagger) and the secondary bronchi (Fig. 4g, asterisk). This expression pattern is maintained in the three stages studied. Lung sectioning confirmed that _ldhb_ is not expressed in the distal epithelial compartment but exclusively present in the distal mesenchyme of the growing tips (Fig. 4h, dagger).
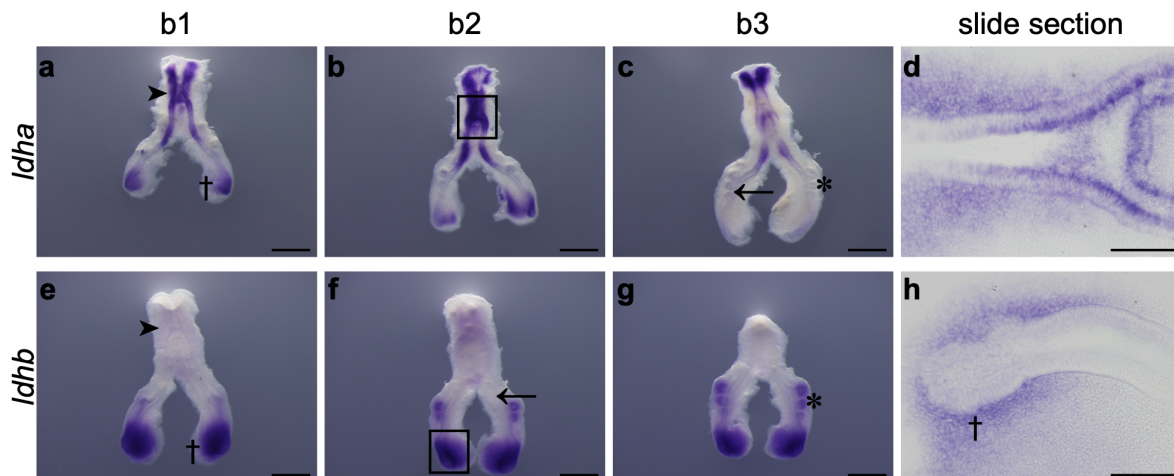

Figure 4 - _ldha_ and _ldhb_ mRNA expression pattern at early stages of chick lung branching. Representative examples of _in situ_ hybridization of stage b1, b2, and b3 lungs for **a–d** _ldha_ and **e–h** _ldhb_, n ≥ 9 per stage. Scale bar: whole mount, 500 μm; slide sections, 100 μm. The black rectangle in images b and f indicates the region shown in the corresponding slide section. Asterisk: secondary bronchi. Black arrow: main bronchus epithelium. Dagger: distal region. Dark arrowhead: trachea region.

Lung active branching sites are associated with high proliferation

To assess the proliferation status of lung branching morphogenesis, we performed an EdU-based proliferation assay using B1 to B3 lung explants (Fig. 1a). Proliferation was determined by directly assessing EdU incorporation into new DNA strands using Alexa Fluor 488 (Green); nuclei were counterstained with Hoechst 33342 (Red) (Fig. 5).

After 48 h of culture, high proliferation levels were detected in the trachea region (white arrowhead) (Fig. 5b), in the distal tip of the lung (white arrow) (Fig. 5e), and in the secondary bronchi/active branching sites (asterisk) (Fig. 5h). The proliferation patterns are maintained in the three stages (B1, B2, and B3).
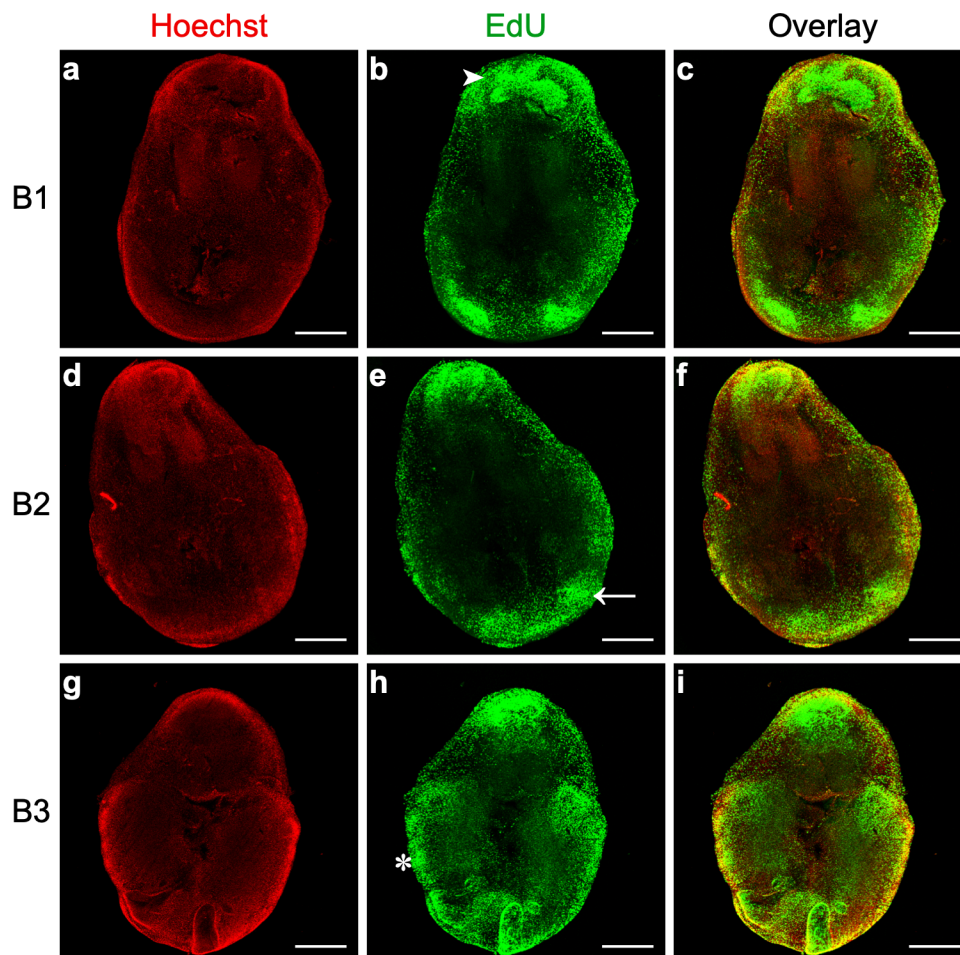

Figure 5 - Proliferation analysis of lung branching morphogenesis. Representative confocal microscopy fluorescence images of lungs explants after 48 h in culture (B1, B2, B3). **a**, **d**, **g** Nuclei were stained with Hoechst 33342 (Red). **b**, **e**, **h** Proliferation was assessed using an EdU-based assay; EdU incorporation in DNA was detected using Alexa Fluor 488 (Green). **c**, **f**, **i** Overlay represents the merged images of Hoechst (Red) and EdU (Green). All images are represented as maximum intensity projection of z-stacks. n ≥ 4 per stage. Scale bar: 500 μm. Asterisk: secondary bronchi/active branching sites. White arrow: distal tip. White arrowhead: trachea region.

LDH protein levels support the increase of lactate production throughout branching

To understand how LDH protein levels may contribute to the observed increase in lactate production, the protein expression levels of LDHA and total LDH (that recognizes both LDHA and LDHB proteins) were assessed.

As seen in Fig. 6a, at 0 h, LDHA protein levels fluctuate between stage/condition. Semi-quantitative analysis (Fig. 6b) revealed that LDHA expression levels increase at 0 h, namely from b1 to b3 ($p < 0.01$). On the other hand, after 48 h of culture, this variation dissipates, and there are no differences between stages. Conversely, when comparing both time points for each stage individually, a statistically significant decrease in LDHA expression levels is observed (Fig. 6b), namely from b1 to B1 ($p < 0.01$), from b2 to B2 ($p < 0.0001$), and from b3 to B3 ($p < 0.0001$).

In contrast, total LDH (LDHA plus LDHB) displays similar levels between stages at 0 h (Fig. 6c). Semi-quantitative analysis (Fig. 6d) exposed that there are no statistically significant differences between the three stages analyzed at 0 h. After 48 h of culture, total LDH protein levels vary between stages, namely from B1 to B2 ($p < 0.05$) and from B1 to B3 ($p < 0.01$). When comparing both time points for each stage individually, there is a statistically significant increase in total LDH expression levels from b2 to B2 ($p < 0.001$) and from b3 to B3 ($p < 0.0001$); in contrast, from b1 to B1 the protein levels remained unaltered.
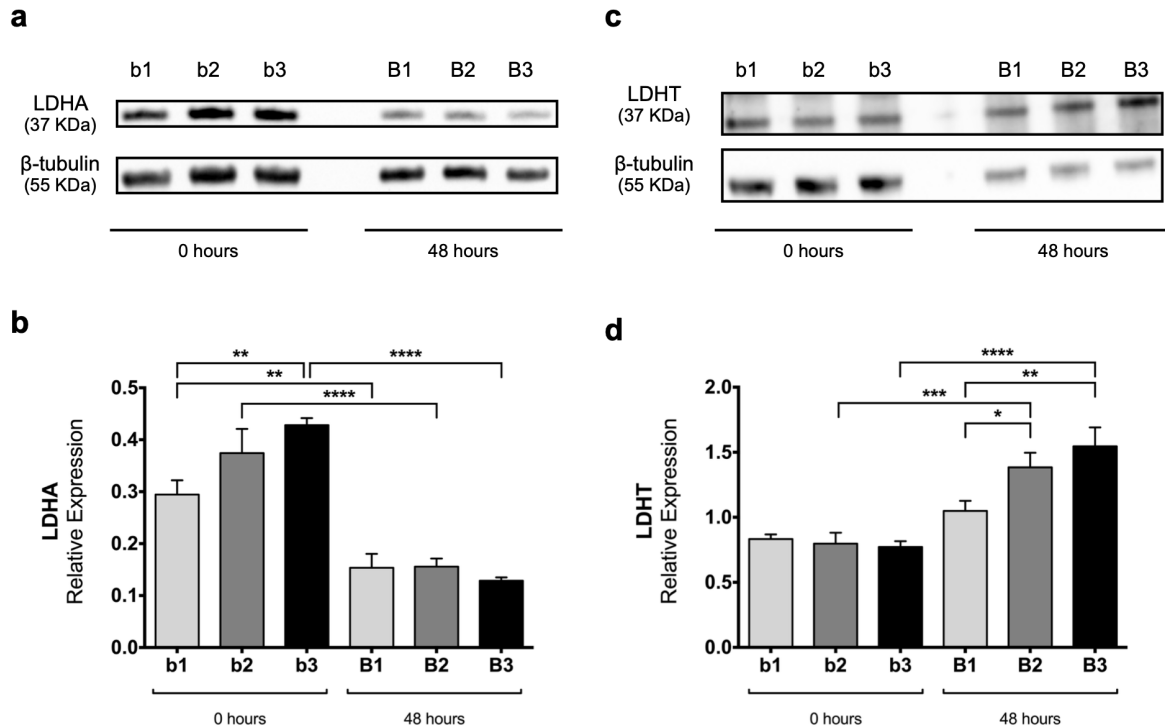
Figure 6 - Western blot analysis of LDHA and total LDH throughout chick lung branching. Representative immunoblots for **a** LDHA and **c** LDHT (LDHA and LDHB contribution) of pooled-tissue samples of embryonic lungs at D0 (0 h) (b1, b2, b3) and D2 (48 h) (B1, B2, B3) of explant culture. Loading control was performed using β-tubulin (55 KDa). LDHA and LDHT correspond to 37 KDa. Semiquantitative analysis, of three independent experiments, for **b** LDHA and for **d** LDHT protein expression levels. Results are represented in arbitrary units, normalized for β-tubulin. Results are expressed as mean ± SEM (n = 3/stage/condition). One-Way ANOVA and Fisher's LSD test were performed. Significantly different results are indicated as: *$p < 0.05$; **$p < 0.01$; ***$p < 0.001$; ****$p < 0.0001$. Full-length blots are presented in Figure S2.

Basal oxygen consumption rate is maintained during branching morphogenesis

To corroborate that the embryonic lung displays a glycolytic preference as branching morphogenesis develops, the respiratory capacity of explant tissue was evaluated. For this purpose, B1 to B3 lung explant tissue was collected after 48 h of culture (Fig. 1a), and the basal oxygen consumption rate (OCR) was measured (Fig. 7).

After 48 h of culture, basal OCR was maintained between B1, B2, and B3 (Fig. 7). However, a slight decrease tendency in explants' respiratory capacity throughout pulmonary branching is detected.
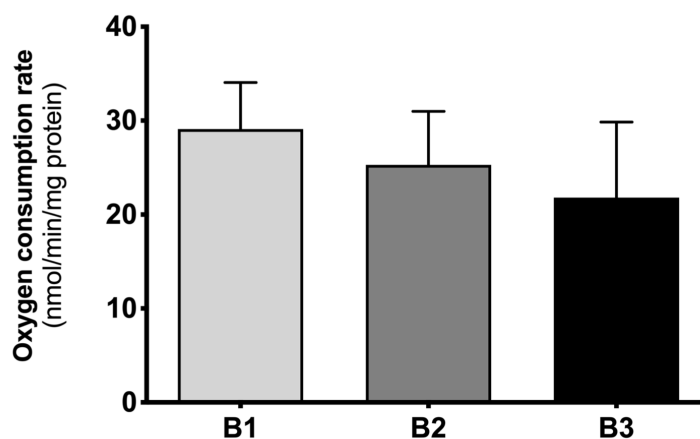
Figure 7 - Basal oxygen consumption rate (OCR) measurements throughout early stages of lung branching. Oxygen consumption rate (OCR) of embryonic lungs after 48 h of explant culture (B1, B2, B3). Results are represented in nmol/min of oxygen consumption normalized for the total amount of protein. Results are expressed as mean ± SEM (n ≥ 5/stage/condition). One-Way ANOVA and Fisher's LSD test were performed. $p < 0.05$ was considered.

DISCUSSION

Lung development is a complex process characterized by epithelial-mesenchymal interactions mediated by signaling cascades, leading to the formation of a fully functional organ [12,26]. Altogether, these processes contribute to the formation of a fully functional adult organ responsible for gas exchange.

The metabolic profile of the mammalian adult pulmonary system was studied in the '70 and '80s, revealing a metabolism that is primarily dependent on glucose utilization [16–18]. On the other hand, little is known about embryonic lung metabolic needs. The importance of metabolism during development, beyond its canonical role, has been recently reported; several studies have shown that metabolism is highly regulated both in time and space, affecting multiple aspects of animal development [19]. Moreover, glucose uptake and catabolism are essential for all cellular processes and are believed to be enhanced in high proliferative systems such as cancer and embryonic development [20,27].

Branching morphogenesis is a crucial step in lung organogenesis since it establishes the future airway conducting system [28]. In the chicken lung, b1, b2, and b3 stages correspond to the sequential appearance of the first three secondary buds, with approximately an 8 h gap between them. These morphologically similar stages revealed to be a useful system to study the molecular mechanisms underlying avian branching morphogenesis. Overall, signaling pathways display similar patterns between stages, and the interaction between different signaling events ultimately shapes airway branching [7–9,11]. In this sense, we wondered if b1, b2, and b3 stages were also similar at the metabolic level or if, despite the molecular similarities, the embryonic lung gradually adapts its metabolic needs to cope with

the progressive tissue growth. Accordingly, in this work, we focused on describing the metabolic profile of the embryonic chicken lung during the abovementioned stages of branching morphogenesis. For this purpose, an *ex vivo* explant culture system was used to precisely measure the metabolic and associated molecular alterations during 48 h of culture [29–31]. This method is particularly relevant to study the whole organ while under very controlled conditions since it preserves the epithelial-mesenchymal interactions that contribute to branching morphogenesis [30,32]. Lung explants are described to maintain the native physiological interactions between cells and tissues, thus mimicking the *in vivo* structure and function [29]. The culture medium from *ex vivo* lung explant culture was collected to study the production/consumption of extracellular metabolites related to glucose catabolism (alanine, lactate, and acetate) by ^{1}H-NMR spectroscopy. Afterward, the molecular machinery associated with glucose catabolism (*glut1*, *glut3*, *glut8*, *mct1*, *mct3*, *mct4*, *mct8*, *hk1*, *hk2*, *pfk1*, *ldha*, *ldhb*, *pdha*, and *pdhb*) was characterized by qPCR. *ldha* and *ldhb* mRNA spatial localization was assessed by *in situ* hybridization. Proliferation status was determined by directly assessing DNA synthesis using an EdU-based assay. LDH protein expression levels were evaluated by western blot. The respiratory capacity of lung explants was evaluated by measuring the basal oxygen consumption rate.

In this study, ^{1}H-NMR results revealed that glucose consumption by chicken lung explants decreases from B1 to B2 and from B1 to B3 stage, and remains stable between B2 and B3 stage (Fig. 1c). In B1, glucose consumption is higher, and we believe this is due to a higher nutrient requirement to cope with the very beginning of branching morphogenesis. As lung branching morphogenesis proceeds, glucose consumption profile variation may reflect the need to cope with specific energy and nutrients requirements needed to maintain high proliferative rates. Similarly, the adult mammalian lung metabolic requirements are mainly achieved through glucose catabolism, although other metabolic substrates might support lung energetic demands [16–18,33].

Glucose cellular uptake relies on the presence of integral membrane glucose transporters (GLUTs) that move glucose from the extracellular space to the cytosol by facilitated diffusion; furthermore, this process depends on the number of glucose transporters expressed in the cell surface. In this sense, the expression levels of selected transporters, *glut1*, *glut3*, and *glut8*, in the chicken developing lung were characterized. *glut1*, *glut3*, and *glut8* are expressed in the three pulmonary stages studied (Fig. 2b–d). After 48 h in culture, major variations of *glut1* and *glut3* are detected in B1 and B2 stages (Fig. 2b, c) but not in the B3 stage (Fig. 2b, c). *glut1* and *glut3* expression level variations may support the observed glucose consumption variations. *glut1* and *glut3* transcripts have already been identified during chicken embryonic development in other tissues than the lung, namely, in the brain, muscle, and heart; moreover,

glut1 and *glut3* expression levels are developmentally regulated in these structures [34]. In the adult, *glut1* and *glut8* are ubiquitously expressed, whereas *glut3* is highly expressed in the brain, similarly to their mammalian counterparts [35–37]. In human fetal lung, GLUT1 is present in bronchial and primitive alveolar epithelial cells during the branching phase but becomes progressively less expressed from week 19 onwards [38]. GLUT1 is widely expressed in adult human tissues, and it is commonly overexpressed in several tumor types [39]. On its turn, GLUT3 is highly expressed in lung cancer and actively contributes to cellular glucose uptake and consequent high proliferation of pulmonary tumor cells [40]. Altogether *glut1*, *glut3*, and *glut8* may likely contribute to sustaining glucose consumption throughout early pulmonary branching morphogenesis stages.

Once inside the cell, glucose is converted into glucose-6-Pi in a reaction catalyzed by hexokinase [41]. *hk1* is expressed in the embryonic chicken lung during branching morphogenesis (Fig. 3a), whereas *hk2* transcript is barely detected (data not shown).

PFK1 catalyzes a key step of glycolysis, the unidirectional conversion of fructose-6-Pi and ATP into fructose-1,6-Pi and ADP [41]. In the embryonic chicken lung, *pfk1* transcript is present in all stages studied without major variations between groups (Fig. 3b). *pfk1* expression levels may contribute to control the relative glucose flux into the glycolytic pathway throughout early branching.

From the glycolytic pathway, each molecule of glucose is converted into two molecules of pyruvate. In our explant culture medium, several pyruvate-derived metabolites (alanine, lactate, and acetate from acetyl-CoA) were detected (Fig. 1d–f). During branching morphogenesis, the embryonic chicken lung progressively increases alanine production that is finally exported to the extracellular medium (Fig. 1d). Previous studies revealed that, in the adult mammalian lung, part of the glucose carbons serves for alanine production through pyruvate transamination [17,18,33]. Similarly, in prostate cancer, the production of significantly high levels of alanine supports the need for proliferating cells for protein synthesis and membranogenesis [42]. Moreover, in pancreatic ductal adenocarcinoma, alanine produced from the surrounding environment is used by tumor cells for biosynthetic purposes [43]. Thus, alanine is an important end product of glucose catabolism and, in the developing lung, may contribute to protein biosynthesis to support active pulmonary growth.

Lactate was detected at high concentrations in the explant culture medium. Indeed, in our culture conditions, there is a sharp increase in lactate production from stage B1 to B3, and from stage B2 to B3 (Fig. 1e), concurrently with the increase in branching (Figure S1). The lactate/glucose ratio revealed that in B1 and B2 explants, 41% and 58% of glucose is directed to lactate production, respectively; in B3 explants, around 76% of glucose is converted into lactate. Likewise, in the mammalian adult lung, around

50% of the glucose carbons are metabolized into lactate [16–18,33]. Therefore, lactate production by the developing lung may be facilitating the uptake and incorporation of nutrients by promoting the activity of biosynthetic pathways to, for instance, form new biomass and regenerate NAD+ required for maximal glycolytic flux [44]. The increase in alanine and lactate production is characteristic of high proliferative systems in which fast energy and macromolecules are necessary to sustain the growth.

Lactate dehydrogenase (LDH) is the enzyme responsible for the interconversion of pyruvate into lactate and NADH into NAD+. This enzyme is a tetramer of two types of subunits, LDHA (formerly LDH-M) and LDHB (formerly LDH-H), encoded by *ldha* and *ldhb*, respectively [45]. In this work, we characterized the expression levels of both *ldha* and *ldhb* in the embryonic chicken lung. *ldha* expression increases from b1 to B1 and from b3 to B3 (Fig. 3c). Regarding 48 h' time point, the expression levels are higher at B1 and then decrease substantially to B2 and B3 (Fig. 3c). On the other hand, *ldhb* expression levels decrease from 0 to 48 h for b1 stage (Fig. 3d). Although the relative expression levels of *ldhb* are greater than *ldha*, higher variations accompanying branching were observed in *ldha* (Fig. 3g). Afterward, we performed *in situ* hybridization to assess *ldha* and *ldhb* spatial localization. *ldha* and *ldhb* displayed region-specific expression patterns in the chicken developing lung. *ldha* is highly expressed in the proximal region of the lung (Fig. 4a and d) and non-existent in the main bronchus epithelium and secondary bronchi (Fig. 4c). In opposition, *ldhb* transcript is absent from the proximal region of the lung (Fig. 4e) but expressed in the distal region. *ldhb* is specifically expressed in the growing tips and secondary buds (Fig. 4e and g), suggesting an association with highly proliferative regions. Interestingly, in the chicken and mouse embryo, *ldhb* is found mostly in the posterior (distal-most) region of the embryo, the tailbud region [25]. *ldha* and *ldhb* specific patterns remind a spatial distribution typical of proximal-distal markers.

To determine the proliferation status of lung branching morphogenesis, we performed an EdU proliferation assay, using B1 to B3 lung explants (Fig. 1a). High levels of proliferation were detected in the trachea region (white arrowhead) (Fig. 5b), matching *ldha* mRNA expression pattern (Fig. 4d). In addition, high levels of proliferation were also present in the secondary bronchi/active branching sites (asterisk) (Fig. 5h), and in the distal tips of the developing lung (white arrow) (Fig. 5e), which coincides with *ldhb* transcripts spatial localization (Fig. 4e–h). These results point towards an association between *ldha* and *ldhb* expression localization and proliferation events occurring during branching morphogenesis.

After the mRNA expression studies, we performed western blot for LDHA and total LDH (LDHA and LDHB contribution). LDHA displayed a decrease between 0 and 48 h (Fig. 6a, b). In contrast, total LDH expression levels increased from 0 to 48 h of *ex vivo* culture (Fig. 6c, d). From these results, we

speculate that LDHB may be contributing to the increase of total LDH protein levels. When we compare mRNA and protein expression data, an inverse pattern between the same *ldh*/LDH isoform is observed (Figs. 3c *vs* 6b; Figs. 3d *vs* 6d). It is generally assumed that mRNA expression levels directly correlate with protein levels. However, several studies have demonstrated that this not always occurs [46,47]. Distinct factors may account for these differences, such as regulatory mechanisms at transcriptional and/or translational level, or mRNA and protein stability, that can collectively impact total protein levels. In addition, given western blot results and mRNA spatial localization, it is possible that during branching, distal regions produce more lactate to cope with high proliferation rates. The increase in LDH total levels may account for the observed rise in extracellular lactate levels, which seem to be a characteristic of the developing lung.

Since lactate exchange between the cytosol and the extracellular space depends on monocarboxylate transporters (MCTs), we decided to study MCTs in the developing lung. *mct1* and *mct8* expression levels behave similarly throughout branching (Fig. 2e, f) and recapitulate GLUTs mRNA expression behavior. *mct1* displays a considerable increase in stage b1 after 48 h in culture (Fig. 2e), suggesting that it may support intracellular lactate export. Likewise, *mct3* and *mct4* were evaluated but displayed very low expression levels (data not shown). MCT1 has been described in both human and rat fetal lung; additionally, MCT inhibition leads to a decrease in rat lung branching [38]. More recently, Oginuma and colleagues found that *mct1* is expressed, in a graded manner, in the tailbud and posterior PSM of the chicken embryo. Moreover, chicken explants cultured with MCTs inhibitor α-cyano-4-hydroxycinnamic acid (CNCn) displayed increased intracellular lactate levels [48]. On the other hand, cancer cells are equipped with MCTs, mainly MCT1 and MCT4, to exchange lactate and regulate pH homeostasis [49]. MCT4 is the predominant monocarboxylate transporter for lactate export in glycolytic cancer cells; conversely, MCT1 is a passive transporter that can operate in both directions and, in cancer systems, it is described to facilitate lactate export [50]. In fact, MCT1 lactate transport depends on the intracellular/extracellular concentrations of lactate and protons [50]. Chicken *mct8*, also known as thyroid hormone transporter, was previously described in the developing brain, retina, spinal cord, kidney, and testis of the chicken [51,52]. Moreover, *mct8* knockdown impacts embryonic chicken development, meaning that *mct8* expression is crucial from the very early stages of organogenesis [53]. However, MCT8 does not transport lactate, but it may transport other monocarboxylates and amino acids [54]. In the embryonic chicken lung, *mct1* can be the transporter responsible for cellular lactate exchange.

Pyruvate can be transformed into acetyl-CoA through an irreversible enzymatic reaction catalyzed by pyruvate dehydrogenase (PDH) and then incorporated in the TCA cycle or converted into acetate [41].

Both isoforms of pyruvate dehydrogenase, *pdha* and *pdhb*, are expressed in the embryonic chicken lung (Fig. 3e, f). In the embryonic lung explant culture medium, we did not find detectable levels of metabolites from the Krebs cycle in the ^{1}H-NMR spectra. On the other hand, acetate was identified, and its production is increased in later stages of early pulmonary branching (Fig. 1f). Altogether, these data suggest that part of pyruvate may be diverted to acetate, through acetyl-CoA, as pulmonary branching proceeds. In mammals, glucose-derived pyruvate can generate acetate, and this phenomenon is more pronounced when under conditions of hyperactive glucose metabolism [55]. Moreover, in the adult mammalian lung, glucose carbons can incorporate acetate for lipogenesis purposes and serve for surfactant production [17,18,33,56]. Thus, in the embryonic lung, acetate may also point to a hyperactive glucose metabolism and can be produced to incorporate the newly synthesized cellular membranes, a common mechanism of high proliferative cells.

Lastly, to assess whether the embryonic lung truly shows a glycolytic preference during branching morphogenesis, mitochondrial respiration was evaluated. For this purpose, the respiratory capacity of explants was assessed by measuring the basal oxygen consumption rate of the embryonic lungs (Fig. 7). After 48 h of culture, explants display a steady basal OCR in the three stages; nonetheless, there is a slight tendency to decrease as branching morphogenesis proceeds (Fig. 7). This phenomenon occurs in parallel to the progressive increase in alanine, lactate, and acetate production, previously described (Fig. 1d–f). Altogether, these results suggest that, under aerobic conditions and with functional mitochondria, the embryonic lung seems to shift to a glycolytic lactate-based metabolism throughout branching morphogenesis.

CONCLUSIONS

This study describes the temporal metabolic changes that occur during early chicken pulmonary branching. Throughout this period, we observed changes in the metabolite profile that occur concurrently with variations in the expression levels of pivotal enzymes and transporters from the glycolytic pathway and with a steady oxygen consumption rate (Fig. 8). It appears that pulmonary branching morphogenesis progressively adapts to a glycolytic lactate-based metabolic profile, suggesting a Warburg-like metabolism. This metabolic rewiring to aerobic glycolysis is also observed in other high proliferative developing systems and allows the production of energy and biomass during embryonic development [20–22, 24, 25, 57]. Moreover, this metabolic adaptation might exert additional signaling functions throughout pulmonary branching, and further studies are required to address this topic. We acknowledge that this study has a strong descriptive perspective, but we are addressing a subject that has not been exploited so far. This

report highlights the importance of metabolic regulation during the early stages of lung development and lays the groundwork for future mechanistic studies on this topic.
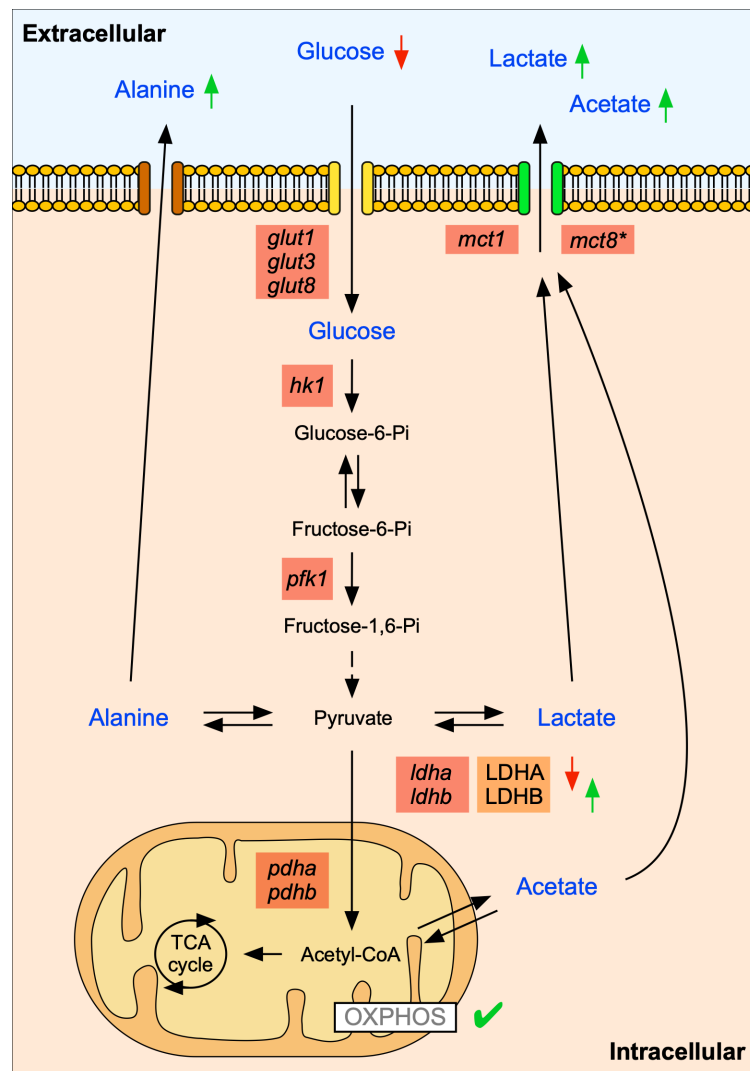

Figure 8 - Schematic representation of the metabolic profile of early pulmonary branching morphogenesis. The metabolites detected in the extracellular medium (blue labeling) can either be consumed (glucose) or produced (alanine, lactate, and acetate) by the lung tissue. The symbols refer to increase (↑) or decrease (↓) in the metabolites, considering their particular fate. Temporal metabolite changes are accompanied by variations in the expression of *glut1*, *glut3*, *glut8*, *hk1*, *pfk1*, *mct1*, *mct8*, *ldha*, *ldhb*, *pdha*, and *pdhb*. Decreased LDHA and increased LDHB protein levels may contribute to the observed increase in the extracellular levels of lactate. OXPHOS is active with mitochondria displaying a constant rate of oxygen consumption. The symbols refer to: does not contribute to lactate transport (*); oxidative phosphorylation is active (✓).

METHODS

Ethical statement

This work was performed at the early stages of chicken embryonic development and, therefore, does not require ethical approval following the European Parliament Directive 2010/63/EU of 22 September 2010 and the Portuguese Directive 113/2013 of 7 August 2013 on the protection of animals used for scientific purposes.

Tissue collection

Fertilized chicken eggs, *Gallus gallus*, were incubated between 4.5 and 5.5 days (Embryonic day 4.5–5.5) in a 49% humidified atmosphere at 37 °C (Termaks KB400, Norway). Embryonic lungs were obtained by microdissection under a stereomicroscope (Olympus SZX16, Japan) and classified in stage b1, b2, or b3 according to the number of secondary buds formed per bronchus; 1, 2, or 3, respectively [7]. Dissected lungs were processed for *ex vivo* lung explant culture or for *in situ* hybridization.

Ex vivo lung explant culture

Chicken lung explant culture was performed, as previously described [30], to study potential temporal metabolic changes while in controlled settings. Briefly, after dissection in PBS, lungs were placed on top of 8 μm nucleopore polycarbonate membranes (Whatman, USA) and incubated for 48 h in 200 μL of medium 199 (5.5 mM glucose; Sigma, USA) supplemented with 10% (V/V) chick serum (Invitrogen, USA), 5% (V/V) heat-inactivated fetal calf serum (Invitrogen), 1% (V/V) L-glutamine (Invitrogen), 1% (V/V) penicillin 5000 IU/mL plus streptomycin 5000 IU/mL (Invitrogen) and 0.25 mg/mL of ascorbic acid (Sigma). The medium was replaced by fresh supplemented medium at 24 h of culture. Lung explants were photographed at 0 h (D0), 24 h (D1), and 48 h (D2) with a camera (Olympus U-LH100HG) coupled to a stereomicroscope (Olympus SZX16). The medium was collected at D0, D1, and D2 for ^{1}H-NMR spectroscopy analysis. D0 and D2 lung explants were collected for RNA and protein extraction; D2 lung explants were collected for EdU proliferation assay and basal oxygen consumption rate assay.

^{1}H-NMR spectroscopy

Samples of 200 μL of medium were collected from *ex vivo* lung explant culture, at D0, D1, and D2, and analyzed by ^{1}H-NMR spectroscopy (n ≥ 5/stage/condition) according to [58]. A Bruker Avance 600 MHz spectrometer with a 5 mm QXI probe and z-gradient (Bruker Biospin, Germany) was used, and spectra accessed at 25 °C. Solvent-suppressed ^{1}H-NMR spectra were acquired with 6 kHz spectral width,

14-s interpulse, 3-s water presaturation, 45-degree pulse angle, 3.5-s acquisition time, and a minimum of 128 scans. Sodium fumarate (singlet, at 6.50 ppm) was used as an internal reference at 10 mM. The following metabolites were detected and quantified: H1-α glucose (doublet, 5.22 ppm), alanine (doublet, 1.46 ppm), lactate (doublet, 1.33 ppm), and acetate (singlet, 1.9 ppm). To quantify the relative areas of ^{1}H-NMR resonances, the curve-fitting routine supplied with the NUTSpro™ NMR spectral analysis program (Acorn NMR, USA) was used. D0 media samples were used as reference/control. The metabolite consumption/production during 48 h of explant culture was calculated following the mathematical formula | (D1-D0) + (D2-D0) |. Metabolite data were normalized to the total amount of protein.

Quantitative PCR

Total RNA was extracted from D0 and D2 lung explants using TripleXtractor directRNA kit (Grisp, Portugal). RNA integrity and purity were determined using the Experion RNA StdSens Analysis Kit (Bio-Rad, USA), and RNA concentration determined by Nanodrop 1000 Spectrophotometer (Thermo Fisher Scientific, USA). Total RNA was treated with DNase I (Thermo Fisher Scientific) and then reversely transcribed to obtain cDNA using GRS cDNA Synthesis kit (Grisp). Specific exon-exon spanning primers were designed for the amplification of target and housekeeping transcripts (Table S1). Primers were optimized for annealing temperature and PCR cycles, using NZY Taq 2×Green Master Mix (NZYTech, Portugal) and, subsequently, for efficiency range. qPCR was performed in duplicate (n ≥ 5/stage/condition) using 1 μL of cDNA and SYBR method according to manufacturer's instructions, NZY qPCR Green Master Mix (2x) (NZYTech). mRNA expression levels were normalized for both *18s* and *actin-β* housekeeping genes. Data on the gene expression levels were calculated following the mathematical model $2^{\wedge}(-\Delta Ct)$ [59].

Western blot

Pooled samples of D0 and D2 explants (3 pools per stage: 8 lungs per pool) were processed for western blot analysis, as described in [8]. Protein was obtained according to [60]. 10 μg of protein was loaded onto 10% acrylamide minigels, electrophoresed at 100 V in a Mini-PROTEAN Tetra Cell (Bio-Rad), and transferred to 0.2 μm nitrocellulose membranes using a Trans-Blot Turbo Transfer System (Bio-Rad). Blots were probed with primary antibodies for LDHA (1:20,000; #3582, Cell Signaling, USA), for total LDH that recognizes both LDHA and LDHB (1:20,000; #ab52488, Abcam, UK), and for β-tubulin (1:200,000; #ab6046, Abcam) as a loading control. Afterward, blots were incubated with anti-rabbit secondary horseradish peroxidase-conjugated antibody (1:2000; #7074, Cell Signaling). Membranes

were developed with Clarity Max Western ECL substrate (Bio-Rad), and the chemiluminescent signal captured using Chemidoc XRS (Bio-Rad). Quantitative analysis was performed with Image Lab software (Bio-Rad). At least three independent experiments per pool were performed (n = 3).

RNA probes

Total RNA and cDNA from b2 lungs were obtained as previously described. Specific primers were designed for *ldha* (Fw: 5'-GCACTTTCCAAGTAGGTCAAATCC-3'; Rv: 5'-AGTCTTTGGTTTCACGTTGTGT-3') and *ldhb* (Fw: 5'-GCAGGTTGTTGAAAGTGCCT-3'; Rv: 5'-AGTGAGTAGAGAGCCCACAT-3'). cDNA was used as a template for conventional PCR (GRS Xpert Taq 2×MasterMix, Grisp). PCR fragments were cloned in the pCR II-TOPO vector (TOPO TA Cloning Kit, Invitrogen) and sequenced to determine the insert orientation (GATC Biotech, Germany). *l-cam* RNA probe was produced as previously described [61]. Antisense digoxigenin-labeled RNA probes were produced from PCR-amplified fragments using SP6 or T7 RNA polymerase and according to the manufacturer's instructions (Roche, Germany).

Whole mount *in situ* hybridization

Dissected lungs were fixed in PBS solution containing 4% formaldehyde, 2 mM EGTA, pH 7.5, at 4 °C overnight. Then, the lungs were dehydrated in a methanol series and stored at −20 °C. Tissues were rehydrated through a methanol/PBT series and processed for whole mount *in situ* hybridization (n ≥ 9 per gene/stage) as previously described by [30]. Briefly, tissues were permeabilized with proteinase K solution (PBT with 0.05% proteinase K) (Roche). PBT washes were made to remove the excess of proteinase K and, tissues were incubated with a post-fixing solution (PBT with 10% formaldehyde, 0.4% glutaraldehyde). After, tissues were incubated with hybridization solution (50% formamide, 6.5% SSC, 1% EDTA 0.5 M pH 9.8, 0.25% t-RNA, 0.2% Tween 20, 0.2% heparin, 0.5% CHAPS), at 70 °C. Then, tissues were incubated with specific probes, in hybridization solution, at 70 °C, overnight. On the following day, several washes were performed with preheated hybridization solution, hybridization solution with MABT (50:50) (5.8% $C_4H_4O_4$, 4.4% NaCl, 7% NaOH, 1% Tween 20, pH 7.5) and subsequently with only MABT. Next, tissues were treated with blocking solutions [MABT with 20% blocking reagent (Roche); MABT with 20% blocking reagent plus 20% goat serum (Invitrogen)]. Then, lungs were incubated in MABT, 20% blocking reagent, 20% goat serum, and 1:2000 anti-digoxigenin antibody (Roche) solution, overnight. On day 3, the tissues were washed with MABT solution. On the last day, tissues were washed in NTMT solution (0.1 M NaCl, 0.1 M Tris–HCl, 50 mM $MgCl_2$, 1% Tween 20) and then incubated in a developing solution (NTMT with BCIP, NBT) (Roche), at 37 °C and protected from light. Each group

of lungs/probes was processed simultaneously and developed for the same amount of time. All the lungs were photographed using a camera (Olympus U-LH100HG) coupled to a stereomicroscope (Olympus SZX16).

Histological sections

Hybridized chicken lungs were dehydrated through increasing ethanol series and embedded in a 2-hydroxy-ethyl methacrylate solution (Heraeus Kulzer, Germany). 25 μm thick histological slides were produced by a rotatory microtome (Leica RM 2155, Germany). Lung histological sections were photographed using a camera (Olympus DP70) coupled to a microscope (Olympus BX61).

Proliferation assay and confocal microscopy

After 48 h of culture, half of the explant's media was replaced by fresh media containing EdU, at a final concentration of 150 μM. Explants were incubated with EdU for 90 min in the same culture conditions. After incubation, tissues were fixed in PBS solution containing 3.7% formaldehyde. Then, tissues were washed in PBS with 3% BSA, and permeabilized in PBS with 0.5% Triton X-100, for 90 min. Tissues were washed again and processed for Click-iT Plus EdU reaction, according to the manufacturer's instructions (Click-iT™ Plus EdU Cell Proliferation Kit for Imaging, Invitrogen). Detection of the incorporated EdU was performed using Alexa Fluor 488. Nuclei were counterstained with Hoechst 33342 (1:2000). Images were acquired using an Olympus LPS Confocal FV3000 microscope (Olympus).

Basal oxygen consumption rate measurements

Pooled samples of D2 (2 lungs per pool/per stage) explants were processed to assess respiratory capacity (n ≥ 5/stage/condition). Lung tissue was washed in PBS and incubated, for 2 min, in respiration medium, at 37 °C. Respiration medium was composed by medium 199 (5.5 mM glucose) supplemented with 1% L-glutamine, 1% ITS (0.01 mg/mL recombinant human insulin, 0.0055 mg/mL human transferrin substantially iron-free, and 0.005 μg/mL sodium selenite) (BD Biosciences, USA) and 10 mM HEPES; pH was adjusted to 7.2–7.4, at 37 °C. To assess Oxygen Consumption Rate (OCR), a Clark-type electrode Oxytherm System (Hansatech, UK) was used [62]. Samples were transferred in 1 mL respiration medium to the pre-calibrated and thermostatized (with a water jacket, at 37 °C) electrode chamber. Oxygen recording protocol was performed for 15 min with an open-chamber plus 15 min with a closed-chamber; data acquisition refers to the last 5 min of closed-chamber mode. After each assay, tissue samples were retrieved, washed in PBS, and processed for protein extraction and quantification. Data

was analyzed using Oxytrace Plus acquisition software (Hansatech) and normalized to the total amount of protein.

Statistical analysis

Statistical analysis was performed using GraphPad Prism 6 (GraphPad Software, USA). The normality of distribution was tested using the Kolmogorov–Smirnov test. One-Way ANOVA was performed and followed by Fisher's Least Significant Difference (LSD) post hoc test for multiple comparisons. All experimental data are presented as mean ± standard error of the mean (SEM) with a statistically significant level of 5% ($p < 0.05$) considered.

SUPPLEMENTARY INFORMATION

Table S1 - Primers and qPCR conditions. Primer sequences forward (Fw) and reverse (Rv), corresponding PCR product size, annealing temperature and number of cycles.

Gene	Sequence 5'-3'	Size (bp)	Annealing T (°C)	Cycles
actin-β	Fw – CTTCTAAACCGGACTGTTACCA Rv – AAACAAATAAAGCCATGCCAATCT	100	58	30
18s	Fw – TCTTTCTCGATTCCGTGGGT Rv – AACGCCACTTGTCCCTCTAC	157	58	30
glut1	Fw – GCAGTTCGGCTACAACACCG Rv – ATCAGCATGGAGTTACGCCG	222	58	40
glut3	Fw – GTACCGTTCGGGTTCCGTTAG Rv – AATGGCAGCAACAGAAACAGC	115	62	35
glut8	Fw – AGCTTTGGCTTCGTGCTAGG Rv – GTAGCCTCCCAGTATTCCTCC	153	58	40
mct1	Fw – TCGGAGCCTTCATCTCCATTG Rv – CAATCAAACCACACCCCGAG	234	58	40
mct3	Fw – CATCGGGCTGGTCCTACTTA Rv – GTCTTCTTCCCTCGGTTCAG	183	58	40
mct4	Fw – GGATCTGCACTCAGGGAACC Rv – GGAAAGGCGTAGGAGAACCC	151	62	40
mct8	Fw – TTCTTCTGCTCTCCCATCGT Rv – CGACGCTTGAAGTAGTGACC	218	58	40
hk1	Fw – CTGGCCTACTACTTCACCGAG Rv – TCACTGTCGCTGTTGGGTTA	166	58	35

|				
hk2	Fw – GCGCAGAAGGTGGACAAATAC Rv – TGCCAAGAAGTCTCCGTCCT	192	58	40
pfk1	Fw – CGTGGGAGGAGCTTTGAGAA Rv – CAGCCCACCTCACGTATCTG	236	56	40
ldha	Fw – AAGACGCCGGCAGTACAC Rv – GAGTGTGCAGTCACGCTGTA	285	58	35
ldhb	Fw – ACTTGGTATCCACCCAACCAG Rv – CTCAGCAACGCTAAGACCAAT	244	54	40
pdha	Fw – TCACGGCTTTACCTATGCCC Rv – ACCTGAGCACCGACAATACC	153	58	35
pdhb	Fw – GCTCAGAAGATGCTAAAGGGC Rv – GCTTCTAAACAGTGCCCAACAG	220	58	40
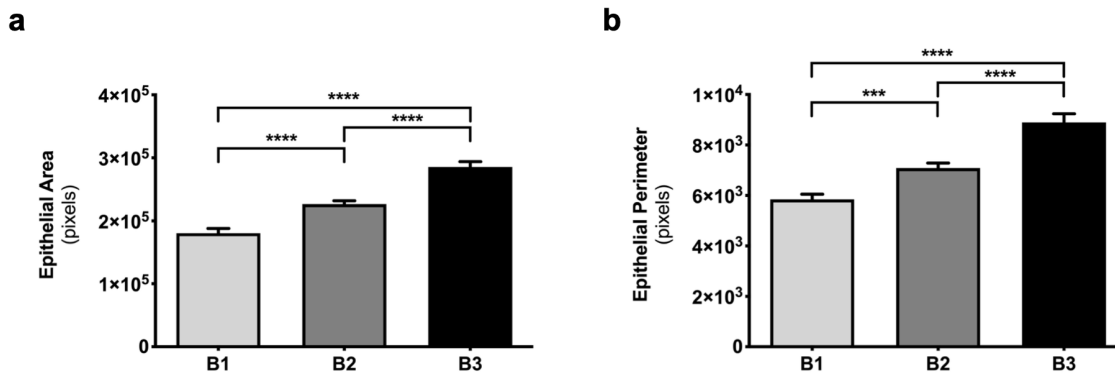
Figure S1 - Morphometric analysis of lung explants. The imaging program AxioVision Rel. 4.9.1 (Carl Zeiss, Germany) was used to outline lung explants at 48 hours (B1, B2, B3) and to calculate **a** Epithelial area and **b** Epithelial perimeter. After 48 hours in culture, explants display a progressive increase of the epithelial compartment when compared between stages (B1 *vs* B2 *vs* B3). Results are expressed as mean ± SEM (n > 10/stage/condition). One-Way ANOVA and Fisher's LSD test were performed. Significantly different results are indicated as: *** $p < 0.001$ **** $p < 0.0001$.
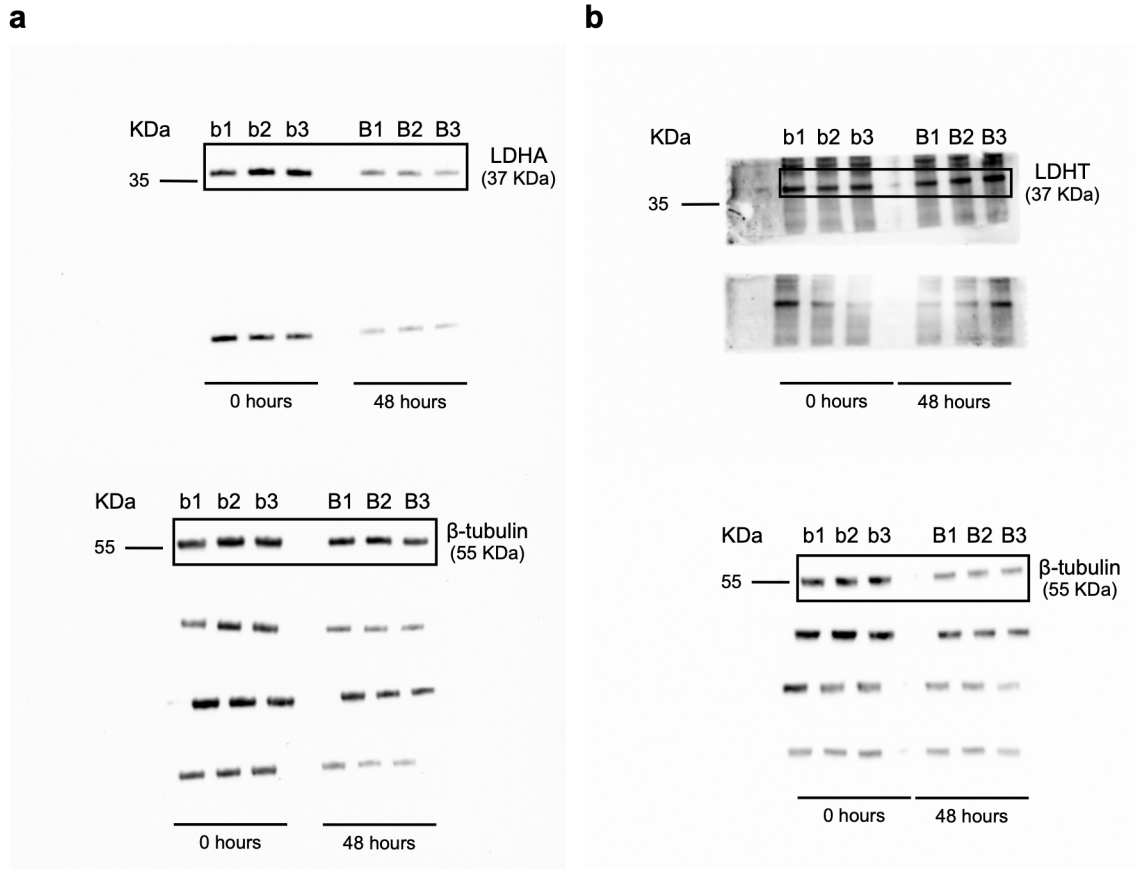
Figure S2 - Uncropped images of LDHA and total LDH immunoblot represented in Fig. 5 of the manuscript. Representative immunoblot for **a** LDHA and **b** LDHT (LDHA and LDHB contribution) of pooled-tissue samples of embryonic lungs at 0 hours (b1, b2, b3) and 48 hours (B1, B2, B3) of explant culture. Loading control was performed using β-tubulin, lower panel of the image (55 KDa). LDHA and LDHT correspond to 37 KDa.

REFERENCES

1.   Whitsett, J.A.; Kalin, T.V.; Xu, Y.; Kalinichenko, V.V. Building and Regenerating the Lung Cell by Cell. Physiol. Rev. 2019, 99, 513-554, doi:10.1152/physrev.00001.2018.

2.   Maina, J.N. A systematic study of the development of the airway (bronchial) system of the avian lung from days 3 to 26 of embryogenesis: a transmission electron microscopic study on the domestic fowl, Gallus gallus variant domesticus. Tissue Cell 2003, 35, 375-391, doi:10.1016/s0040-8166(03)00058-2.

3.   Kim, H.Y.; Varner, V.D.; Nelson, C.M. Apical constriction initiates new bud formation during monopodial branching of the embryonic chicken lung. Development 2013, 140, 3146-3155, doi:10.1242/dev.093682.

4.   Metzger, R.J.; Klein, O.D.; Martin, G.R.; Krasnow, M.A. The branching programme of mouse lung development. Nature 2008, 453, 745-750, doi:10.1038/nature07005.

5.   Maina, J.N. Comparative molecular developmental aspects of the mammalian- and the avian lungs, and the insectan tracheal system by branching morphogenesis: recent advances and future directions. Front. Zool. 2012, 9, 16, doi:10.1186/1742-9994-9-16.

6. Moura, R.S.; Correia-Pinto, J. Molecular aspects of avian lung development. In: Maina JN, editor. The biology of the avian respiratory system. Cham: Springer. 2017; pp. 129–146.

7. Moura, R.S.; Coutinho-Borges, J.P.; Pacheco, A.P.; Damota, P.O.; Correia-Pinto, J. FGF signaling pathway in the developing chick lung: expression and inhibition studies. PLoS ONE 2011, 6, e17660, doi:10.1371/journal.pone.0017660.

8. Moura, R.S.; Carvalho-Correia, E.; daMota, P.; Correia-Pinto, J. Canonical Wnt signaling activity in early stages of chick lung development. PLoS ONE 2014, 9, e112388, doi:10.1371/journal.pone.0112388.

9. Moura, R.S.; Silva-Goncalves, C.; Vaz-Cunha, P.; Correia-Pinto, J. Expression analysis of Shh signaling members in early stages of chick lung development. Histochem. Cell Biol. 2016, 146, 457-466, doi:10.1007/s00418-016-1448-1.

10. Fernandes-Silva, H.; Correia-Pinto, J.; Moura, R.S. Canonical Sonic Hedgehog Signaling in Early Lung Development. J. Dev. Biol. 2017, 5, doi:10.3390/jdb5010003.

11. Fernandes-Silva, H.; Vaz-Cunha, P.; Barbosa, V.B.; Silva-Goncalves, C.; Correia-Pinto, J.; Moura, R.S. Retinoic acid regulates avian lung branching through a molecular network. Cell. Mol. Life Sci. 2017, 74, 4599-4619, doi:10.1007/s00018-017-2600-3.

12. Warburton, D.; El-Hashash, A.; Carraro, G.; Tiozzo, C.; Sala, F.; Rogers, O.; De Langhe, S.; Kemp, P.J.; Riccardi, D.; Torday, J.; et al. Lung organogenesis. Curr. Top. Dev. Biol. 2010, 90, 73-158, doi:10.1016/S0070-2153(10)90003-3.

13. Fernandes-Silva, H.; Araujo-Silva, H.; Correia-Pinto, J.; Moura, R.S. Retinoic Acid: A Key Regulator of Lung Development. Biomolecules 2020, 10, doi:10.3390/biom10010152.

14. Engle, M.J.; Dooley, M.; Brown, D.J. Evidence for lactate utilization for fetal lung glycogen synthesis. Biochem. Biophys. Res. Commun. 1987, 145, 397-401, doi:10.1016/0006-291x(87)91335-0.

15. Engle, M.J.; Brown, D.J.; Dehring, A.F.; Dooley, M. Effect of lactate on glucose incorporation into fetal lung phospholipids. Exp. Lung Res. 1988, 14, 121-129, doi:10.3109/01902148809062854.

16. Yeager, H., Jr.; Massaro, D. Glucose metabolism and glycoprotein synthesis by lung slices. J. Appl. Physiol. 1972, 32, 477-482, doi:10.1152/jappl.1972.32.4.477.

17. Fisher, A.B. Normal and pathologic biochemistry of the lung. Environ. Health Perspect. 1976, 16, 3-9, doi:10.1289/ehp.76163.

18. Fisher, A.B. Intermediary metabolism of the lung. Environ. Health Perspect. 1984, 55, 149-158, doi:10.1289/ehp.8455149.

19. Krejci, A.; Tennessen, J.M. Metabolism in time and space - exploring the frontier of developmental biology. Development 2017, 144, 3193-3198, doi:10.1242/dev.150573.

20. Miyazawa, H.; Aulehla, A. Revisiting the role of metabolism during development. Development 2018, 145, doi:10.1242/dev.131110.

21. Miyazawa, H.; Yamaguchi, Y.; Sugiura, Y.; Honda, K.; Kondo, K.; Matsuda, F.; Yamamoto, T.; Suematsu, M.; Miura, M. Rewiring of embryonic glucose metabolism via suppression of PFK-1 and aldolase during mouse chorioallantoic branching. Development 2017, 144, 63-73, doi:10.1242/dev.138545.

22. Slaninova, V.; Krafcikova, M.; Perez-Gomez, R.; Steffal, P.; Trantirek, L.; Bray, S.J.; Krejci, A. Notch stimulates growth by direct regulation of genes involved in the control of glycolysis and the tricarboxylic acid cycle. Open Biol. 2016, 6, 150155, doi:10.1098/rsob.150155.

23. Homem, C.C.F.; Steinmann, V.; Burkard, T.R.; Jais, A.; Esterbauer, H.; Knoblich, J.A. Ecdysone and mediator change energy metabolism to terminate proliferation in Drosophila neural stem cells. Cell 2014, 158, 874-888, doi:10.1016/j.cell.2014.06.024.

24. Bulusu, V.; Prior, N.; Snaebjornsson, M.T.; Kuehne, A.; Sonnen, K.F.; Kress, J.; Stein, F.; Schultz, C.; Sauer, U.; Aulehla, A. Spatiotemporal Analysis of a Glycolytic Activity Gradient Linked to Mouse Embryo Mesoderm Development. Dev. Cell 2017, 40, 331-341 e334, doi:10.1016/j.devcel.2017.01.015.

25. Oginuma, M.; Moncuquet, P.; Xiong, F.; Karoly, E.; Chal, J.; Guevorkian, K.; Pourquie, O. A Gradient of Glycolytic Activity Coordinates FGF and Wnt Signaling during Elongation of the Body Axis in Amniote Embryos. Dev. Cell 2017, 40, 342-353 e310, doi:10.1016/j.devcel.2017.02.001.

26. Herriges, M.; Morrisey, E.E. Lung development: orchestrating the generation and regeneration of a complex organ. Development 2014, 141, 502-513, doi:10.1242/dev.098186.

27. Vander Heiden, M.G.; DeBerardinis, R.J. Understanding the Intersections between Metabolism and Cancer Biology. Cell 2017, 168, 657-669, doi:10.1016/j.cell.2016.12.039.

28. Schittny, J.C. Development of the lung. Cell Tissue Res. 2017, 367, 427-444, doi:10.1007/s00441-016-2545-0.

29. Yeganeh, B.; Bilodeau, C.; Post, M. Explant culture for studying lung development. In: Delgado-Olguin P, editor. Mouse embryogenesis; methods in molecular biology. New York: Humana Press: 2018; pp. 81–90.

30. Moura, R.S. Retinoic acid as a modulator of proximal-distal patterning and branching morphogenesis of the avian lung. In: Ray S, editor. Retinoid and rexinoid signaling; methods in molecular biology. New York: Humana Press: 2019; pp. 209–224.

31. Spurlin, J.W.; Siedlik, M.J.; Nerger, B.A.; Pang, M.F.; Jayaraman, S.; Zhang, R.; Nelson, C.M. Mesenchymal proteases and tissue fluidity remodel the extracellular matrix during airway epithelial branching in the embryonic avian lung. Development 2019, 146, doi:10.1242/dev.175257.

32. Carraro, G.; del Moral, P.M.; Warburton, D. Mouse embryonic lung culture, a system to evaluate the molecular mechanisms of branching. J. Vis. Exp. 2010, doi:10.3791/2035.

33. Tierney, D.F. Lung metabolism and biochemistry. Annu. Rev. Physiol. 1974, 36, 209-231, doi:10.1146/annurev.ph.36.030174.001233.

34. Carver, F.M.; Shibley, I.A., Jr.; Pennington, J.S.; Pennington, S.N. Differential expression of glucose transporters during chick embryogenesis. Cell. Mol. Life Sci. 2001, 58, 645-652, doi:10.1007/PL00000887.

35. Seki, Y.; Sato, K.; Kono, T.; Abe, H.; Akiba, Y. Broiler chickens (Ross strain) lack insulin-responsive glucose transporter GLUT4 and have GLUT8 cDNA. Gen. Comp. Endocrinol. 2003, 133, 80-87, doi:10.1016/s0016-6480(03)00145-x.

36. Kono, T.; Nishida, M.; Nishiki, Y.; Seki, Y.; Sato, K.; Akiba, Y. Characterisation of glucose transporter (GLUT) gene expression in broiler chickens. Br. Poult. Sci. 2005, 46, 510-515, doi:10.1080/00071660500181289.

37. Byers, M.S.; Howard, C.; Wang, X. Avian and Mammalian Facilitative Glucose Transporters. Microarrays (Basel) 2017, 6, doi:10.3390/microarrays6020007.

38. Granja, S.; Morais-Santos, F.; Miranda-Goncalves, V.; Viana-Ferreira, M.; Nogueira, R.; Nogueira-Silva, C.; Correia-Pinto, J.; Baltazar, F. The monocarboxylate transporter inhibitor alpha-cyano-4-hydroxycinnamic acid disrupts rat lung branching. Cell. Physiol. Biochem. 2013, 32, 1845-1856, doi:10.1159/000356617.

39. Ganapathy, V.; Thangaraju, M.; Prasad, P.D. Nutrient transporters in cancer: relevance to Warburg hypothesis and beyond. Pharmacol. Ther. 2009, 121, 29-40, doi:10.1016/j.pharmthera.2008.09.005.

40. Masin, M.; Vazquez, J.; Rossi, S.; Groeneveld, S.; Samson, N.; Schwalie, P.C.; Deplancke, B.; Frawley, L.E.; Gouttenoire, J.; Moradpour, D.; et al. GLUT3 is induced during epithelial-

mesenchymal transition and promotes tumor cell proliferation in non-small cell lung cancer. Cancer Metab 2014, 2, 11, doi:10.1186/2049-3002-2-11.

41. Nelson, D.L.; Cox, M.M. Lehninger principles of biochemistry. 5th ed. New York: Worth Publishers: 2008.

42. Tessem, M.B.; Swanson, M.G.; Keshari, K.R.; Albers, M.J.; Joun, D.; Tabatabai, Z.L.; Simko, J.P.; Shinohara, K.; Nelson, S.J.; Vigneron, D.B.; et al. Evaluation of lactate and alanine as metabolic biomarkers of prostate cancer using 1H HR-MAS spectroscopy of biopsy tissues. Magn. Reson. Med. 2008, 60, 510-516, doi:10.1002/mrm.21694.

43. Sousa, C.M.; Biancur, D.E.; Wang, X.; Halbrook, C.J.; Sherman, M.H.; Zhang, L.; Kremer, D.; Hwang, R.F.; Witkiewicz, A.K.; Ying, H.; et al. Pancreatic stellate cells support tumour metabolism through autophagic alanine secretion. Nature 2016, 536, 479-483, doi:10.1038/nature19084.

44. Vander Heiden, M.G.; Cantley, L.C.; Thompson, C.B. Understanding the Warburg effect: the metabolic requirements of cell proliferation. Science 2009, 324, 1029-1033, doi:10.1126/science.1160809.

45. Porporato, P.E.; Dhup, S.; Dadhich, R.K.; Copetti, T.; Sonveaux, P. Anticancer targets in the glycolytic metabolism of tumors: a comprehensive review. Front. Pharmacol. 2011, 2, 49, doi:10.3389/fphar.2011.00049.

46. Vogel, C.; Marcotte, E.M. Insights into the regulation of protein abundance from proteomic and transcriptomic analyses. Nat. Rev. Genet. 2012, 13, 227-232, doi:10.1038/nrg3185.

47. Koussounadis, A.; Langdon, S.P.; Um, I.H.; Harrison, D.J.; Smith, V.A. Relationship between differentially expressed mRNA and mRNA-protein correlations in a xenograft model system. Sci. Rep. 2015, 5, 10775, doi:10.1038/srep10775.

48. Oginuma, M.; Harima, Y.; Tarazona, O.A.; Diaz-Cuadros, M.; Michaut, A.; Ishitani, T.; Xiong, F.; Pourquie, O. Intracellular pH controls WNT downstream of glycolysis in amniote embryos. Nature 2020, 584, 98-101, doi:10.1038/s41586-020-2428-0.

49. Payen, V.L.; Hsu, M.Y.; Radecke, K.S.; Wyart, E.; Vazeille, T.; Bouzin, C.; Porporato, P.E.; Sonveaux, P. Monocarboxylate Transporter MCT1 Promotes Tumor Metastasis Independently of Its Activity as a Lactate Transporter. Cancer Res. 2017, 77, 5591-5601, doi:10.1158/0008-5472.CAN-17-0764.

50. Perez-Escuredo, J.; Van Hee, V.F.; Sboarina, M.; Falces, J.; Payen, V.L.; Pellerin, L.; Sonveaux, P. Monocarboxylate transporters in the brain and in cancer. Biochim. Biophys. Acta 2016, 1863, 2481-2497, doi:10.1016/j.bbamcr.2016.03.013.

51. Bourgeois, N.M.; Van Herck, S.L.; Vancamp, P.; Delbaere, J.; Zevenbergen, C.; Kersseboom, S.; Darras, V.M.; Visser, T.J. Characterization of Chicken Thyroid Hormone Transporters. Endocrinology 2016, 157, 2560-2574, doi:10.1210/en.2015-2025.

52. Vancamp, P.; Bourgeois, N.M.A.; Houbrechts, A.M.; Darras, V.M. Knockdown of the thyroid hormone transporter MCT8 in chicken retinal precursor cells hampers early retinal development and results in a shift towards more UV/blue cones at the expense of green/red cones. Exp. Eye Res. 2019, 178, 135-147, doi:10.1016/j.exer.2018.09.018.

53. Delbaere, J.; Vancamp, P.; Van Herck, S.L.; Bourgeois, N.M.; Green, M.J.; Wingate, R.J.; Darras, V.M. MCT8 deficiency in Purkinje cells disrupts embryonic chicken cerebellar development. J. Endocrinol. 2017, 232, 259-272, doi:10.1530/JOE-16-0323.

54. Friesema, E.C.; Ganguly, S.; Abdalla, A.; Manning Fox, J.E.; Halestrap, A.P.; Visser, T.J. Identification of monocarboxylate transporter 8 as a specific thyroid hormone transporter. J. Biol. Chem. 2003, 278, 40128-40135, doi:10.1074/jbc.M300909200.

55. Liu, X.; Cooper, D.E.; Cluntun, A.A.; Warmoes, M.O.; Zhao, S.; Reid, M.A.; Liu, J.; Lund, P.J.; Lopes, M.; Garcia, B.A.; et al. Acetate Production from Glucose and Coupling to Mitochondrial Metabolism in Mammals. Cell 2018, 175, 502-513 e513, doi:10.1016/j.cell.2018.08.040.

56.   Veldhuizen, R.; Nag, K.; Orgeig, S.; Possmayer, F. The role of lipids in pulmonary surfactant. Biochim. Biophys. Acta 1998, 1408, 90-108, doi:10.1016/s0925-4439(98)00061-1.

57.   Gandara, L.; Wappner, P. Metabo-Devo: A metabolic perspective of development. Mech. Dev. 2018, 154, 12-23, doi:10.1016/j.mod.2018.02.004.

58.   Alves, M.G.; Oliveira, P.F.; Martins, F.O.; Oliveira, P.J.; Carvalho, R.A. Gender-dependent metabolic remodeling during heart preservation in cardioplegic celsior and histidine buffer solution. J. Cardiovasc. Pharmacol. 2012, 60, 227-233, doi:10.1097/FJC.0b013e3182391d17.

59.   Livak, K.J.; Schmittgen, T.D. Analysis of relative gene expression data using real-time quantitative PCR and the 2(-Delta Delta C(T)) Method. Methods 2001, 25, 402-408, doi:10.1006/meth.2001.1262.

60.   Kling, D.E.; Lorenzo, H.K.; Trbovich, A.M.; Kinane, T.B.; Donahoe, P.K.; Schnitzer, J.J. MEK-1/2 inhibition reduces branching morphogenesis and causes mesenchymal cell apoptosis in fetal rat lungs. Am. J. Physiol. Lung Cell Mol. Physiol. 2002, 282, L370-378, doi:10.1152/ajplung.00200.2001.

61.   Dady, A.; Blavet, C.; Duband, J.L. Timing and kinetics of E- to N-cadherin switch during neurulation in the avian embryo. Dev. Dyn. 2012, 241, 1333-1349, doi:10.1002/dvdy.23813.

62.   Silva, A.M.; Oliveira, P.J. Evaluation of respiration with clark-type electrode in isolated mitochondria and permeabilized animal cells. In: Palmeira C, Monero A, editors. Mitochondrial bioenergetics; methods in molecular biology. New York: Humana Press: 2018; pp. 7–29.

Statement regarding data collection

For the record, we state that some data included in this article were obtained by the first author as part of a Master project. Specifically, *ldha* and *ldhb* expression pattern, *glut3*, *hk1*, *ldha*, *ldhb*, *pdha*, *pdhb* expression levels and some metabolite data. These preliminary data set the groundwork for the PhD project. Nonetheless, all data were reevaluated and reanalyzed. Moreover, all data interpretation, integration, discussion, and article writing, and submission were performed during this PhD project.

CHAPTER 3.2

RETINOIC ACID SIGNALING REGULATES THE METABOLIC PROFILE OF LUNG BRANCHING MORPHOGENESIS

Hugo Fernandes-Silva, Marco G. Alves, Marcia R. Garcez, Jorge Correia-Pinto, Pedro F. Oliveira, Catarina C. F. Homem and Rute S. Moura

ABSTRACT

Lung branching morphogenesis is characterized by epithelial-mesenchymal interactions and mediated by complex signaling that ultimately defines the airway conducting system. Retinoic Acid (RA) signaling modulates lung organogenesis, specifically proximal-distal patterning and lung branching morphogenesis. Growing evidence suggests that signaling-metabolism interactions are essential to understanding developmental processes. Here, we investigate how RA signaling influences the metabolic profile of early lung development. We show that RA signaling modulation elicits changes in lung metabolism at the transcript, protein, and metabolite levels. RA signaling stimulation increases lung branching and maintains proper morphology by promoting optimal growth conditions. RA signaling inhibition decreases lung branching, induces a cystic-like phenotype, and affects mitochondrial function. Moreover, a RA-AMPK-dependent mechanism regulates lipid synthesis in the embryonic lung. This report reveals novel insights on signaling-metabolism interaction during embryonic lung development. This study also highlights the importance of metabolic regulation in this phase and may contribute to understanding the etiology of congenital lung disorders.

INTRODUCTION

Pulmonary branches are formed during the early stages of embryonic lung development through an intricate process known as lung branching morphogenesis. Lung branching shapes the pulmonary airway conducting system and is characterized by epithelial-mesenchymal interactions mediated by complex signaling [1,2].

In the chicken (*Gallus gallus*), the lung arises from the primitive foregut, around day 3 of embryogenesis [3]. The primary bronchus (mesobronchus) grows distally, and the secondary bronchi (buds) sprout laterally into the surrounding mesenchyme [4]. This lateral/monopodial branching is similar to the domain branching subroutine observed during mammalian lung development [5,6]. Beyond the structural similarities, the molecular mechanisms underlying the avian respiratory system are highly conserved from the mammalian, indicating similar functions [7]. For example, FGF (Fibroblast Growth Factor), SHH (Sonic Hedgehog), WNT (Wingless-related Integration Site), and RA (Retinoic Acid) play crucial roles in both chicken and mammalian pulmonary branching morphogenesis [8–11].

RA signaling is fundamental for vertebrate embryonic development, and it is a major player in lung organogenesis [12–14]. Intracellularly, RA binds to specific nuclear Retinoic Acid Receptors (RARs), of which there are three subtypes (RARα, RARβ, and RARγ). Then, RARs form a heterodimer with Retinoic

X Receptors (RXRs) that mediates downstream cellular signaling and the transcription of RA target genes [15]. Additionally, RA modulates multiple aspects of embryonic lung development, specifically proximal-distal patterning and lung branching morphogenesis [11,16,17].

Regarding metabolism, it is known that the adult lung metabolic requirements are achieved mainly through the uptake and catabolism of glucose, representing the primary energy source for the adult lung tissue [18–20]. As for the embryonic lung, it has been recently described that chicken lung branching morphogenesis gradually adapts to a glycolytic lactate-based metabolism to sustain the lung energetic demands, revealing the importance of metabolic regulation in this phase [21].

The interaction between cell signaling and metabolism is emerging as a central concept for understanding developmental processes. Hence, it is crucial to comprehend how metabolism impacts cellular and developmental decisions and how metabolism is dynamically regulated during development [22–25]. Recent studies have demonstrated that metabolism can have additional roles beyond the classic bioenergetic function and that signaling-metabolism interactions shape developmental processes. For instance, in *Drosophila*, activation of the Notch signaling pathway promotes glycolysis and downregulates the Krebs cycle, resembling the Warburg effect [26]. On the other hand, loss of Notch signaling in *Drosophila* wing discs and human microvascular cells results in downregulation of glycolytic genes [26]. In *Drosophila* wing discs, the expression of glucose catabolism genes is regulated by Notch signaling, and this mechanism is proposed to promote the growth of this developing tissue [26]. In a different study, during *Zebrafish* neural tissue development, Notch signaling is described to regulate the expression of glycolysis-related genes in a context-dependent manner at different developmental stages [27]. Moreover, an FGF/Wnt signaling coordinated glycolytic gradient was reported to regulate cell motility and control specification, contributing to presomitic mesoderm development during vertebrate embryo somite formation [28].

Considering the well-known role of RA as a modulator of lung organogenesis, we aimed to investigate how the RA signaling pathway influences the metabolic profile of early stages of chicken lung branching morphogenesis. Our study reveals that alterations in RA signaling elicit changes in the lung metabolic profile, specifically at the transcript, protein, and metabolite levels. The mitochondria function is affected by RA signaling inhibition, and RA signaling might control fatty acid metabolism through an AMP-activated protein kinase (AMPK) pathway molecular mechanism. Also, RA stimulation increases lung branching, whereas RA inhibition decreases lung branching and induces a cystic-like phenotype. Overall, this report reveals new insights on signaling-metabolism interaction during embryonic lung development that may eventually contribute to understanding the etiology of congenital lung disorders.

RESULTS

Retinoic Acid signaling downregulation decreases lung branching and induces a cystic-like phenotype

Retinoic Acid is crucial for lung development, and it is a known modulator of lung branching morphogenesis. Previous studies showed that RA signaling stimulation triggers an increase in lung branching. On the other hand, the effect of BMS493 (BMS), a specific inhibitor of the RA signaling cascade, on lung branching morphogenesis has not been characterized so far.

To describe the impact of BMS treatment on lung branching morphogenesis, a 48-hour *ex vivo* lung explant culture was performed using b2 lungs (2 secondary buds per bronchus). Lung explants were treated with increasing doses of BMS: 0.1 µM, 1 µM, or 10 µM. DMSO was used as a control. Afterward, D0 (0 hours) and D2 (48 hours) explants were morphometrically analyzed, and results were represented as D2/D0 ratio. Additionally, *rarβ* expression levels were evaluated in D2 lungs by *in situ* hybridization.

BMS treated lungs revealed a dose-dependent decrease in *rarβ* expression, suggesting a gradual downregulation of RA signaling (Fig. S1 A). Moreover, a progressive decrease in the epithelial perimeter was observed (Fig. S1 B). No major alterations were detected in the epithelial area (Fig. S1 C). From this point onwards, the selected dose to inhibit the RA signaling pathway was 10 µM of BMS. To compare the effect of RA signaling stimulation *versus* inhibition on lung branching morphogenesis, *in vitro* lung explants were treated with 1 µM of RA (stimulation) or 10 µM of BMS (inhibition). Explants were morphometrically analyzed as previously described, and D2 explants probed for *rarβ*. *In situ* hybridization revealed that RA supplementation increases while BMS treatment decreases *rarβ* expression compared to control (Fig. 1 A). Additionally, BMS treated lungs displayed wider primary bronchus (Fig. 1 A; arrow) and larger epithelial pouches (Fig. 1 A; asterisk) that resemble cystic-like structures. Regarding branching morphogenesis, the epithelial perimeter of RA-treated lungs increased, while BMS showed a significant decrease, compared to the DMSO (Fig. 1 B). Concerning the epithelial area, no variations were detected (Fig. 1 C).
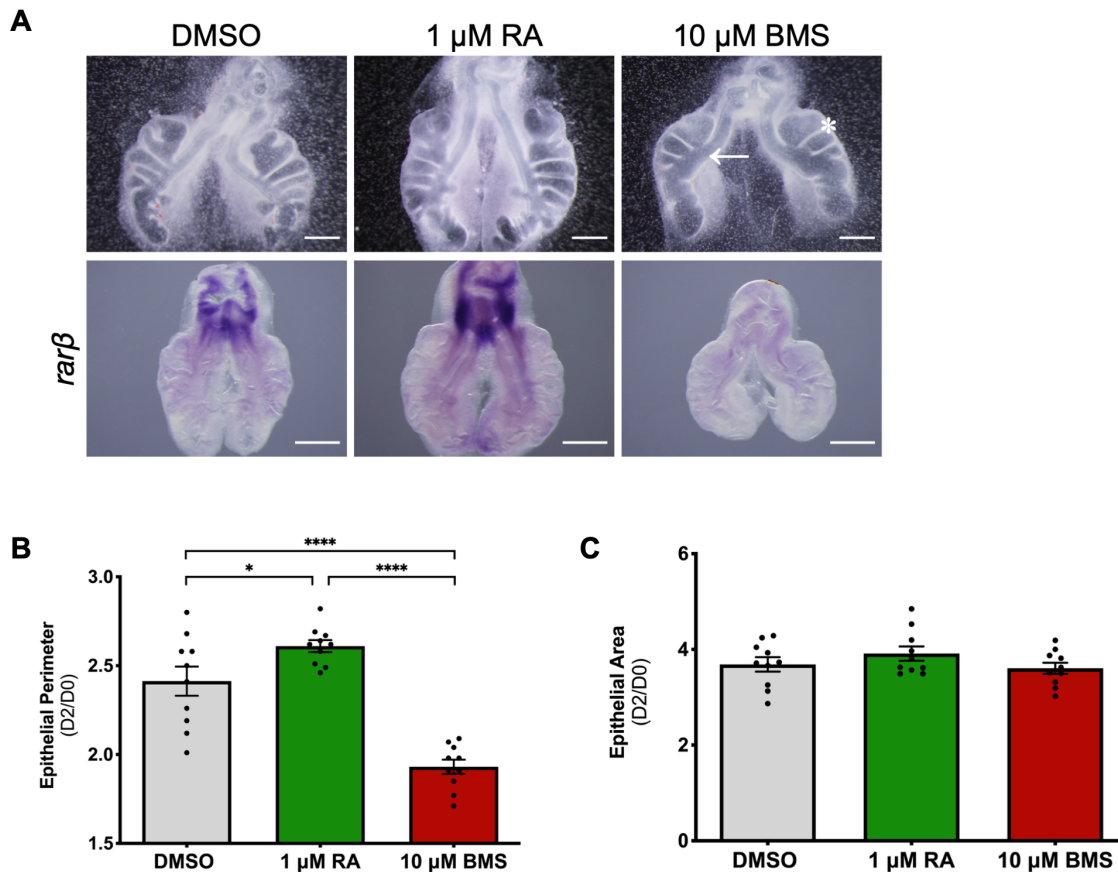
Figure 1 - Effect of RA signaling stimulation *versus* inhibition on lung branching morphogenesis. (A) Representative examples of b2 lungs after 48 hours of explant culture (DMSO, 1 μM of RA, or 10 μM of BMS) (upper panel); and probed for *rarβ* (lower panel) (n ≥ 4/condition). Scale bar: 500 μm. Arrow: wider primary bronchus. Asterisk: large epithelial pouches; Morphometric analysis of (B) Epithelial perimeter and (C) Epithelial area. Results are expressed as D2/D0 and represented as mean ± SEM (n = 10/condition). One-Way ANOVA and Fisher's LSD test were performed. Significantly different results are indicated as: $^*p < 0.05$; $^{****}p < 0.0001$.

Retinoic Acid signaling stimulation requires less glucose consumption

To determine the metabolic alterations that occur upon RA signaling stimulation *versus* inhibition, we started by focusing on glucose metabolism (Fig. 2 A). For that purpose, lung explants were exposed to one of the following conditions: DMSO, 1 μM of RA, or 10 μM of BMS. The explant culture was performed for 48 h and refreshed at D1 (24 h). The medium was collected at D0 (0 h; reference/control), D1, and D2 and analyzed by ^{1}H-NMR spectroscopy. Extracellular metabolite production/consumption was calculated following the mathematical formula | (D1-D0) + (D2-D0) | and expressed in fold variation to DMSO. D2 lung tissues were collected to perform qPCR for phosphofructokinase 1 (*pfk1*), glucose-6-phosphate dehydrogenase (*g6pd*), and 6-phosphogluconate dehydrogenase (*pgd*).

^{1}H-NMR analysis revealed that in both RA signaling stimulation and inhibition, the lung tissue consumes equal amounts of glucose compared to the control (Fig. 2 B). Nevertheless, between

121

treatments, glucose consumption is significantly lower under RA stimulation compared to the RA inhibition (Fig. 2 B). RA signaling stimulation promotes pulmonary branching morphogenesis, but its metabolic needs seem to require less glucose consumption. Additionally, *pfk1* expression levels remained unaltered among the three experimental conditions (Fig. 2 C), suggesting that RA signaling modulation does not affect this glycolysis rate-limiting step.

In what refers to the pentose phosphate pathway (PPP), *g6pd* expression levels were virtually undetected (data not shown). As for the *pgd*, the expression levels decreased from the DMSO to 10 μM of BMS (Fig. 2 D). The same tendency was observed for the 1 μM RA condition but without statistically significant differences (Fig. 2 D), suggesting that the amount of glucose catabolized into PPP decreases under RA signaling modulation.
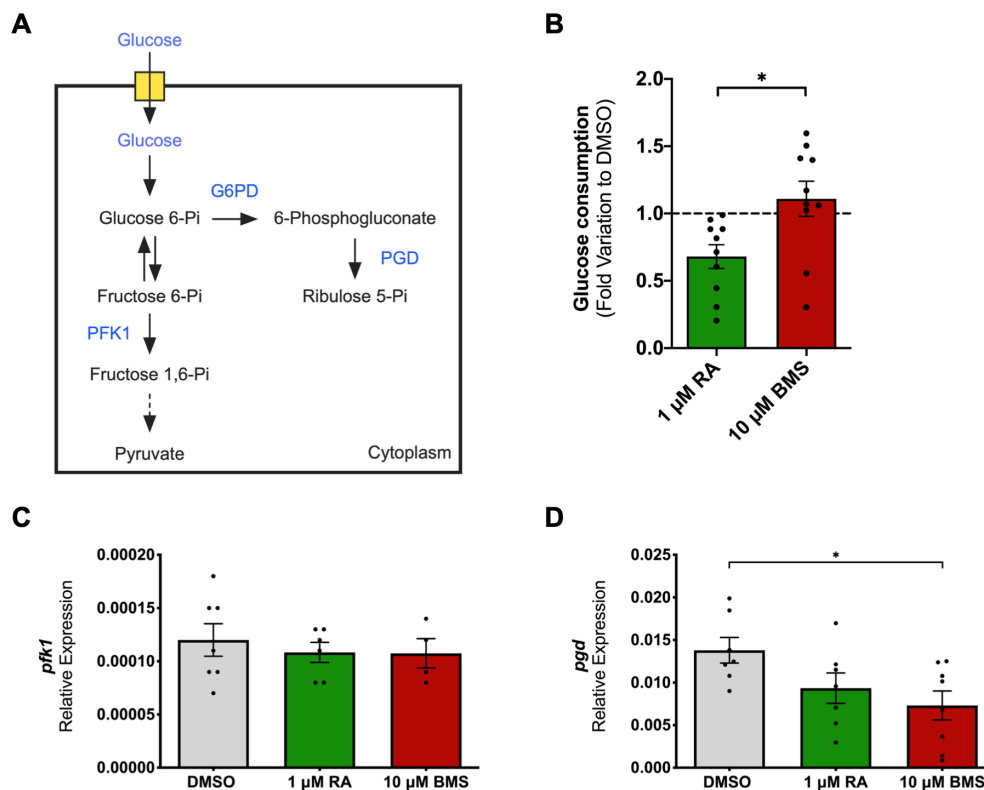

Figure 2 - Impact of RA signaling modulation on glucose metabolism during lung branching morphogenesis. (A) Schematic representation of glucose metabolism through the glycolytic and pentose phosphate pathways. Blue labeling indicates the molecular targets analyzed; ^{1}H-NMR analysis of (B) glucose consumption (n ≥ 8/condition), during 48 hours of lung explant culture (DMSO, 1 μM of RA, or 10 μM of BMS). Metabolite consumption/production was calculated following the mathematical formula | (D1-D0) + (D2-D0) | and represented in fold variation to DMSO. D2 lung mRNA relative expression levels of (C) *pfk1* (n ≥ 4/condition) and (D) *pgd* (n ≥ 7/condition) All results are expressed as mean ± SEM. One-Way ANOVA and Fisher's LSD test were performed. Significantly different results are indicated as: *p < 0.05.

Retinoic Acid signaling controls pyruvate fates and metabolism

We searched for additional glycolysis-related products using the previous experimental approach to further study potential metabolite alterations promoted by RA signaling stimulation/inhibition. In the ^{1}H-NMR spectra, it was possible to detect the final product of glycolysis, pyruvate. Furthermore, several pyruvate metabolic fates were present, namely alanine, lactate, acetate, and succinate (Fig. 3 A). RA signaling stimulation promotes a sharp increase in pyruvate production compared to DMSO and the BMS-treated group (Fig. 3 B). In addition, under BMS treatment, pyruvate production is lower than in the DMSO (Fig. 3 B). No differences were detected in alanine production when compared to the DMSO, still 1 μM of RA produces less alanine than the 10 μM of BMS-treated group (Fig. 3 C). Lastly, RA signaling stimulation leads to a decrease in lactate production compared to the control and the BMS group (Fig. 3 D).

After entering into the mitochondria, pyruvate is converted into acetyl-CoA, which can be shuttled into acetate or directly fuel the Krebs cycle. There are no major variations in acetate production among the three experimental conditions (Fig. 3 E). Lastly, succinate production displays a sharp increase upon RA signaling stimulation in comparison with the control and the BMS-treated group (Fig. 3 F).
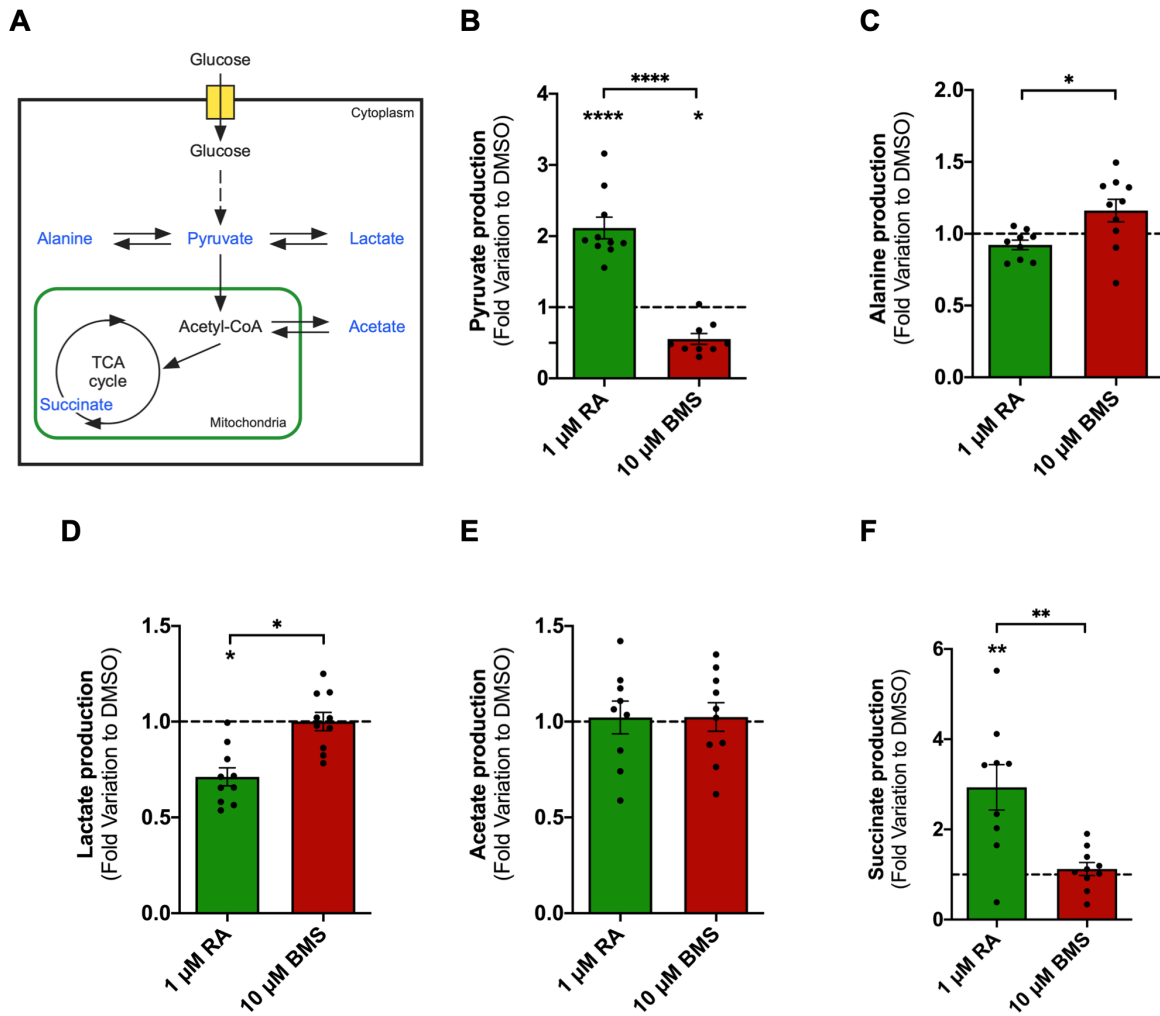
Figure 3 - Extracellular metabolite changes induced by RA signaling modulation during lung branching morphogenesis. (A) Schematic representation of pyruvate metabolic fates. Blue labeling indicates the metabolites detected and quantified in the ^{1}H-NMR spectra; ^{1}H-NMR analysis of (B) pyruvate production; (C) alanine production, (D) lactate production; (E) acetate production; and (F) succinate production, during 48 hours of lung explant culture (DMSO, 1 μM of RA, or 10 μM of BMS). Metabolite consumption/production was calculated following the mathematical formula | (D1-D0) + (D2-D0) | and represented in fold variation to DMSO. Results are expressed as mean ± SEM (n ≥ 8/condition). One-Way ANOVA and Fisher's LSD test were performed. Significantly different results are indicated as: *$p < 0.05$; **$p < 0.01$; ****$p < 0.0001$.

Retinoic Acid signaling modulates lactate dehydrogenase expression

This study revealed that RA signaling stimulation promotes a decrease in lactate production (Fig. 3 D). To understand how Lactate dehydrogenase (LDH) might be affected by RA signaling stimulation/inhibition, LDHA and LDHB isoforms were evaluated. Treated explants were processed for *in situ* hybridization to analyze *ldha* and *ldhb* spatial localization and relative expression levels. D2 lungs were also collected to assess LDHA and LDHB protein expression levels by western blot.

ldha transcript is present in the ventral region of D2 lung explants in all experimental conditions (Fig. 4 A; arrow). RA stimulation increases the expression levels of *ldha* transcript compared to the DMSO (Fig. 4 A). Conversely, the BMS treatment decreases *ldha* expression compared to both DMSO and RA-treated lungs (Fig. 4 A). Regarding *ldhb*, it is restricted to active branching sites (Fig. 4 B; asterisk). When supplemented with 1 µM of RA, the expression pattern of *ldhb* is maintained but, its expression levels increase (Fig. 4 B). On the other hand, lung explants treated with 10 µM of BMS displayed a decrease in *ldhb* expression levels compared to DMSO and RA supplemented lungs (Fig. 4 B).

Western blot analysis revealed that LDHA (Fig. 4 C) and LDHB (Fig. 4 D) protein expression levels exhibited similar trends between the three experimental conditions. Compared directly to the corresponding transcript, LDHA and LDHB protein levels showed a similar tendency, except for the 10 µM of BMS condition, where the protein expression levels decrease is not so pronounced (Fig. 4 C and 4 D, respectively). In this case, statistically significant differences were only present between RA stimulation and RA inhibition of both isoforms (Fig. 4 C and D, respectively). Full-length blots and total protein stain are presented in SourceDataF4.
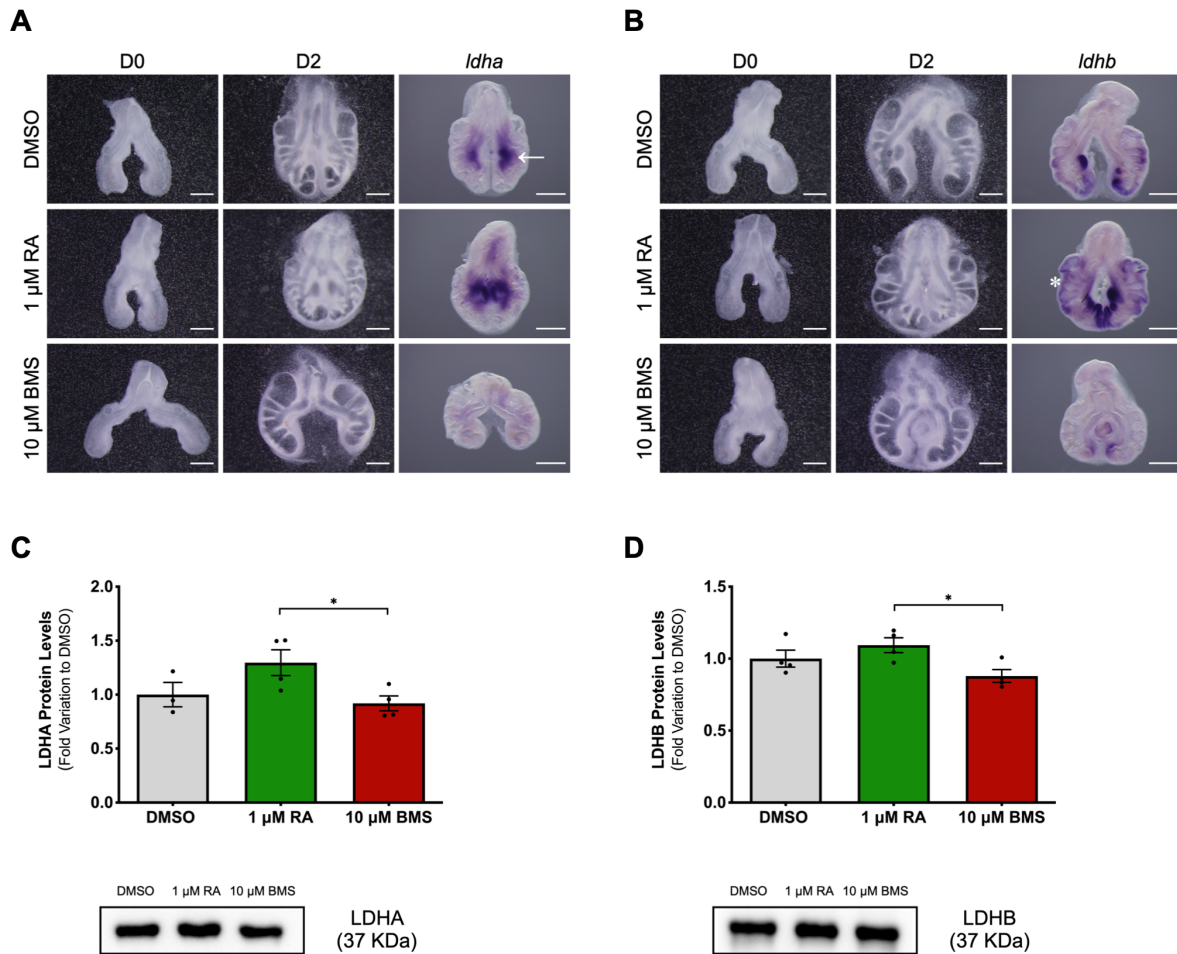
Figure 4 - LDHA and LDHB expression alterations induced by RA signaling modulation during lung branching morphogenesis. Representative examples of b2 lung explant culture at D0 and at D2, treated with DMSO, 1 μM of RA, and 10 μM of BMS. D2 lungs were probed for (A) *ldha* and (B) *ldhb* (n ≥ 4 /condition). scale bar: 500 μm. Arrow: ventral region. Asterisk: active branching sites; D2 lungs were analyzed for (C) LDHA and (D) LDHB protein expression levels. LDHA and LDHB immunoblots correspond to 37 KDa. Full-length blots and total protein are presented in SourceDataF4. Results are represented in fold variation to DMSO. Results are expressed as mean ± SEM (n ≥ 3/condition). One-Way ANOVA and Fisher's LSD test were performed. Significantly different results are indicated as: *p < 0.05.

High proliferation is associated with active branching regions

To evaluate the proliferation status of lung branching morphogenesis upon RA signaling stimulation/inhibition, we assessed EdU incorporation into new DNA strands using Alexa Fluor 488 (Green) in the three experimental conditions. The nuclei were counterstained with Hoechst 33342 (Red) (Fig. 5).

DMSO-treated explants revealed high proliferative areas in the trachea region (arrowhead), in the distal area of the lung (arrow), and at active branching sites (asterisk) (Fig. 5 B). Moreover, the proliferation pattern remained unaltered for 1 μM of RA and 10 μM of BMS conditions (Fig. 5 B, 5 E, 5 H). Since RA stimulation increases lung branching, and high proliferation is characteristic of active

126

branching sites (asterisk), this condition is associated with more proliferation (Fig. 5 E). In contrast, 10 μM of BMS decreases lung branching morphogenesis and induces a cystic-like phenotype. Thus, in this condition, high proliferation levels are restricted to the branching structures (asterisk), which are fewer and with an enlarged appearance (Fig. 5 H).
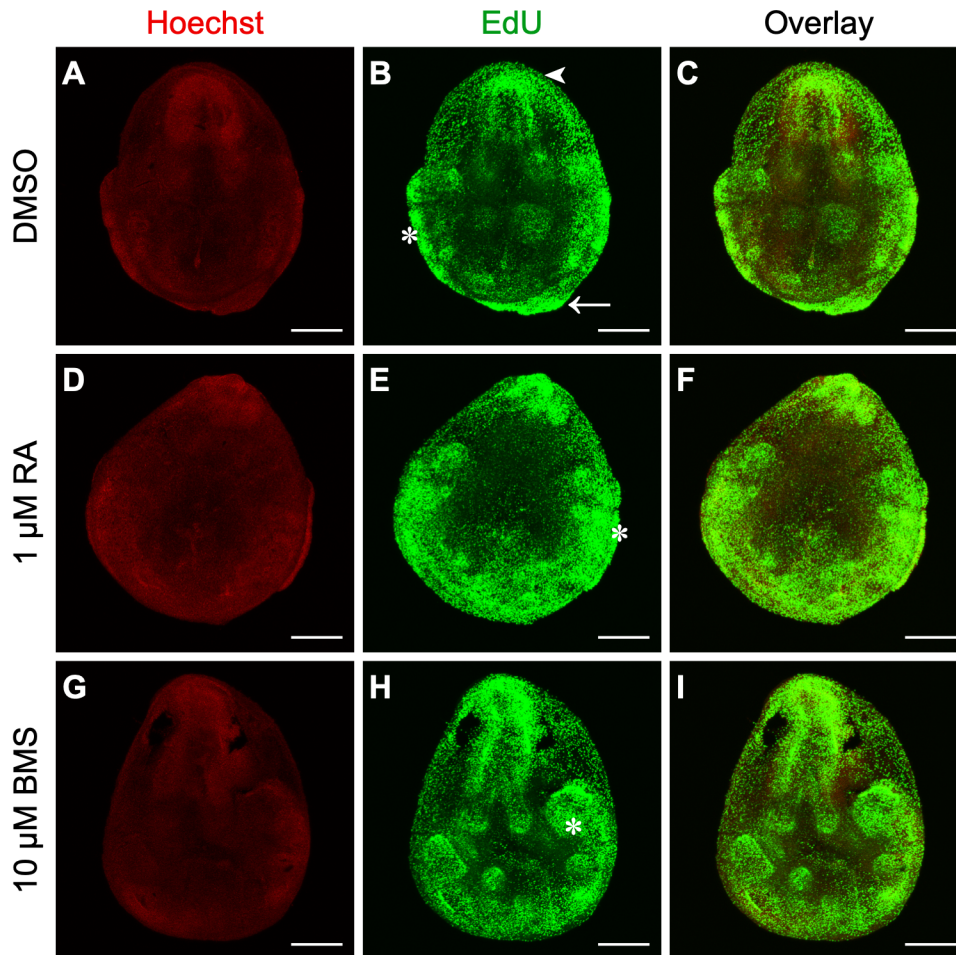

Figure 5 - Proliferation analysis of lung branching morphogenesis upon RA signaling stimulation/inhibition. Representative confocal microscopy fluorescence images of b2 lung explants after 48 hours in culture, supplemented with: (A-C) DMSO, (D-F) 1 μM of RA, and (G-I) 10 μM of BMS. (A, D, G) Nuclei were stained with Hoechst 33342 (Red). (B, E, H) Proliferation was assessed through EdU incorporation in DNA, followed by detection using Alexa Fluor 488 (Green). (C, F, I) Merged images. n ≥ 4 /condition. Scale bar: 500 μm. Arrowhead: trachea region. Asterisk: active branching sites. Arrow: distal tip.

Retinoic Acid signaling downregulation increases mitochondrial function

To assess how RA signaling stimulation/inhibition affects mitochondrial function, mitochondrial respiration was evaluated in the three experimental conditions. 48-hour lung explant tissues were processed for real-time measurement of oxygen consumption rate (OCR), and results were expressed in pmol/min/mg protein (Fig. S2).

Regarding basal respiration, the OCR from BMS-treated lungs increased, compared to DMSO and to RA-treated lungs (Fig. 6 A). Similarly, for ATP production, the 10 μM of BMS condition displayed higher OCR levels than DMSO and 1 μM of RA (Fig. 6 B). Likewise, the maximal respiration component revealed an increase in the OCR levels of the RA inhibition group, compared to DMSO and 1 μM of RA (Fig. 6 C). The OCR component corresponding to the proton leak was also increased in BMS-treated lungs in comparison to DMSO and RA-treated lungs (Fig. 6 D). The OCR portion of the non-mitochondrial respiration was higher in the BMS-treated lungs with a statistically significant increase from the control (Fig. 6 E).

As for the spare respiratory capacity, there is a decrease from DMSO to the BMS-treated explants (Fig. 6 F). Lastly, the coupling efficiency decreased from the DMSO to the RA-treated condition and increased from RA to BMS-treated lungs (Fig. 6 G).

To assess mitochondrial biogenesis, treated explants were evaluated for the mtDNA copy number and transcription factor A mitochondrial (*tfam*) expression levels by qPCR. Regarding mitochondrial copy number, no differences were observed among the three experimental conditions (Fig. S3 A). Similarly, the expression levels of *tfam* remained unaltered between conditions (Fig. S3 B).
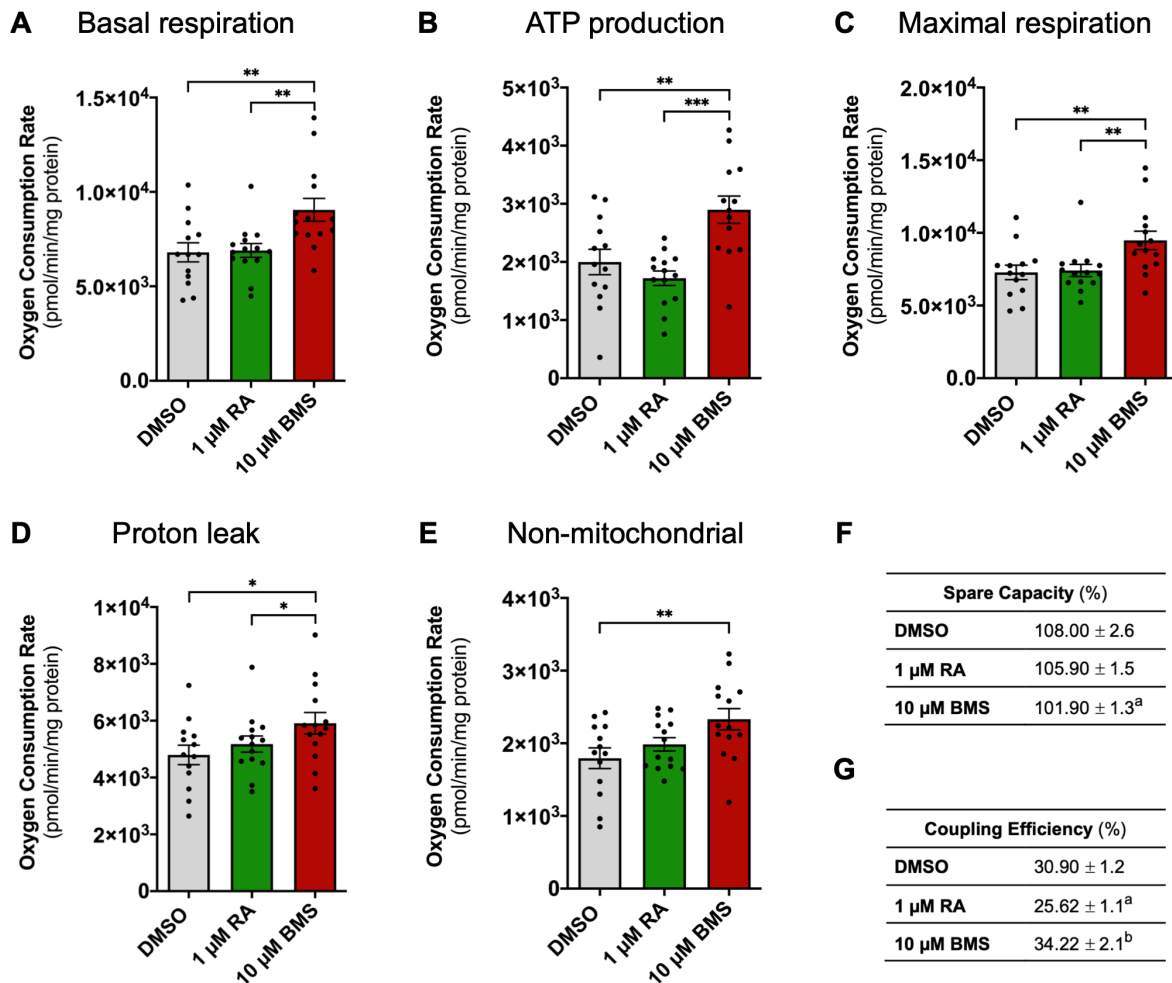
A Basal respiration

B ATP production

C Maximal respiration

D Proton leak

E Non-mitochondrial

F

Spare Capacity (%)	
DMSO	108.00 ± 2.6
1 µM RA	105.90 ± 1.5
10 µM BMS	101.90 ± 1.3[a]

G

Coupling Efficiency (%)	
DMSO	30.90 ± 1.2
1 µM RA	25.62 ± 1.1[a]
10 µM BMS	34.22 ± 2.1[b]

Figure 6 - Mitochondrial oxygen consumption of lung explants upon RA signaling stimulation/inhibition. Real-time measurement of oxygen consumption rate (OCR) corresponding to (A) Basal respiration; (B) ATP production; (C) Maximal respiration; (D) Proton leak; (E) Non-mitochondrial; (F) Spare capacity; and (G) Coupling efficiency, after 48 hours of lung explant culture (DMSO, 1 µM of RA, or 10 µM of BMS). Results are represented in pmol/min and normalized to the total amount of protein. Results are expressed as mean ± SEM (n ≥ 13/condition). One-Way ANOVA and Fisher's LSD test were performed. Significantly different results are indicated as: *p < 0.05; **p < 0.01; ***p < 0.001. a *vs* DMSO; b *vs* 1 µM of RA.

Retinoic Acid signaling downregulation decreases mitochondrial complexes expression

To further study the impact of RA signaling stimulation/inhibition on mitochondria, we evaluated the expression of the mitochondrial complexes by determining the OXPHOS protein expression levels expressed in fold variation to DMSO.

Regarding complex I, the protein expression levels of BMS-treated lungs displayed a statistically significant decrease compared to both the DMSO and RA-treated explants (Fig. 7 A). Likewise, in complex III, the protein expression levels were equal between the DMSO and RA-treated lungs, and a decrease was observed between RA and the BMS-treated group (Fig. 7 A). Lastly, complex V showed a decrease from DMSO and RA-treated explants to the BMS-treated group (Fig. 7 A). Although with a similar

tendency, no significant differences were observed for complex II and IV (Fig. 7 A). Total OXPHOS complexes and corresponding molecular weights are represented in (Fig. 7 B). Full-length blots and total protein are presented in SourceDataF7.
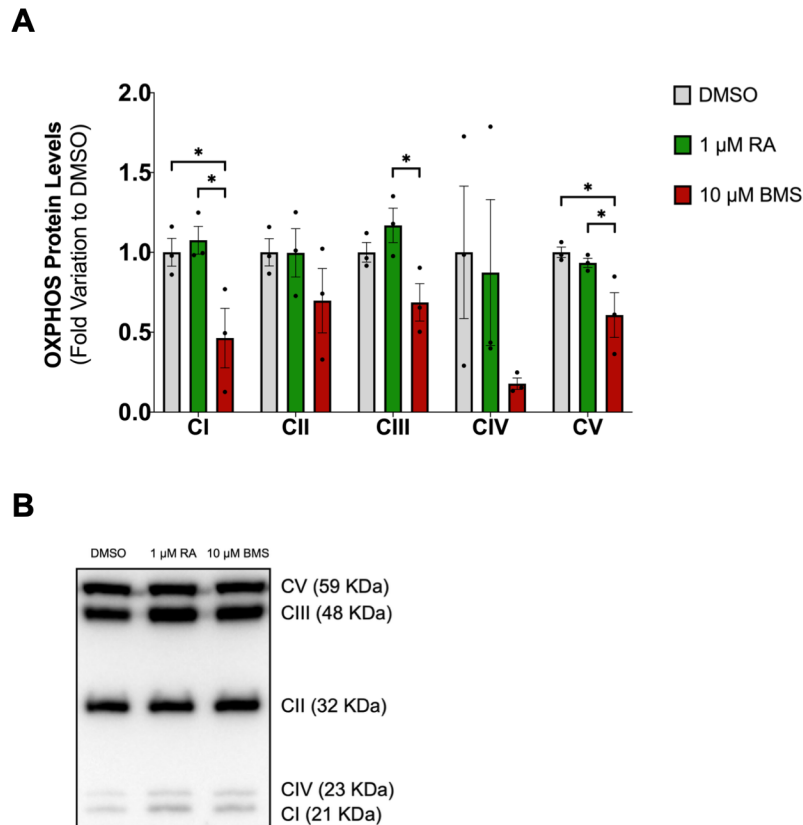
A

B

Figure 7 - Mitochondrial complexes protein expression levels upon RA signaling modulation in lung branching morphogenesis. D2 lungs were analyzed for (A) OXPHOS complexes protein expression levels, after 48 hours of lung explant culture (DMSO, 1 µM of RA, or 10 µM of BMS); (B) OXPHOS complexes immunoblot corresponds to complex V (59 KDa), Complex III (48 KDa), Complex II (32 KDa), Complex IV (23 KDa), and Complex I (21 KDa), molecular weights according to UniProt database. Full-length blots and total protein are presented in SourceDataF7. Results are represented in fold variation to DMSO. Results are expressed as mean ± SEM (n ≥ 3/condition). One-Way ANOVA and Fisher's LSD test were performed. Significantly different results are indicated as: *p < 0.05.

Retinoic Acid signaling controls fatty acid metabolism through AMPK

To study the potential impact of RA signaling stimulation/inhibition on lipid metabolism, we focused on AMPK and fatty acids and analyzed protein and transcript expression levels in the three experimental conditions. Since the AMPK pathway controls lipid metabolism, we wondered if it was regulated by RA signaling. Western blot results revealed that upon RA stimulation, pAMPK/AMPK protein levels increased, compared to the control group (Fig. 8 A). Likewise, upon RA inhibition, pAMPK/AMPK

protein levels increased even more, compared to both the DMSO and RA-treated lungs (Fig. 8 A). Full-length blots and total protein are presented in SourceDataF8.

Regarding lipogenesis, sterol regulatory element-binding transcription factor 1 (*srebf1*) and fatty acid synthase (*fasn*) expression levels were evaluated. *srebf1* expression levels decreased from DMSO to 1 µM of RA, and to 10 µM of BMS (Fig. 8 B). Therefore, *fasn* expression levels decreased from the control group to the BMS-treated group (Fig. 8 C). As to fatty acid oxidation, carnitine palmitoyltransferase I (*cpt1*) expression was measured, unveiling stable expression levels among the three experimental conditions (Fig. 8 D).
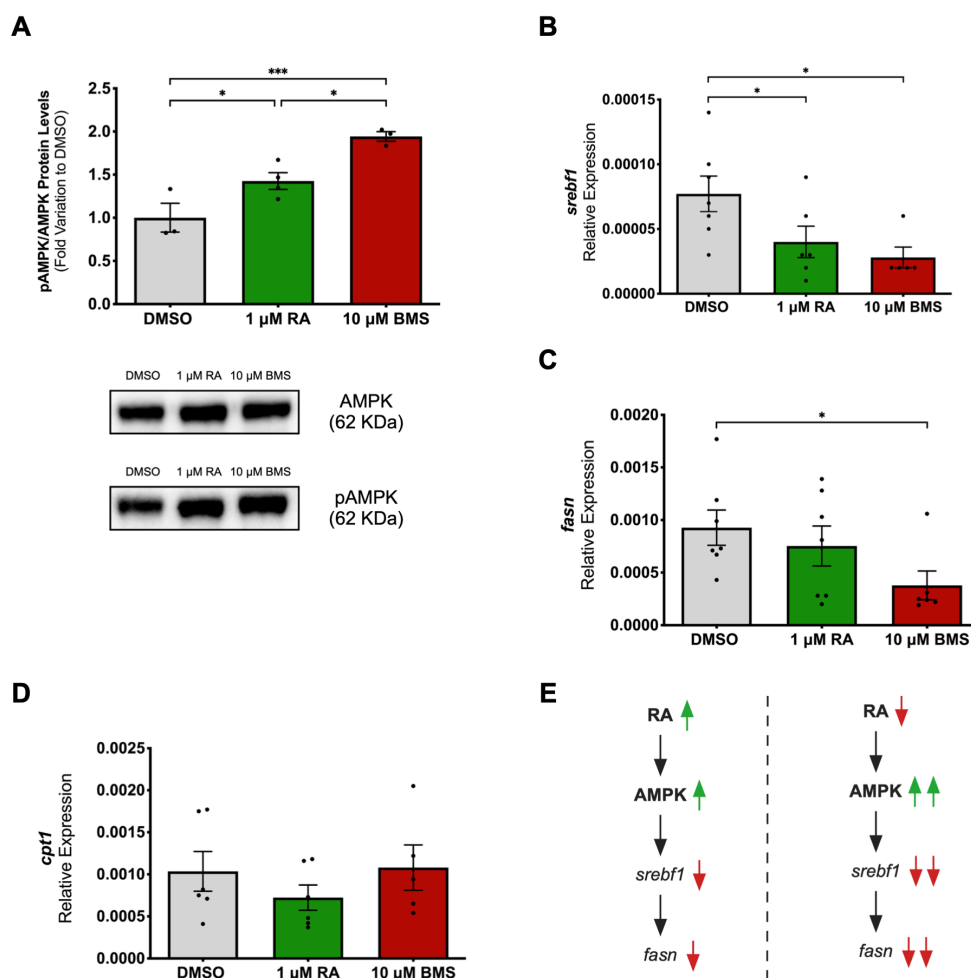

Figure 8 - Impact of RA signaling modulation on AMPK pathway and lipid metabolism in early lung branching morphogenesis. D2 lungs were analyzed for (A) pAMPK/AMPK protein expression levels (n ≥ 3/condition), after 48 hours of lung explant culture (DMSO, 1 µM of RA, or 10 µM of BMS). pAMPK and AMPK immunoblots correspond to 62 KDa. Full-length blots and total protein are presented in SourceDataF8. Results are represented in fold variation to DMSO; mRNA relative expression levels of (B) *srebf1*, (C) *fasn*, and (D) *cpt1* (n ≥ 7/condition), after 48 hours of lung explant culture (DMSO, 1 µM of RA, or 10 µM of BMS). Results are expressed as mean ± SEM. One-Way ANOVA and Fisher's LSD test were performed. Significantly different results are indicated as: *$p < 0.05$; ***$p < 0.001$. (E) Proposed molecular mechanism involving RA and AMPK signaling pathways, and respective impact on lipid synthesis machinery during lung branching morphogenesis. The symbols refer to increase (↑) or decrease (↓).

DISCUSSION

Growing evidence suggests that signaling-metabolism interactions are essential to understanding developmental processes. To gain new insights into this subject, we asked whether RA signaling could affect the metabolic profile of early lung development. In this work, we began by evaluating the impact of RA signaling stimulation *versus* inhibition on lung branching morphogenesis. *Ex vivo* lung explant culture supplemented with DMSO, 1 μM of RA (stimulation), or 10 μM of BMS (inhibition; dose selected according to dose-response studies Fig. S1) was performed. The RA signaling pathway activation status was assessed by performing *in situ* hybridization for *rarβ*, a recognized target of this pathway [11,29,30].

RA-supplemented lungs displayed an increase in *rarβ* expression (Fig. 1 A), suggesting an activation of the RA signaling cascade. BMS-treated lungs showed the opposite effect, with a decrease in *rarβ* implying a downregulation of the RA pathway (Fig. 1 A). BMS493 (BMS) is a pan-RAR inverse agonist which suppresses RA signaling pathway by establishing associations between the RARs and transcriptional co-repressors, thus blocking RA signaling dependent transcription [12,31]. The effect of BMS on lung branching morphogenesis had not been described so far.

Then, lung explants were morphometrically analyzed for branching morphogenesis. RA signaling stimulation increased the pulmonary epithelial perimeter; conversely, RA inhibition decreased branching (Fig. 1 B). As for the epithelial area, no alterations were detected in both conditions compared to the DMSO (Fig. 1 C). RA is a known modulator of lung branching morphogenesis, and these results are in agreement with previous RA supplementation studies using the mouse, rat, and chicken embryonic lungs [11,30,32]. BMS is a chemical inhibitor of the RA signaling pathway [31], and here we show that BMS supplementation downregulates RA signaling and decreases the branching morphogenesis of the embryonic chicken lung.

Interestingly, lungs treated with BMS exhibited cystic-like morphological alterations, namely wider primary bronchus (Fig. 1 A, arrow) and larger epithelial pouches (Fig. 1 A, asterisk). Likewise, rat overexpression of *fgf10* induces cystic malformations comparable to human Congenital Pulmonary Airway Malformation (CPAM) [33]. Also, mouse DICER mutant lungs display an upregulation of mesenchymal *fgf10* accompanied by branching arrest and the formation of large epithelial pouches [34]. During lung branching morphogenesis, a gradient of RA is produced from the pleura region to the periepithelial mesenchyme that surrounds the distal region of the growing bud [16]. RA availability is described to regulate *fgf10* expression levels in the mesenchymal compartment surrounding the distal bud tips [9,11,35,36]. In our study, the occurrence of cystic-like structures might be due to an impairment of *fgf10* levels due to defective RA signaling.

Having established the RA/BSM effect on lung branching, we explored potential metabolic alterations induced by RA signaling modulation on lung branching morphogenesis. *Ex vivo* lung explant culture allows to study the whole organ and precisely assess metabolic and associated molecular alterations in a very controlled environment [21,37,38]. Briefly, the culture system was supplemented with DMSO, 1 μM of RA, or 10 μM of BMS for 48 h and refreshed at D1 (24 hours). The medium was collected at D0 (0 h; reference/control), D1, and D2 (48 hours) and analyzed by ^{1}H-NMR spectroscopy. Extracellular metabolite production/consumption was calculated following the mathematical formula | (D1-D0) + (D2-D0) |, according to described in [21]. Additionally, qPCR, *in situ* hybridization, or western blot was performed to assess the expression levels and spatial distribution of key targets from the selected metabolic pathways.

Since both the adult and the embryonic lung use glucose as a primary energy source [18-21,39], we initially focused on glycolysis and pentose phosphate pathway (PPP) (Fig. 2 A). ^{1}H-NMR analysis revealed that RA stimulation and inhibition consume the same amount of glucose as the DMSO (Fig. 2 B). Nevertheless, glucose consumption is significantly lower under RA stimulation compared to RA inhibition (Fig. 2 B). It has been previously demonstrated that the embryonic chicken lung has the molecular machinery for the transport and uptake glucose and that glucose consumption profile adapts to cope with the specific energy and nutrient requirements to sustain proper branching morphogenesis [21].

Additionally, to assess the rate-controlling step of glycolysis, we measured *pfk1* expression. Under these conditions, *pfk1* expression levels remained unaltered (Fig. 2 C). PFK1 is the main glycolysis enzyme, and it is allosterically regulated by ATP and the accumulation of ATP breakdown products [40]. The expression of *pfk1* was previously described without major variations throughout lung branching morphogenesis [21]. Here, we described that RA signaling does not impact *pfk1* transcript expression.

The main catabolic fate of glucose-6-phosphate is the glycolytic breakdown into pyruvate through glycolysis. However, part of glucose-6-phosphate can be oxidized into pentose phosphate by PPP (according to the cell needs or NADP+/NADPH concentrations) [40]. To study how RA signaling modulation impacts PPP, the expression levels of glucose-6-phosphate dehydrogenase (*g6pd*) and phosphogluconate dehydrogenase (*pgd*) were evaluated. Both transcripts encode enzymes responsible for the oxidative reactions of PPP that produce NADPH. In the embryonic lung, *g6pd* expression levels are low, regardless RA stimulation or inhibition conditions (data not shown). As for the *pgd*, the expression levels decrease from DMSO to BMS-treated lungs, and RA stimulation displays the same tendency but without statistically significant differences (Fig. 2 D). According to our results, RA signaling modulation is

not directing glucose-6-phosphate into the pentose phosphate pathway, and glucose-6-phosphate is available to be used by glycolysis. Moreover, the RA stimulation condition seems to make better use of glucose or uses other metabolic substrates since it promotes lung branching morphogenesis (Fig. 1 A and 1 B) with less glucose consumption (Fig. 2 B).

To study additional glycolysis-related products, we further explored the ¹H-NMR spectra. Pyruvate, the final product of glycolysis, and several pyruvate metabolic fates such as alanine, lactate, acetate from acetyl-CoA, and succinate (Krebs cycle) were present (Fig. 3 A). RA signaling stimulation promotes a sharp increase in pyruvate production compared to DMSO and BMS-treated lungs (Fig. 3 B). BMS treatment promotes a decrease in pyruvate production when compared to the DMSO group (Fig. 3 B).

Regarding alanine, RA-stimulated lungs produce less alanine compared to BMS treatment (Fig. 3 C). This decrease in alanine production follows the decrease in glucose consumption (Fig. 2 B). Moreover, the production of alanine was formerly described during embryonic lung development and might contribute to protein biosynthesis to support active tissue growth [21]. Similarly, in the adult lung, it is described that part of glucose is used to produce alanine through pyruvate transamination [19,20,39].

Also, pyruvate can be inter-converted into lactate through an enzymatic reaction catalyzed by Lactate dehydrogenase, which regenerates NAD+ [40]. The conversion of pyruvate to lactate is a crucial step for lung branching morphogenesis [21]. Moreover, it facilitates the uptake and incorporation of nutrients to form new biomass and sustain active tissue growth [21,41]. Here, we showed that lactate production decreases upon RA stimulation compared to DMSO and BMS-treated lungs (Fig. 3 D). This lactate decrease seems to follow the slight decrease in glucose consumption promoted by RA stimulation (Fig. 2 B). In this sense, upon RA stimulation, there is an increase in the portion of glucose that is directed into pyruvate rather than into the alanine and lactate branches. Moreover, it is known that the embryonic chicken lung is able to convert glucose into lactate during branching morphogenesis [21]. To further explore the molecular mechanism underlying lactate production, we analyzed LDHA and LDHB isoforms under RA signaling modulation. *In situ* hybridization revealed that the *ldha* expression pattern is limited to the ventral region of the lung (Fig. 4 A; arrow), and its expression is dependent on RA signaling. RA stimulation increases *ldha* expression considerably, and BMS promotes the opposite effect (Fig. 4 A). *ldhb* expression localization is restricted to active branching regions (Fig. 4 B; asterisk) and considerably increases upon RA stimulation, while BMS does the reverse effect (Fig. 4 B). Protein expression levels changes are not as pronounced as in the transcripts, but they follow a similar trend (Fig. 4 C and D). Previous data from our team have shown that both *ldha* and *ldhb* isoforms are present at earlier stages of lung branching and are expressed in a region-specific manner [21]. Moreover, *ldhb* transcript

localization is associated with active branching regions [21]. In addition, protein expression studies suggest that LDHB has a role in lung branching morphogenesis [21]. Here, we describe that LDH reaction is likely to be modulated by RA signaling and that both *ldha* and *ldhb* are downstream targets of the RA pathway.

Besides, previous data from our research group indicate an association between *ldha* and *ldhb* spatial localization and proliferation events [21]. In this sense, we evaluated how the RA signaling modulation would impact cellular proliferation during lung branching morphogenesis (Fig. 5). DMSO-treated explants display high proliferation in the trachea region (Fig. 5 B; arrowhead), in the distal lung (Fig. 5 B; arrow), and at active branching sites (Fig. 5 B; asterisk). These results match previous data described in [21]. Moreover, since RA stimulation increases branching morphogenesis, the regions of high proliferation expand substantially (Fig. 5 E). Under BMS treatment, branching morphogenesis decreases, and lungs display cystic-like structures (Fig. 1 A). The proliferation of BMS-treated lungs is restricted to the branching regions, thus generally decreasing compared to the other conditions (Fig. 5 H). Furthermore, high proliferation matches *ldhb* expression localization, namely when the RA signaling pathway is stimulated (Fig. 4 B).

Inside mitochondria, pyruvate is converted by pyruvate dehydrogenase (PDH) complex into acetyl-CoA, which can be shuttled to acetate or fuel the Krebs cycle (Fig. 3 A). Acetate can be used as a substrate for lipid synthesis and might incorporate new cellular membranes to sustain embryonic lung growth [21]. However, no alterations were observed for acetate production among the experimental groups (Fig. 3 E). Under RA stimulation, succinate production abruptly increases compared to DMSO and BMS-treated lungs (Fig. 3 F). Succinate is the only direct link between the Krebs cycle and the mitochondrial respiratory chain. During oxidative phosphorylation, the electrons obtained from the succinate/fumarate oxidation through mitochondrial complex II/succinate dehydrogenase (SDH) are used to reduce ubiquinone to ubiquinol [40]. In addition, the export of succinate from the mitochondrial matrix to the cytosol can act as a signal of mitochondrial status that might contribute to regulating overall metabolic homeostasis [42]. Nevertheless, succinate accumulation can trigger numerous cellular events, namely act as a metabolic signaling molecule [42,43].

To assess mitochondrial function upon RA signaling modulation, we performed a real-time measurement of oxygen consumption rate (OCR). Mitochondrial respiration data (Basal respiration, ATP production, and Maximal respiration) revealed that while RA stimulation presents an overall mitochondrial respiration profile similar to DMSO, whereas the BMS-treated lungs display increased mitochondrial function (Fig. 6 A-C). Additionally, BMS-treated lungs showed increased proton leak (Fig. 6 D). Proton leak

constitutes the remaining basal respiration not coupled to ATP production, and can be related to mitochondrial damage/stress induced by the BMS cystic-like phenotype or additional regulatory mechanisms to regulate mitochondrial ATP production. The portion of OCR that corresponds to non-mitochondrial respiration was also increased upon BMS treatment (Fig. 6 E). Non-mitochondrial respiration is due to a subset of enzymes and biochemical reactions that consume oxygen and are not coupled to mitochondrial respiration. In addition, the mitochondrial spare capacity of the embryonic lung is modest (Fig. 6 F). Moreover, BMS-treated lungs perform basal mitochondrial respiration closely to its maximal respiration (Fig. 6 F and S2), suggesting low mitochondrial plasticity/fitness to cope with pathophysiological stress conditions [44]. Lastly, the embryonic lung mitochondrial coupling efficiency fluctuates between the experimental conditions (26% - 34%) (Fig. 6 G). Overall, these results point to a more oxidative metabolism when RA signaling is inhibited, compared to control and RA-treated lungs.

To assess if these differences were due to changes in mitochondrial biogenesis, mitochondrial copy number and *tfam* expression levels were evaluated [45,46]. Both mtDNA and *tfam* remained unaltered, thus suggesting the same number of mitochondria in the three experimental groups (Fig. S3 A and B, respectively). Notably, RA signaling does not affect mitochondrial biogenesis during lung branching morphogenesis. Additionally, the protein expression levels of the mitochondrial respiratory complexes were analyzed (Fig. 7 B). Compared to DMSO, RA stimulation displays a similar OXPHOS complexes expression profile (Fig. 7 A). On the other hand, BMS-treated lungs displayed decreased protein expression levels of OXPHOS complexes, with statistically significant differences for complexes I, III, and V (Fig. 7 A). From these data, we propose that RA inhibition increases mitochondrial OXPHOS complexes activity since, based on Seahorse analysis (Fig. 6 and S2), the mitochondrial function is promoted under the same conditions (Fig. 6 A-C).

RA is a known modulator of lipid metabolism [47–49]. Moreover, AMPK is a master regulator of metabolism and a sensor of cellular energy status. AMPK can restore energy balance and modulate glucose and lipid metabolism, and mitochondria homeostasis [50,51]. In this sense, we explored whether AMPK and lipid metabolism could be affected by RA signaling during lung branching morphogenesis. In our experimental settings, RA stimulation upregulated the AMPK pathway through increased pAMPK/AMPK protein expression levels (Fig. 8 A). Still, under RA signaling inhibition, pAMPK/AMPK protein expression increased even more (Fig. 8 A). This suggests that during lung branching morphogenesis, AMPK is activated by RA signaling under stimulation or inhibition conditions. Moreover, the increased activation of AMPK under RA signaling inhibition might be due to a compensatory mechanism to reestablish tissue homeostasis as consequence of the cystic-like phenotype. Besides, RA

modulates AMPK in other systems, for instance, it inhibits neointimal hyperplasia and suppress vascular smooth muscle cells proliferation and migration through AMPK signaling activation [52]. RA activates AMPK signaling pathway and sensitizes hepatocellular carcinoma cells to apoptosis induced by sorafenib [53]. RA activates AMPK in skeletal muscle cells [54].

In addition, *srebf1*, *fasn*, and *cpt1* expression levels were evaluated to assess lipid biosynthesis and fatty acid oxidation. Lipogenesis is in part regulated by sterol regulatory element-binding transcription factor 1 (*srebf1*). Our results showed that *srebf1* (SREBP1) is present in the embryonic lung with the expression levels decreasing from DMSO to RA-supplemented and BMS-treated conditions (Fig. 8 B). Fatty acid synthase (FAS) is a rate-limiting enzyme of fatty acid synthesis and converts acetyl-CoA and malonyl-CoA into palmitate [40]. In the chicken lung, *fasn* expression decreased from DMSO to BMS-treated lungs (Fig. 8 C). Together, our data suggest a potential mechanism during early lung branching, in which RA signaling modulation activates the AMPK pathway, which in turn downregulates *srebf1*. Downregulation of *srebf1* decreases the expression of the downstream target *fasn* and, consequently, lipid synthesis might be reduced (Fig. 8 E). Likewise, in human liver cells, AMPK activation is associated with inhibition of SREBP-1c [55]. Moreover, RA treatment can inhibit lipid biosynthesis in mice liver [47]. SREBP influences genes that control epithelial development, proliferation, and cell death. Moreover, SREBP has a role in controlling the lung lipid transcriptional network [56]. Additionally, SREBP1-c is expressed during lung development, and its expression increases in late gestation associated with increased surfactant lipid synthesis [57].

Fatty acid β-oxidation is the process by which fatty acids are oxidized to acetyl-CoA to produce energy. Carnitine palmitoyltransferase I (CPT1) catalyzes the rate-limiting step of the long-chain fatty acid oxidation and promotes the translocation of fatty acids from the cytosol to the mitochondrial matrix [40]. In the embryonic chicken lung, *cpt1* expression levels remained unaltered between the three experimental conditions (Fig. 8 D). Such data indicates that RA signaling is not modulating lung branching fatty acid oxidation in contrast to what occurs in other systems [47–49].

In conclusion, this study describes the metabolic changes produced by RA signaling modulation on lung branching morphogenesis. RA signaling inhibition decreases lung branching morphogenesis and induces a cystic-like phenotype, which is accompanied by an increase in mitochondrial function. Since typical lung branching relies on a glycolytic lactate-based metabolism, the opposite metabolic phenotype, the OXPHOS-based BMS-induced metabolism, might explain the observed disease phenotype. On the other hand, RA signaling stimulation increased lung branching while maintaining proper morphology. RA signaling stimulation required less glucose consumption and produced less lactate. Nonetheless, RA

stimulation displayed a similar OCR mitochondrial profile as control lungs. Such data support the extracellular accumulation of pyruvate and succinate, which are not being used to fuel OXPHOS. Still, pyruvate and succinate might be exerting an additional metabolic or signaling role. We hypothesize that RA signaling stimulation might promote optimal growth conditions, while RA signaling inhibition promotes a less efficient metabolism for branching morphogenesis. Moreover, a RA-AMPK-dependent molecular mechanism seems to regulate lipid synthesis in the embryonic lung.

Undoubtedly, RA signaling modulation induces alterations at the transcript, protein, and metabolite levels. This report unveils novel insights on signaling-metabolism interaction during embryonic lung development and highlights the importance of metabolic regulation in this phase. Furthermore, our data may contribute to the understanding of the etiology of congenital lung disorders, namely cystic-related. We realize that this is a very new and unexplored topic, and several questions that require additional mechanistic understandings have been raised. Still, this report lays the groundwork for future studies in this emerging field.

MATERIALS AND METHODS

Ethical statement

Under the European Parliament Directive 2010/63/EU of 22 September 2010 and the Portuguese Directive 113/2013 of 7 August 2013 on the protection of animals used for scientific purposes, no ethical approval is required to carry out this work, performed at the early stages of chicken embryonic development.

Tissue collection

Fertilized chicken eggs, *Gallus gallus*, were incubated between 4.5 and 5.5 days (Embryonic day 4.5-5.5) in an incubator with a 49% humidified atmosphere, at 37 °C (Termaks KB400, Norway). b2 stage lungs (two secondary buds formed per bronchus) were microdissected using a stereomicroscope (Olympus SZX16, Japan) [9]. Dissected lung tissues were processed for *ex vivo* lung explant culture.

Ex vivo lung explant culture

Ex vivo lung explant culture was performed to study potential metabolic alterations in a very controlled environment [21]. Lungs were dissected in PBS and placed on 8 μm nucleopore polycarbonate membranes (Whatman, USA). Lung explants were cultured in 200 μL of medium 199 containing 5.5 mM glucose (Sigma, USA), supplemented with 1% (V/V) L-glutamine (Invitrogen), 0.25 mg/mL of ascorbic

acid (Sigma), 5% (V/V) heat-inactivated fetal calf serum (Invitrogen), 10% (V/V) chick serum (Invitrogen, USA), and 1% (V/V) penicillin 5000 IU/mL plus streptomycin 5000 IU/mL (Invitrogen). Lung explants were supplemented with increasing doses of BMS (BMS493, Sigma): 0.1 μM of BMS, 1 μM of BMS, or 10 μM of BMS; or in a different experimental setting with 1 μM of RA (Sigma), and 10 μM of BMS. DMSO 0.1% was used as control. Lung explants were incubated for 48 h, at 37 °C with 5% CO_2 (Heraeus HeraCell CO_2 incubator, Netherlands). At 24 hours, the culture medium was replaced by a fresh supplemented medium. Lung explants were photographed at 0 h (D0), 24 h (D1), and 48 h (D2) to be morphometrically analyzed (Olympus U-LH100HG coupled to Olympus SZX16). Media samples were collected at D0, D1, and D2 for ^{1}H-NMR spectroscopy. D2 tissues were collected for RNA, DNA, and protein extraction. D2 explants were also collected for *in situ* hybridization, proliferation assay, and seahorse analysis.

RNA probes

D2 lung explants total RNA was extracted using TripleXtractor directRNA kit (Grisp, Portugal). After, 1 μg of RNA was treated with DNase I (Thermo Fisher Scientific) and reversely transcribed into cDNA using the GRS cDNA Synthesis kit (Grisp). *rarβ* [58], *ldha*, and *ldhb* [21] RNA probes were produced as previously described. Antisense digoxigenin-labeled RNA probes were produced, using T3 (*rarβ*) or SP6 (*ldha* and *ldhb*) RNA polymerase, according to the manufacturer's instructions (Roche, Germany).

Whole-mount *in situ* hybridization

After explant culture, lungs were fixed in PBS solution with 4% formaldehyde, 2 mM EGTA, pH 7.5, at 4 °C overnight. Afterward, lung explants were dehydrated in a methanol series and stored at −20 °C. Tissues were rehydrated in a methanol/PBT series and processed for whole-mount *in situ* hybridization (n ≥ 4 per gene/condition) [59]. Tissues were permeabilized with proteinase K solution (PBT with 0.05% proteinase K) (Roche). After, tissues were incubated in a post-fixing solution (PBT with 10% formaldehyde and 0.4% glutaraldehyde). Subsequently, tissues were incubated with hybridization solution containing: 50% formamide, 6.5% SSC, 1% EDTA 0.5 M pH 9.8, 0.5% CHAPS, 0.25% t-RNA, 0.2% heparin, and 0.2% Tween 20, at 70 °C. Then, tissues were incubated with specific RNA probes, in the hybridization solution, at 70 °C, overnight. The next day, washes were performed with preheated hybridization solution, hybridization solution with MABT (50:50) (5.8% $C_4H_4O_4$, 4.4% NaCl, 7% NaOH, 1% Tween 20, pH 7.5), and MABT. Next, tissues were treated with blocking solutions [MABT with 20% blocking reagent (Roche); MABT with 20% blocking reagent plus 20% goat serum (Invitrogen)]. Then, lungs were incubated in MABT,

20% goat serum, 20% blocking reagent, and anti-digoxigenin antibody (1:2000) (Roche) solution overnight. Day 3 was committed to performing MABT solution washes. On the last day, tissues were washed in NTMT solution (0.1 M Tris-HCl, 0.1 M NaCl, 50 mM MgCl$_2$, 1% Tween 20) and then incubated in a developing solution (NTMT with BCIP and NBT) (Roche), protected from light, at 37 °C. The reaction was stopped, for each group of lungs/probes, at the same time. Lastly, lung explants were photographed (Olympus U-LH100HG coupled to Olympus SZX16).

Morphometric analysis

Morphometric analysis was performed to evaluate lung branching morphogenesis. Lung explants were outlined at D0 and D2, using AxioVision Rel. 4.9.1 (Carl Zeiss, Germany). The epithelial perimeter and epithelial area parameters were calculated, and results were expressed as D2/D0 ratio (n = 10/condition) [11].

^{1}H-NMR spectroscopy

Explant culture media samples (200 μL) were collected at D0, D1, and D2 and analyzed by ^{1}H-NMR spectroscopy (n ≥ 8/condition) according to [60]. Spectra were accessed at 25 °C, using a Bruker Avance 600 MHz spectrometer with a 5 mm QXI probe and z-gradient (Bruker Biospin, Germany). Solvent-suppressed ^{1}H-NMR spectra were acquired with 6 kHz spectral width, 14-s interpulse, 3-s water presaturation, 45-degree pulse angle, 3.5-s acquisition time, and 128 scans (minimum). Sodium fumarate 10 mM (singlet, at 6.50 ppm) was used as an internal reference. The following metabolites were detected and quantified: H1-α glucose (doublet, 5.22 ppm), pyruvate (singlet, 2.35 ppm), alanine (doublet, 1.46 ppm), lactate (doublet, 1.33 ppm), acetate (singlet, 1.9 ppm), and succinate (singlet, 2.39 ppm). The relative areas of ^{1}H-NMR resonances were quantified using NUTSpro™ NMR spectral analysis program (Acorn NMR, USA). D0 media samples were used as reference/control. Metabolite consumption or production was calculated using the mathematical formula | (D1-D0) + (D2-D0) | [21] and normalized to the total amount of protein.

Quantitative PCR

b2 lungs total RNA and cDNA were obtained as previously described. qPCR method was performed as described in [21]. Specific exon-exon spanning primers were designed for the amplification of target (*pfk1*, *g6pd*, *pgd*, *tfam*, *srebf1*, *fasn*, and *cpt1*) and housekeeping transcripts (*18s* and *actin-β*) (Table S1). Primers were optimized for annealing temperature and PCR cycles, using NZY Taq 2×Green

Master Mix (NZYTech, Portugal). Afterward, primers were optimized for the efficiency range. Each qPCR was performed in duplicate, using 1 µL of cDNA, and SYBR method, NZY qPCR Green Master Mix (2x) (NZYTech). *18s* and *actin-β* housekeeping genes were used to normalize the mRNA expression levels. Data on relative expression levels were calculated using the mathematical model $2^{\wedge}(-\Delta Ct)$ [61].

Western blot

Pooled samples 10 lungs/pool of D2 lung explants were processed for western blot as described in [10]. Protein was extracted and quantified according to [62]. 40 µg or 20 µg (Total OXPHOS) of protein were loaded onto 10% or 15% (Total OXPHOS) acrylamide minigels and electrophoresed at 100 V in a Mini-PROTEAN Tetra Cell (Bio-Rad). Blotting was performed using low fluorescence PVDF membranes (Bio-Rad) and a Trans-Blot Turbo Transfer System (Bio-Rad). After, membranes were incubated with AzureRed Fluorescent Total Protein Stain (Azure Biosystems, USA) according to the manufacturer's instructions. Immunoblots were probed with primary antibodies for LDHA (1:40000; #3582, Cell Signaling, USA), LDHB (1:10000; #ab240482, Abcam, UK), Total OXPHOS (1:1000; ab110413, Abcam), AMPKα (1:2000; #2532, Cell Signaling), Phospho-AMPKα (Thr172) (1:2000; #2531, Cell Signaling). Subsequently, blots were incubated with anti-rabbit IgG HRP-linked secondary antibody (1:2000; #7074, Cell Signaling), anti-mouse IgG HRP-linked secondary antibody (#7076, Cell Signaling), or anti-goat secondary IgG (H+L) HRP cross-adsorbed antibody (#R-21459, Invitrogen). Membranes were developed with Clarity or Clarity Max Western ECL substrate (Bio-Rad). To capture the chemiluminescent signal, a Sapphire Biomolecular Imager (Azure Biosystems) was used. Western blot quantifications were performed using AzureSpot Analysis Software (Azure Biosystems) and normalized to the total protein. Two or more independent experiments were performed per pool of tissue (n ≥ 3/condition).

Proliferation assay and confocal microscopy

Proliferation assay (n ≥ 4/condition) was performed as described in [21]. After 48 hours of lung explant culture, half of the explant's media was replaced by fresh media containing EdU (150 µM final concentration). Explants were incubated with EdU solution for 90 min, at 37 °C with 5% CO_2 (Heraeus HeraCell CO_2 incubator). Then, tissues were fixed in PBS with 3.7% formaldehyde. Afterward, tissues were washed in PBS with 3% BSA and permeabilized in PBS with 0.5% Triton X-100, for 90 min. Tissues were washed and processed for Click-iT Plus EdU reaction, according to the manufacturer's instructions (Click-iT™ Plus EdU Cell Proliferation Kit for Imaging, Invitrogen). Alexa Fluor 488 was used to detect EdU, and

the nuclei were counterstained with Hoechst 33342 (1:2000). Image acquisition was performed using an Olympus LPS Confocal FV3000 microscope (Olympus).

Seahorse analysis

After 48 hours of *in vitro* lung explant culture, D2 lungs were processed for real-time measurement of oxygen consumption rate (OCR) (n ≥ 13/condition), using a Seahorse XFe24 (Agilent, USA). Seahorse Mito Stress Test was performed according to the manufacturer's instructions (Agilent, USA). On the previous day, the Seahorse sensor cartridge (Agilent) was hydrated in Seahorse XF calibrant (Agilent), in a non-CO_2 incubator with humidity, at 37 °C overnight. On the protocol day, the Seahorse assay medium was freshly prepared with medium 199 without phenol red (Sigma), supplemented with 1 mM pyruvate (Sigma) and 1% (V/V) L-glutamine (Invitrogen), pH 7.3, warmed at 37 °C until use. Drugs were freshly prepared in Seahorse assay medium and sequentially loaded into the sensor cartridge injection ports: oligomycin 15 μM (Sigma), FFCP 20 μM (Sigma), and Rotenone/Antimycinn A 8 μM (Sigma), final concentrations. After explant culture, D2 lungs were washed in PBS and placed on Seahorse assay media. Islet capture microplates (Agilent) were prepared with 500 μL of Seahorse assay medium, then D2 tissues were placed on the wells' inner depression, and the islet capture screens (Agilent) were placed into the wells. After preparation, both islet capture microplates (tissues) and Seahorse sensor cartridge (drugs) were pre-warmed and calibrated at 37 °C. The Seahorse protocol cycles (5;5;5;8) and moment of injections are represented in Fig. S2. Each OCR measurement was performed with 3 min of mixing, 2 min of waiting, and 3 min of measuring. In the end, tissues were collected, washed in PBS several times, and processed for protein extraction and quantification. OCR data (pmol/min) was normalized to the total amount of protein.

mtDNA copy number

A qPCR method was performed to evaluate the mtDNA copy number, as described by [63], with minor modifications. D2 lungs total DNA was extracted using a GRS Genomic DNA kit (Grisp). DNA integrity was assessed by electrophoresis in a 0.6% agarose gel. Specific primers were designed for mitochondrial NADH dehydrogenase 1 (*nd1*); Nuclear angiotensin II receptor type 1 (*agrt1*) primers were produced according to [64] (Table S1). Primers were optimized for annealing temperature and PCR cycles, using NZY Taq 2×Green Master Mix (NZYTech). Then, primers were optimized for the efficiency range. qPCR was performed in duplicate (n ≥ 8/condition), using 20 ng of DNA per reaction, and SYBR

method NZY qPCR Green Master Mix (2x) (NZYTech). Ct value differences between *nd1* and *agrt1* were used to quantify the mtDNA copy number, using the mathematical model $2^{(-\Delta Ct)}$ [61].

Statistical analysis

Statistical analysis was performed using GraphPad Prism 8 (GraphPad Software, USA). The normality of distribution was tested using the Kolmogorov-Smirnov test. One-Way ANOVA was performed and followed by a post hoc Fisher's Least Significant Difference (LSD) test for multiple comparisons. All data are presented as mean ± standard error of the mean (SEM) with a statistically significant level of 5% ($p < 0.05$) considered.

SUPPLEMENTAL MATERIAL
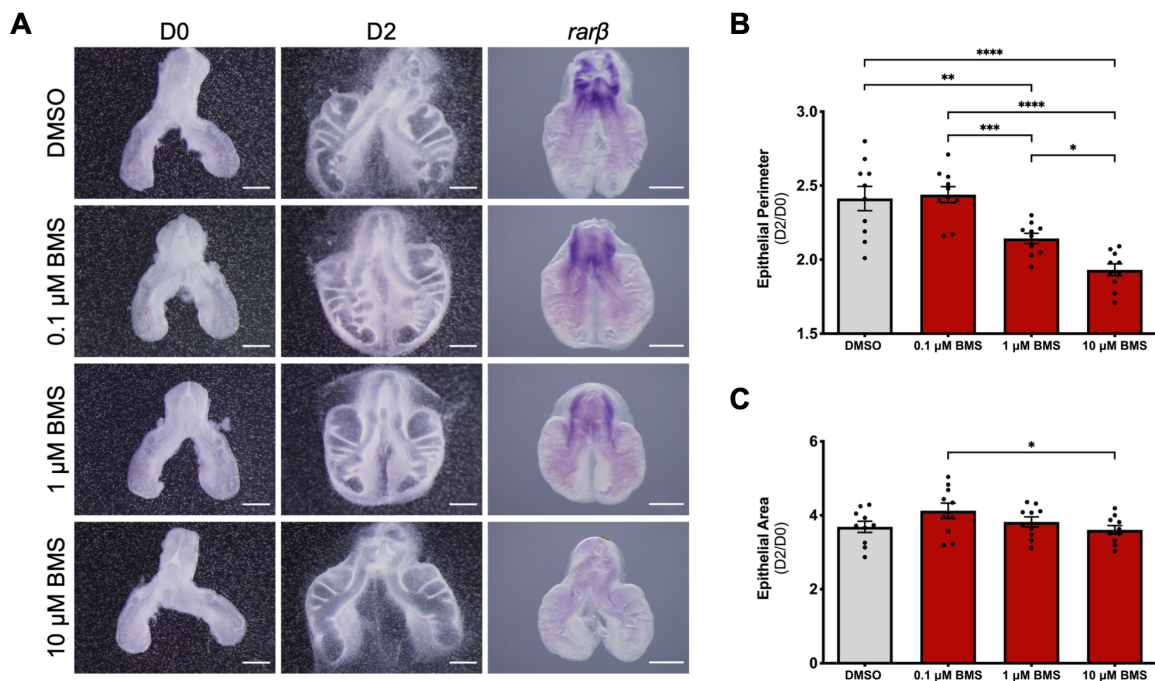
Figure S1 - Dose-dependent effect of BMS treatment on RA signaling pathway and lung branching morphogenesis. (A) Representative examples of b2 lung explant culture at D0 and D2, treated with DMSO, 0.1 μM of BMS, 1 μM of BMS, and 10 μM of BMS; D2 lungs were probed for *rarβ* (n = 5 /condition). scale bar: 500 μm. Morphometric analysis of lung explants: (B) epithelial perimeter and (C) epithelial area. Results are expressed as D2/D0 ratio and represented as mean ± SEM (n = 10/condition). One-Way ANOVA and Fisher's LSD test were performed. Significantly different results are indicated as: *p < 0.05; **p < 0.01; ***p < 0.001; ****p < 0.0001.
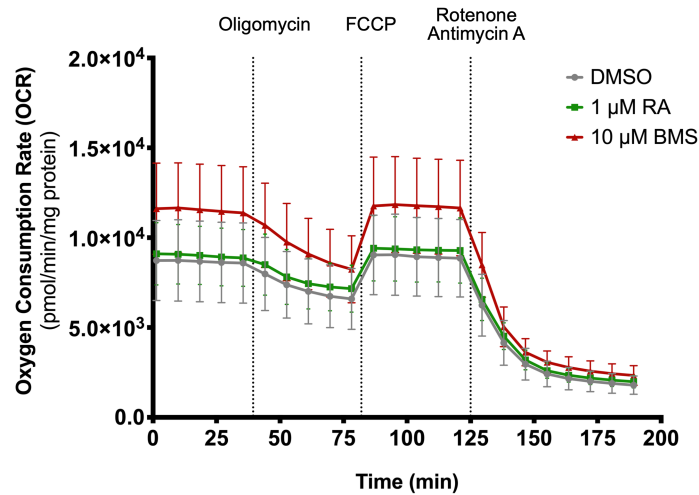
Figure S2 - Seahorse OCR profile. Real-time measurement of oxygen consumption rate (OCR) of D2 lung explants supplemented with DMSO, 1 μM of RA, and 10 μM of BMS. Time of measurements and moment of injections: Oligomycin (inhibition of complex V), FFCP (mitochondrial oxidative phosphorylation uncoupler), Rotenone/Antimycin A (inhibition of complex I and III, respectively). Results are represented in pmol/min/mg protein. Results are expressed as mean ± SEM (n ≥ 13/condition).
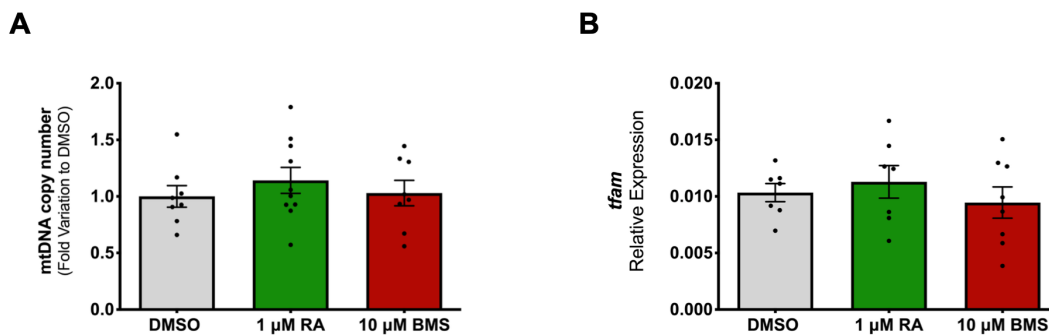

Figure S3 - Mitochondrial biogenesis in lung branching morphogenesis. Mitochondrial biogenesis analysis of lung explants after 48 hours in culture supplemented with DMSO, 1 μM of RA, and 10 μM of BMS. (A) mtDNA copy number (n ≥ 8/condition). Results are represented in fold variation to DMSO. (B) *tfam* relative expression levels (n ≥ 7/condition). Results are represented in fold variation to DMSO. Results are expressed as mean ± SEM. One-Way ANOVA and Fisher's LSD test were performed. Significantly different results are indicated as: *p < 0.05.
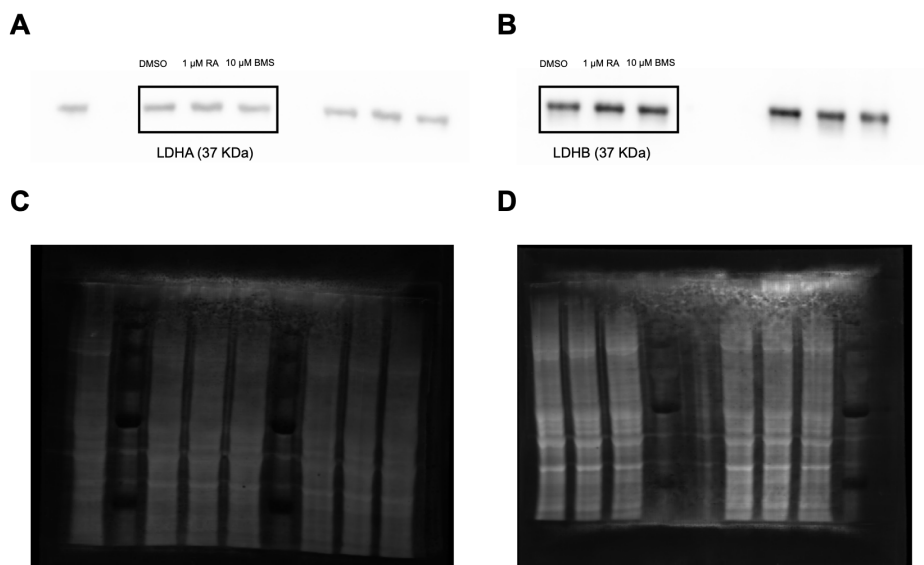
Table S1 - Primers sequences and qPCR conditions. Primer sequences forward (Fw) and reverse (Rv), corresponding PCR product size, annealing temperature, and the number of cycles.

Gene	Sequence 5'-3'	Size (bp)	Annealing T (°C)	Cycles
actin-β	Fw – CTTCTAAACCGGACTGTTACCA	100	58	30
	Rv – AAACAAATAAAGCCATGCCAATCT			
18s	Fw – TCTTTCTCGATTCCGTGGGT	157	58	30
	Rv – AACGCCACTTGTCCCTCTAC			

pfk1	Fw – CGTGGGAGGAGCTTTGAGAA Rv – CAGCCCACCTCACGTATCTG	236	56	40
g6pd	Fw – CTGGGGCAGTACGTGGGTAA Rv – CCGAAATATCGCCCGGAACC	232	62	40
pgd	Fw – AATAAATTAGTGCCGTTGTTGGA Rv – TGGCATGAGTGAAGGACCAT	174	60	40
tfam	Fw – GGAGAAAACGGCTGGCAAAA Rv – AGCTGAAGGTATGGCTGCTT	211	60	40
srebf1	Fw – GCTCTCGGCTTCGACGAT Rv – CGAACAGCCCTGAGAAGTCAT	145	60	40
fasn	Fw – CGGATCTCTCCCACTCTGGA Rv – CCGTGCAATGCCATCTTAGC	143	60	40
cpt1	Fw – TCATTGCGGGGGAAAACCTC Rv – CCCCACGGCCTTTATTGCTC	158	64	40
nd1	Fw – TGTAGAATATGCCGCCGGAC Rv – GTCATAGCGGAACCGTGGAT	214	62	40
agrt1	Fw – TGGCCATAGTGCATCCAGTG Rv – ACGATGAATGATGACGGGCA	119	62	40

SOURCE DATA

SourceDataF4
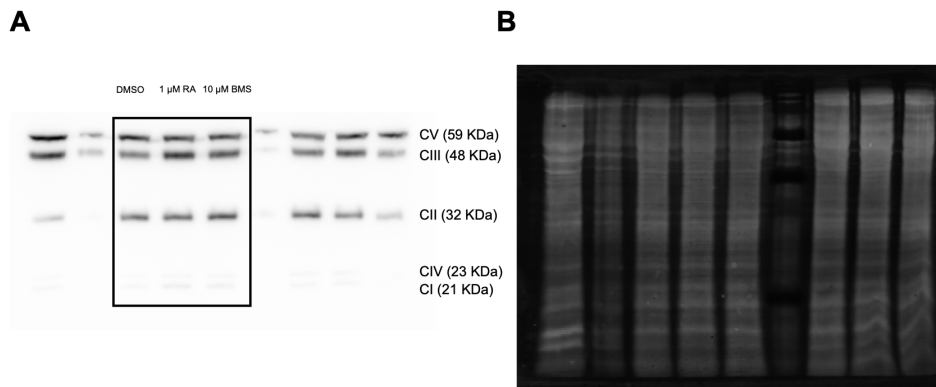
A

LDHA (37 KDa)

B

LDHB (37 KDa)

C

D

SourceDataF7

A

DMSO 1 µM RA 10 µM BMS

CV (59 KDa)
CIII (48 KDa)

CII (32 KDa)

CIV (23 KDa)
CI (21 KDa)

B

SourceDataF8

A

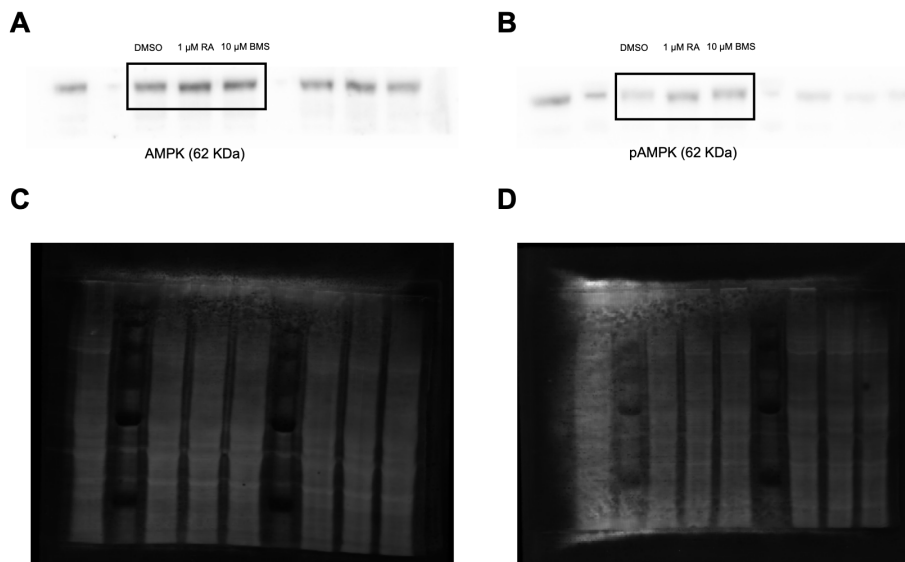DMSO 1 µM RA 10 µM BMS

AMPK (62 KDa)

B

DMSO 1 µM RA 10 µM BMS

pAMPK (62 KDa)

C

D

REFERENCES

1. Caldeira, I.; Fernandes-Silva, H.; Machado-Costa, D.; Correia-Pinto, J.; Moura, R.S. Developmental Pathways Underlying Lung Development and Congenital Lung Disorders. Cells 2021, 10, doi:10.3390/cells10112987.
2. Schittny, J.C. Development of the lung. Cell Tissue Res. 2017, 367, 427-444, doi:10.1007/s00441-016-2545-0.
3. Maina, J.N. A systematic study of the development of the airway (bronchial) system of the avian lung from days 3 to 26 of embryogenesis: a transmission electron microscopic study on the domestic fowl, Gallus gallus variant domesticus. Tissue Cell 2003, 35, 375-391, doi:10.1016/s0040-8166(03)00058-2.
4. Kim, H.Y.; Varner, V.D.; Nelson, C.M. Apical constriction initiates new bud formation during monopodial branching of the embryonic chicken lung. Development 2013, 140, 3146-3155, doi:10.1242/dev.093682.

5. Maina, J.N. Comparative molecular developmental aspects of the mammalian- and the avian lungs, and the insectan tracheal system by branching morphogenesis: recent advances and future directions. Front. Zool. 2012, 9, 16, doi:10.1186/1742-9994-9-16.

6. Metzger, R.J.; Klein, O.D.; Martin, G.R.; Krasnow, M.A. The branching programme of mouse lung development. Nature 2008, 453, 745-750, doi:10.1038/nature07005.

7. Moura, R.S.; Correia-Pinto, J. Molecular aspects of avian lung development. In: Maina JN, editor. The biology of the avian respiratory system. Cham: Springer: 2017; pp. 129–146.

8. Moura, R.S.; Silva-Goncalves, C.; Vaz-Cunha, P.; Correia-Pinto, J. Expression analysis of Shh signaling members in early stages of chick lung development. Histochem. Cell Biol. 2016, 146, 457-466, doi:10.1007/s00418-016-1448-1.

9. Moura, R.S.; Coutinho-Borges, J.P.; Pacheco, A.P.; Damota, P.O.; Correia-Pinto, J. FGF signaling pathway in the developing chick lung: expression and inhibition studies. PLoS ONE 2011, 6, e17660, doi:10.1371/journal.pone.0017660.

10. Moura, R.S.; Carvalho-Correia, E.; daMota, P.; Correia-Pinto, J. Canonical Wnt signaling activity in early stages of chick lung development. PLoS ONE 2014, 9, e112388, doi:10.1371/journal.pone.0112388.

11. Fernandes-Silva, H.; Vaz-Cunha, P.; Barbosa, V.B.; Silva-Goncalves, C.; Correia-Pinto, J.; Moura, R.S. Retinoic acid regulates avian lung branching through a molecular network. Cell. Mol. Life Sci. 2017, 74, 4599-4619, doi:10.1007/s00018-017-2600-3.

12. Cunningham, T.J.; Duester, G. Mechanisms of retinoic acid signalling and its roles in organ and limb development. Nat. Rev. Mol. Cell Biol. 2015, 16, 110-123, doi:10.1038/nrm3932.

13. Morrisey, E.E.; Hogan, B.L. Preparing for the first breath: genetic and cellular mechanisms in lung development. Dev. Cell 2010, 18, 8-23, doi:10.1016/j.devcel.2009.12.010.

14. Marquez, H.A.; Cardoso, W.V. Vitamin A-retinoid signaling in pulmonary development and disease. Mol. Cell. Pediatr. 2016, 3, 28, doi:10.1186/s40348-016-0054-6.

15. Ghyselinck, N.B.; Duester, G. Retinoic acid signaling pathways. Development 2019, 146, doi:10.1242/dev.167502.

16. Fernandes-Silva, H.; Araujo-Silva, H.; Correia-Pinto, J.; Moura, R.S. Retinoic Acid: A Key Regulator of Lung Development. Biomolecules 2020, 10, 152, doi:10.3390/biom10010152.

17. Marquez, H.A.; Chen, F. Retinoic Acid Signaling and Development of the Respiratory System. Subcell. Biochem. 2020, 95, 151-174, doi:10.1007/978-3-030-42282-0_6.

18. Yeager, H., Jr.; Massaro, D. Glucose metabolism and glycoprotein synthesis by lung slices. J. Appl. Physiol. 1972, 32, 477-482, doi:10.1152/jappl.1972.32.4.477.

19. Fisher, A.B. Normal and pathologic biochemistry of the lung. Environ. Health Perspect. 1976, 16, 3-9, doi:10.1289/ehp.76163.

20. Fisher, A.B. Intermediary metabolism of the lung. Environ. Health Perspect. 1984, 55, 149-158, doi:10.1289/ehp.8455149.

21. Fernandes-Silva, H.; Alves, M.G.; Araujo-Silva, H.; Silva, A.M.; Correia-Pinto, J.; Oliveira, P.F.; Moura, R.S. Lung branching morphogenesis is accompanied by temporal metabolic changes towards a glycolytic preference. Cell Biosci. 2021, 11, 134, doi:10.1186/s13578-021-00654-w.

22. Krejci, A.; Tennessen, J.M. Metabolism in time and space - exploring the frontier of developmental biology. Development 2017, 144, 3193-3198, doi:10.1242/dev.150573.

23. Miyazawa, H.; Aulehla, A. Revisiting the role of metabolism during development. Development 2018, 145, doi:10.1242/dev.131110.

24. Teleman, A.A. Metabolism meets development at Wiston House. Development 2016, 143, 3045-3049, doi:10.1242/dev.138800.

25. Cable, J.; Pourquie, O.; Wellen, K.E.; Finley, L.W.S.; Aulehla, A.; Gould, A.P.; Teleman, A.; Tu, W.B.; Garrett, W.S.; Miguel-Aliaga, I.; et al. Metabolic decisions in development and disease-a Keystone Symposia report. Ann. N. Y. Acad. Sci. 2021, doi:10.1111/nyas.14678.

26. Slaninova, V.; Krafcikova, M.; Perez-Gomez, R.; Steffal, P.; Trantirek, L.; Bray, S.J.; Krejci, A. Notch stimulates growth by direct regulation of genes involved in the control of glycolysis and the tricarboxylic acid cycle. Open Biol. 2016, 6, 150155, doi:10.1098/rsob.150155.

27. Kuwabara, S.; Yamaki, M.; Yu, H.; Itoh, M. Notch signaling regulates the expression of glycolysis-related genes in a context-dependent manner during embryonic development. Biochem. Biophys. Res. Commun. 2018, 503, 803-808, doi:10.1016/j.bbrc.2018.06.079.

28. Oginuma, M.; Moncuquet, P.; Xiong, F.; Karoly, E.; Chal, J.; Guevorkian, K.; Pourquie, O. A Gradient of Glycolytic Activity Coordinates FGF and Wnt Signaling during Elongation of the Body Axis in Amniote Embryos. Dev. Cell 2017, 40, 342-353 e310, doi:10.1016/j.devcel.2017.02.001.

29. Mendelsohn, C.; Lohnes, D.; Decimo, D.; Lufkin, T.; LeMeur, M.; Chambon, P.; Mark, M. Function of the retinoic acid receptors (RARs) during development (II). Multiple abnormalities at various stages of organogenesis in RAR double mutants. Development 1994, 120, 2749-2771, doi:10.1242/dev.120.10.2749.

30. Pereira-Terra, P.; Moura, R.S.; Nogueira-Silva, C.; Correia-Pinto, J. Neuroendocrine factors regulate retinoic acid receptors in normal and hypoplastic lung development. J. Physiol. 2015, 593, 3301-3311, doi:10.1113/JP270477.

31. Germain, P.; Gaudon, C.; Pogenberg, V.; Sanglier, S.; Van Dorsselaer, A.; Royer, C.A.; Lazar, M.A.; Bourguet, W.; Gronemeyer, H. Differential action on coregulator interaction defines inverse retinoid agonists and neutral antagonists. Chem. Biol. 2009, 16, 479-489, doi:10.1016/j.chembiol.2009.03.008.

32. Schuger, L.; Varani, J.; Mitra, R., Jr.; Gilbride, K. Retinoic acid stimulates mouse lung development by a mechanism involving epithelial-mesenchymal interaction and regulation of epidermal growth factor receptors. Dev. Biol. 1993, 159, 462-473, doi:10.1006/dbio.1993.1256.

33. Gonzaga, S.; Henriques-Coelho, T.; Davey, M.; Zoltick, P.W.; Leite-Moreira, A.F.; Correia-Pinto, J.; Flake, A.W. Cystic adenomatoid malformations are induced by localized FGF10 overexpression in fetal rat lung. Am. J. Respir. Cell Mol. Biol. 2008, 39, 346-355, doi:10.1165/rcmb.2007-0290OC.

34. Harris, K.S.; Zhang, Z.; McManus, M.T.; Harfe, B.D.; Sun, X. Dicer function is essential for lung epithelium morphogenesis. Proc. Natl. Acad. Sci. 2006, 103, 2208-2213, doi:10.1073/pnas.0510839103.

35. Malpel, S.; Mendelsohn, C.; Cardoso, W.V. Regulation of retinoic acid signaling during lung morphogenesis. Development 2000, 127, 3057-3067.

36. Bellusci, S.; Grindley, J.; Emoto, H.; Itoh, N.; Hogan, B.L. Fibroblast growth factor 10 (FGF10) and branching morphogenesis in the embryonic mouse lung. Development 1997, 124, 4867-4878, doi:10.1242/dev.124.23.4867.

37. Carraro, G.; del Moral, P.M.; Warburton, D. Mouse embryonic lung culture, a system to evaluate the molecular mechanisms of branching. J. Vis. Exp. 2010, doi:10.3791/2035.

38. Yeganeh, B.; Bilodeau, C.; Post, M. Explant Culture for Studying Lung Development. Methods Mol. Biol. 2018, 1752, 81-90, doi:10.1007/978-1-4939-7714-7_8.

39. Tierney, D.F. Lung metabolism and biochemistry. Annu. Rev. Physiol. 1974, 36, 209-231, doi:10.1146/annurev.ph.36.030174.001233.

40. Nelson, D.; Cox, M. Lehninger principles of biochemistry, 5th edition ed.; New York: Worth Publishers: 2008.

41.   Vander Heiden, M.G.; Cantley, L.C.; Thompson, C.B. Understanding the Warburg effect: the metabolic requirements of cell proliferation. Science 2009, 324, 1029-1033, doi:10.1126/science.1160809.

42.   Murphy, M.P.; O'Neill, L.A.J. Krebs Cycle Reimagined: The Emerging Roles of Succinate and Itaconate as Signal Transducers. Cell 2018, 174, 780-784, doi:10.1016/j.cell.2018.07.030.

43.   Guo, Y.; Cho, S.W.; Saxena, D.; Li, X. Multifaceted Actions of Succinate as a Signaling Transmitter Vary with Its Cellular Locations. Endocrinol. Metab. (Seoul) 2020, 35, 36-43, doi:10.3803/EnM.2020.35.1.36.

44.   Marchetti, P.; Fovez, Q.; Germain, N.; Khamari, R.; Kluza, J. Mitochondrial spare respiratory capacity: Mechanisms, regulation, and significance in non-transformed and cancer cells. FASEB J 2020, 34, 13106-13124, doi:10.1096/fj.202000767R.

45.   Ventura-Clapier, R.; Garnier, A.; Veksler, V. Transcriptional control of mitochondrial biogenesis: the central role of PGC-1alpha. Cardiovasc. Res. 2008, 79, 208-217, doi:10.1093/cvr/cvn098.

46.   Gureev, A.P.; Shaforostova, E.A.; Popov, V.N. Regulation of Mitochondrial Biogenesis as a Way for Active Longevity: Interaction Between the Nrf2 and PGC-1alpha Signaling Pathways. Front. genet. 2019, 10, 435, doi:10.3389/fgene.2019.00435.

47.   Amengual, J.; Ribot, J.; Bonet, M.L.; Palou, A. Retinoic acid treatment enhances lipid oxidation and inhibits lipid biosynthesis capacities in the liver of mice. Cell. Physiol. Biochem. 2010, 25, 657-666, doi:10.1159/000315085.

48.   Amengual, J.; Ribot, J.; Bonet, M.L.; Palou, A. Retinoic acid treatment increases lipid oxidation capacity in skeletal muscle of mice. Obesity (Silver Spring) 2008, 16, 585-591, doi:10.1038/oby.2007.104.

49.   Amengual, J.; Garcia-Carrizo, F.J.; Arreguin, A.; Musinovic, H.; Granados, N.; Palou, A.; Bonet, M.L.; Ribot, J. Retinoic Acid Increases Fatty Acid Oxidation and Irisin Expression in Skeletal Muscle Cells and Impacts Irisin In Vivo. Cell. Physiol. Biochem. 2018, 46, 187-202, doi:10.1159/000488422.

50.   Garcia, D.; Shaw, R.J. AMPK: Mechanisms of Cellular Energy Sensing and Restoration of Metabolic Balance. Mol. Cell 2017, 66, 789-800, doi:10.1016/j.molcel.2017.05.032.

51.   Herzig, S.; Shaw, R.J. AMPK: guardian of metabolism and mitochondrial homeostasis. Nat. Rev. Mol. Cell Biol. 2018, 19, 121-135, doi:10.1038/nrm.2017.95.

52.   Zhang, J.; Deng, B.; Jiang, X.; Cai, M.; Liu, N.; Zhang, S.; Tan, Y.; Huang, G.; Jin, W.; Liu, B.; et al. All-Trans-Retinoic Acid Suppresses Neointimal Hyperplasia and Inhibits Vascular Smooth Muscle Cell Proliferation and Migration via Activation of AMPK Signaling Pathway. Front. Pharmacol. 2019, 10, 485, doi:10.3389/fphar.2019.00485.

53.   Ishijima, N.; Kanki, K.; Shimizu, H.; Shiota, G. Activation of AMP-activated protein kinase by retinoic acid sensitizes hepatocellular carcinoma cells to apoptosis induced by sorafenib. Cancer Sci. 2015, 106, 567-575, doi:10.1111/cas.12633.

54.   Lee, Y.M.; Lee, J.O.; Jung, J.H.; Kim, J.H.; Park, S.H.; Park, J.M.; Kim, E.K.; Suh, P.G.; Kim, H.S. Retinoic acid leads to cytoskeletal rearrangement through AMPK-Rac1 and stimulates glucose uptake through AMPK-p38 MAPK in skeletal muscle cells. J. Biol. Chem. 2008, 283, 33969-33974, doi:10.1074/jbc.M804469200.

55.   Li, Y.; Xu, S.; Mihaylova, M.M.; Zheng, B.; Hou, X.; Jiang, B.; Park, O.; Luo, Z.; Lefai, E.; Shyy, J.Y.; et al. AMPK phosphorylates and inhibits SREBP activity to attenuate hepatic steatosis and atherosclerosis in diet-induced insulin-resistant mice. Cell Metab. 2011, 13, 376-388, doi:10.1016/j.cmet.2011.03.009.

56.   Xu, Y.; Zhang, M.; Wang, Y.; Kadambi, P.; Dave, V.; Lu, L.J.; Whitsett, J.A. A systems approach to mapping transcriptional networks controlling surfactant homeostasis. BMC Genom. 2010, 11, 451, doi:10.1186/1471-2164-11-451.

57. Zhang, F.; Pan, T.; Nielsen, L.D.; Mason, R.J. Lipogenesis in fetal rat lung: importance of C/EBPalpha, SREBP-1c, and stearoyl-CoA desaturase. Am. J. Respir. Cell Mol. Biol. 2004, 30, 174-183, doi:10.1165/rcmb.2003-0235OC.

58. Michaille, J.J.; Kanzler, B.; Blanchet, S.; Garnier, J.M.; Dhouailly, D. Characterization of cDNAs encoding two chick retinoic acid receptor alpha isoforms and distribution of retinoic acid receptor alpha, beta and gamma transcripts during chick skin development. Int. J. Dev. Biol. 1995, 39, 587-596.

59. Moura, R.S. Retinoic Acid as a Modulator of Proximal-Distal Patterning and Branching Morphogenesis of the Avian Lung. Methods Mol. Biol. 2019, 2019, 209-224, doi:10.1007/978-1-4939-9585-1_15.

60. Alves, M.G.; Oliveira, P.F.; Martins, F.O.; Oliveira, P.J.; Carvalho, R.A. Gender-dependent metabolic remodeling during heart preservation in cardioplegic celsior and histidine buffer solution. J. Cardiovasc. Pharmacol. 2012, 60, 227-233, doi:10.1097/FJC.0b013e3182391d17.

61. Livak, K.J.; Schmittgen, T.D. Analysis of relative gene expression data using real-time quantitative PCR and the 2(-Delta Delta C(T)) Method. Methods 2001, 25, 402-408, doi:10.1006/meth.2001.1262.

62. Kling, D.E.; Lorenzo, H.K.; Trbovich, A.M.; Kinane, T.B.; Donahoe, P.K.; Schnitzer, J.J. MEK-1/2 inhibition reduces branching morphogenesis and causes mesenchymal cell apoptosis in fetal rat lungs. Am. J. Physiol. Lung Cell Mol. Physiol. 2002, 282, L370-378, doi:10.1152/ajplung.00200.2001.

63. Martins, A.D.; Monteiro, M.P.; Silva, B.M.; Barros, A.; Sousa, M.; Carvalho, R.A.; Oliveira, P.F.; Alves, M.G. Metabolic dynamics of human Sertoli cells are differentially modulated by physiological and pharmacological concentrations of GLP-1. Toxicol. Appl. Pharmacol. 2019, 362, 1-8, doi:10.1016/j.taap.2018.10.009.

64. Liu, R.; Jin, L.; Long, K.; Tang, Q.; Ma, J.; Wang, X.; Zhu, L.; Jiang, A.; Tang, G.; Jiang, Y.; et al. Analysis of mitochondrial DNA sequence and copy number variation across five high-altitude species and their low-altitude relatives. Mitochondrial DNA B Resour 2018, 3, 847-851, doi:10.1080/23802359.2018.1501285.

CHAPTER 4. GENERAL DISCUSSION

Pulmonary development depends on epithelial-mesenchymal interactions and conserved signaling pathways that promote spatial-temporal synchronization of lung morphogenesis [1–3]. The molecular mechanisms underlying lung branching morphogenesis have been extensively explored over the last years [3]. Most of our knowledge regarding the signaling mechanisms triggering early lung development was attained through the use of mammalian models such as the mouse and rat [4,5]. More recently, the chicken embryo, *Gallus gallus*, has emerged as an excellent alternative to study branching morphogenesis because its lateral/monopodial branching is remarkably similar to the domain branching subroutine of the mammalian lung system [6,7]. In addition to this morphological resemblance, the molecular mechanisms that lie beneath early avian lung development are highly conserved with the mammalian, pointing towards similar functions [8–11]. Furthermore, the chicken embryo offers additional advantages compared to the mammalian models. For instance, it has a progenitor-independent development, does not need special housing facilities, is cheaper and easily accessible to surgical manipulation, allows direct observation of embryogenesis, and presents symmetric lung structure.

On the other hand, little is known regarding lung metabolic needs. In this sense, one of the main goals of this thesis was to investigate how metabolism contributes and is dynamically regulated during lung development, using the chicken embryo as a model. In **chapter 3.1**, we explored the metabolic profile associated with pulmonary branching. We described the temporal metabolite changes that occur concurrently with variations in the expression levels of key enzymes and transporters from the glycolytic pathway in the early stages of branching morphogenesis. This metabolic profile is accompanied by functional mitochondria, which perform steady basal oxygen consumption. Also, we established that active lung branching sites are associated with high proliferation rates. Furthermore, we propose that LDH is pivotal for lung branching morphogenesis as *ldha* and *lhdb* exhibit region-specific expression patterns and behave as proximal-distal markers. Furthermore, LDH seems to support the increase in lactate production throughout lung branching [12]. This study demonstrates that the chicken embryo is a valuable model for lung metabolism studies, and we show that the embryonic lung has a glycolytic preference with a shift to lactate production as pulmonary branching proceeds. This metabolic rewiring into aerobic glycolysis resembles a Warburg-like metabolism, observed in other high proliferative systems such as cancer and specific developmental processes. This type of metabolism is associated with the production of energy and biomass critical for embryonic development [12].

The coordination between cell signaling and metabolism is arising as a central concept for understanding developmental processes, and it is crucial to comprehend how metabolism impacts cellular and developmental decisions and is dynamically regulated during development [13–15]. In other

contexts, it has been shown that PSM glycolytic activity is coordinated by an FGF/WNT signaling network, NOTCH signaling regulates glycolytic genes expression in *Zebrafish* neural tissue development, and NOTCH controls *Drosophila* wing disc development by regulating glucose catabolism [16–18].

In **chapter 3.2**, we investigated how the RA signaling pathway influences the metabolic profile of chicken lung branching morphogenesis. RA signaling stimulation increases lung branching and maintains proper lung morphology [11]. On the other hand, the impact of RA signaling inhibition had not been assessed so far. Our study revealed that RA signaling inhibition decreases lung branching and induces a phenotype that resembles the airway dilation observed in Congenital Pulmonary Airway Malformation (CPAM) [19,20]. After establishing the RA/BMS model, we explored the potential metabolic alterations induced by RA signaling modulation. Notably, RA signaling modulation elicits changes in lung metabolism at the transcript, protein, and metabolite levels. RA signaling stimulation induces metabolic changes towards an optimal growth condition to sustain an increase in lung branching morphogenesis. Since typical lung branching relies on a glycolytic lactate-based metabolism, RA signaling inhibition seems to promote a less efficient metabolism by inducing mitochondrial function and, consequently, oxidative metabolism. Such metabolic alteration during lung branching morphogenesis might explain the observed disease phenotype. RA signaling modulation also controls lipid synthesis through an AMPK indirect molecular mechanism thus contributing to the overall metabolic profile. In this study, we uncovered new insights on the signaling-metabolism interaction and highlighted the importance of metabolic and signaling regulation during lung branching morphogenesis. Additionally, our findings may contribute to understanding the etiology of congenital cystic-related lung disorders.

Congenital lung lesions may result from impairments during lung branching morphogenesis [3]. Likewise, it has been recently reported that bronchial variations in the central pulmonary airway tree, which occur in one-quarter of the general population, may represent a susceptibility factor for developing Chronic Obstructive Pulmonary Disease (COPD) [21,22]. In this sense, the scientific contributions presented in this thesis may contribute to better understanding the etiology of congenital lung disorders and also chronic conditions in which the airway architecture might be defective due to impairments during lung development.

References:

1.   Schittny, J.C. Development of the lung. Cell Tissue Res. 2017, 367, 427-444, doi:10.1007/s00441-016-2545-0.
2.   Whitsett, J.A.; Kalin, T.V.; Xu, Y.; Kalinichenko, V.V. Building and Regenerating the Lung Cell by Cell. Physiol. Rev. 2019, 99, 513-554, doi:10.1152/physrev.00001.2018.

3. Caldeira, I.; Fernandes-Silva, H.; Machado-Costa, D.; Correia-Pinto, J.; Moura, R.S. Developmental Pathways Underlying Lung Development and Congenital Lung Disorders. Cells 2021, 10(11):2987, doi:10.3390/cells10112987.

4. Bellusci, S.; Grindley, J.; Emoto, H.; Itoh, N.; Hogan, B.L. Fibroblast growth factor 10 (FGF10) and branching morphogenesis in the embryonic mouse lung. Development 1997, 124, 4867–4878, doi:10.1242/dev.124.23.4867.

5. Pereira-Terra, P.; Moura, R.S.; Nogueira-Silva, C.; Correia-Pinto, J. Neuroendocrine factors regulate retinoic acid receptors in normal and hypoplastic lung development. J. Physiol. 2015, 593, 3301–3311, doi:10.1113/JP270477.

6. Metzger, R.J.; Klein, O.D.; Martin, G.R.; Krasnow, M.A. The branching programme of mouse lung development. Nature 2008, 453, 745–750, doi:10.1038/nature07005.

7. Maina, J.N. Comparative molecular developmental aspects of the mammalian- and the avian lungs, and the insectan tracheal system by branching morphogenesis: recent advances and future directions. Front. Zool. 2012, 9, 16, doi:10.1186/1742-9994-9-16.

8. Moura, R.S.; Coutinho-Borges, J.P.; Pacheco, A.P.; Damota, P.O.; Correia-Pinto, J. FGF signaling pathway in the developing chick lung: expression and inhibition studies. PLoS ONE 2011, 6, e17660, doi:10.1371/journal.pone.0017660.

9. Moura, R.S.; Carvalho-Correia, E.; daMota, P.; Correia-Pinto, J. Canonical Wnt signaling activity in early stages of chick lung development. PLoS ONE 2014, 9, e112388, doi:10.1371/journal.pone.0112388.

10. Moura, R.S.; Silva-Goncalves, C.; Vaz-Cunha, P.; Correia-Pinto, J. Expression analysis of Shh signaling members in early stages of chick lung development. Histochem. Cell Biol. 2016, 146, 457-466, doi:10.1007/s00418-016-1448-1.

11. Fernandes-Silva, H.; Vaz-Cunha, P.; Barbosa, V.B.; Silva-Goncalves, C.; Correia-Pinto, J.; Moura, R.S. Retinoic acid regulates avian lung branching through a molecular network. Cell. Mol. Life Sci. 2017, 74, 4599-4619, doi:10.1007/s00018-017-2600-3.

12. Fernandes-Silva, H.; Alves, M.G.; Araujo-Silva, H.; Silva, A.M.; Correia-Pinto, J.; Oliveira, P.F.; Moura, R.S. Lung branching morphogenesis is accompanied by temporal metabolic changes towards a glycolytic preference. Cell Biosci. 2021, 11, 134, doi:10.1186/s13578-021-00654-w.

13. Krejci, A.; Tennessen, J.M. Metabolism in time and space - exploring the frontier of developmental biology. Development 2017, 144, 3193-3198, doi:10.1242/dev.150573.

14. Miyazawa, H.; Aulehla, A. Revisiting the role of metabolism during development. Development 2018, 145, doi:10.1242/dev.131110.

15. Cable, J.; Pourquie, O.; Wellen, K.E.; Finley, L.W.S.; Aulehla, A.; Gould, A.P.; Teleman, A.; Tu, W.B.; Garrett, W.S.; Miguel-Aliaga, I.; et al. Metabolic decisions in development and disease-a Keystone Symposia report. Ann. N. Y. Acad. Sci. 2021, 1506, 55-73, doi:10.1111/nyas.14678.

16. Slaninova, V.; Krafcikova, M.; Perez-Gomez, R.; Steffal, P.; Trantirek, L.; Bray, S.J.; Krejci, A. Notch stimulates growth by direct regulation of genes involved in the control of glycolysis and the tricarboxylic acid cycle. Open Biol. 2016, 6, 150155, doi:10.1098/rsob.150155.

17. Oginuma, M.; Moncuquet, P.; Xiong, F.; Karoly, E.; Chal, J.; Guevorkian, K.; Pourquie, O. A Gradient of Glycolytic Activity Coordinates FGF and Wnt Signaling during Elongation of the Body Axis in Amniote Embryos. Dev. Cell 2017, 40, 342-353 e310, doi:10.1016/j.devcel.2017.02.001.

18. Kuwabara, S.; Yamaki, M.; Yu, H.; Itoh, M. Notch signaling regulates the expression of glycolysis-related genes in a context-dependent manner during embryonic development. Biochem. Biophys. Res. Commun. 2018, 503, 803-808, doi:10.1016/j.bbrc.2018.06.079.

19. Gonzaga, S.; Henriques-Coelho, T.; Davey, M.; Zoltick, P.W.; Leite-Moreira, A.F.; Correia-Pinto, J.; Flake, A.W. Cystic adenomatoid malformations are induced by localized FGF10 overexpression

in fetal rat lung. Am. J. Respir. Cell Mol. Biol. 2008, 39, 346-355, doi:10.1165/rcmb.2007-0290OC.

20. Rockich, B.E.; Hrycaj, S.M.; Shih, H.P.; Nagy, M.S.; Ferguson, M.A.; Kopp, J.L.; Sander, M.; Wellik, D.M.; Spence, J.R. Sox9 plays multiple roles in the lung epithelium during branching morphogenesis. Proc. Natl. Acad. Sci. 2013, 110, E4456–4464, doi:10.1073/pnas.1311847110.

21. Sun, X.W.; Lin, Y.N.; Ding, Y.J.; Li, S.Q.; Li, H.P.; Li, Q.Y. Bronchial Variation: Anatomical Abnormality May Predispose Chronic Obstructive Pulmonary Disease. Int. J. Chron. Obstruct. Pulmon. Dis. 2021, 16, 423-431, doi:10.2147/COPD.S297777.

22. Smith, B.M.; Traboulsi, H.; Austin, J.H.M.; Manichaikul, A.; Hoffman, E.A.; Bleecker, E.R.; Cardoso, W.V.; Cooper, C.; Couper, D.J.; Dashnaw, S.M.; et al. Human airway branch variation and chronic obstructive pulmonary disease. Proc. Natl. Acad. Sci. 2018, 115, E974-E981, doi:10.1073/pnas.1715564115.

CHAPTER 5. CONCLUSIONS AND FUTURE PERSPECTIVES

The main goal of this thesis was to investigate the metabolic profile associated with the early stages of pulmonary branching and to study a potential interaction between the Retinoic Acid signaling pathway and the lung metabolism throughout lung branching morphogenesis.

We described the temporal metabolic changes accompanying early lung branching morphogenesis using the chicken model. We observed that as lung branching morphogenesis proceeds, the lung progressively adapts to a glycolytic lactate-based metabolic profile. This metabolic rewiring into aerobic glycolysis resembles a Warburg-like metabolism, typical of high proliferative systems such as cancer and specific developmental processes.

Then, we explored the metabolic changes induced by RA signaling modulation on lung branching morphogenesis metabolism. RA modulation impacts branching morphogenesis and regulates lung metabolism. RA signaling stimulation is associated with increased lung branching morphogenesis and an optimization of growth conditions. On the other hand, RA signaling inhibition causes impairment in branching morphogenesis and seems to induce a less efficient metabolism. This study unveiled novel insights on signaling-metabolism interactions during embryonic lung development.

Overall, we have highlighted the importance of metabolic regulation during lung branching morphogenesis, and we believe our findings may contribute to a better understanding of the etiology of congenital and chronic branching-related disorders.

Lung development and metabolism are undeniably interlinked. This is a new, unexplored, and exciting topic, and several questions have been raised. Future mechanistic studies exploring metabolic regulation and the interaction between classical signaling pathways and metabolism will certainly, contribute to a better understanding of lung development and other developmental processes. Of particular interest is to further explore the role of MCTs, perform LDH inhibition and enzymatic activity studies, explore the role of reactive oxygen species, and further explore the role of lipids throughout lung branching. Still, we recognize that our data can lay the groundwork for uncovering early biomarkers of congenital and chronic branching-related disorders.

CHAPTER 6. APPENDIX

COPYRIGHTS

Search for Articles: [Title / Keyword]   [Author / Affiliation]   [All Journals ▾]   [All Article Types ▾]   **Search**   Advanced

Information

- For Authors
- For Reviewers
- For Editors
- For Librarians
- For Publishers
- For Societies
- For Conference Organizers
- Article Processing Charges
- **Open Access Policy**
  - Permissions
  - External Open Access Resources
  - Open Access Explained!
  - Meaning of Open Access
  - Advantages of Open Access for Authors
  - Links and Notes
- Institutional O.A. Program
- Editorial Process
- Awards
- Research and Publication Ethics

MDPI Open Access Information and Policy

All articles published by MDPI are made immediately available worldwide under an open access license. This means:

- everyone has free and unlimited access to the full-text of *all* articles published in MDPI journals;
- everyone is free to re-use the published material if proper accreditation/citation of the original publication is given;
- open access publication is supported by the authors' institutes or research funding agencies by payment of a comparatively low **Article Processing Charge (APC)** for accepted articles.

Permissions

No special permission is required to reuse all or part of article published by MDPI, including figures and tables. For articles published under an open access Creative Common CC BY license, any part of the article may be reused without permission provided that the original article is clearly cited. Reuse of an article does not imply endorsement by the authors or MDPI.

External Open Access Resources

Those who are new to the concept of open access might find the following websites or the *Open Access Explained!* video informative:

- **Wikipedia article on Open Access**
- Information Platform Open Access [in **English**, in **German**]

Meaning of Open Access

In accordance with major definitions of open access in scientific literature (namely the Budapest, Berlin, and Bethesda declarations), MDPI defines *open access* by the following conditions:

- peer-reviewed literature is freely available without subscription or price barriers,
- literature is immediately released in open access format (no embargo period), and
- published material can be re-used without obtaining permission as long as a correct citation to the original publication is given.

Open Access Explained!

Until 2008, most articles published by MDPI contained the note: "© *year* by MDPI (http://www.mdpi.org). Reproduction is permitted for noncommercial purposes". During 2008, MDPI journals started to publish articles under the **Creative Commons Attribution License** and are now using the latest version of the CC BY license, which grants authors the most extensive rights. All articles published by MDPI before and during 2008 should now be considered as having been released under the post-2008 Creative Commons Attribution License.

This means that all articles published in MDPI journals, including data, graphics, and supplements, can be linked from external sources, scanned by search engines, re-used by text mining applications or websites, blogs, *etc.* free of charge under the sole condition of proper accreditation of the source and original publisher. MDPI believes that open access publishing fosters the exchange of research results amongst scientists from different disciplines, thus facilitating interdisciplinary research. Open access publishing also provides access to research results to researchers worldwide, including those from developing countries, and to an interested general public. Although MDPI publishes all of its journals under the open access model, we believe that open access is an enriching part of the scholarly communication process that can and should co-exist with other forms of communication and publication, such as society-based publishing and conferencing activities.

Important Note: some articles (especially *Reviews*) may contain figures, tables or text taken from other publications, for which MDPI does not hold the copyright or the right to re-license the published material. Please note that you should inquire with the original copyright holder (usually the original publisher or authors) whether or not this material can be re-used.

Advantages of Open Access for Authors

The High Availability and Visibility of our open access articles is guaranteed through the free and unlimited accessibility of the publication over the Internet. Everyone can freely access and download the full text of all articles published with MDPI: readers of open access journals, *i.e.*, mostly other researchers, do not need to pay any subscription or pay-per-view charges to read articles published by MDPI. Open access publications are also more likely to be included in search engines and indexing databases.

The Higher Citation Impact of open access articles results from their high publicity and availability. Open access publications are demonstrably more frequently cited [1,2].
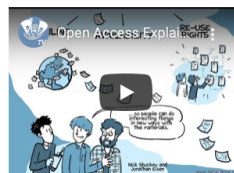
Lower Publishing Costs: Open access publishers cover their costs for editorial handling and editing of a paper by charging authors' institutes or research funding agencies. The cost of handling and producing an article is covered through the one-time payment of an **article processing charge (APC)** for each accepted article. The APCs of open access publishers are only a fraction of the average income per paper earned by traditional, subscription-based publishers. MDPI's **article processing charge (APC)** is the same, irrespective of article length, because we wish to encourage publication of long papers with complete results and full experimental or computational details [3].

Faster Publication in MDPI's open access journals is achieved by online-only availability. Accepted articles are typically published online more rapidly in MDPI journals than those of traditional, subscription-based and printed journals are [4].

Links and Notes

1. Open access citation impact advantage: **http://en.wikipedia.org/wiki/Open_access#Authors_and_researchers**. For example, a standard research paper "Shutalev, A.D.; Kishko, E.A.; Sivova, N.V.; Kuznetsov, A.Y. *Molecules* **1998**, *3*, 100-106" has been cited 51 times, the highest number among all the papers published so far by the same author.

2. Lin, S.-K. *Editorial:* Non-Open Access and Its Adverse Impact on Molecules. *Molecules* **2007**, *12*, 1436-1437 (PDF format 16 K, HTML format).

3. Recently a research paper of 30 pages has been published: *Molecules* **2008, 13(5), 1081-1110**.

4. Some well written papers have been peer reviewed and published in less than two weeks from manuscript submission, see e.g.: *Molecules* **2006, 11(4), 212-218**.